AD

USAAVLABS TECHNICAL REPORT 68-42

AN ANALYTICAL AND MODEL TEST RESEARCH STUDY ON THE KAMAN DYNAMIC ANTIRESONANT VIBRATION ISOLATOR (DAVI)

By

Robert Jones

November 1968

U. S. ARMY AVIATION MATERIEL LABORATORIES
FORT EUSTIS, VIRGINIA

CONTRACT DA 44-177-AMC-391(T)
KAMAN AIRCRAFT DIVISION
KAMAN CORPORATION
BLOOMFIELD, CONNECTICUT

241

Disclaimers

The findings in this report are not to be construed as an official Department of the Army position unless so designated by other authorized documents.

When Government drawings, specifications, or other data are used for any purpose other than in connection with a definitely related Government procurement operation, the United States Government thereby incurs no responsibility nor any obligation whatsoever; and the fact that the Government may have formulated, furnished, or in any way supplied the said drawings, specifications, or other data is not to be regarded by implication or otherwise as in any manner licensing the holder or any other person or corporation, or conveying any rights or permission, to manufacture, use, or sell any patented invention that may in any way be related thereto.

Trade names cited in this report do not constitute an official endorsement or approval of the use of such commercial hardware or software.

Disposition Instructions

Destroy this report when no longer needed. Do not return it to originator.

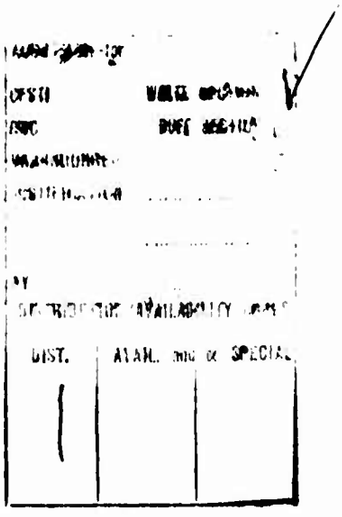

DEPARTMENT OF THE ARMY
U S ARMY AVIATION MATERIEL LABORATORIES
FORT EUSTIS, VIRGINIA 23604

This contract was initiated to:

1. Assess the relative merits of the Alpha, Beta, Gamma, and Delta configurations of the Dynamic Antiresonant Vibration Isolator (DAVI). A generalized parametric study of the four DAVI circuits was conducted, setting forth in the form of design charts the relationships between DAVI performance and DAVI's key parameters.

2. Determine, through tests and analyses, the design feasibility and the isolation characteristics of the two-dimensional DAVI Alpha, which is an isolator simultaneously offering isolation in two orthogonal directions.

Results show that the DAVI, a passive mechanical isolator, simultaneously offers high static stiffness while exhibiting very low transmissibility. The low transmissibility associated with antiresonance is independent of the isolated mass. Test results demonstrated that the DAVI could be tuned to give an antiresonance over a broad frequency range without any change of hardware.

From the operational point of view, there appears to be little difference between the Beta and Gamma configurations. The Delta configuration exhibits one key advantage: zero deflection of the inertia bar under static load. For some applications, however, the price of the very definite advantage may be too high, because the DAVI Delta does not have the versatility of simple tuning without a hardware change. The DAVI Delta, it is noted, is the impedance equivalent of a Wheatstone Bridge and thus might be suitable for impedance measurements. Tests and analyses show the two-dimensional DAVI Alpha to be very promising for attenuating discrete frequency excitations common to helicopter vibration problems.

This report has been reviewed by the U. S. Army Aviation Materiel Laboratories and is considered to be technically sound. It is published for the exchange of information and the stimulation of ideas.

Task 1F125901A14608
Contract DA 44-177-AMC-391(T)
USAAVLABS Technical Report 68-42
November 1968

AN ANALYTICAL AND MODEL TEST RESEARCH STUDY ON THE KAMAN DYNAMIC ANTIRESONANT VIBRATION ISOLATOR (DAVI)

Kaman Report No. R-690

By

Robert Jones

Prepared By

Kaman Aircraft
Division of Kaman Corporation
Bloomfield, Connecticut

For

U. S. ARMY AVIATION MATERIEL LABORATORIES
Fort Eustis, Virginia

SUMMARY

This report covers the analysis and experimental model testing of the Dynamic Antiresonant Vibration Isolator (DAVI), including the basic DAVI Alpha and the series-type DAVI models.

A parametric study was conducted on the basic unidirectional and two-dimensional DAVI Alpha to determine its isolation performance, and a general design criterion was obtained. Theoretical analyses, including damping across the series element, were done on the series-type DAVI's. A comparison was made of the series-type DAVI Beta and Gamma. Shock analyses for various types of inputs were done for the DAVI Alpha configuration.

Experimental models of the unidirectional and two-dimensional DAVI Alpha and the series-type DAVI Beta and Gamma were constructed and tested to corroborate the theoretical results. Drop tests with three different inputs were done to determine the shock characteristics of the DAVI Alpha.

Results of the analysis and tests show that the DAVI Alpha can be designed to give over 98-percent isolation at much lower frequencies than a conventional isolator with the same static frequencies. The isolation obtained at the antiresonant frequency is independent of the mass to be isolated. Analysis and tests show that the DAVI Alpha can be designed to give better shock attenuation than the conventional isolator with the same spring rate.

Analysis and tests show that a DAVI Beta or Gamma can be designed to retain the advantages of the DAVI Alpha and to obtain better high-frequency isolation than the equivalent conventional isolator. Damping across the series element can be used to attenuate the amplitude obtained at the second natural frequency without affecting the isolation obtained at the antiresonance.

FOREWORD

This research program for the parametric study and testing of the Kaman Dynamic Antiresonant Vibration Isolator (DAVI) was performed by Kaman Aircraft, Division of Kaman Corporation, under Contract DA 44-177-AMC-391(T) for the U. S. Army Aviation Materiel Laboratories, Fort Eustis, Virginia.

The program was conducted under the technical direction of Mr. J. H. McGarvey, Contracting Officer's Representative.

Principal Kaman personnel in this program were Messrs. R. C. Anderson and M. F. Smith, Research Engineers; H. A. Cooke and R. F. Metzger, Research Technicians; W. G. Flannelly, Assistant Chief of Vibrations Research; and R. Jones, Chief of Vibrations Research.

BLANK PAGE

TABLE OF CONTENTS

LIST OF ILLUSTRATIONS

LIST OF TABLES

LIST OF SYMBOLS

C_A Convenient Viscous Damping Coefficient Definition of the DAVI at Antiresonance, lb/ft/sec

C_c Critical Viscous Damping Coefficient of a Conventional Spring-Mass System, lb/ft/sec

C_D Viscous Damping Coefficient Which is in Parallel With the DAVI Inertia Bar and Also the Viscous Damping Coefficient of the Conventional Isolation System, lb/ft/sec

C_S Viscous Damping Coefficient Which is in Series With the DAVI Element in a Series DAVI Configuration, lb/ft/sec

C_{IP} Viscous Damping Coefficient in the DAVI Delta Between the Isolated Mass and DAVI Inertia Bar Pivot, lb/ft/sec

C_{PB} Viscous Damping Coefficient in the DAVI Delta Between the DAVI Inertia Bar Pivot and the Base or Input, lb/ft/sec

C_1 Viscous Damping Coefficient of the Flexible Pivot of the DAVI Alpha Attached to the Isolated Mass, lb/ft/sec

C_2 Viscous Damping Coefficient of the Flexible Pivot of the DAVI Alpha Attached to the Base at Input Pivot, lb/ft/sec

C_θ Viscous Torsional Damping Coefficient of the Flexible Pivots of the DAVI Alpha, ft-lb/rad/sec

D Dissipation Function, ft-lb/sec

f_A Antiresonant Frequency of the DAVI - c.p.s.

f_B Displacement of the Base Along the Direction of Excitation in the Two-Dimensional DAVI Alpha, ft

f_x Displacement of the Isolated Mass of the Two-Dimensional DAVI in a Direction Parallel to the Excitation, ft

I Moment of Inertia About the Center of Gravity of the DAVI Inertia Bar, slug-ft^2

I_y Mass Moment of Inertia About the Center of Gravity of the Two-Dimensional DAVI Alpha Inertia Bar About the Lateral Axis, slug-ft^2

I_z Mass Moment of Inertia About the Center of Gravity of the Two-Dimensional DAVI Alpha Inertia Bar About the Vertical Axis, slug-ft^2

K_D Spring Constant Which is Parallel With the DAVI Inertia Bar and Also the Spring Constant of the Conventional Isolation System, lb/ft

K_{Dy} Lateral Spring Constant of the Two-Dimensional DAVI Alpha Along the Lateral Axis, lb/ft

K_{Dz} Vertical Spring Constant of the Two-Dimensional DAVI Alpha Along the Vertical Axis, lb/ft

K_{IP} Spring Constant in the DAVI Delta Between the DAVI Inertia Bar Pivot and the Isolated Mass, lb/ft

K_{PB} Spring Constant in the DAVI Delta Between the DAVI Inertia Bar Pivot and the Base or Input, lb/ft

K_S Spring Constant Which is in Series With the DAVI Element in a Series DAVI Configuration, lb/ft

K_1 Spring Constant of the Flexible Pivot of the DAVI Alpha Attached to the Isolated Mass, lb/ft

K_2 Spring Constant of the Flexible Pivot of the DAVI Alpha Attached to the Base or Input, lb/ft

K_θ	Torsional Spring Constant of the Flexible Pivots of the DAVI Alpha, ft-lb/rad
M_A	Effective Mass of the DAVI at Antiresonance, slugs
M_C	Mass of the Carriage of the Drop Test Fixture, slugs
M_D	Mass of the DAVI Inertia Bar, slugs
M_I	Isolated Mass, slugs
M_R	Effective Mass Term in the DAVI Alpha and Beta at Resonance, Slugs
M_R'	Effective Mass Term in the DAVI Gamma, slugs
M_R''	Effective Mass Term in the DAVI Delta, slugs
M_S	Intermediate Mass of the Series DAVI, slugs
M_T	Effective Mass Term in the DAVI Beta, slugs
P_B	Displacement of the Base Orthogonal to the Direction of Excitation, ft
P_I	Displacement of the Isolated Mass of the Two-Dimensional DAVI Alpha Orthogonal to the Direction of Excitation, ft
R	Distance of the Center of Gravity of the DAVI Inertia Bar From the Pivot Attached to the Isolated Mass. Positive When the Direction of the Center of Gravity is in the Direction of the Base or Input Pivot, ft
r	Distance Between Pivots, ft
s	Frequency Used in the Laplace transformation, rad/sec
T	Kinetic Energy, ft-lb
t	Time, sec

V Potential Energy, ft-lb

W_D DAVI Inertia Bar Weight, lb

W_I Isolated Weight, lb

Y_B Lateral Displacement of the Base or Input, ft

Y_D Lateral Displacement of the DAVI Inertia Bar Mass, ft

Y_I Lateral Displacement of the Isolated Mass, ft

Z_B Vertical Displacement of the Base or Input, ft

Z_D Vertical Displacement of the DAVI Inertia Bar Mass, ft

Z_I Vertical Displacement of the Isolated Mass, ft

Z_P Vertical Displacement of Pivot in DAVI Delta, ft

Z_S Vertical Displacement of the Intermediate Mass of Series DAVI, ft

Z_1 Vertical Displacement of Flexible Pivot in the DAVI Alpha, ft

Z_2 Vertical Displacement of Flexible Pivot in DAVI Alpha, ft

δ_{ST} Static Deflection, ft

δ''_{ST} Static Deflection, in.

θ Angular Rotation of the DAVI Inertia Bar, rad or deg

θ_Y Angular Rotation of the Two-Dimensional DAVI Inertia Bar About the Vertical Axis of the Inertia Bar, rad

θ_Z Angular Rotation of the Two-Dimensional DAVI Inertia Bar About the Lateral Axis, rad

ρ	Radius of Gyration of the DAVI Inertia Bar, ft
ϕ	Angle Between the Principal Axis of the Two-Dimensional DAVI Alpha and the Direction of Excitation, rad
τ	Duration of the Transient Inputs, sec
ω	Frequency of Excitation, rad/sec
ω_A	Antiresonant Frequency of the DAVI, rad/sec
ω_N	Natural Frequency of a Conventional Isolation System, rad/sec
ω_R	Natural Frequency of the DAVI, rad/sec
ω_S	Uncoupled Natural Frequency of the Conventional System in the Series-Type DAVI, rad/sec
T_C	Transmissibility of the Conventional Isolator
$T_{C_{VHF}}$	Transmissibility of the Conventional Isolator at Very High Frequency
T_α	Transmissibility of the DAVI Alpha
T_{α_y}	Lateral Transmissibility of the Two-Dimensional DAVI Alpha
T_{α_z}	Vertical Transmissibility of the Two-Dimensional DAVI Alpha
$T_{\alpha_{VHF}}$	Transmissibility of the DAVI Alpha at Very High Frequency
T_β	Transmissibility of the DAVI Beta
$T_{\beta_{VHF}}$	Transmissibility of the DAVI Beta at Very High Frequency
T_δ	Transmissibility of the DAVI Gamma

$T_{\delta_{VHF}}$	Transmissibility of the DAVI Gamma at Very High Frequency
T_{δ}	Transmissibility of the DAVI Delta
ζ_A	Percent Damping of the DAVI
ζ_S	Percent Critical Damping of the Series Element in the Series DAVI
μ_D	Ratio of DAVI Inertia Bar Mass to the Isolated Mass
μ_S	Ratio of the Intermediate Mass of the Series DAVI to the Isolated Mass

INTRODUCTION

The design problems of conventional isolation for low frequency are well-known. The greater the isolation desired, the larger the static deflection required. The solution to this problem is to provide a device which will give a high percentage of isolation with a very small static deflection. The Dynamic Antiresonant Vibration Isolator (DAVI) is such a device; research on the DAVI was sponsored by the U. S. Army Aviation Materiel Laboratories (USAAVLABS) under Contract DA 44-177-AMC-196(T) and is reported in Reference 1.

This research through analysis and tests showed that the DAVI, which is a passive vibration isolator, can provide a high degree of isolation at low frequency with very low static deflection. At a predetermined antiresonant frequency, the nearly zero transmissibility across a DAVI is independent of the isolated mass. The analysis and tests showed that the DAVI gives significantly better shock isolation than a standard isolator with the same spring rate.

However, further research was required to determine engineering design parameters of the DAVI and to determine more thoroughly the isolation characteristics of the series-type DAVI's, especially to determine the effects of damping in the series element. This report discloses the results of the analytical and experimental research conducted on the unidirectional DAVI Alpha, the two-dimensional DAVI Alpha, and the series-type DAVI which includes the Beta, Gamma, and Delta. The analytical phases determined design criteria for the unidirectional and two-dimensional DAVI Alpha. Comparisons were made of the series-type DAVI's. Shock analysis was done for various types of inputs. The experimental work on the DAVI models corroborated the analytical predictions of the DAVI concept in vibration isolation.

DAVI ALPHA

UNIDIRECTIONAL DAVI ALPHA

Analysis

The equations of motion of the DAVI Alpha have been derived in USAAVLABS Technical Report 65-75 (Reference 1). However, for completeness, the equations of motion are rederived, and the transmissibility equation is then nondimensionalized and programmed for the digital computer. The transmissibility equation is then used to determine design criteria for the DAVI Alpha and is compared to the conventional isolator. This comparison is made of these systems with equivalent static deflection (δ_{ST}'' inches).

For the following schematic, the equations of motion can be derived.

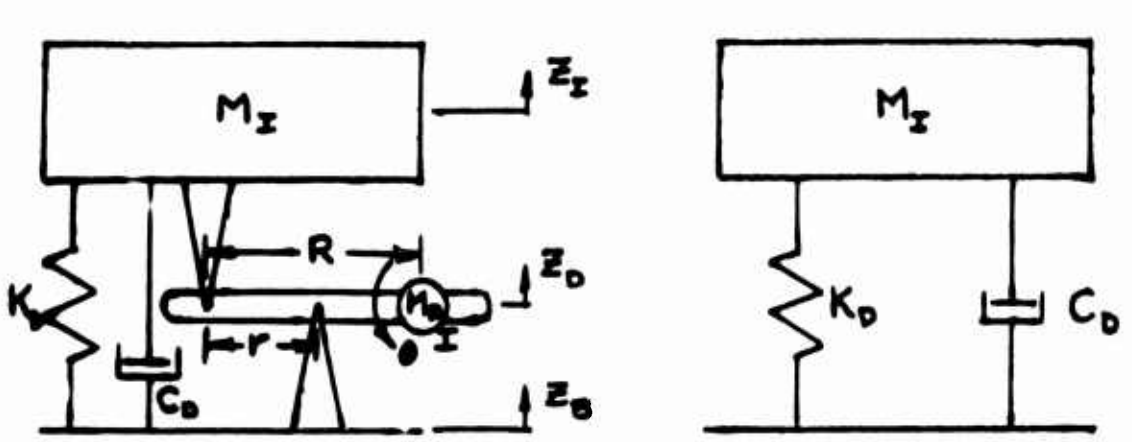

A - DAVI Alpha B - Conventional

Figure 1. Schematic of a Simple Isolation System

From the above schematic, the energies of the DAVI Alpha system are

$$T = \frac{1}{2} M_I \dot{Z}_I^2 + \frac{1}{2} I \dot{\theta}^2 + \frac{1}{2} M_D \dot{Z}_D \quad (1)$$

$$V = \frac{1}{2} K_D (Z_I - Z_D)^2 \quad (2)$$

$$D = \frac{1}{2} C_D (\dot{Z}_I - \dot{Z}_D)^2 \quad (3)$$

But

$$\theta = \frac{Z_B - Z_I}{r} \quad \text{and} \tag{4}$$

$$Z_D = Z_B \frac{R}{r} - Z_I \left(\frac{R}{r} - 1\right) \tag{5}$$

Substituting the above in the kinetic energy equation, Equation (1) becomes

$$T = \frac{1}{2} M_I \dot{Z}_I^2 + \frac{1}{2} I \left(\frac{\dot{Z}_B - \dot{Z}_I}{r}\right)^2 + \frac{1}{2} M_D \left[\dot{Z}_B \frac{R}{r} - \dot{Z}_I \left(\frac{R}{r} - 1\right)\right]^2 \tag{6}$$

Using Lagrange's equation, the equation of motion is

$$\left[M_I + M_D \left(\frac{R}{r} - 1\right)^2 + \frac{I}{r^2}\right] \ddot{Z}_I + C_D \dot{Z}_I + K_D Z_I - \left[M_D \frac{R}{r} \left(\frac{R}{r} - 1\right) + \frac{I}{r^2}\right] \ddot{Z}_B - C_D \dot{Z}_B - K_D Z_B = 0 \tag{7}$$

Assuming a steady-state solution of the form $e^{i\omega t}$, the transmissibility equation of the DAVI Alpha is

$$T_\alpha = \frac{Z_I}{Z_B} = \frac{K_D - \left[M_D \left(\frac{R}{r} - 1\right) \frac{R}{r} + \frac{I}{r^2}\right] \omega^2 + i C_D \omega}{K_D - \left[M_I + M_D \left(\frac{R}{r} - 1\right)^2 + \frac{I}{r^2}\right] \omega^2 + i C_D \omega} \tag{8}$$

However, $I = M_D \rho^2$

and let

$$M_A = M_D \left[\left(\frac{R}{r} - 1\right) \frac{R}{r} + \frac{\rho^2}{r^2}\right] \tag{9}$$

$$M_R = M_I + M_D \left[\left(\frac{R}{r} - 1\right)^2 + \frac{\rho^2}{r^2}\right] \tag{10}$$

where M_A and M_R are the effective mass of the DAVI Alpha at the antiresonant frequency and resonant frequency, respectively.

Substituting Equations (9) and (10) into Equation (8), Equation (8) becomes

$$T_\alpha = \frac{K_D - M_A\omega^2 + i C_D \omega}{K_D - M_R\omega^2 + i C_D \omega} \tag{11}$$

It is seen from the above equations that zero transmissibility or the antiresonant frequency of the DAVI Alpha, neglecting damping (C_D), is obtained when the numerator is zero, or

$$\omega^2 = \omega_A^2 = \frac{K_D}{M_A} \tag{12}$$

and the natural frequency of the DAVI, neglecting damping, is obtained when the denominator of Equation (11) is zero, or

$$\omega^2 = \omega_R^2 = \frac{K_D}{M_R} \tag{13}$$

The transmissibility equation can be rewritten by dividing the numerator and denominator by M_A as

$$T_\alpha = \frac{(\omega_A^2 - \omega^2) + i \frac{C_D}{M_A}\omega}{(\omega_A^2 - \frac{M_R}{M_A}\omega^2) + i \frac{C_D}{M_A}\omega} \tag{14}$$

The critical damping in a conventional isolation system is

$$C_c = 2M_2\omega_N \tag{15}$$

in which

$$\omega_N = \sqrt{\frac{K_D}{M_I}}$$

The critical damping in the DAVI Alpha system is defined in a similar manner, as

$$C_C = 2 M_R \omega_R \tag{16}$$

in which

$$\omega_R = \sqrt{\frac{K_D}{M_R}}$$

However, for the DAVI Alpha isolation system, since the antiresonant frequency or the null is not affected by the mass of the isolated item, a damping criterion similar to critical damping can be defined as

$$C_A = 2 M_A \omega_A \tag{17}$$

in which

$$\omega_A = \sqrt{\frac{K_D}{M_A}}$$

Further defining,

$$\frac{C_D}{C_A} = f_A \tag{18}$$

Equation (14) can now be nondimensionalized by dividing denominator and numerator by ω_A^2 and by utilizing the percent of damping at the null from Equation (18). Equation (14) becomes

$$T_{dA} = \frac{\left(1 - \frac{\omega^2}{\omega_A^2}\right) + 2i \frac{\omega}{\omega_A} f_A}{\left(1 - \frac{M_R}{M_A} \frac{\omega^2}{\omega_A^2}\right) + 2i \frac{\omega}{\omega_A} f_A} \tag{19}$$

and the absolute transmissibility is

$$|T_\alpha| = \sqrt{\frac{\left(1-\frac{\omega^2}{\omega_2^2}\right)^2 + 4\zeta_A^2\frac{\omega^2}{\omega_A^2}}{\left(1-\frac{M_R}{M_A}\frac{\omega^2}{\omega_A^2}\right)^2 + 4\zeta_A^2\frac{\omega^2}{\omega_A^2}}} \qquad (20)$$

The above nondimensional transmissibility equation was programmed for the 360 digital computer. This program is primarily useful in obtaining the complete transmissibility equation versus frequency, and in obtaining the effects of damping in the DAVI after the DAVI has been properly sized. To facilitate estimating the size of key DAVI parameters for a given application, design criteria follow.

Design Criteria

In these design criteria, a series of graphs have been produced from which rapid approximations may be made in predicting the physical parameters and performance expectations of DAVI Alpha vibration mounts. These graphs allow the determination of r, R, ρ, θ, M_D, the DAVI Alpha transmissibility curves, and the bandwidth of isolation about the tuned frequency. For comparison with a conventional system, the transmissibility curves of a conventional isolator of equivalent stiffness are also presented.

In any comparison, there must be a mutual base from which to draw related conclusions. In vibration isolation, the system natural frequency is the logical base. However, the natural frequency is a function of the isolated mass and the stiffness of the system; and as Reference 1 has shown, the DAVI exhibits a characteristic of antiresonance which is independent of the isolated mass. It has, therefore, been chosen to compare DAVI Alpha and conventional isolation systems of equivalent stiffness, using then the mutual base of static deflection (δ_{ST}'' inches).

In many vibration problems, such as helicopter applications, isolation is usually concerned with a particular excitation frequency, and the application of the DAVI principle to such a problem would be to create a null or antiresonance at this discrete frequency. The antiresonant frequency (f_A cycles per second) is then a key parameter also.

The following design criteria will make use of the above two functions, which will occur as a ζ_{ST}'' f_A^2 term, and will relate this comparative term to the other system parameters. The resulting graphical representations of these relationships will provide an expeditious means from which DAVI Alpha physical parameters and performance may be predicted and compared to a conventional system for given isolation requirements.

The schematic of the undamped DAVI Alpha showing a negative and positive R is given below.

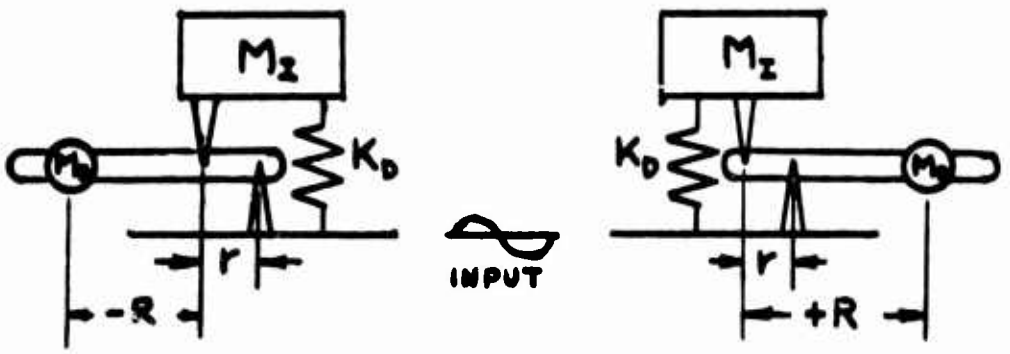

Figure 2. Undamped DAVI Alpha

Dividing the numerator and denominator of Equation (8) by M_I, letting $I = \rho^2 M_D$, and neglecting the damping terms, the equation becomes

$$T_\alpha = \frac{\frac{K_D}{M_I} - \omega^2 \frac{M_D}{M_I}\left[\frac{R}{r}\left(\frac{R}{r}-1\right)+\frac{\rho^2}{r^2}\right]}{\frac{K_D}{M_I} - \omega^2\left\{1+\frac{M_D}{M_I}\left[\left(\frac{R}{r}-1\right)^2+\frac{\rho^2}{r^2}\right]\right\}} \qquad (21)$$

Letting $\frac{K_D}{M_I} = \omega_N^2$ and $\frac{M_D}{M_I} = \mu_D$, and dividing numerator and denominator by ω_N^2,

$$T_\alpha = \frac{1-\left(\frac{\omega}{\omega_N}\right)^2 \mu_D \left[\frac{R}{r}\left(\frac{R}{r}-1\right)+\frac{\rho^2}{r^2}\right]}{1-\left(\frac{\omega}{\omega_N}\right)^2\left\{1+\mu_D\left[\left(\frac{R}{r}-1\right)^2+\frac{\rho^2}{r^2}\right]\right\}} \qquad (22)$$

To determine the effectiveness of the inertia of the DAVI bar, first let $\rho = 0$. Equation (22) reduces to

$$T_{\alpha_{\rho=0}} = \frac{1-\left(\frac{\omega}{\omega_N}\right)^2 \mu_D \left(\frac{R}{r}\right)\left(\frac{R}{r}-1\right)}{1-\left(\frac{\omega}{\omega_N}\right)^2\left[1+\mu_D\left(\frac{R}{r}-1\right)^2\right]} \qquad (23)$$

Then, consider a thin rod as the DAVI inertia bar with one end pivoted to the isolated mass, as shown in Figure 3.

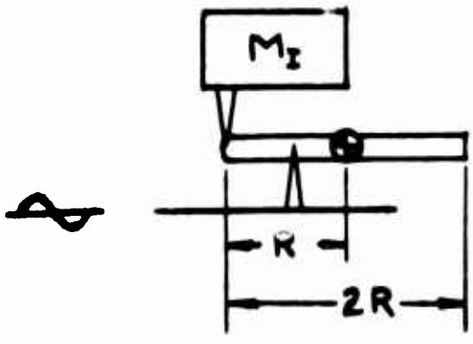

Figure 3. DAVI Alpha With Thin Rod Inertia Bar

The mass moment of inertia is $I = M_D\rho^2$ and for a thin rod $\rho^2 = \ell^2/12$. But $\ell = 2R$; therefore $\rho^2 = \frac{R^2}{3}$.

Substituting that $\rho^2 = \frac{R^2}{3}$ in Equation (22) gives

$$T_{\alpha_{\rho^2=\frac{R^2}{3}}} = \frac{1-\left(\frac{\omega}{\omega_N}\right)^2 \mu_0 \left[\frac{4}{3}\left(\frac{R}{r}\right)^2 - \left(\frac{R}{r}\right)\right]}{1-\left(\frac{\omega}{\omega_N}\right)^2 \left\{1+\mu_0\left[\frac{4}{3}\left(\frac{R}{r}\right)^2 - 2\frac{R}{r}+1\right]\right\}} \qquad (24)$$

For very high frequency, $1 << (\omega/\omega_N)^2$. Therefore, Equations (22), (23), and (24) can be rewritten for transmissibility at very high frequency as

$$T_{\alpha_{VHF}} = \frac{\mu_0\left[\frac{R}{r}\left(\frac{R}{r}-1\right) + \frac{\rho^2}{r^2}\right]}{1+\mu_0\left[\left(\frac{R}{r}-1\right)^2 + \frac{\rho^2}{r^2}\right]} \qquad (25)$$

$$T_{\alpha_{\substack{VHF \\ \rho=0}}} = \frac{\mu_0 \frac{R}{r}\left(\frac{R}{r}-1\right)}{1+\mu_0\left(\frac{R}{r}-1\right)^2} \qquad (26)$$

$$T_{\alpha_{\substack{VHF \\ \rho^2=\frac{R^2}{3}}}} = \frac{\mu_0\left[\frac{4}{3}\left(\frac{R}{r}\right)^2 - \frac{R}{r}\right]}{1+\mu_0\left[\frac{4}{3}\left(\frac{R}{r}\right)^2 - 2\frac{R}{r}+1\right]} \qquad (27)$$

The foregoing equations describe the primary parametric relationships of the DAVI Alpha. The following analysis will now relate the DAVI and the conventional isolator in terms of the static deflection (δ_{ST}'') and the tuned frequency (f_A).

The natural frequency for a conventional isolator is

$$\omega_N^2 = \frac{K_D}{M_I} \tag{28}$$

and the static deflection is

$$\delta_{ST} = \frac{M_I g}{K_D} \tag{29}$$

Multiplying both sides of Equation (29) by ω_A^2 ,

$$\delta_{ST}\omega_A^2 = \frac{M_I g\, \omega_A^2}{K_D} \tag{30}$$

Substituting Equations (9) and (12) for ω_A^2 on the right side, and using $I = M_D\rho^2$, Equation (30) becomes

$$\delta_{ST}\omega_A^2 = \frac{M_I g}{M_D\left[\frac{R}{r}\left(\frac{R}{r}-1\right)+\frac{\rho^2}{r^2}\right]} \tag{31}$$

Dividing the numerator and denominator by M_I, and letting $\mu_D = \frac{M_D}{M_I}$, the above equation may be arranged to

$$\mu_D\left[\frac{R}{r}\left(\frac{R}{r}-1\right)+\frac{\rho^2}{r^2}\right] = \frac{g}{\delta_{ST}\omega_A^2} \tag{32}$$

Substituting Equation (32) into Equation (25), the transmissibility at VHF becomes

$$T_{\alpha_{VHF}} \simeq \frac{1}{\frac{\delta_{ST}\omega_A^2}{g}\left[1-\mu_D\left(\frac{R}{r}-1\right)\right]+1} \qquad (33)$$

By letting $C \simeq 1-\mu_D\left(\frac{R}{r}-1\right)$, Equation (33) may be expressed as

$$T_{\alpha_{VHF}} \simeq \frac{1}{\delta''_{ST} f_A^2 C\left(\frac{4\pi^2}{386}\right)+1} \qquad (34)$$

where δ''_{ST} is in inches, and f_A is in cycles per second. If $.01 \leq \mu_D \leq .1$, and

$-10 \leq \frac{R}{r} \leq +10$, then $.1 \leq C \leq 2.1$.

The relationship of C versus R/r for various μ_D is plotted in Figure 8, and Equation (34) is plotted in Figure 9.

Figure 4 describes the bandwidth for the DAVI, where ω_L is the frequency below the null, and ω_U is the frequency above the null at a given transmissibility less than unity.

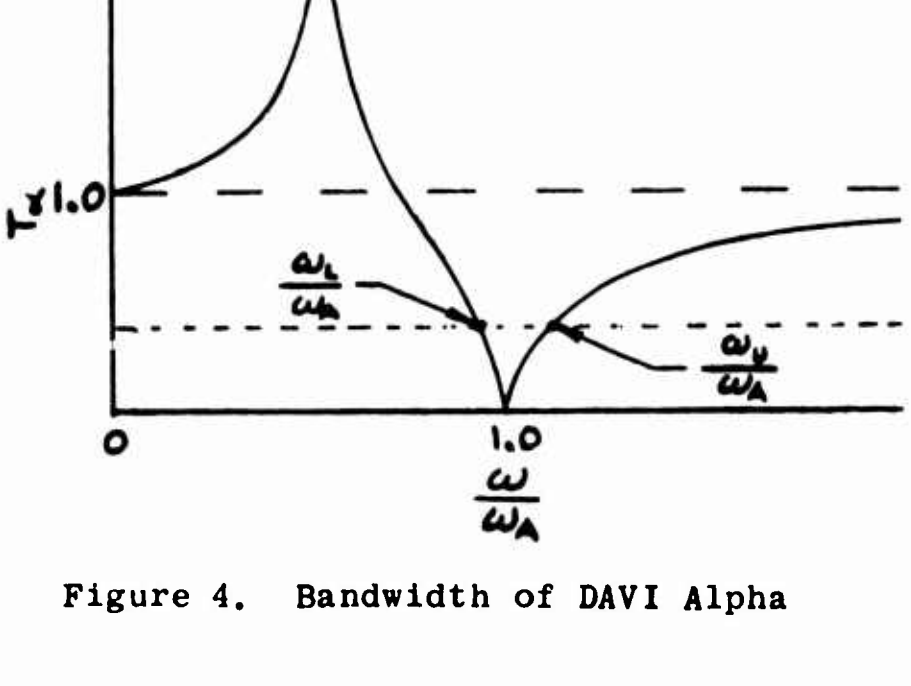

Figure 4. Bandwidth of DAVI Alpha

Analytical determination of this bandwidth is as follows. Ignoring damping, Equation (19) becomes

$$T_\alpha = \frac{\omega_A^2 - \omega^2}{\omega_A^2 - \frac{M_R}{M_A}\omega^2} \tag{35}$$

and $$\frac{M_R}{M_A} = \frac{\omega_R^2}{\omega_A^2} = T_{\alpha_{VHF}}$$

then,

$$T_\alpha = \frac{\omega_A^2 - \omega^2}{\omega_A^2 - \frac{\omega^2}{T_{\alpha_{VHF}}}} \tag{36a}$$

$$T_\alpha = \frac{\omega_A^2 - \omega^2}{\omega_A^2 - \omega^2\left(\frac{\omega_A^2}{\omega_R^2}\right)} \tag{36b}$$

Dividing the numerator and denominator of Equations (36a) and (36b) by ω_A^2,

$$T_\alpha = \frac{1 - \left(\frac{\omega}{\omega_A}\right)^2}{1 - \left(\frac{1}{T_{\alpha_{VHF}}}\right)\left(\frac{\omega}{\omega_A}\right)^2} \tag{37a}$$

$$T_\alpha = \frac{1-\left(\frac{\omega}{\omega_A}\right)^2}{1-\left(\frac{\omega}{\omega_R}\right)^2} \qquad (37b)$$

From Equation (37b), it is apparent that for $1<(\omega/\omega_R)^2<(\omega/\omega_A)^2$ the transmissibility is negative.

Solving for $(\omega/\omega_A)^2$, Equation (37a) becomes

$$\left(\frac{\omega}{\omega_A}\right)^2 = \frac{1-T_\alpha}{1-\frac{T_\alpha}{T_{\alpha_{VHF}}}} \qquad (38)$$

For $T_{\alpha_{VHF}} < 1$ and $\omega = \omega_L < \omega_A$, T_α is negative, and Equation (38) becomes

$$\left(\frac{\omega_L}{\omega_A}\right)^2 = \frac{1+T_\alpha}{1+\frac{T_\alpha}{T_{\alpha_{VHF}}}} \qquad (39)$$

For $T_{\alpha_{VHF}} < 1$ and $\omega = \omega_U > \omega_A$, T_α is positive, and Equation (38) becomes

$$\left(\frac{\omega_U}{\omega_A}\right)^2 = \frac{1-T_\alpha}{1-\frac{T_\alpha}{T_{\alpha_{VHF}}}} \qquad (40)$$

Substituting Equation (34) into Equations (39) and (40),

$$\left(\frac{\omega_L}{\omega_A}\right)^2 = \frac{1+|T_\alpha|}{1+|T_\alpha|\left(\delta''_{ST} f_A^2 C \frac{4\pi^2}{386}+1\right)} \qquad (41)$$

2

$$\left(\frac{\omega_U}{\omega_A}\right)^2 = \frac{1 - |T_\alpha|}{1 - |T_\alpha|\left(S_{ST}'' f_A^2 C \frac{4\pi^2}{386} + 1\right)} \qquad (42)$$

Equations (41) and (42), therefore, define the bandwidth limits of the DAVI Alpha for $T_{\alpha_{VHF}} < 1.0$ and zero damping. Figures 10A, 10B, and 10C are plots of these equations.

The transmissibility of an undamped conventional isolator is

$$T_C = \frac{K_D}{K_D - M_I \omega^2} = \frac{1}{1 - \left(\frac{\omega}{\omega_N}\right)^2} \qquad (43)$$

Rearranging,

$$\left(\frac{\omega}{\omega_N}\right)^2 = 1 - \frac{1}{T_C} \qquad (44)$$

Below resonance, T_C is positive, and Equation (44) becomes

$$\left(\frac{\omega_{LC}}{\omega_N}\right)^2 = 1 - \frac{1}{|T_C|} \qquad (45)$$

Above resonance, T_C is negative, and Equation (44) becomes

$$\left(\frac{\omega_{UC}}{\omega_N}\right)^2 = 1 + \frac{1}{|T_C|} \qquad (46)$$

From Equation (30),

$$\left(\frac{\omega_N}{\omega_A}\right)^2 = \frac{g}{S_{ST}'' \omega_A^2} \qquad (47)$$

Multiplying Equations (45) and (46) by Equation (47), and converting to units of inches and cycles per second, Equations (45) and (46) become

$$\left(\frac{\omega_{LC}}{\omega_A}\right)^2 = \frac{386(2\pi)^{-2}}{\delta''_{ST} f_A^2}\left(1 - \frac{1}{|T_d|}\right) \tag{48}$$

and

$$\left(\frac{\omega_{UC}}{\omega_A}\right)^2 = \frac{386(2\pi)^{-2}}{\delta''_{ST} f_A^2}\left(1 + \frac{1}{|T_d|}\right) \tag{49}$$

Equations (48) and (49) are plotted in Figures 5A and 5B.

To determine the parameter $\delta''_{ST}\,\omega_A^2\,\mu_D$, rewrite Equation (32) or

$$\delta''_{ST}\,\omega_A^2\,\mu_D = \frac{g}{\left(\frac{R}{r}\right)\left(\frac{R}{r}-1\right) + \frac{\rho^2}{r^2}}$$

For the thin rod inertia bar where $\rho^2 = \frac{R^2}{3}$, then

$$\delta''_{ST}\,\omega_A^2\,\mu_D = \frac{g}{\frac{4}{3}\left(\frac{R}{r}\right)^2 - \frac{R}{r}}$$

or

$$\delta''_{ST}\,f_A^2\,\mu_D = \frac{386(2\pi)^{-2}}{\frac{4}{3}\left(\frac{R}{r}\right)^2 - \frac{R}{r}} \tag{50}$$

Equation (50) is plotted in Figures 6A and 6B for R/r positive and negative, respectively. If inertia is neglected, $\rho = 0$, and the equation becomes

$$\delta''_{ST}\,\omega_A^2\,\mu_D = \frac{g}{\left(\frac{R}{r}\right)^2 - \frac{R}{r}}$$

or

$$\delta''_{ST}\,f_A^2\,\mu_D = \frac{386(2\pi)^{-2}}{\left(\frac{R}{r}\right)^2 - \frac{R}{r}} \tag{51}$$

Equation (51) is plotted in Figures 7A and 7B for R/r positive and negative, respectively.

The angular vibratory motion of the inertia bar for values of r and vibratory input at antiresonance is shown in Figure 11. Figure 11 is obtained from Equation (4), when $\ddot{z}_I = 0$.

Below is the procedure for using the design charts.

Step 1 — Figure 5 - $\delta''_{ST} f_A^2$ versus ω/ω_A for various T_C. For the given problem, determine the required $\delta''_{ST} f_A^2$. With this input, enter Figures 5A and 5B and read the values of T_C for various values of ω/ω_A. With this data, plot the transmissibility of a conventional isolator exhibiting the same static deflection as chosen.

Step 2 — Figure 6 - $\delta''_{ST} f_A^2 \mu_D$ versus R/r for $\rho^2 = R^2/3$. Making the assumption of a thin rod inertia bar DAVI, choose an R/r ratio, enter Figures 6A or 6B, and read the corresponding $\delta''_{ST} f_A^2 \mu_D$. Solve for μ_D.

Step 3 — Figure 8 - Value C versus R/r for various μ_D. Using previously determined R/r and μ_D, use Figure 8 and read the value of C. Determine $\delta''_{ST} f_A^2 C$.

Step 4 — Figure 9 - $T_{\alpha VHF}$ versus $\delta''_{ST} f_A^2 C$ at $\delta''_{ST} f_A^2 C$. Enter Figure 9 and read the corresponding $T_{\alpha VHF}$.

Step 5 — Figure 10 - $\delta''_{ST} f_A^2 C$ versus ω/ω_A for various T_α. At $\delta''_{ST} f_A^2 C$, enter Figures 10A, 10B, and 10C, and read data to plot transmissibility of DAVI Alpha for the chosen R/r.

Step 6 — Figure 11 - r versus $\ddot{z}_B$ for various values of θ. At the required $\ddot{z}_B$, determine r for the desired angular motion of the inertia bar, θ.

Step 7 — Repeat Steps 2 through 6 for various R/r ratios for optimization of specific problems.

In order to best illustrate the design procedure, the following examples are given:

For Example 1, it is desired to isolate 100 pounds from 10 cps with 0.11-inch static deflection using the DAVI Alpha. The vibration level at the excitation frequency is $\pm$0.3g or $\pm$0.029 inch.

Step 1 — Using Figure 5B with the input $\delta''_{ST} f_A^2 = .11(10)^2 = 11.0$, determine values of T_C for various values of ω/ω_A to plot transmissibility of the conventional isolator with $\delta''_{ST} = 0.11$, and plot as shown in Figure 12.

Step 2 — With $R/r = +3$ as input and using a thin rod as the DAVI inertia bar, read Figure 6A.

$\delta''_{ST} f_A^2 \mu_D = 1.15$

But $\delta''_{ST} f_A^2 = 11.0$; therefore,

$$\mu_D = \frac{1.15}{11.0} = 0.104$$

or $W_D = (.104)(100) = 10.4$ pounds.

Step 3 — Using Figure 8 with the inputs $R/r = +3$ and $\mu_D = 0.104$, determine that $C = 0.79$. Therefore, $\delta''_{ST} f_A^2 C = (11.0)(0.79) = 8.69$.

Step 4 — Using Figure 9 with the input that $\delta''_{ST} f_A^2 C = 8.69$, then $T_{\alpha VHF} = 0.52$.

Step 5 — Using Figures 10A and 10B, determine the DAVI Alpha transmissibility, and plot as shown in Figure 12.

Step 6 — With $Z_B = 0.029$ inch, using Figure 11 determine the desired angular motion (θ) of the bar and the required distance between pivots (r). For two degrees of angular motion, $r = 0.86$. Therefore, $R = 2.58$ inches and the length of the bar is $2R$ or 5.16 inches.

Repeat steps 2 through 6 for a $R/r = -3$.

Step 2 — With $R/r = -3$ as input and using a thin rod as the DAVI inertia bar, read Figure 6B.

$\delta''_{ST} f_A^2 \mu_D = 0.73$

But $\delta''_{ST} f_A^2 = 11.0$; therefore,

$$\mu_D = \frac{0.73}{11.0} = 0.0662$$

or $W_D = (0.0662)(100) = 6.62$ pounds.

Step 3 — Using Figure 8 with the inputs $R/r = -3$ and $\mu_D = 0.0662$, determine that $C = 1.26$. Therefore, $\delta''_{ST} f_A^2 C = (11.0)(1.26) = 13.82$.

Step 4 — Using Figure 9 with the input that $\delta''_{ST} f_A^2 C = 13.82$, then $T_{\alpha_{VHF}} = 0.42$.

Step 5 — Using Figure 10C, determine the DAVI Alpha transmissibility, and plot as shown in Figure 12.

Step 6 — This step is identical to Step 6 for $R/r = +3$. Therefore, $R/r = -3$ is a more efficient design due to the lower weight of the inertia bar. If a shorter inertia bar is desired, again using Figure 11 with $Z_B = 0.029$ inch and allowing three degrees of angular motion of the bar, then $r = 0.6$ inch and $R = 1.8$; thus the length of the bar is reduced.

Repeat Steps 2 through 6 for an $R/r = -10$.

Step 2 — With $R/r = -10$ as input and using a thin rod as the DAVI inertia bar, read Figure 6B.

$$\delta''_{ST} f_A^2 \mu_D = 0.071$$

$$\delta''_{ST} f_A^2 = 11.0 ; \quad \text{therefore } \mu_D = \frac{0.071}{11.0} = 0.00645$$

or $W_D = (0.00645)(100) = 0.645$ pound.

Step 3 — Using Figure 8 with the inputs $R/r = -10$ and $\mu_D = 0.00645$, determine that $C = 1.065$. Therefore

$$\delta''_{ST} f_A^2 C = (11.0)(1.065) = 11.72$$

Step 4 — Using Figure 9 with the input $\delta''_{ST} f_A^2 C = 11.72$, then $T_{\alpha_{VHF}} = 0.45$.

Step 5 — Using Figure 10C, determine the DAVI Alpha transmissibility, and plot as shown in Figure 12.

Step 6 — With $Z_B = 0.029$ inch, using Figure 11 determine the desired angular motion (θ) of the bar and the required pivot separation (r). For 2 degrees of angular motion, $r = 0.86$ inch. Therefore $R = 8.60$ inches and the bar length is 17.2 inches. For 3 degrees of angular motion, $r = 0.60$ inch and the bar length ℓ is 12.0 inches.

Summary Example 1:

W_I = 100 pounds

f_A = 10 cps

δ''_{ST} = .11 inch

Z_B = $\pm$.029 inch

R/r	Inertia Bar Weight, W_D	Angular Motion θ	Pivot Separation r	Bar Length ℓ
+3.0	10.4 lbs	2^o	.86"	5.16"
-3.0	6.62 lbs	2^o	.86"	5.16"
-3.0	6.62 lbs	3^o	.60"	3.60"
-10.0	.645 lbs	2^o	.86"	17.20"
-10.0	.645 lbs	3^o	.60"	12.00"

By inspection, a large negative R/r ratio yields the optimum (lightest) isolator with operation at the highest permissible angular excursion, θ, requiring the smallest isolator envelope based on bar length, ℓ.

For Example 2, it is desired to isolate 100 pounds from 3 cps with 0.11-inch static deflection using the DAVI Alpha. The excitation level is $\pm$0.3g or $\pm$0.326 inch.

Step 1 — The results of this step are identical to Step 1 in Example 1, and the transmissibility of the conventional isolator is the same as shown in Figure 12.

Step 2 — With $R/r = -10$ as input and using a thin rod as the DAVI inertia bar, read Figure 6B.

$$\delta''_{ST} f_A^2 \mu_0 = 0.071$$

But $\delta''_{ST} f_A^2 = (0.11)(3)^2 = 0.99$; therefore,

$$\mu_0 = \frac{0.071}{0.99} = 0.0717 \text{ or } W_D = 7.17 \text{ pounds.}$$

Step 3 — Using Figure 8 with the input $R/r = -10$ and $\mu_0 = 0.0717$, determine that $C = 1.8$. Therefore,

$$\delta''_{ST} f_A^2 C = (0.99)(1.8) = 1.78.$$

Step 4 — Using Figure 9 with the input that $\delta''_{ST} f_A^2 C = 1.78$, then $T_{\alpha_{VHF}} = 0.82$.

Step 5 — Using Figures 10A and 10B, determine the DAVI Alpha transmissibility, and plot as shown in Figure 12.

Step 6 — With $z_B = 0.326$ inch, from Figure 11, determine that for a reasonable angular motion of the bar of $12^o > \theta > 9^o$, then $1.5" < r < 2.0"$ and therefore $15" < R < 20"$, which for most applications would give an inertia bar that is too long.

Repeat the Steps 2 through 6 for an $\frac{R}{r} = -4$.

Step 2 — With $R/r = -4$ as input and using a thin rod as the DAVI inertia bar, read Figure 6B.

$$\delta''_{ST} f_A^2 \mu_D = 0.39$$

But $\delta''_{ST} f_A^2 = (0.11)(3)^2 = 0.99$; therefore,

$$\mu_D = (0.39)/(0.99) = 0.394 \text{ or}$$

$$W_D = 39.4 \text{ pounds.}$$

For some applications, this may be a reasonable weight and the steps may be continued. However, if further reduction of weight of the inertia bar is required, then an increase in static deflection is required. Therefore, repeat steps 1 through 6 for a $\delta''_{ST} = 0.29$ and $R/r = -4$.

Step 1 — Using Figure 5A with the input $\delta''_{ST} f_A^2 = (0.29)(3)^2 = 2.61$, determine values of T_C for various values of ω/ω_A to plot transmissibility of conventional isolator with $\delta''_{ST} = 0.29$, and plot as shown in Figure 12.

Step 2 — With $R/r = -4$ as input and using a thin rod as the DAVI inertia bar, read Figure 6B.

$$\delta''_{ST} f_A^2 \mu_D = 0.39$$

But $\delta''_{ST} f_A^2 = 2.61$; therefore,

$$\mu_D = (0.39)/(2.61) = 0.15$$

or $W_D = 15.0$ pounds.

Step 3 — Using Figure 8 with the input $R/r = -4$ and $\mu_D = 0.15$, determine that $C = 1.85$. Therefore,

$$\delta''_{ST} f_A^2 C = (2.61)(1.85) = 4.82$$

Step 4 — Using Figure 9 with the input that $\delta''_{ST} f_A^2 C = 4.82$, then $T_{\alpha_{VHF}} = 0.66$.

Step 5 — Using Figures 10A and 10B, determine the DAVI Alpha transmissibility and plot as shown in Figure 12.

Step 6 — With $Z_B = 0.326$ inch, from Figure 11, determine that for a reasonable angular motion of the bar of $12^\circ > \theta > 9^\circ$, then $1.5 < r < 2.0$; therefore, $6 < R < 8.0$, which will give an inertia bar length of 12 to 16 inches.

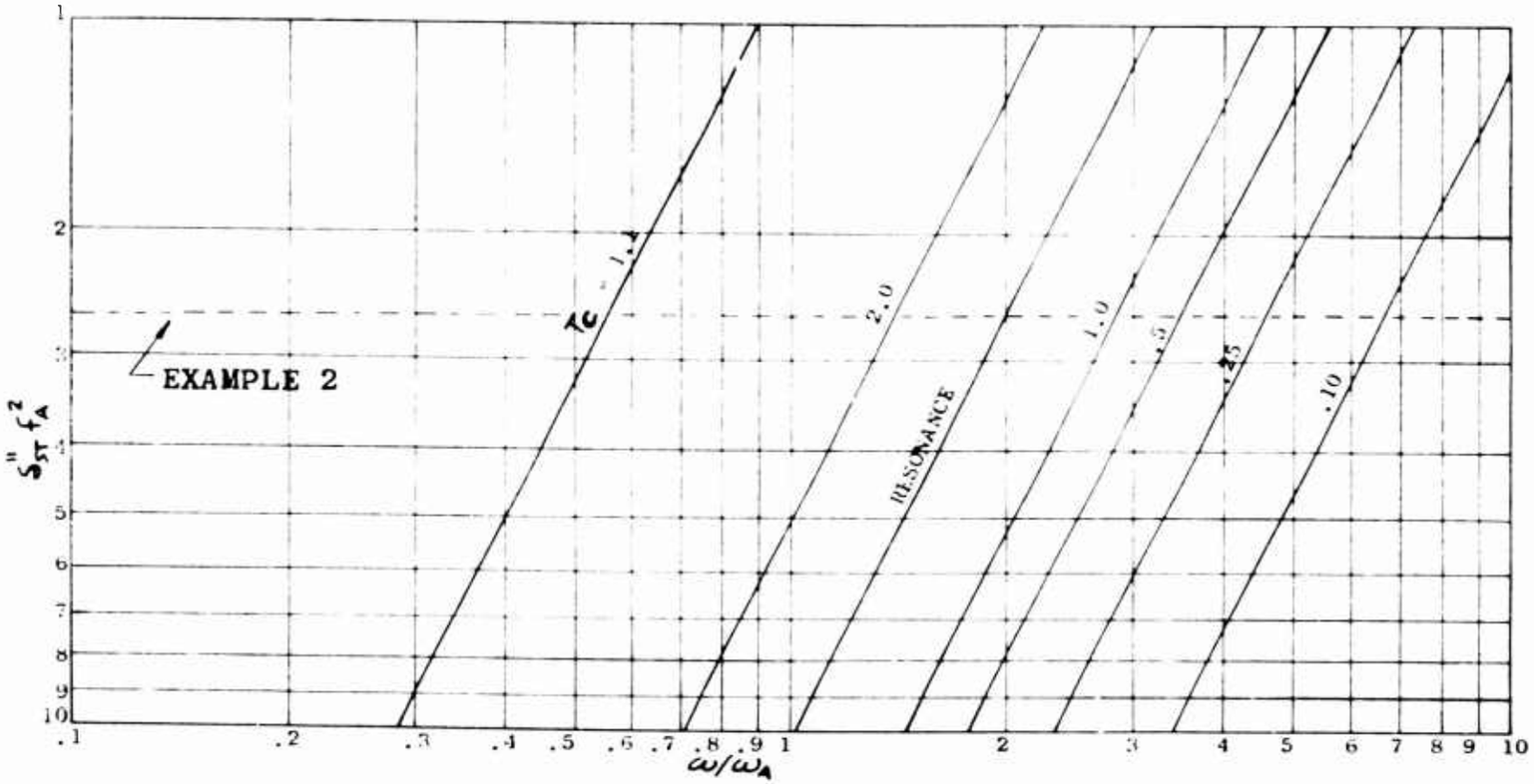

Figure 5A. DAVI Alpha Design Chart, $\zeta''_{ST} f_A^2$ Versus ω/ω_A

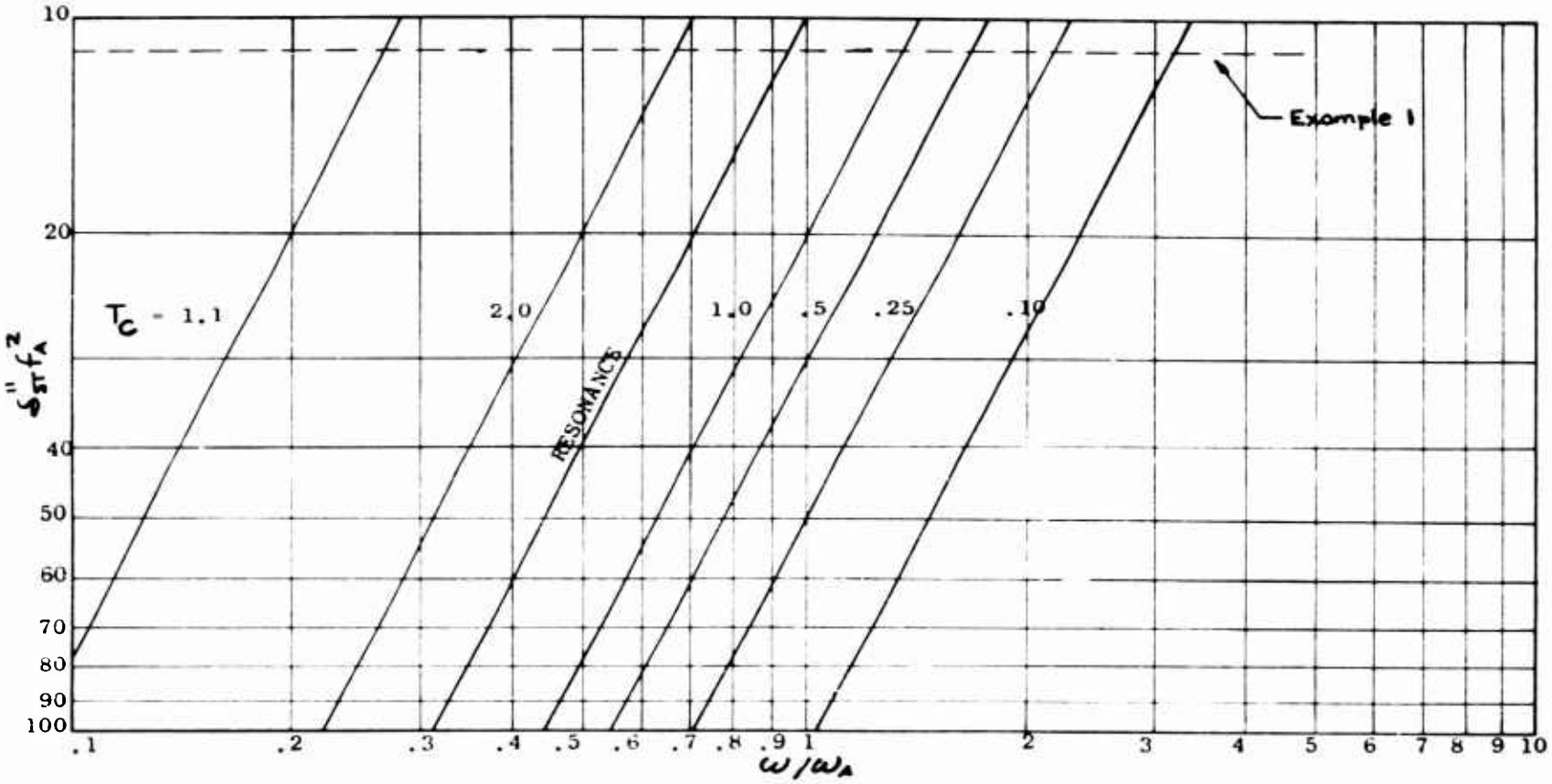

Figure 5B. DAVI Alpha Design Chart, $\zeta''_{ST} f_A^2$ Versus ω/ω_A

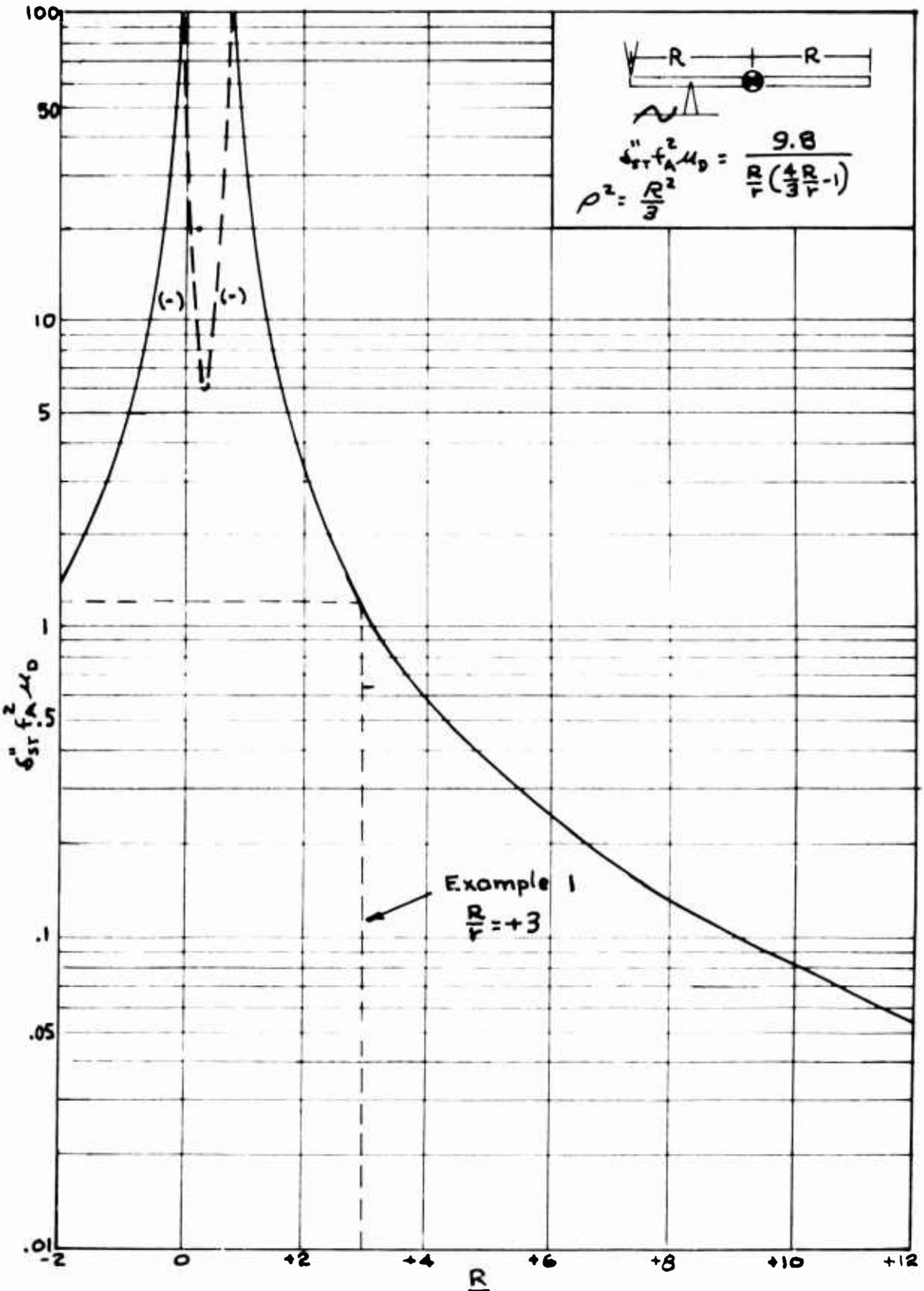

Figure 6A. DAVI Alpha Design Chart, $S''_{ST} f_A^2 \mu_D$ Versus $\frac{R}{r}$

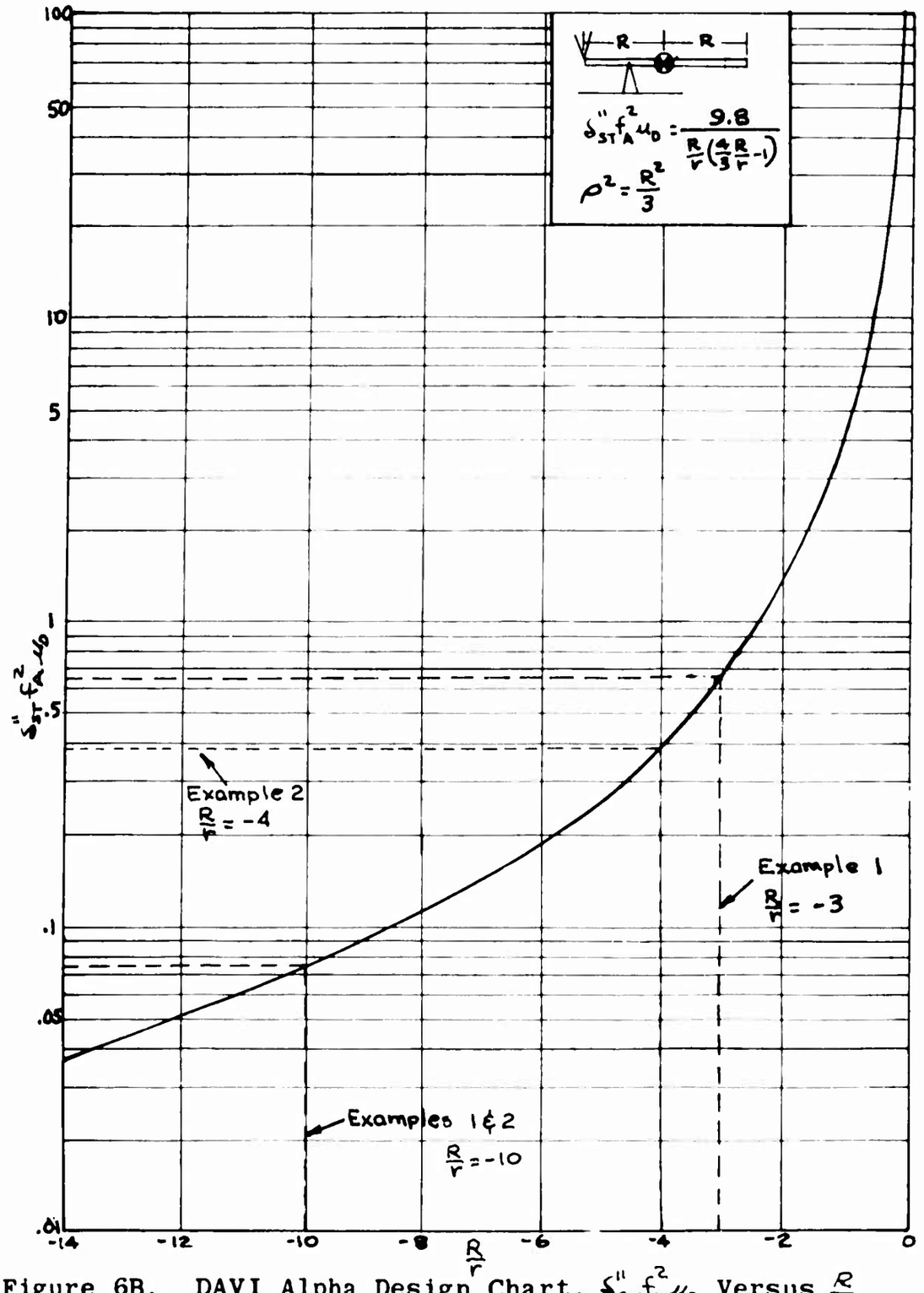

Figure 6B. DAVI Alpha Design Chart, $\delta''_{ST} f_A^2 \mu_D$ Versus $\frac{R}{r}$

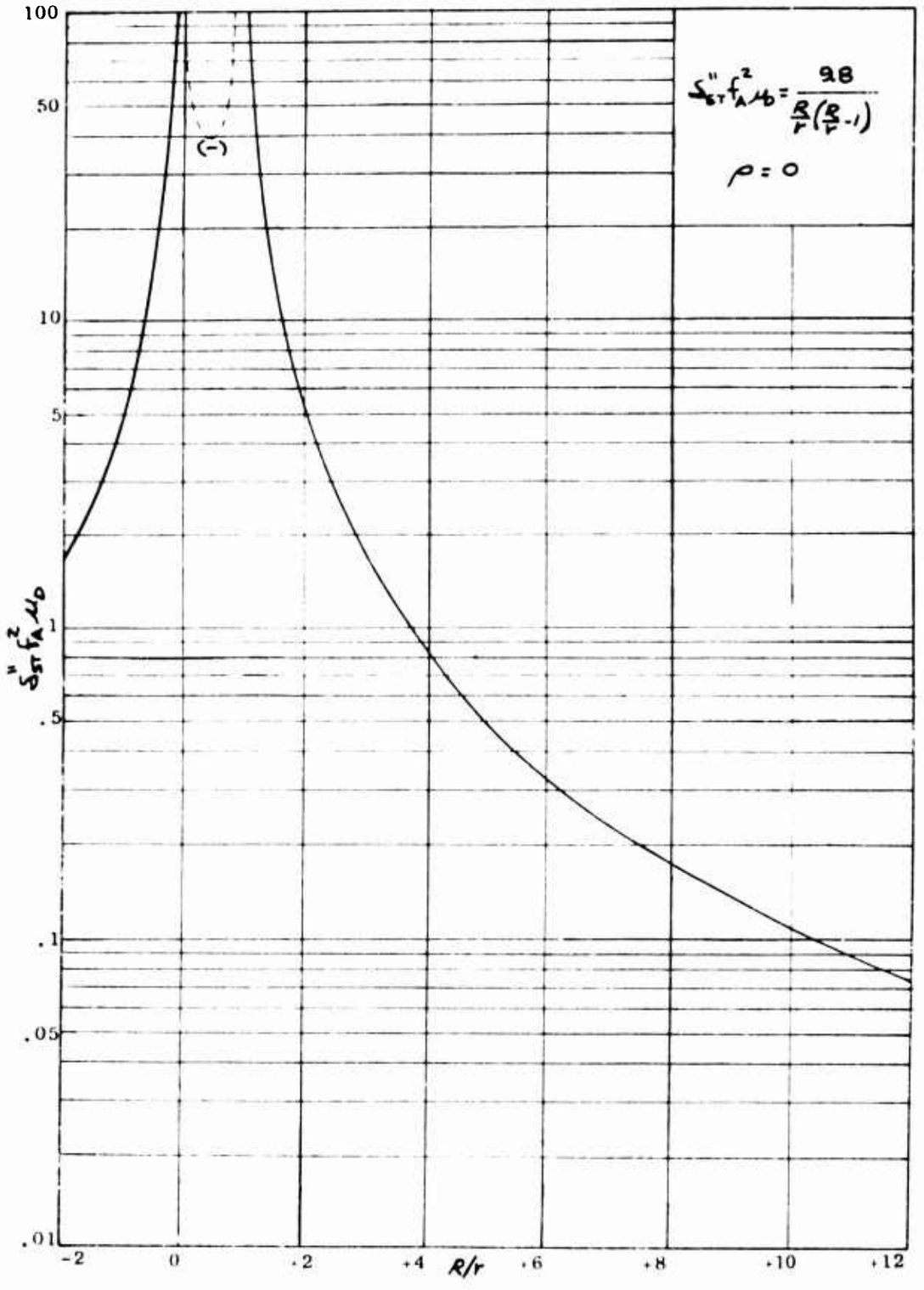

Figure 7A. DAVI Alpha Design Chart, $S''_{ST} f_A^2 \mu_D$ Versus $\frac{R}{r}$

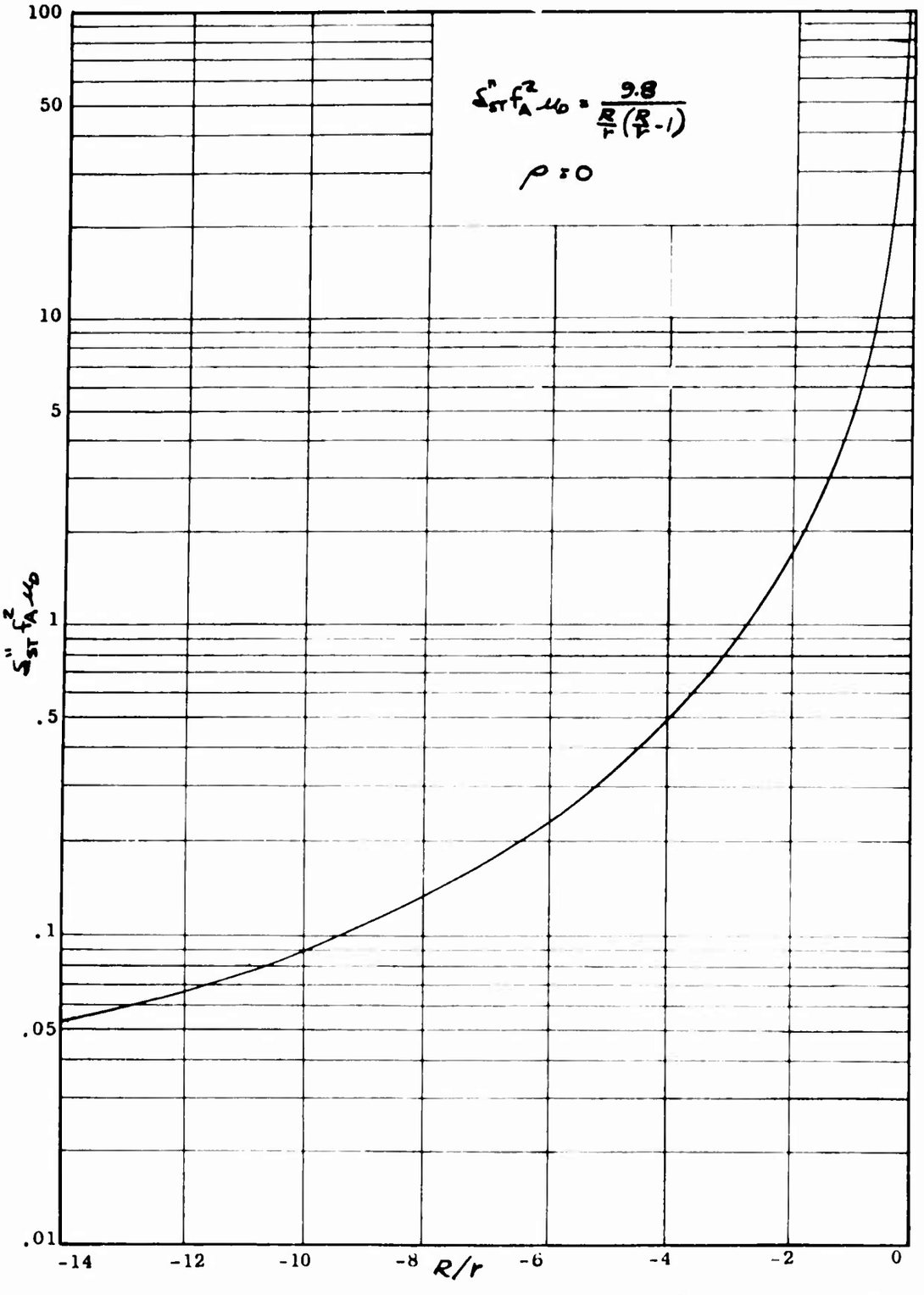

Figure 7B. DAVI Alpha Design Chart, $\delta''_{ST} f_A^2 \mu_0$ Versus $\frac{R}{r}$

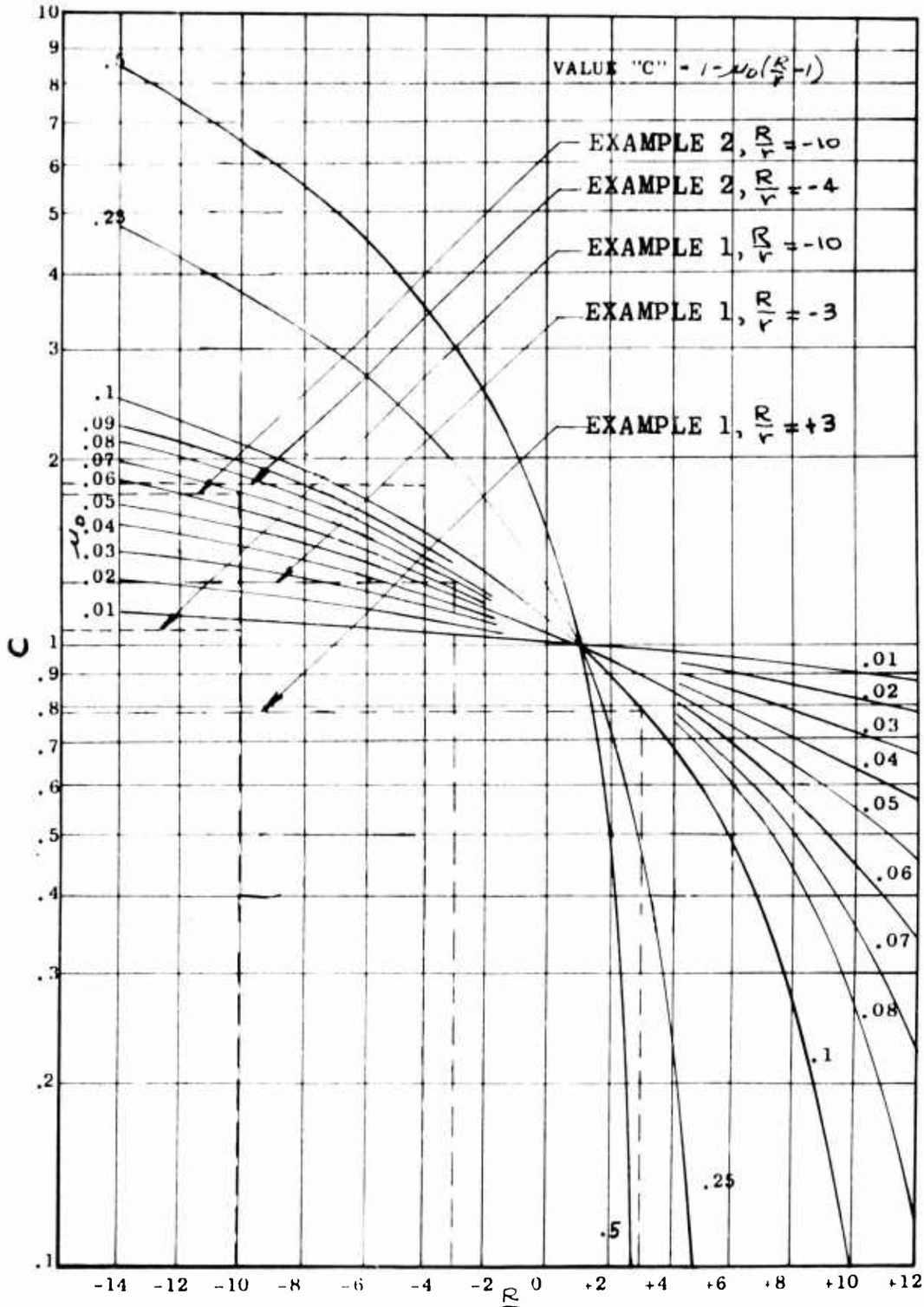

Figure 8. DAVI Alpha Design Chart, Value of C Versus $\frac{R}{r}$

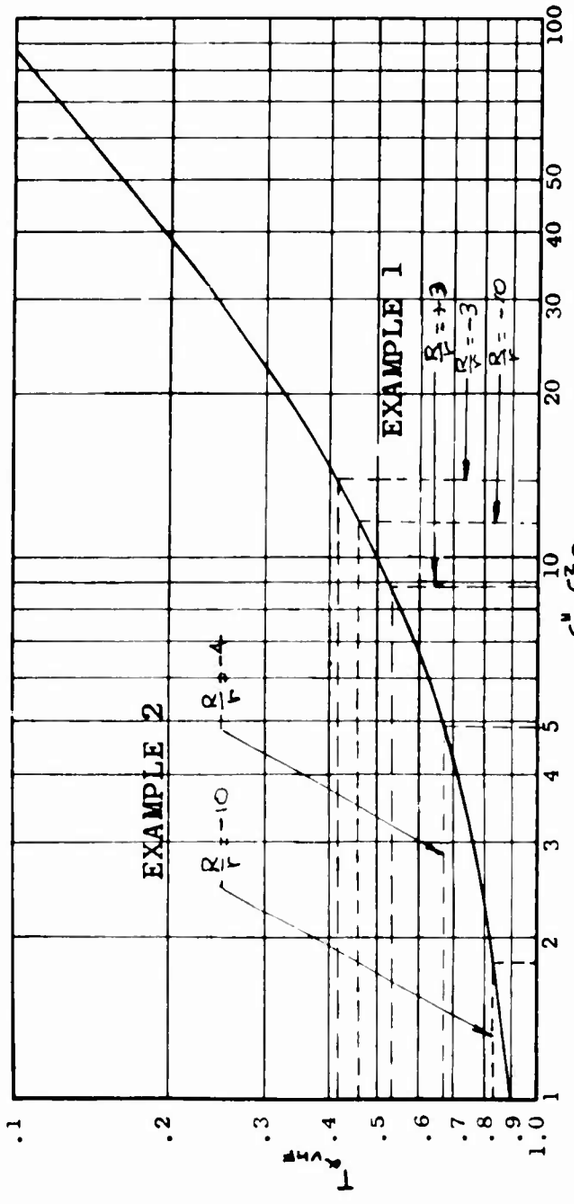

Figure 9. DAVI Alpha Design Chart, $T_{\alpha_{VHF}}$ Versus $S''_{ST} f_A^2 C$

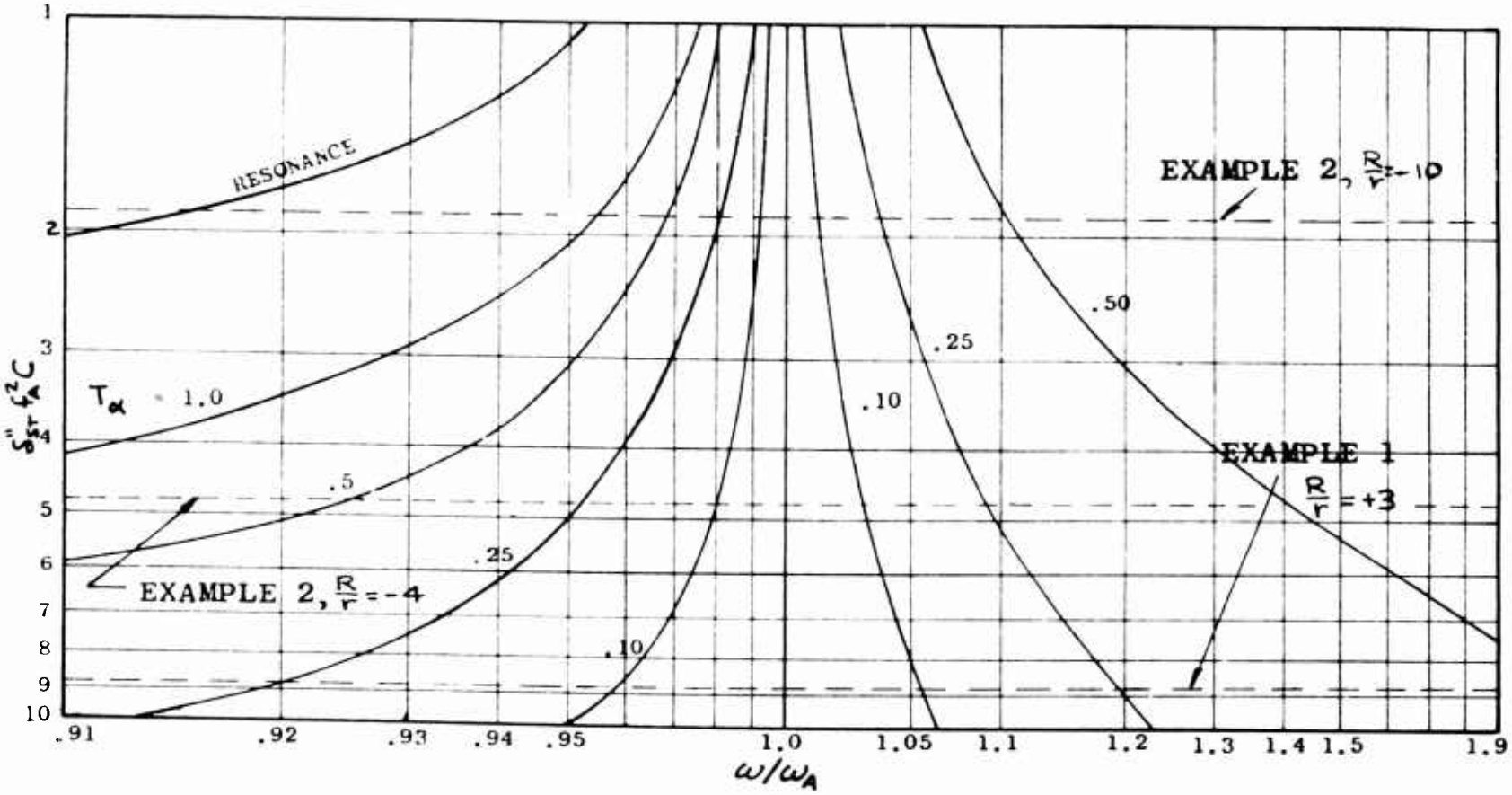

Figure 10A. DAVI Alpha Design Chart, $\zeta''_{ST} f_A^2 C$ Versus ω/ω_A

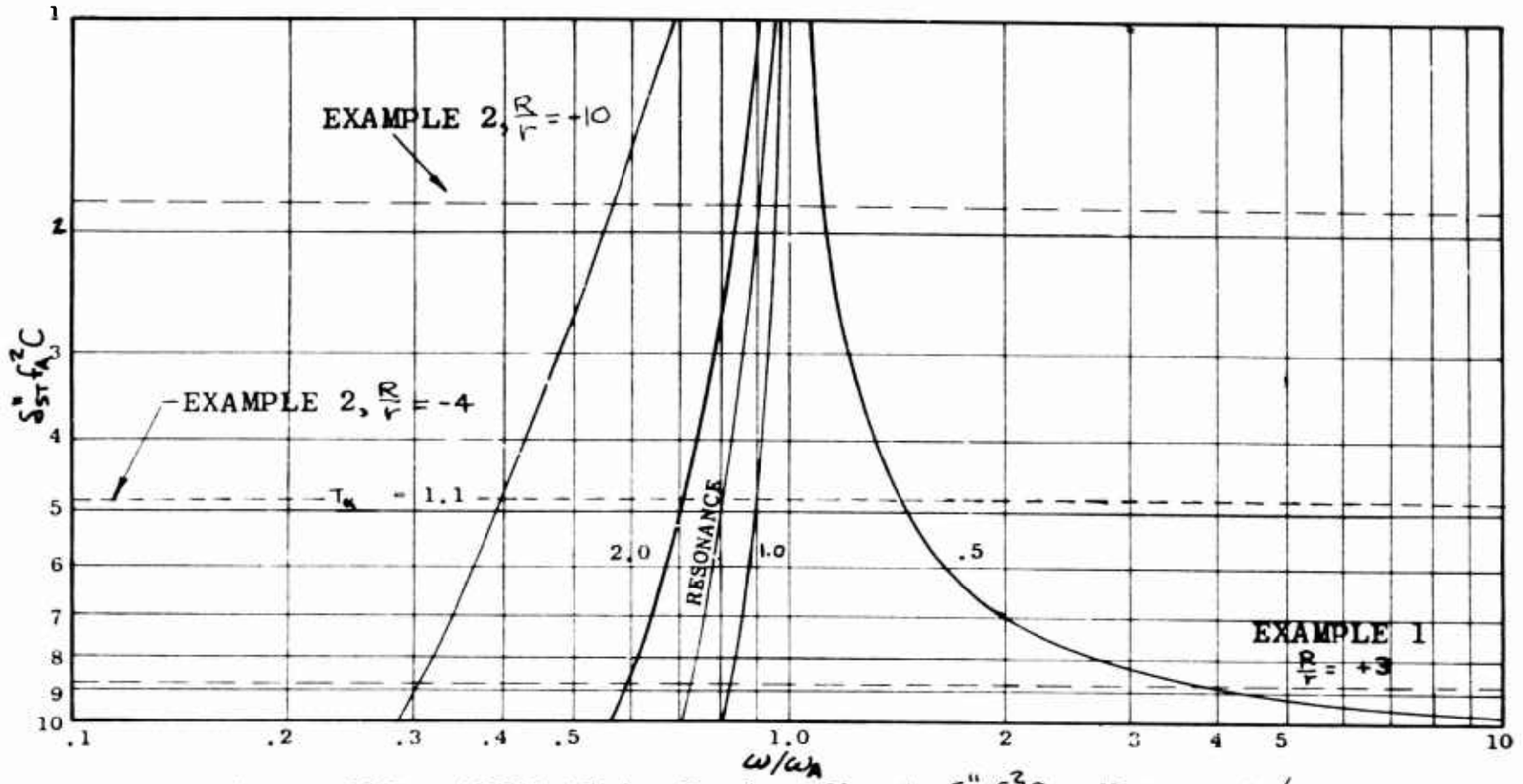

Figure 10B. DAVI Alpha Design Chart, $\delta''_{st} f_A^2 C$ Versus ω/ω_A

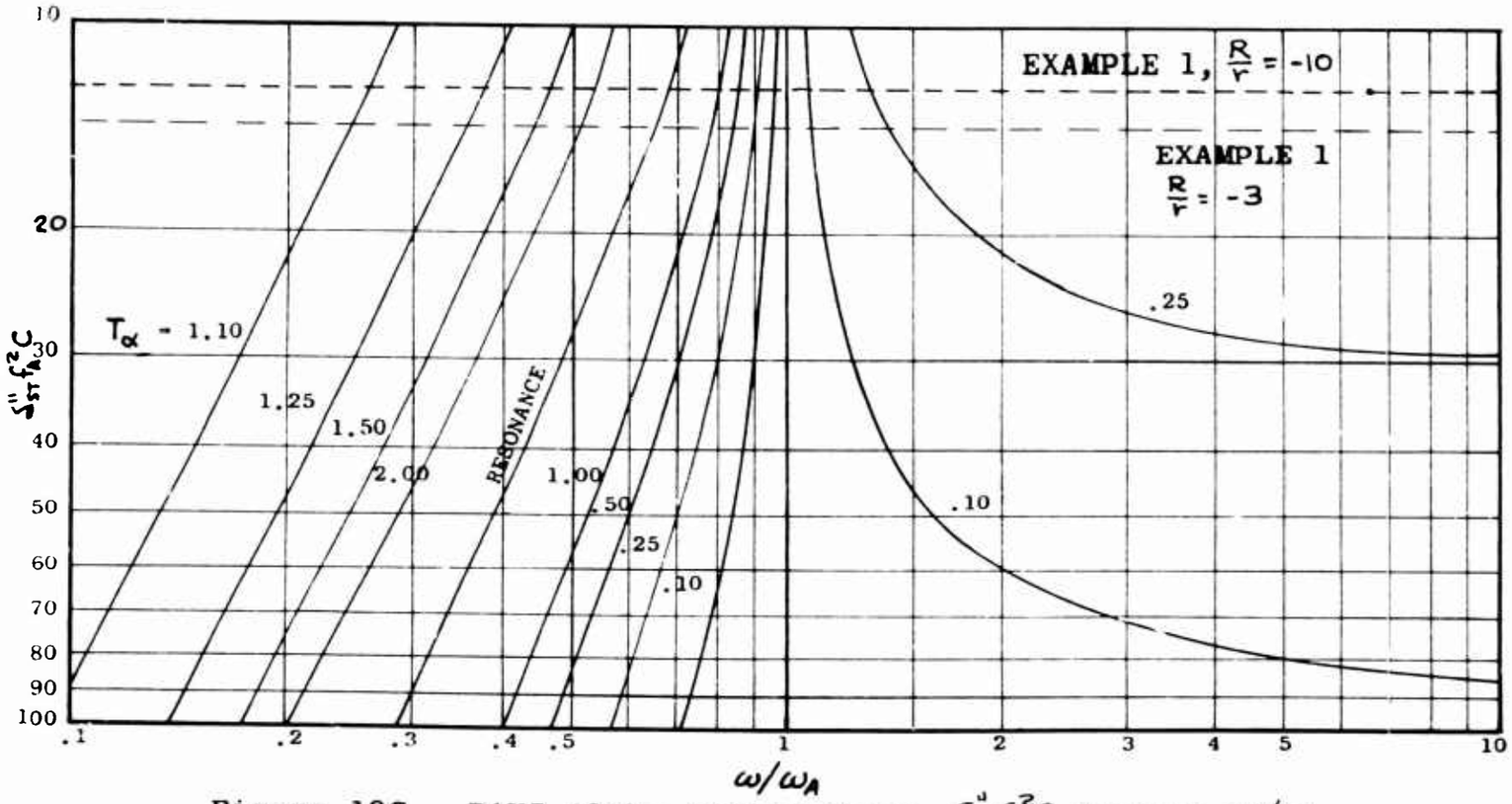

Figure 10C. DAVI Alpha Design Chart, $\zeta''_{st} f_A^2 C$ Versus ω/ω_A

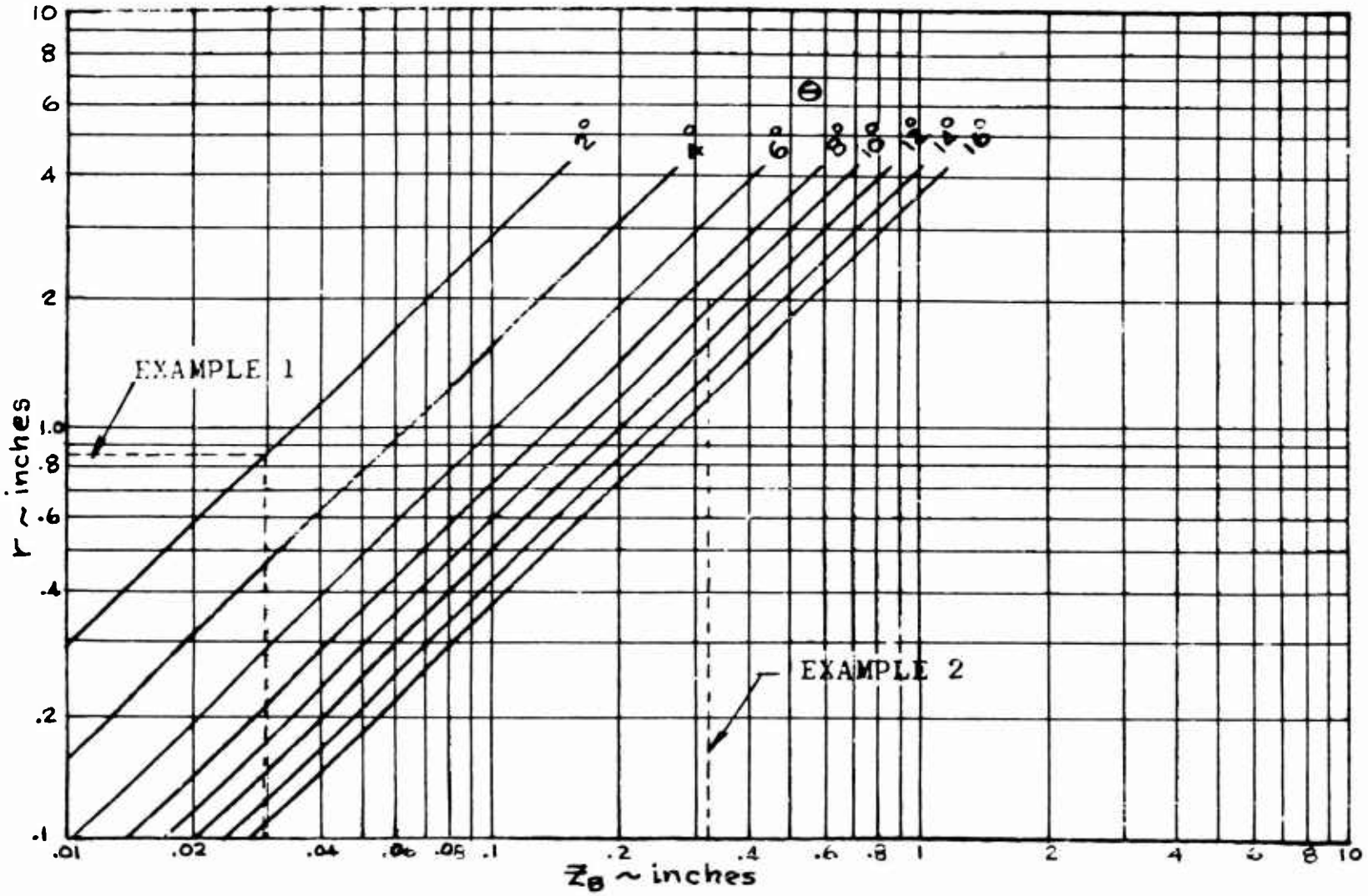

Figure 11. DAV Alpha Design Chart r Versus Z_B

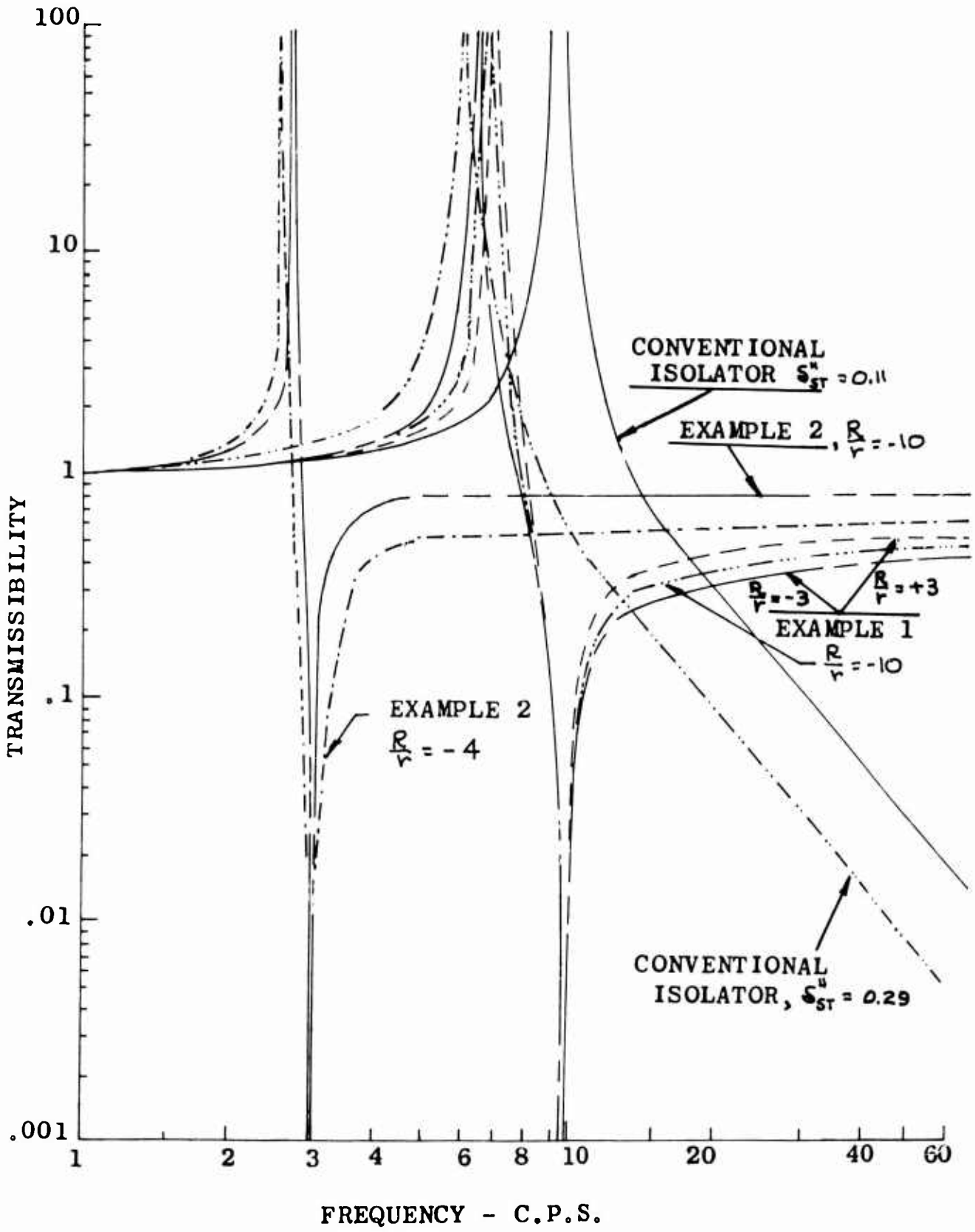

Figure 12. Transmissibilities Obtained From Design Charts

Test Fixture

In order that better correlation between theoretical and test results could be obtained, a unidirectional test rig was designed. Figures 14A and 14B are pictures of this test rig. As indicated in these photographs, the test rig consists of a 3/4-horsepower electric motor turning two counterrotating shafts through two 1:1 right-angle drives at 1750 rpm.

Seated on these two counterrotating shafts are the base weight and isolated weight. The weights are constrained to move axially along the rotating shafts, as illustrated by one weight in Figure 13.

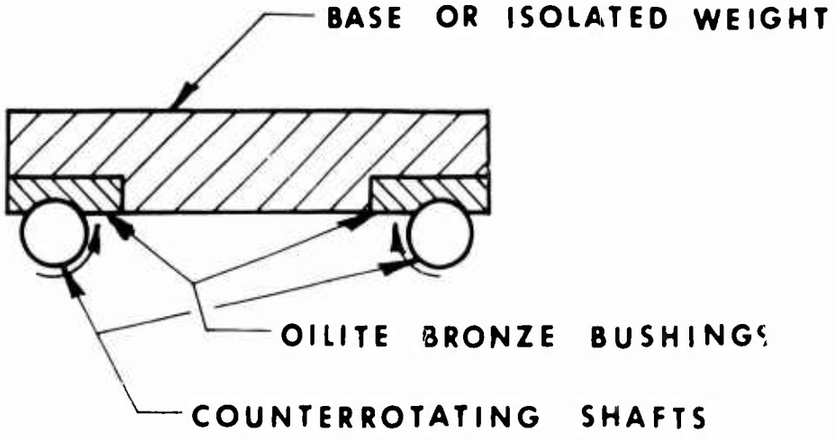

Figure 13. Schematic of Weight on Shafts

It is seen from the above schematic that only axial translation of the base weight and isolated weight can occur. In-house research has shown that Coulomb damping is eliminated and only viscous-type damping occurs. This viscous damping is proportioned to the tangential velocity of the rotating shafts, and it is minimized or controlled by the rpm of the shafts.

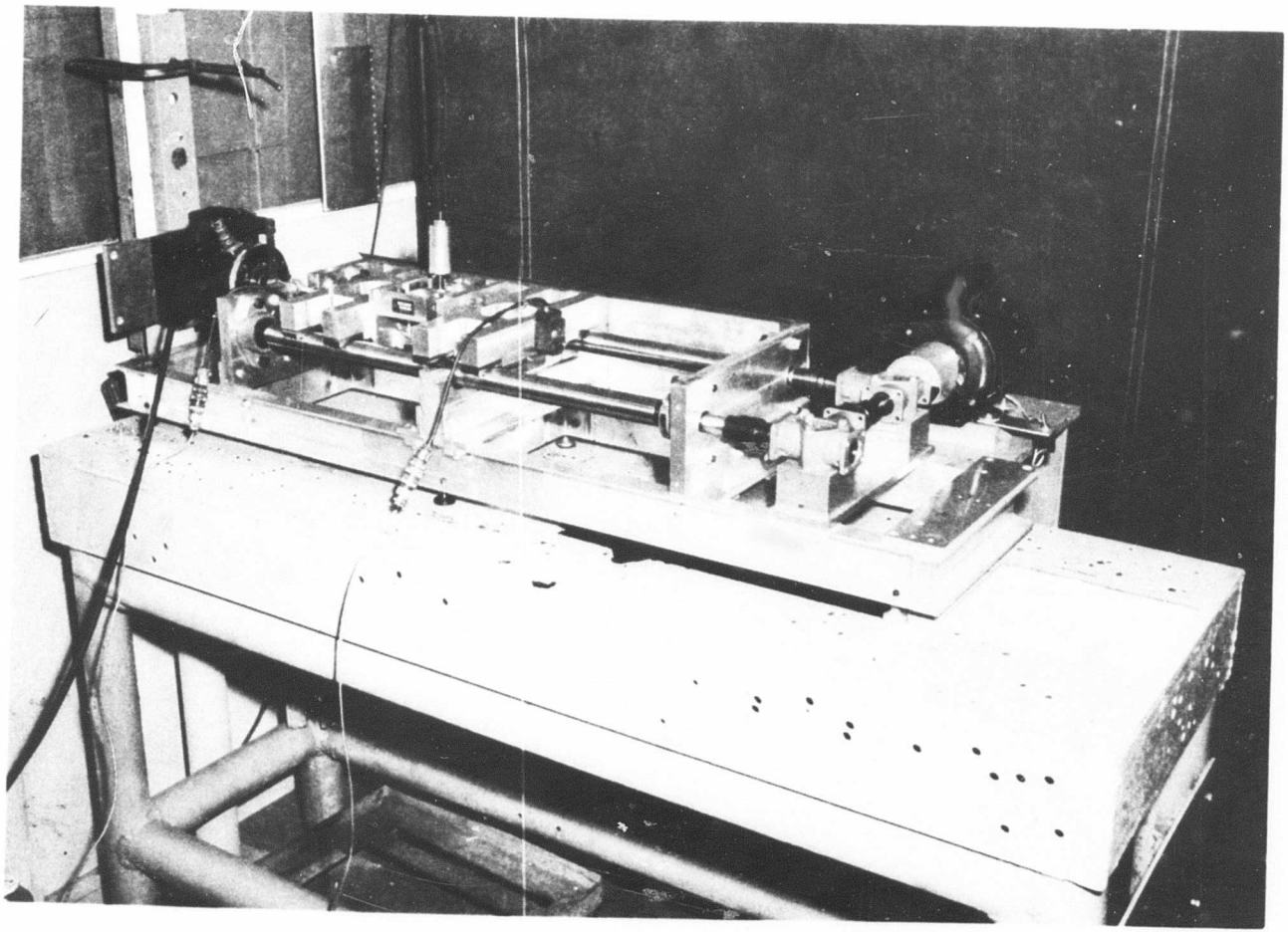

Figure 14A. Side View of Unidirectional Test Rig

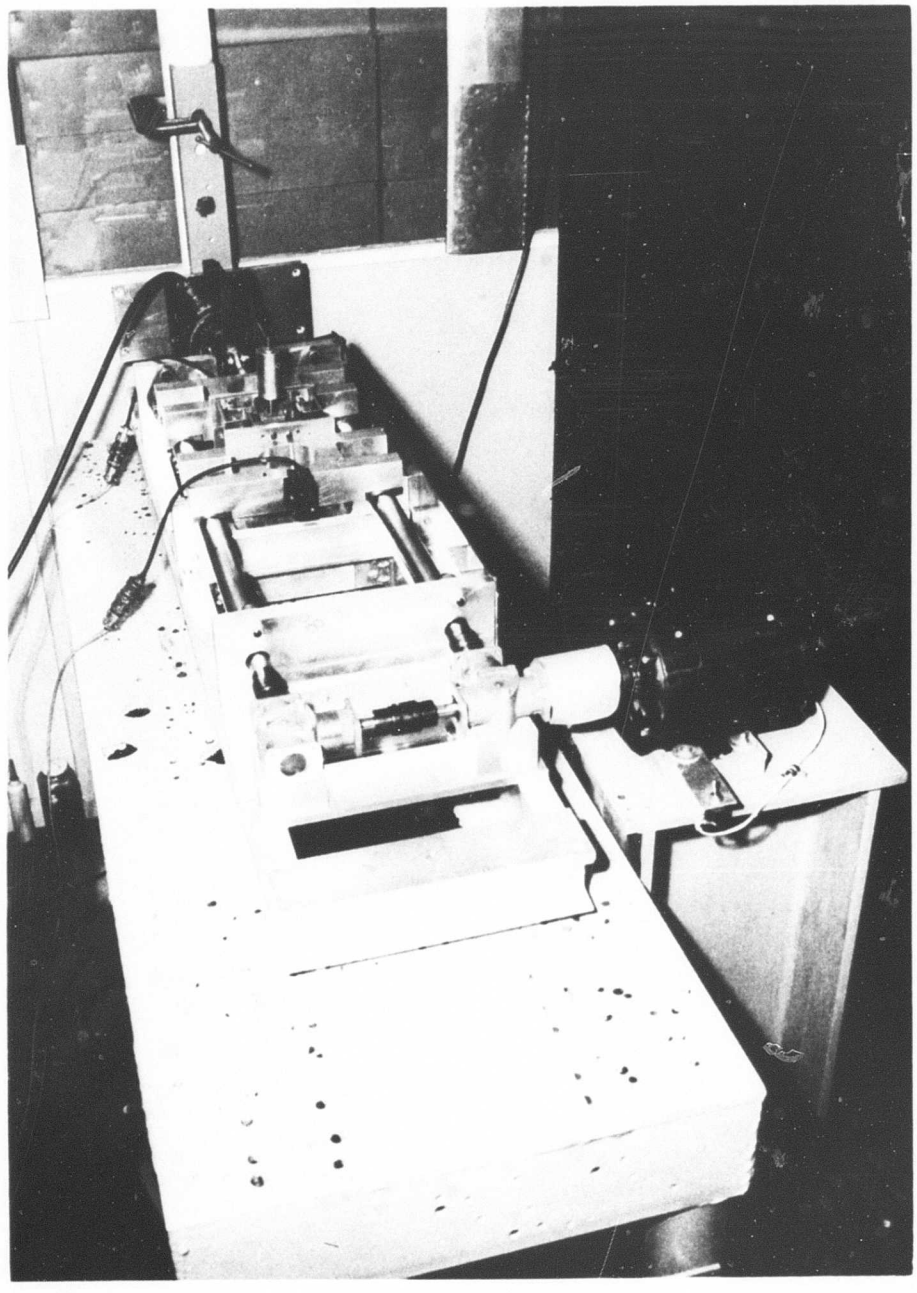

Figure 14B. Longitudinal View of Unidirectional Test Rig

Test Equipment and Procedure

Figure 15 is an overall view of the test setup. An MB model S-DA electromagnetic shaker with a force capability of 10 pounds was connected to the base weight and was used for the excitation. Two MB velocity pickups, which were calibrated at USAAVLABS facilities, were attached to the input and isolated weights. The outputs of the pickups were fed to an MB vibration meter and the results manually recorded. The output velocity of the isolated weight was then divided by the input velocity of the base to obtain the transmissibility of the DAVI Alpha. The DAVI Alpha that was used in this series of tests is shown in Figure 16. This prototype model was designed to have a variable r (distance between pivots) from .75 inch to 2.0 inches. Without changing any of the physical hardware, such as springs, an antiresonant frequency can be obtained from 4 cycles per second to 30 cycles per second. By removing the weight on the inertia bar, much higher antiresonant frequencies can be obtained. Figure 17 shows the installation of this model in the test rig. For this particular installation, it can be seen that the R/r is negative.

Test Results

Figures 18 through 23 give the results of the test of the DAVI Alpha. Table I gives the configurations tested.

It should be noted that the change in spring rate is not due to a physical change of springs; it is due to the change in offset of the pivots. The torsional spring rate of the Bendix flexural pivots and therefore the pivot distance affect the overall spring rate of the DAVI.

The results, as seen in Figures 18 through 23, are as expected. In each series of tests, that is, for a given R/r, the natural frequency of the DAVI Alpha was reduced by an increase in the isolated weight, and the high frequency isolation approached a finite value, rather than zero as in a conventional isolator. However, as expected, the antiresonant frequency was not affected by the magnitude of the isolated weight.

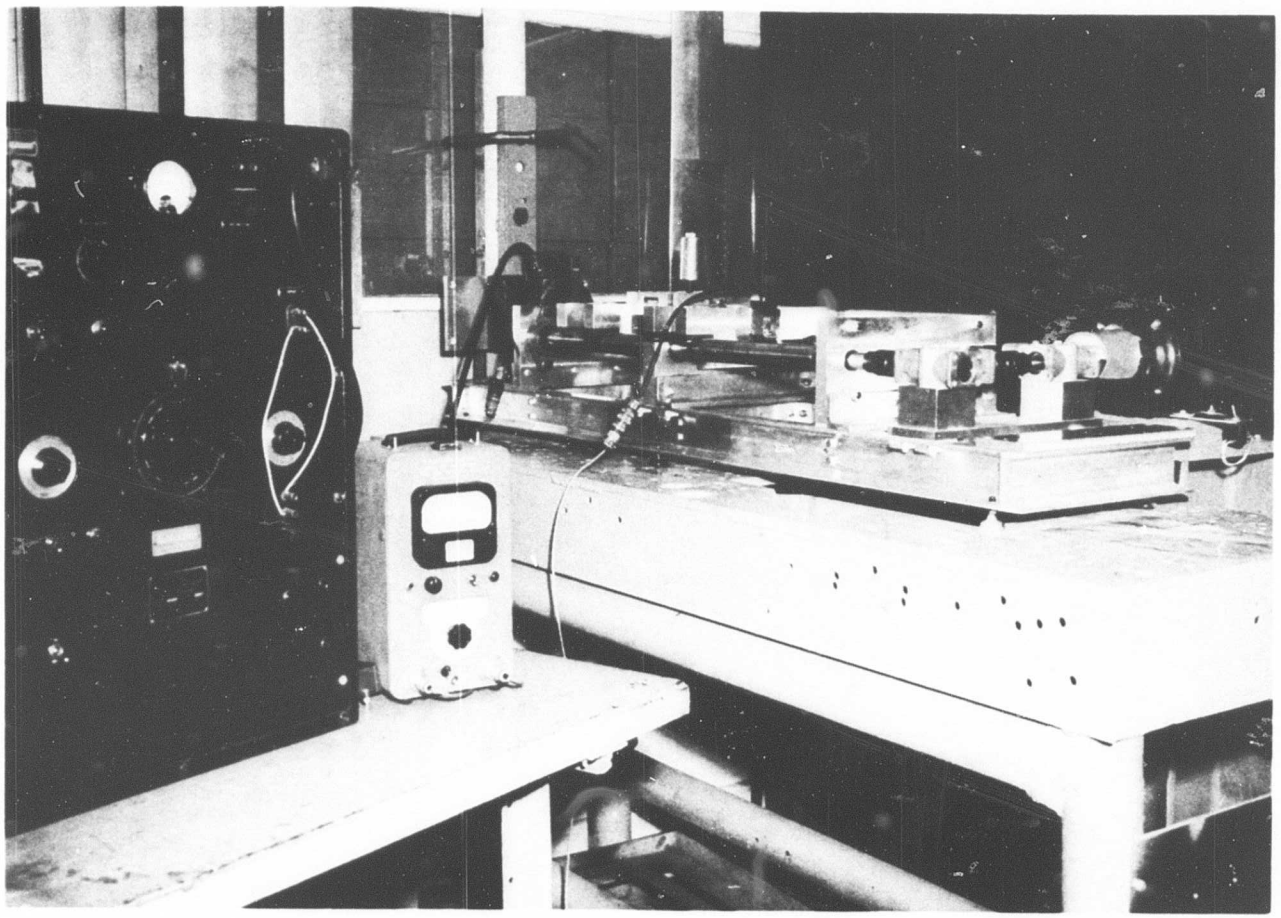

Figure 15. Test Setup

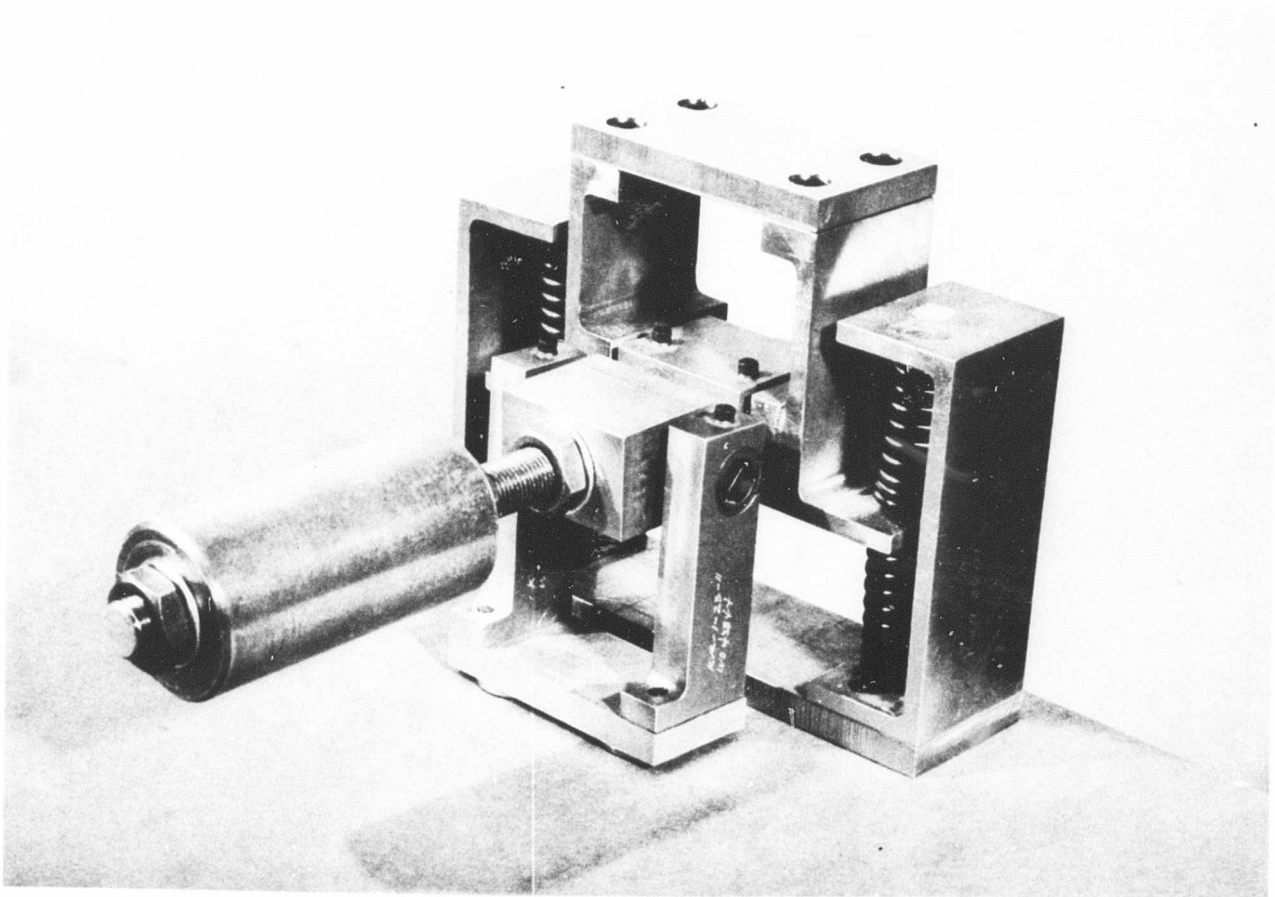

Figure 16. Prototype DAVI Alpha

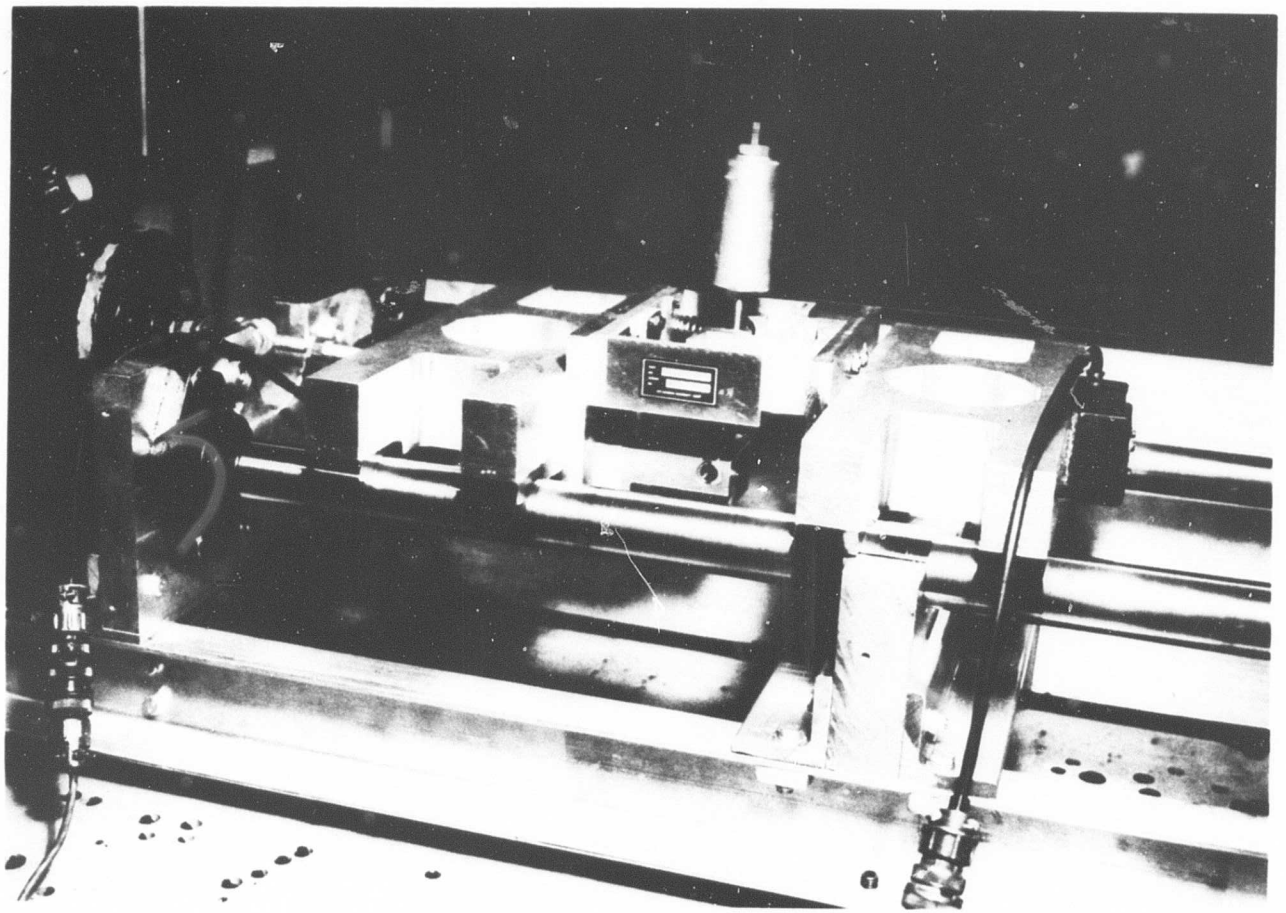

Figure 17. DAVI Alpha Installation

TABLE I

DAVI ALPHA CONFIGURATIONS TESTED

Isolated Weight (Pounds)	DAVI Inertia Bar · Weight (Pounds)	K_D Spring Rate (Pounds/In.)	R (In.)	r (In.)	ρ (In.)	Figure Number
11 27 42	2.25	428	-2.27	2.00	2.405	18
11 27 42	2.25	450	-2.40	1.00	2.125	19
11 27 42	2.25	484	-4.66	.76	3.480	20
11 27 42	2.25	428	4.20	2.00	2.435	21
11 27 42	2.25	450	2.95	1.00	1.92	22
11 27 42	2.25	484	3.68	.76	2.30	23

Correlation

Figures 24 through 41 show the results of the correlation of analytical and test results. A comparison is also made of a conventional and DAVI Alpha isolation system having the same spring rate.

Table II, on the following page, gives the results of this comparison. The physical parameters used in the analytical comparison are those given in Table I, and the theoretical transmissibility curves are obtained from the digital program. For the analytical study, .01-percent damping (ζ_A) at the antiresonant frequency was used.

It is also seen from Table II and Figures 24 through 41 that very good correlation was obtained between the analytical and test results. The natural frequencies and antiresonant frequencies of the DAVI Alpha were predicted very accurately.

There is some discrepancy between the predicted and actual transmissibility of the DAVI Alpha obtained at the antiresonant frequency. In approximately 50 percent of the cases, lower transmissibility than predicted was actually obtained from the tests.

It is also seen that there is a discrepancy between the calculated and test natural frequency and transmissibility of the conventional system. This is due to the fact that in the analysis, the effective spring rate of the conventional system includes the spring rate of the pivots; whereas in the test, the spring rate of the pivots was not included.

It is seen in every case that the natural frequency of the DAVI was lower than that of the equivalent conventional system. In Figure 30, it is seen that an antiresonant frequency was obtained at 5.6 cycles per second, whereas the equivalent conventional system had a natural frequency of 20.02 cycles per second. It is also seen that in 13 of the 18 tests, at the antiresonant frequency of the DAVI Alpha, amplification occurred in the equivalent conventional system.

TABLE II

COMPARISON OF THEORETICAL AND TEST RESULTS

Figure Number	Isolated Weight (Pounds)	R/r	Natural Frequency (c.p.s.) DAVI Test	DAVI Theory	Conventional Test	Conventional Theory	Antiresonant Frequency (c.p.s.) Test	Antiresonant Frequency (c.p.s.) Theory	Transmissibility At Antiresonant Frequency DAVI Test	DAVI Theory	Conventional Test	Conventional Theory	Frequency At Which Equivalent Transmissibility For DAVI And Conventional System Occurs
24	11	-1.135	12.2	12.58	-	18.8	20.5	20.49	.008	.012	-	5.67	35
25	27	-1.135	10.0	9.95	11.5	12.3	20.5	20.49	.012	.006	.420	.562	31
26	42	-1.135	9.0	8.54	-	9.9	20.5	20.49	.022	.004	-	.304	29
27	11	-2.40	9.6	9.59	-	19.4	12.25	12.42	.023	.029	-	1.696	30
28	27	-2.40	8.4	8.29	11.5	12.6	12.25	12.42	.027	.016	5.00	29.208	24
29	42	-2.40	7.3	7.48	-	10.16	12.25	12.42	.027	.011	-	2.004	21
30	11	-6.1316	5.1	5.23	-	20.02	5.6	5.69	.018	.104	-	1.087	30
31	27	-6.1316	4.8	5.0	11.5	13.05	5.6	5.69	.053	.066	1.15	1.234	20
32	42	-6.1316	4.7	4.81	-	10.51	5.6	5.69	.016	.050	-	1.414	16
33	11	2.10	15.0	14.8	-	18.8	20.5	20.49	.025	.022	-	5.678	32
34	27	2.10	11.25	10.9	11.5	12.3	20.5	20.49	.021	.008	.420	.562	30
35	42	2.10	9.4	9.14	-	9.9	20.5	20.49	.020	.005	-	.304	29
36	11	2.95	12.5	12.41	-	19.4	14.5	14.40	.027	.058	-	2.229	30
37	27	2.95	10.0	9.95	11.5	12.6	14.25	14.40	.012	.018	1.10	3.265	23
38	42	2.95	8.8	8.61	-	10.16	14.25	14.40	.029	.011	-	.988	21
39	11	4.8421	7.9	8.49	-	20.02	8.3	8.70	.25	.379	-	1.230	29
40	27	4.8421	7.8	7.63	11.5	13.05	8.6	8.70	.04	.06	1.80	1.80	20
41	42	4.8421	7.0	7.0	-	10.51	8.4	8.70	.025	.03	-	2.70	17

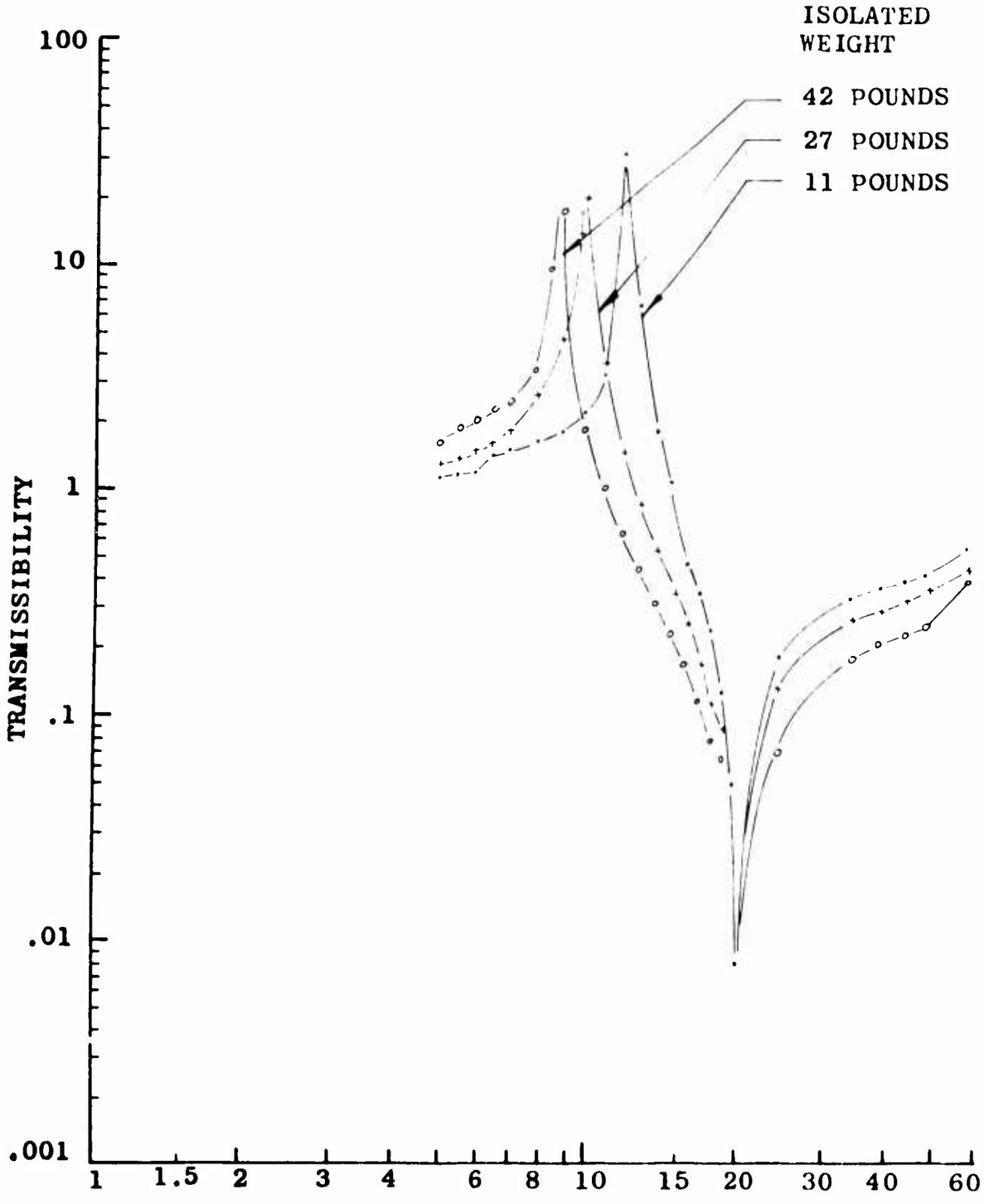

Figure 18. Experimental Response Curve of Unidirectional DAVI Alpha for $\frac{\rho}{r}$ = -1.135

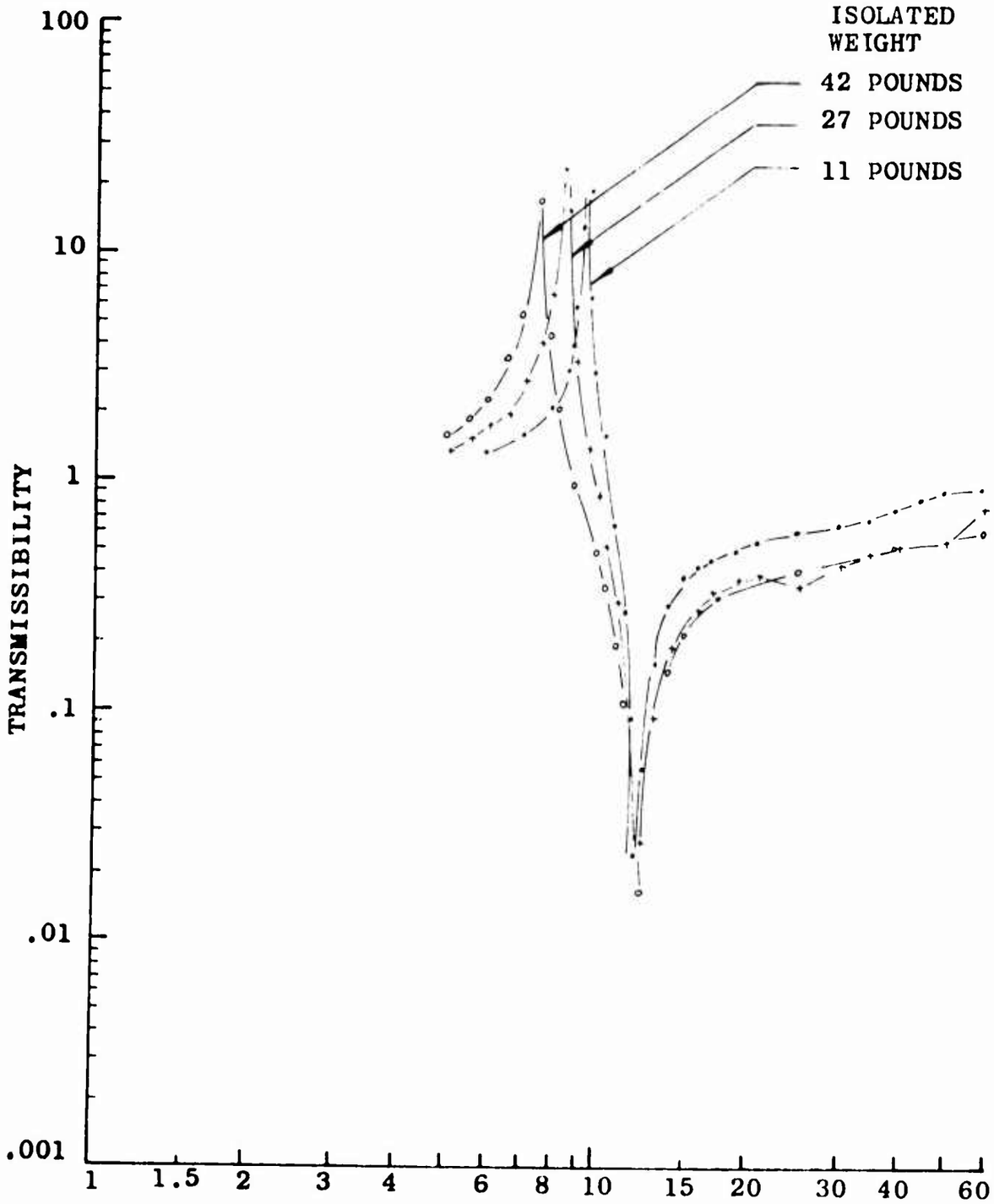

Figure 19. Experimental Response Curve of Unidirectional DAVI Alpha for $\frac{R}{r}$ = -2.40

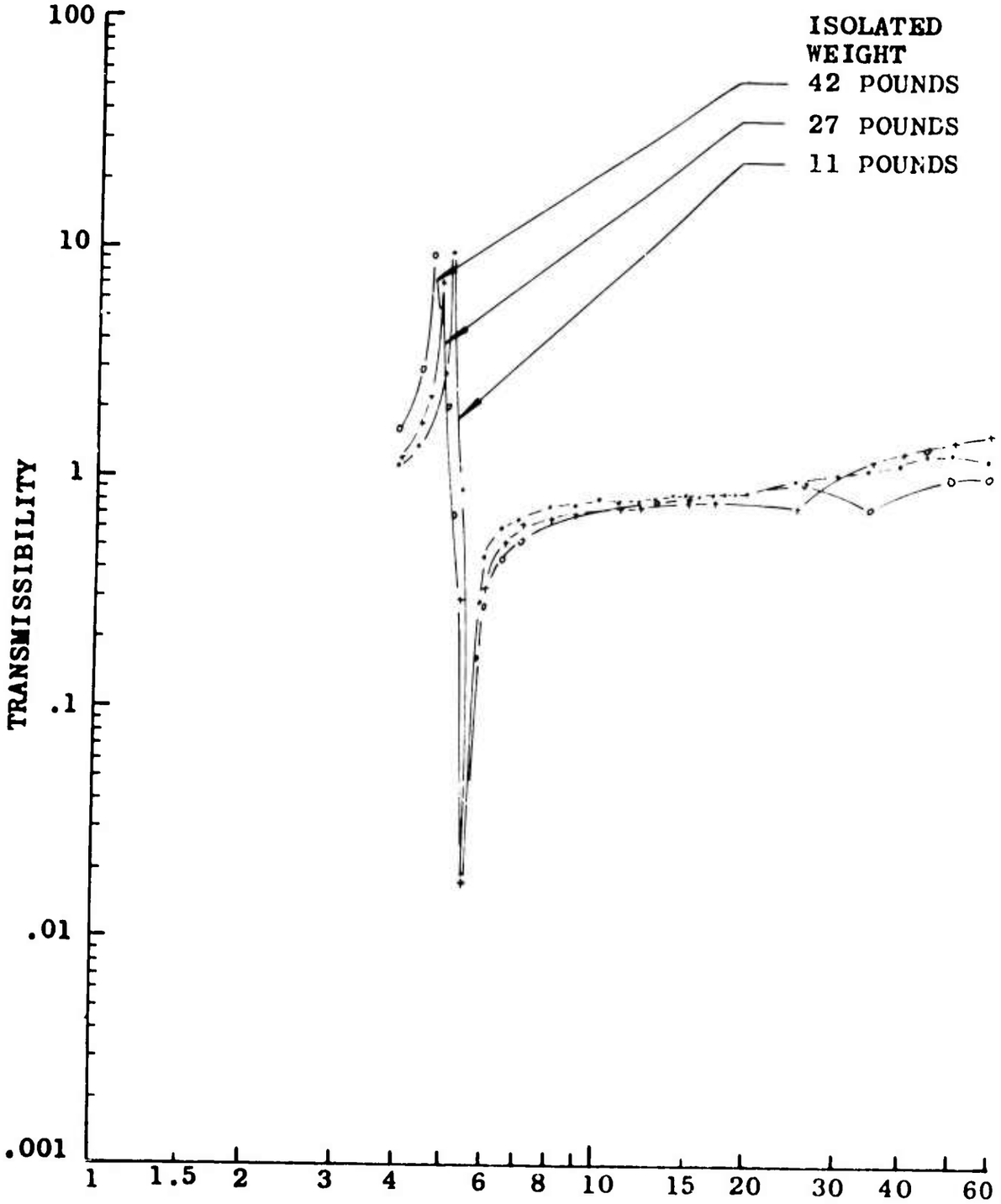

Figure 20. Experimental Response Curve of Unidirectional DAVI Alpha for $\frac{R}{r}$ = -6.131

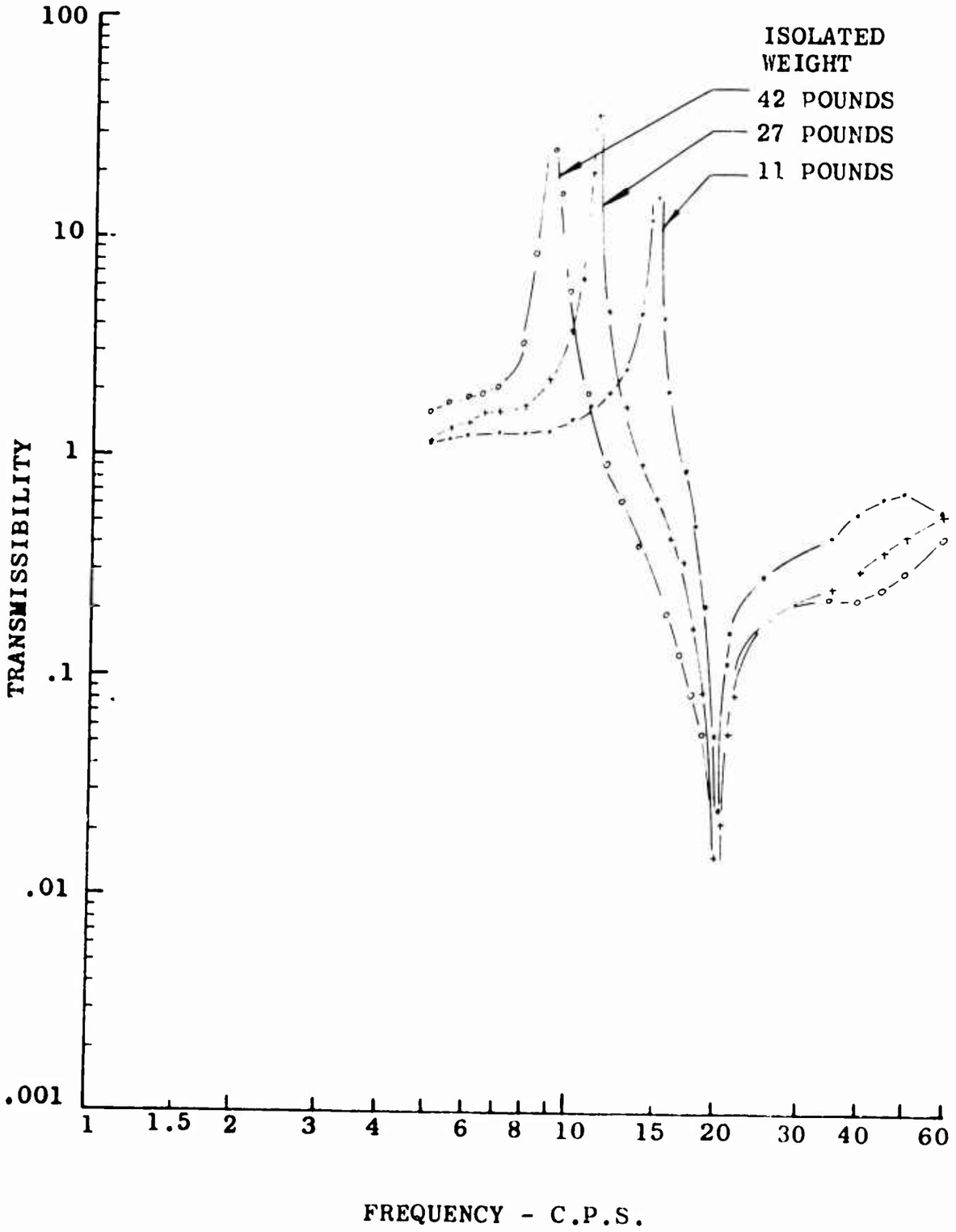

Figure 21. Experimental Response Curve of Unidirectional DAVI Alpha for $\frac{R}{r} = 2.26$

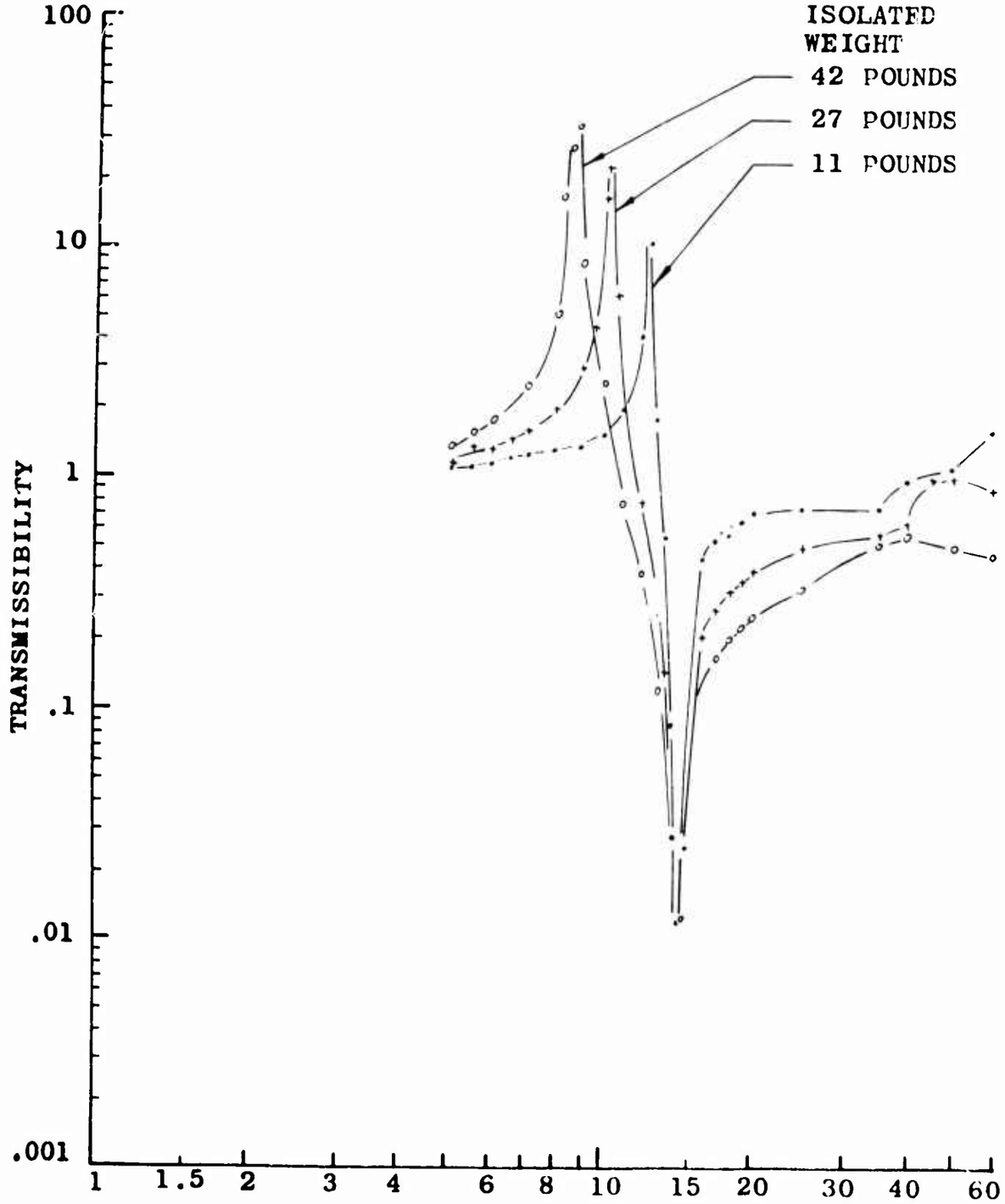

Figure 22. Experimental Response Curve of Unidirectional DAVI Alpha for $\frac{R}{r} = 2.950$

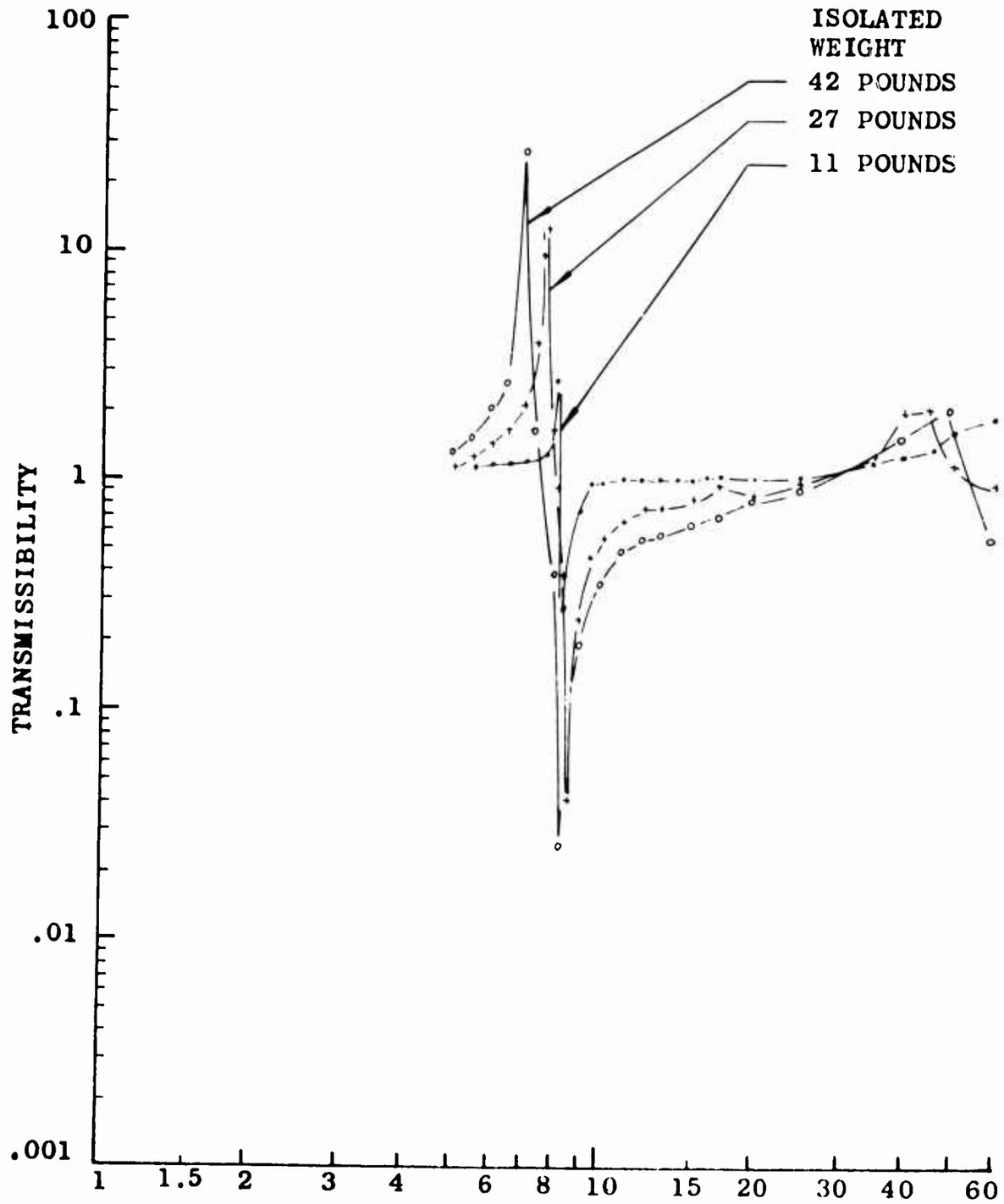

Figure 23. Experimental Response Curve of Unidirectional DAVI Alpha for $\frac{R}{r_1} = 4.842$

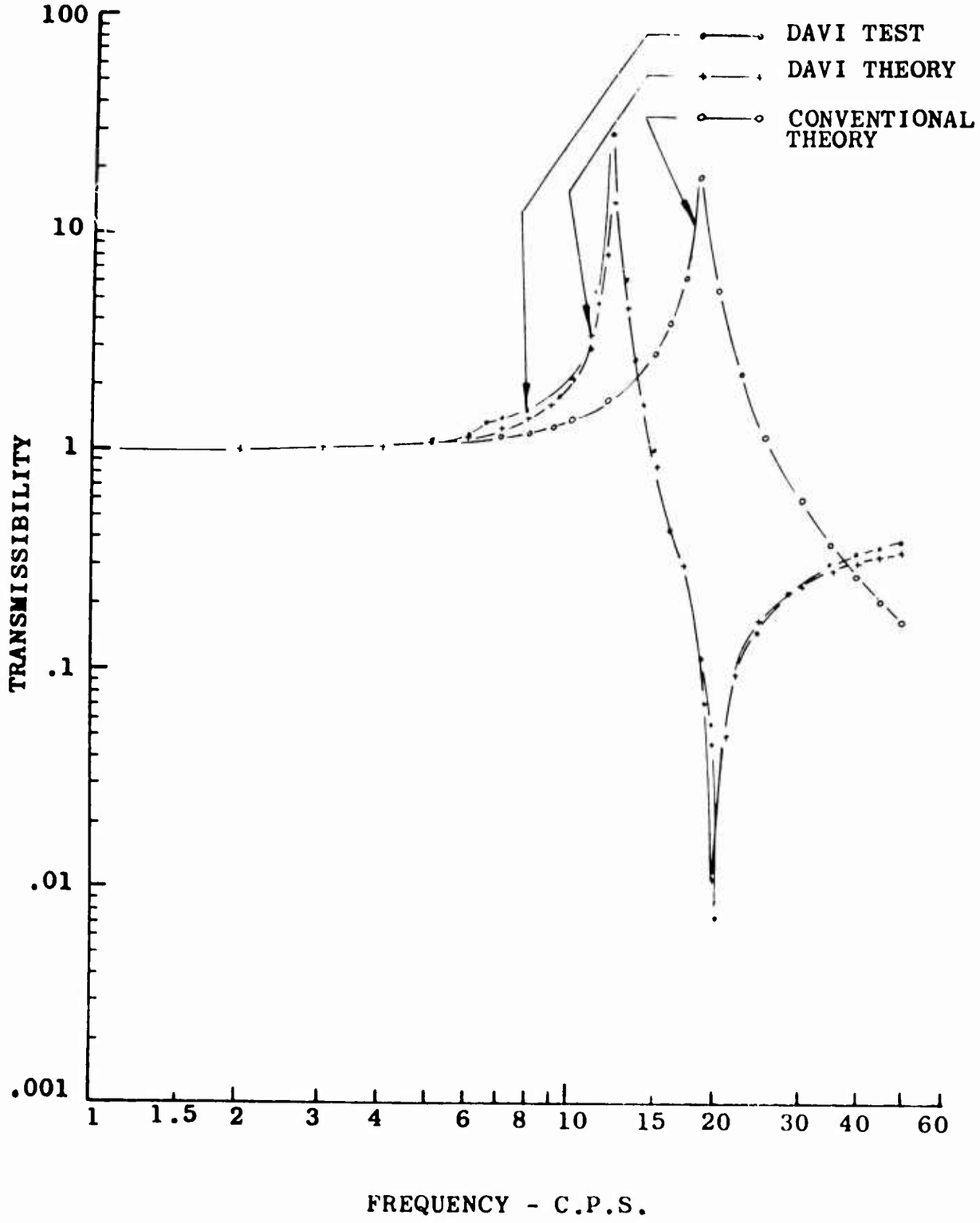

Figure 24. Analytical and Test Response Curves of Unidirectional DAVI Alpha for Isolated Weight of 11 Pounds and $\frac{R}{r}$ = -1.135

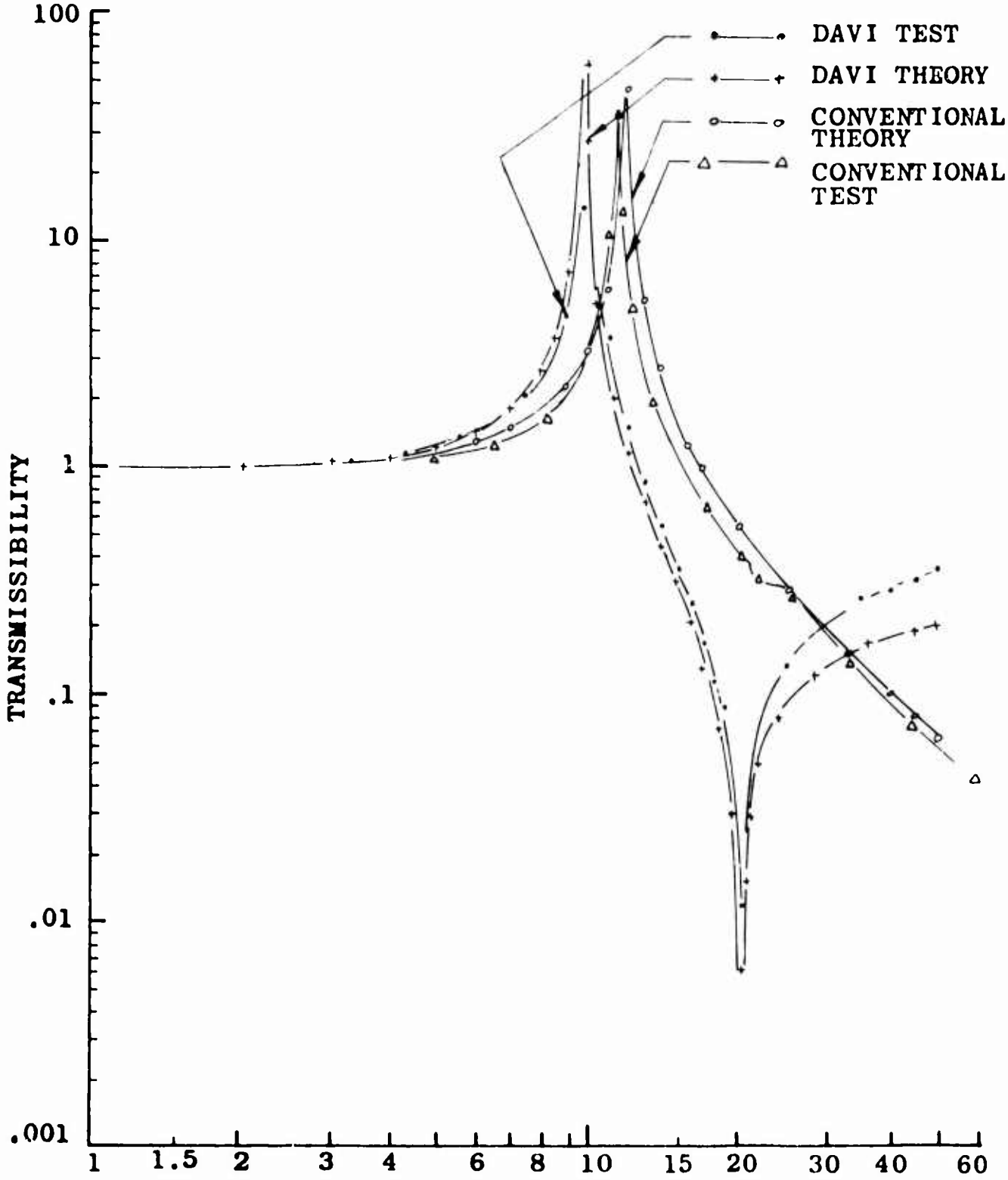

Figure 25. Analytical and Experimental Response Curves of Unidirectional DAVI Alpha for Isolated Weight of 27 Pounds and $\frac{R}{r}$ = -1.135

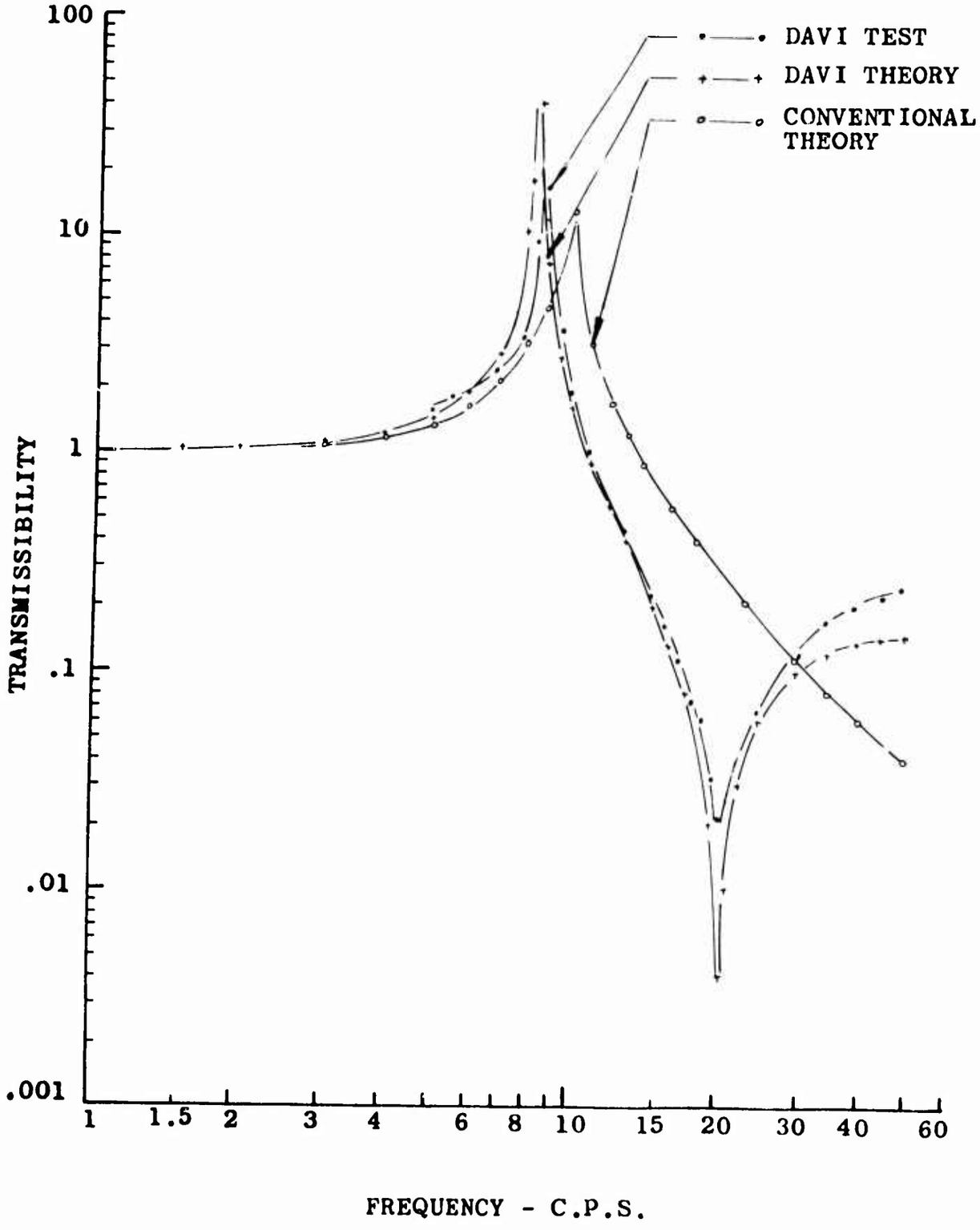

Figure 26. Analytical and Experimental Test Response Curves of Unidirectional DAVI Alpha for Isolated Weight of 42 Pounds and $\frac{R}{r} = -1.135$

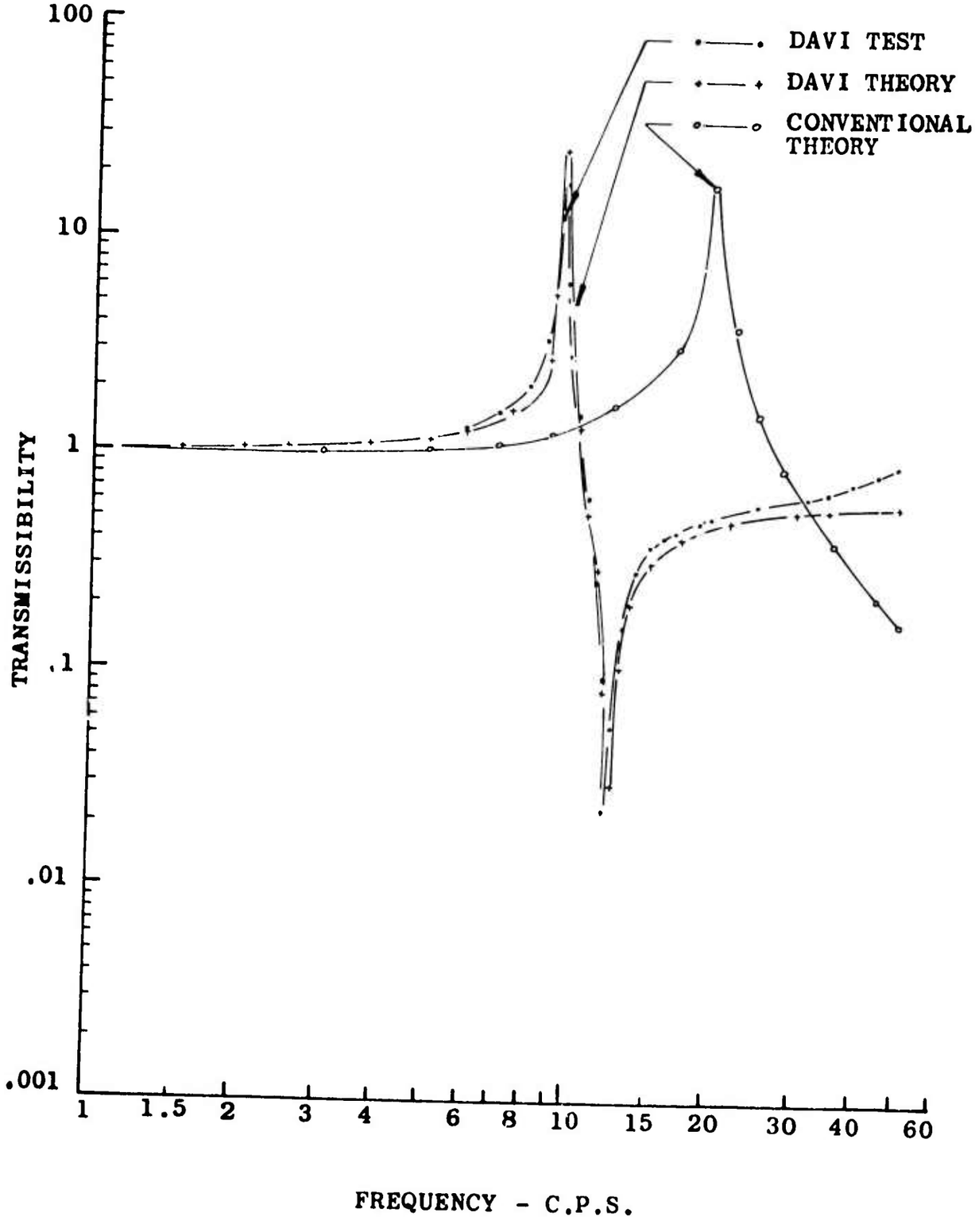

Figure 27. Analytical and Experimental Response Curves of Unidirectional DAVI Alpha for Isolated Weight of 11 Pounds and $\frac{B}{r}$ = -2.40

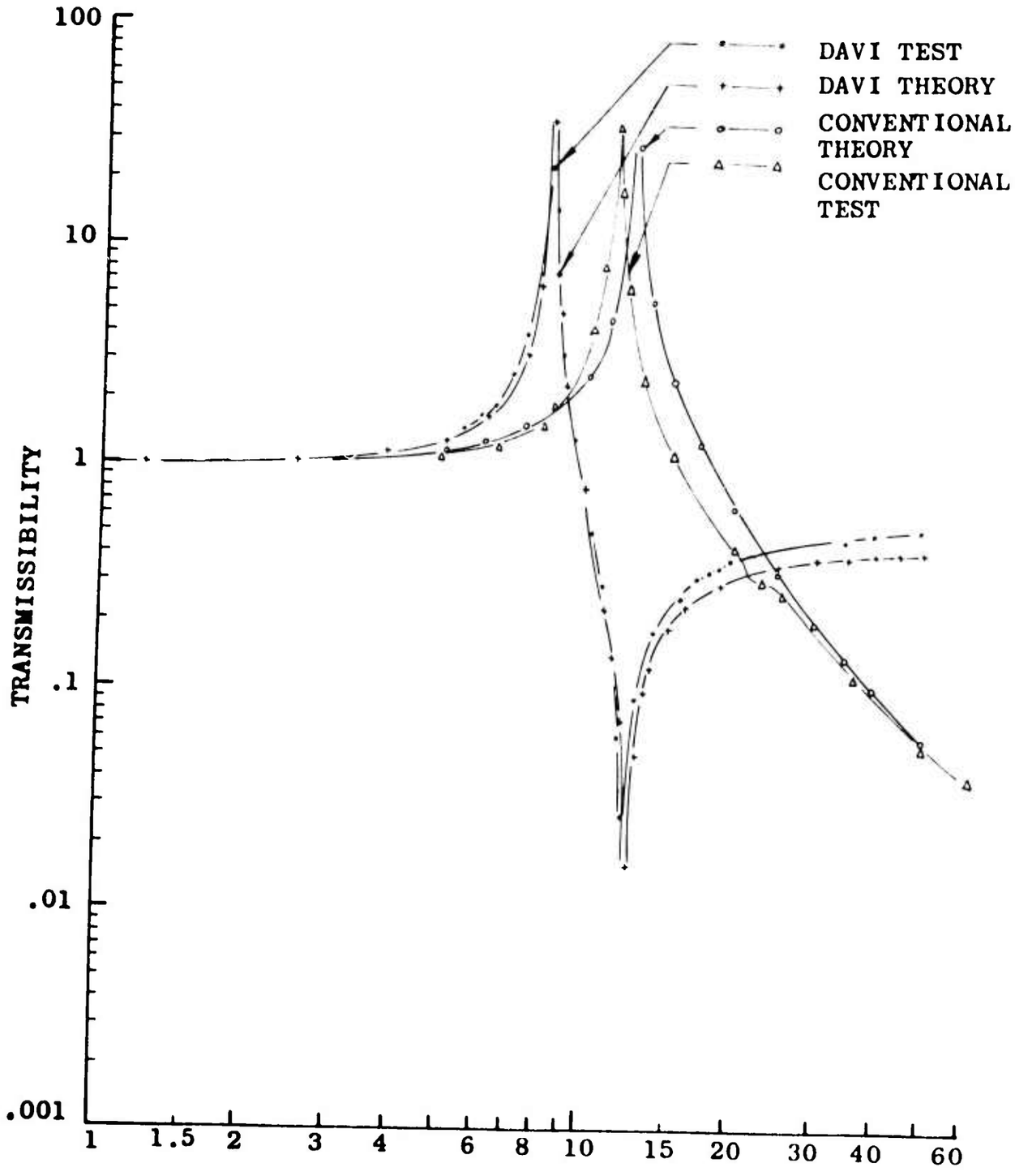

Figure 28. Analytical and Experimental Response Curves of Unidirectional DAVI Alpha for Isolated Weight of 27 Pounds and $\frac{R}{r}$ = -2.40

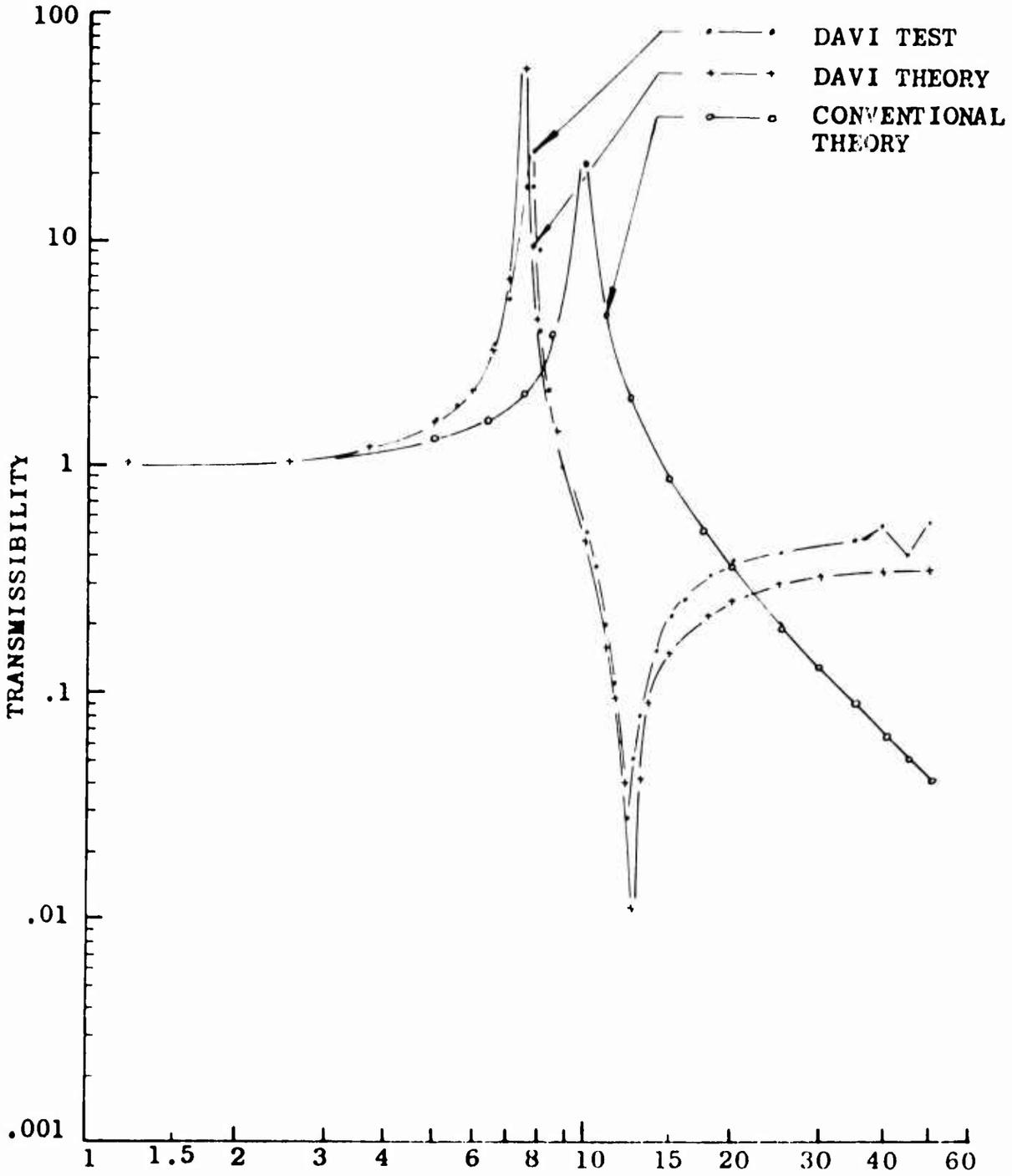

Figure 29. Analytical and Experimental Response Curves of Unidirectional DAVI Alpha for Isolated Weight of 42 Pounds and $\frac{R}{r}$ = -2.40

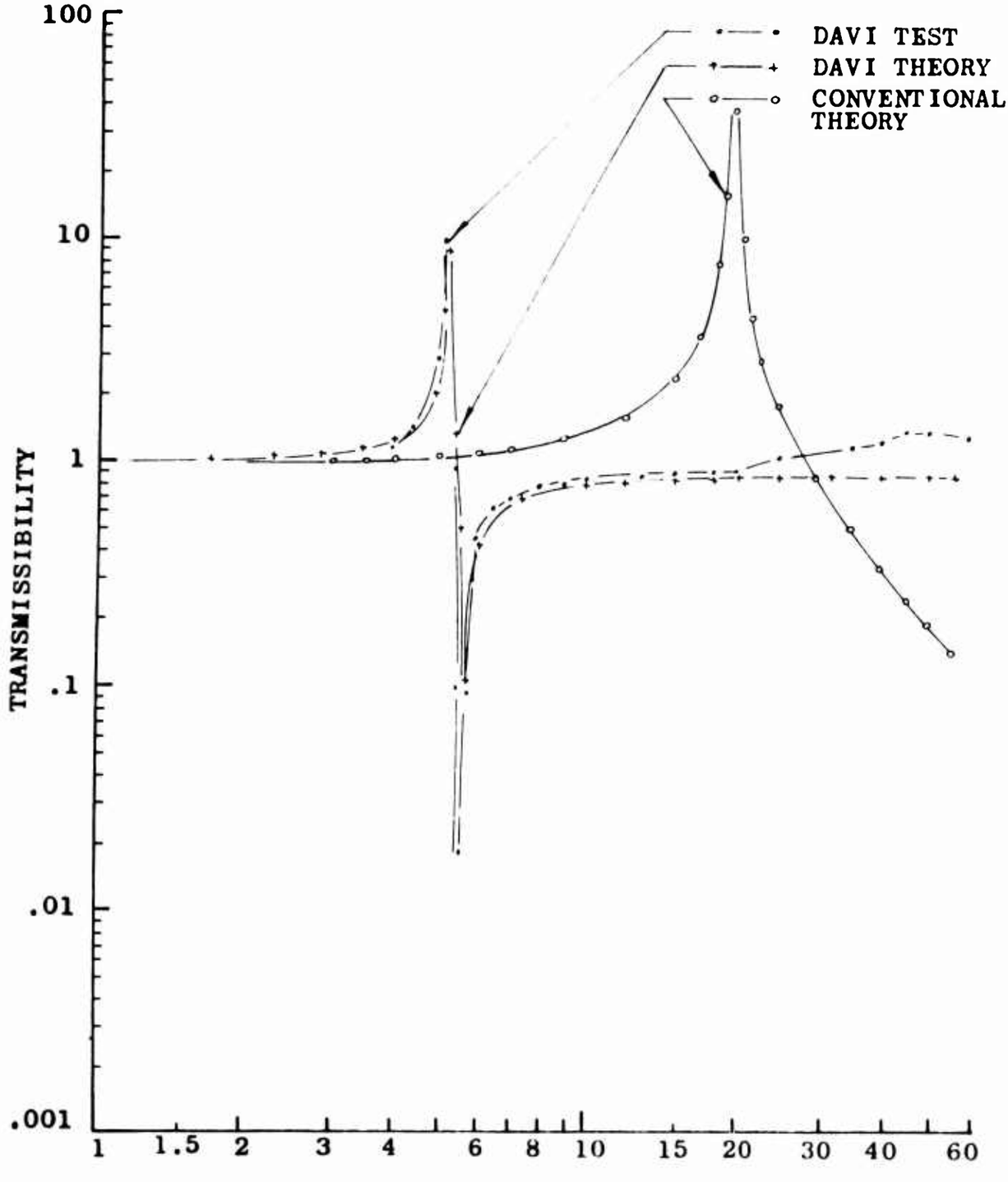

Figure 30. Analytical and Experimental Response Curves of Unidirectional DAVI Alpha for Isolated Weight of 11 Pounds and $\frac{R}{r}$ = -6.131

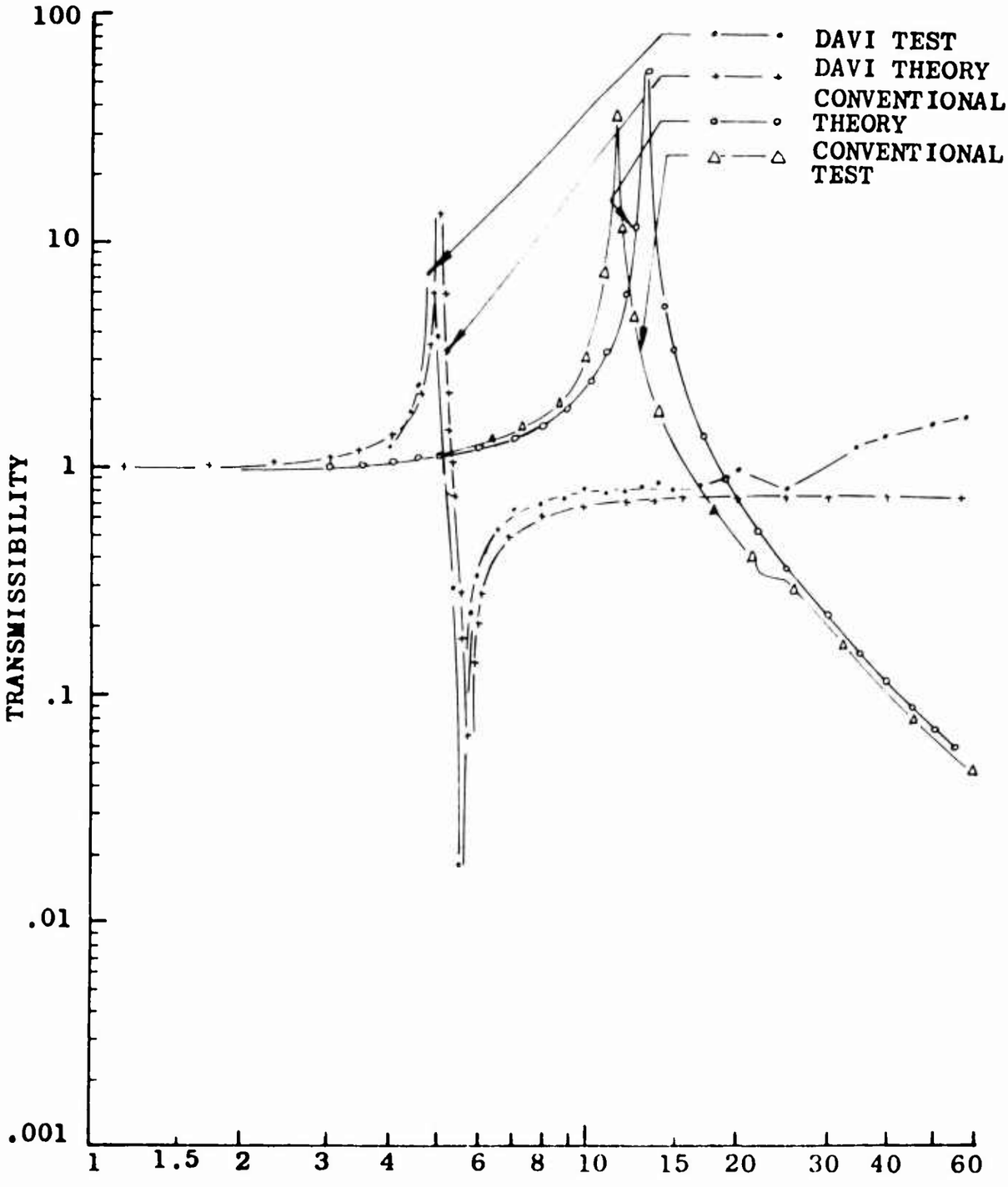

Figure 31. Analytical and Experimental Response Curves of Unidirectional DAVI Alpha for Isolated Weight of 27 Pounds and $\frac{R}{r}$ = -6.131

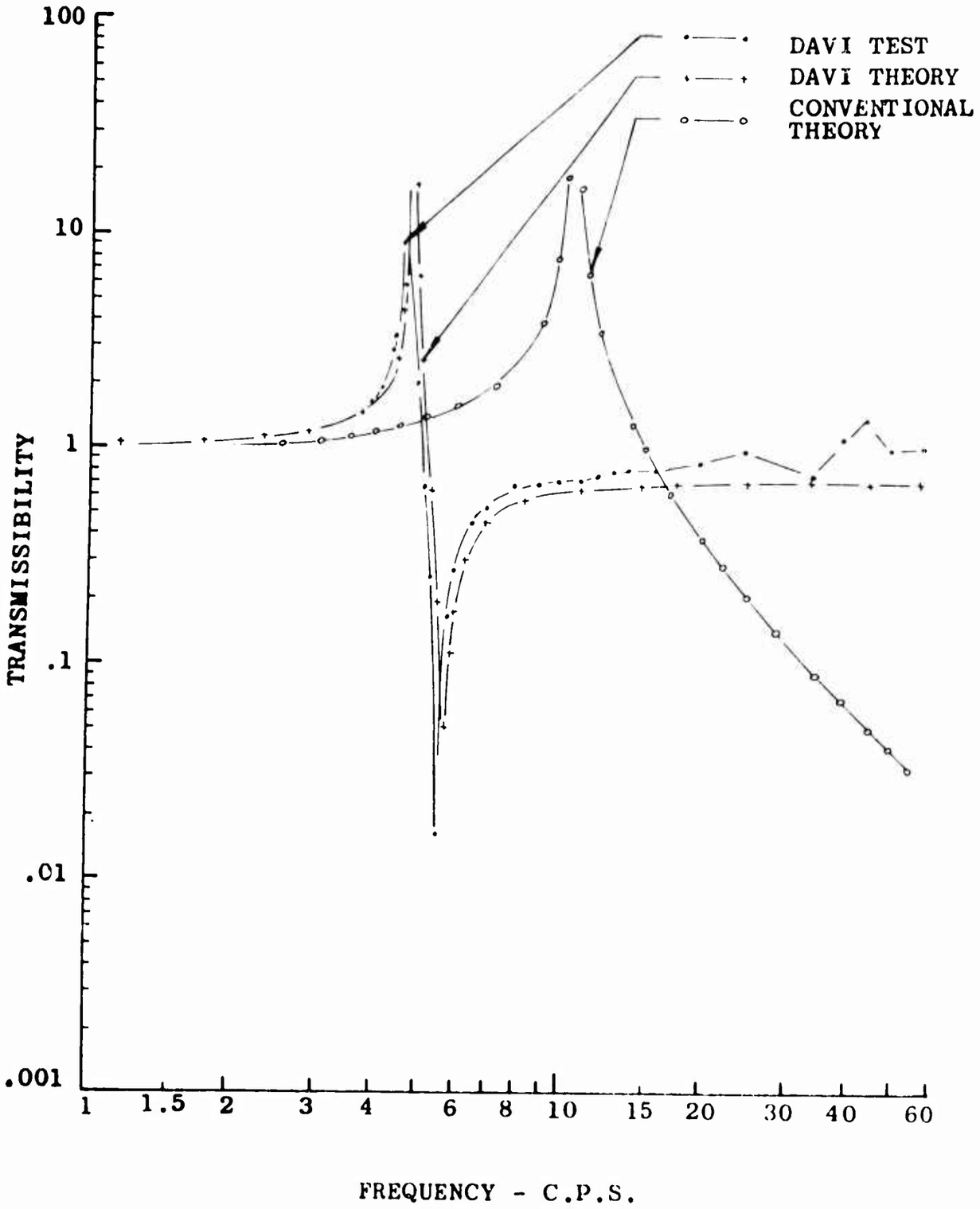

Figure 32. Analytical and Experimental Response Curves of Unidirectional DAVI Alpha for Isolated Weight of 42 Pounds and $\frac{R}{r}$ = -6.131

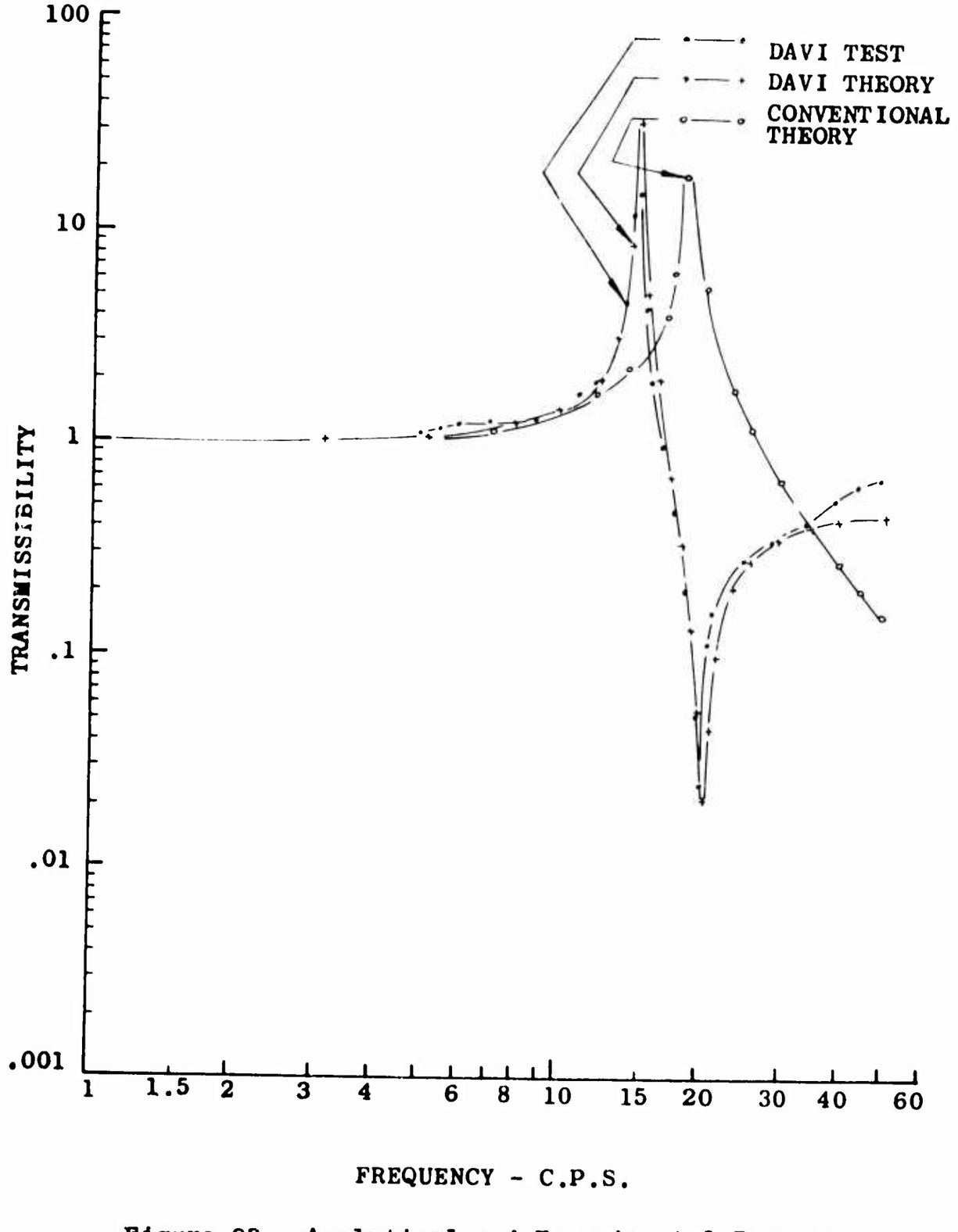

Figure 33. Analytical and Experimental Response Curves of Unidirectional DAVI Alpha for Isolated Weight of 11 Pounds and $\frac{R}{r} = 2.100$

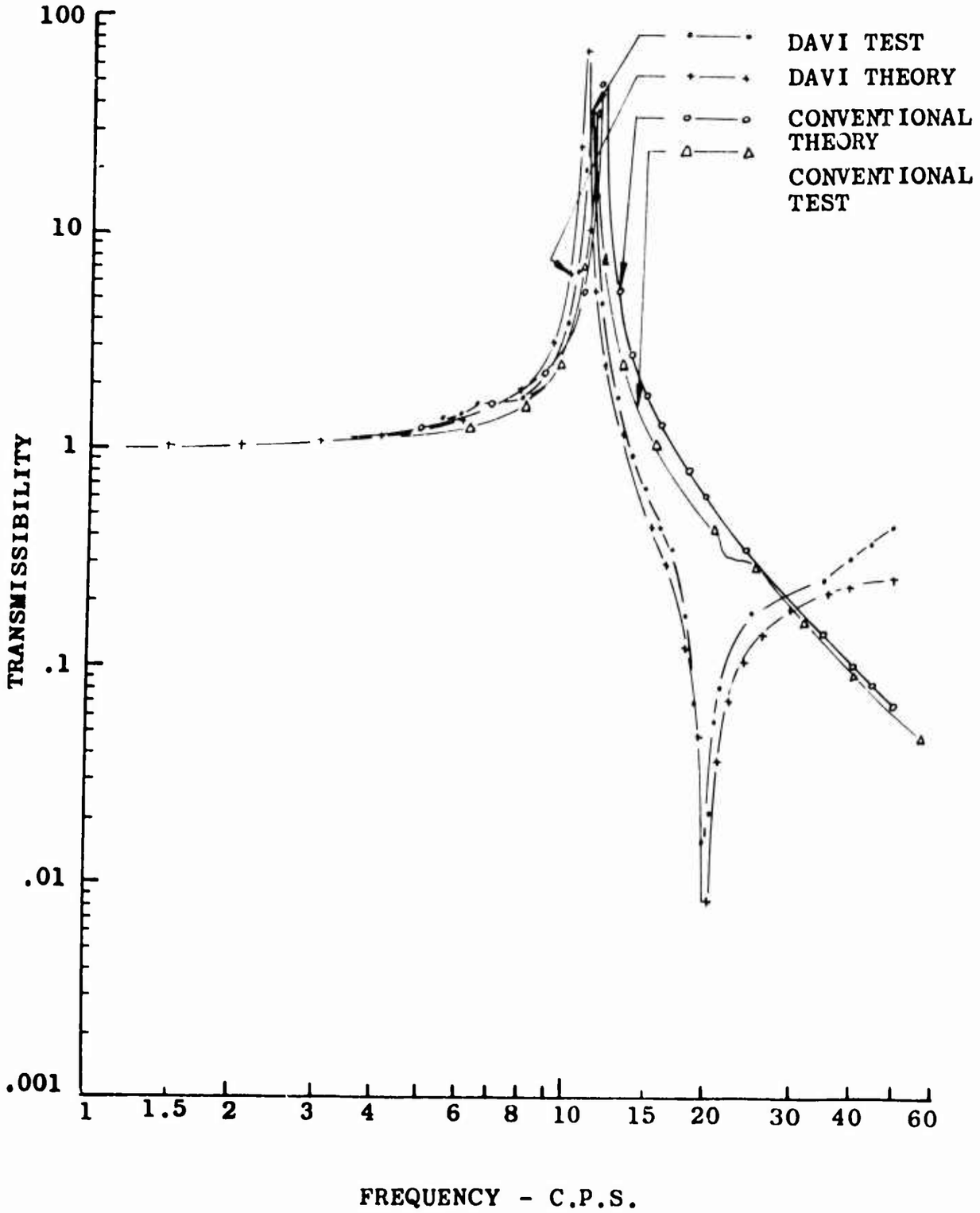

Figure 34. Analytical and Experimental Response Curves of the Unidirectional DAVI Alpha for Isolated Weight of 27 Pounds and $\frac{R}{r}$ = 2.100

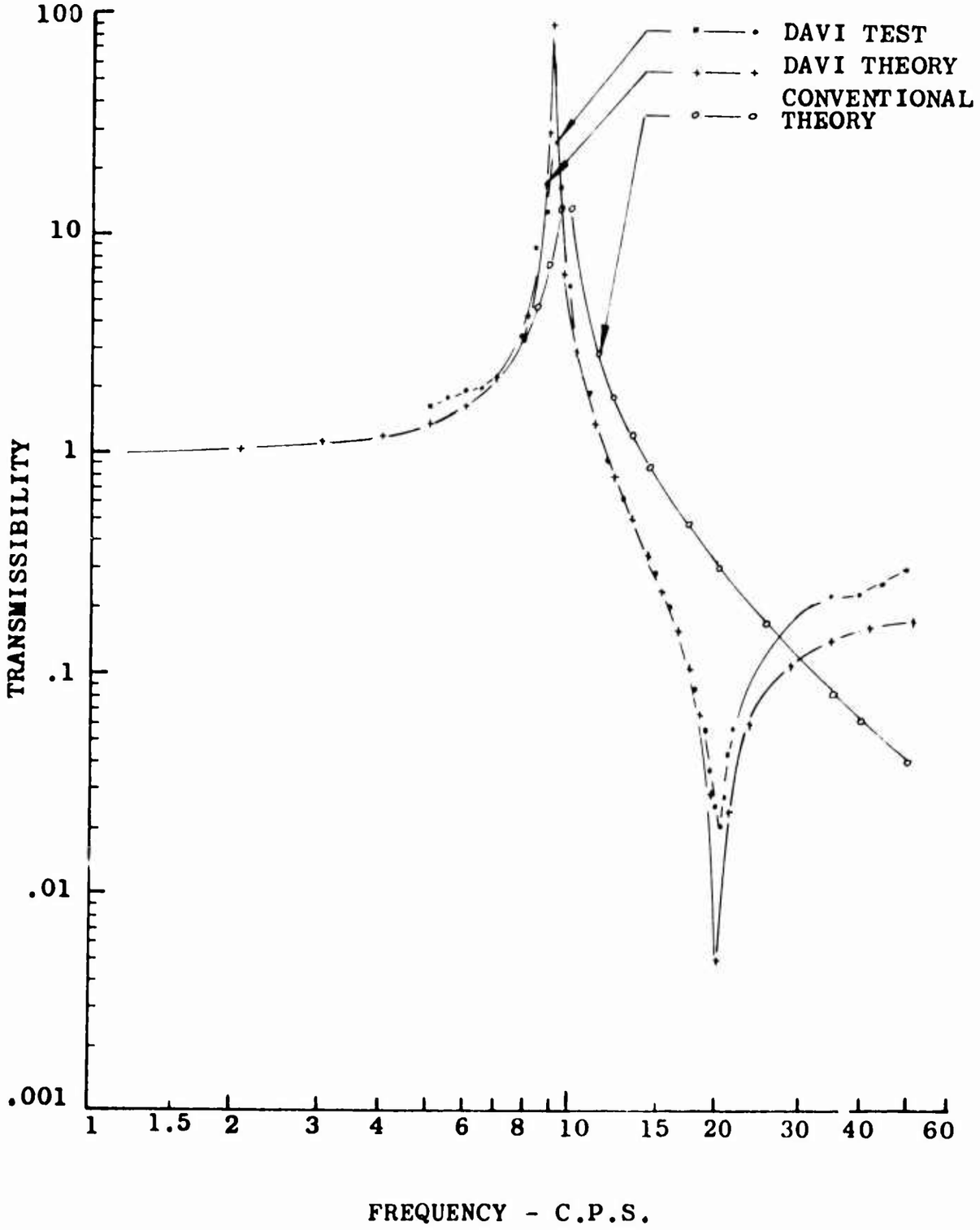

Figure 35. Analytical and Experimental Response Curves of the Unidirectional DAVI Alpha for Isolated Weight of 42 Pounds and $\frac{R}{T}$ = 2.100

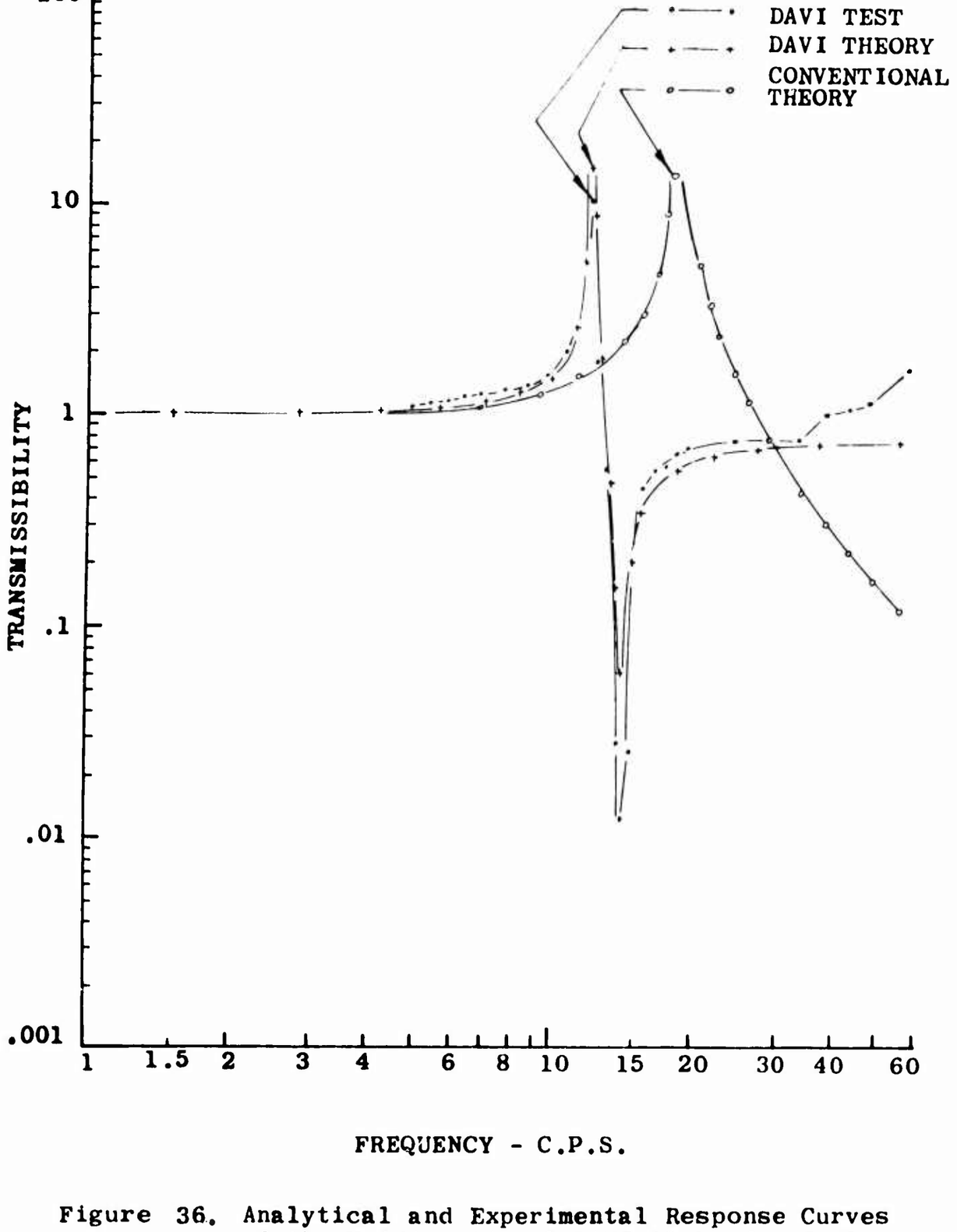

Figure 36. Analytical and Experimental Response Curves of the Unidirectional DAVI Alpha for Isolated Weight of 11 Pounds and $\frac{R}{r} = 2.950$

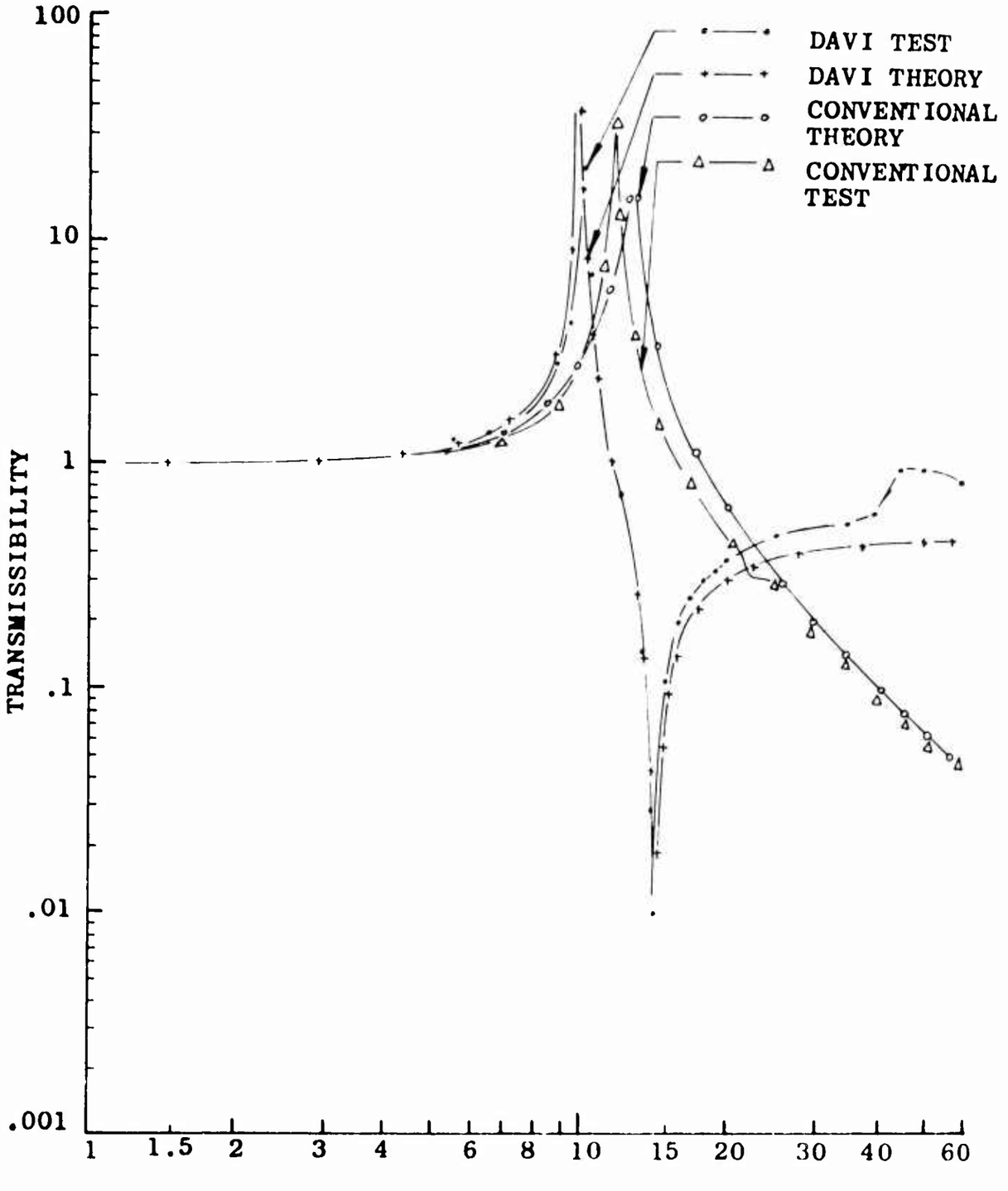

Figure 37. Analytical and Experimental Response Curves of the Unidirectional DAVI Alpha for Isolated Weight of 27 Pounds and $\frac{R}{r}$ = 2.950

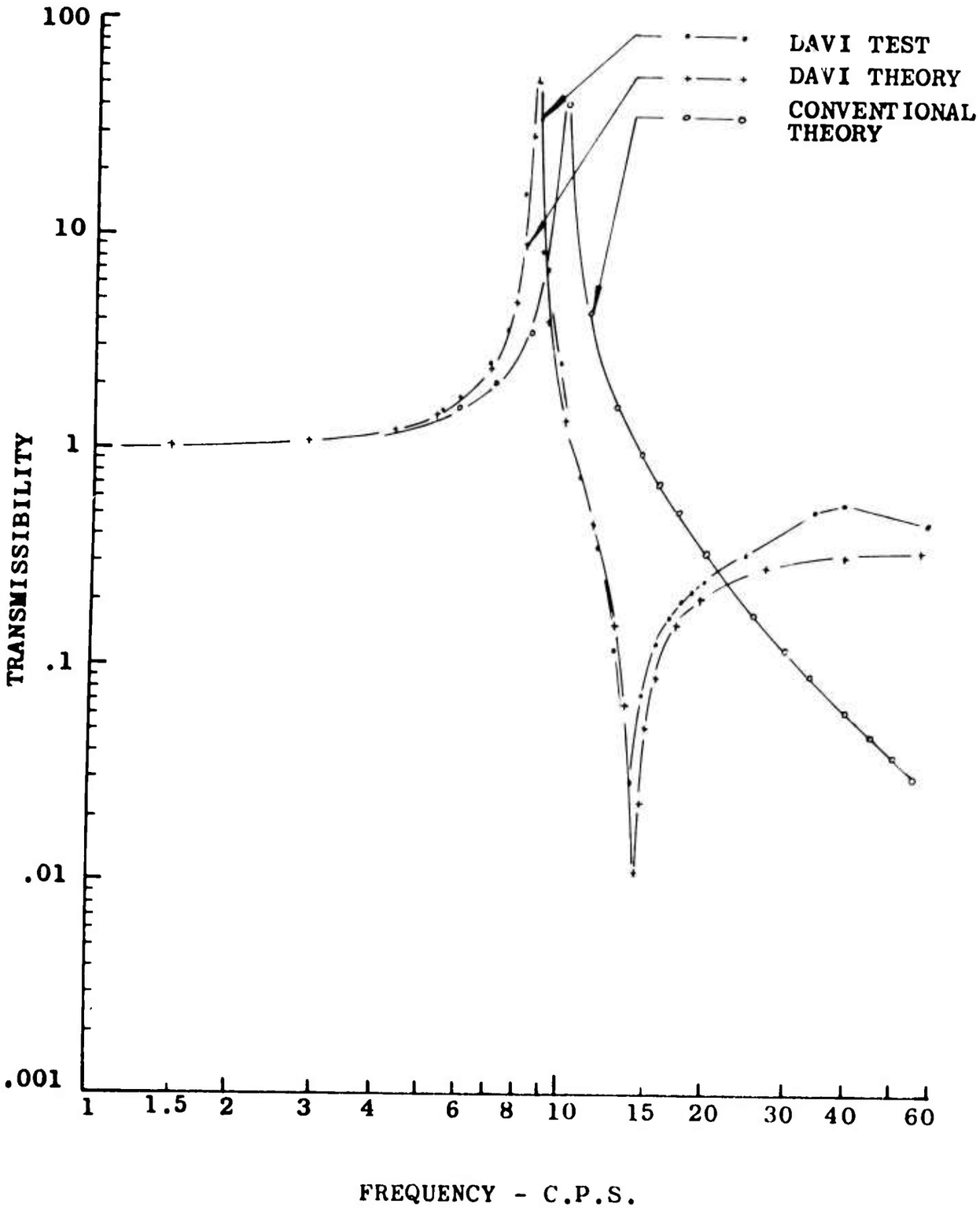

Figure 38. Analytical and Experimental Response Curves of the Unidirectional DAVI Alpha for Isolated Weight of 42 Pounds and $\frac{R}{r}$ = 2.950

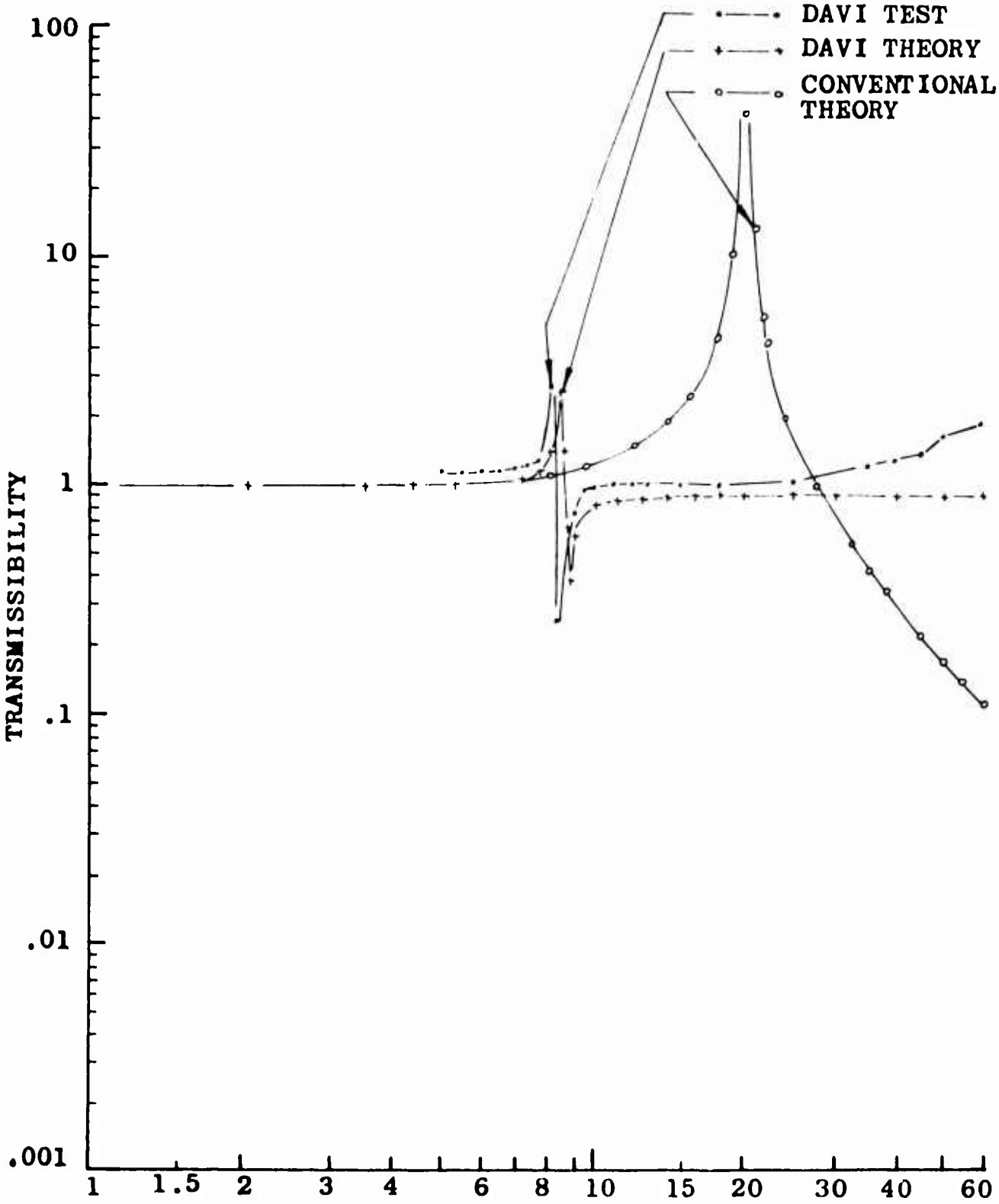

Figure 39. Analytical and Experimental Response Curves of the Unidirectional DAVI Alpha for Isolated Weight of 11 Pounds and $\frac{R}{r} = 4.872$

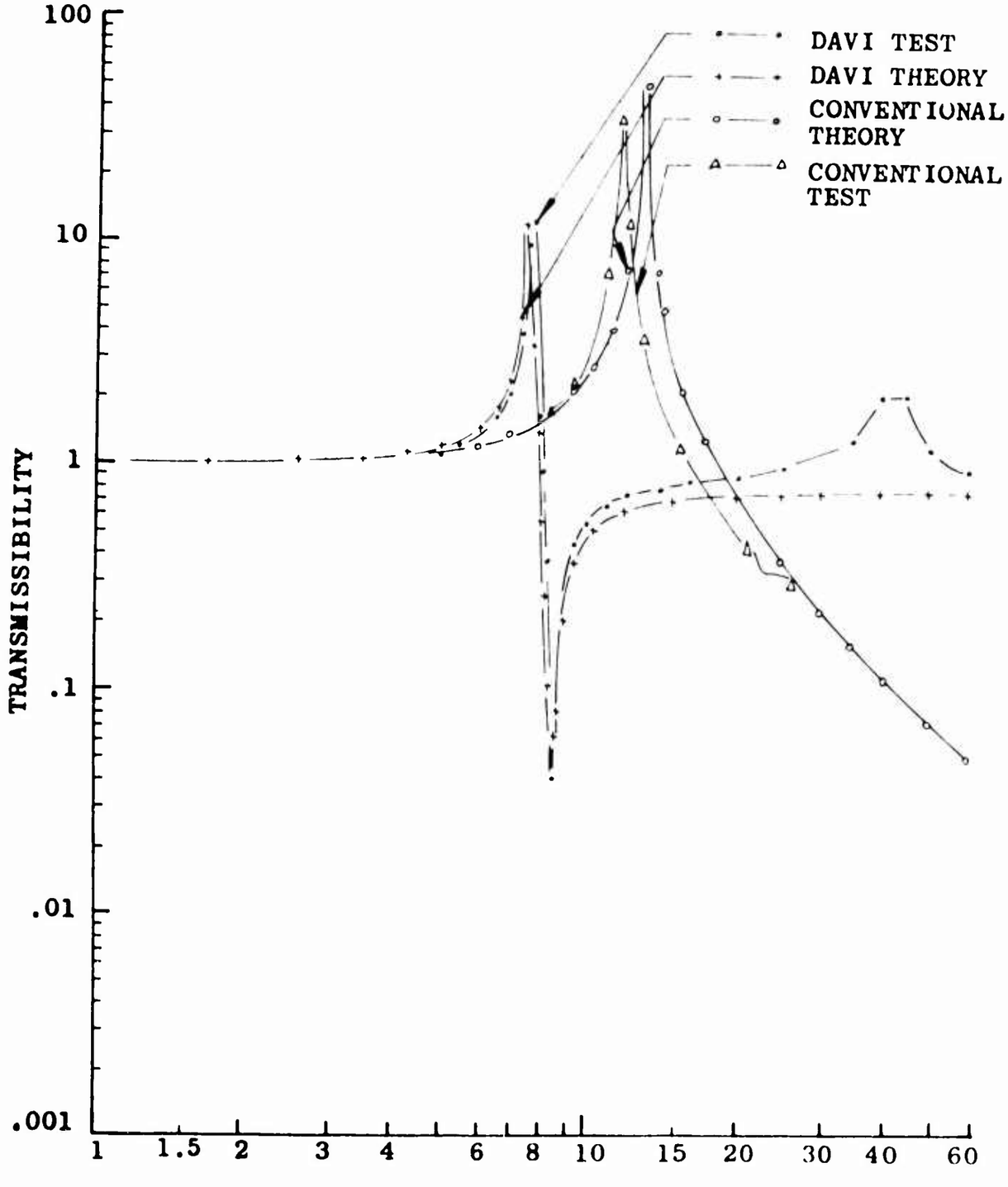

Figure 40. Analytical and Experimental Response Curves of the Unidirectional DAVI Alpha for Isolated Weight of 27 Pounds and $\frac{R}{r} = 4.872$

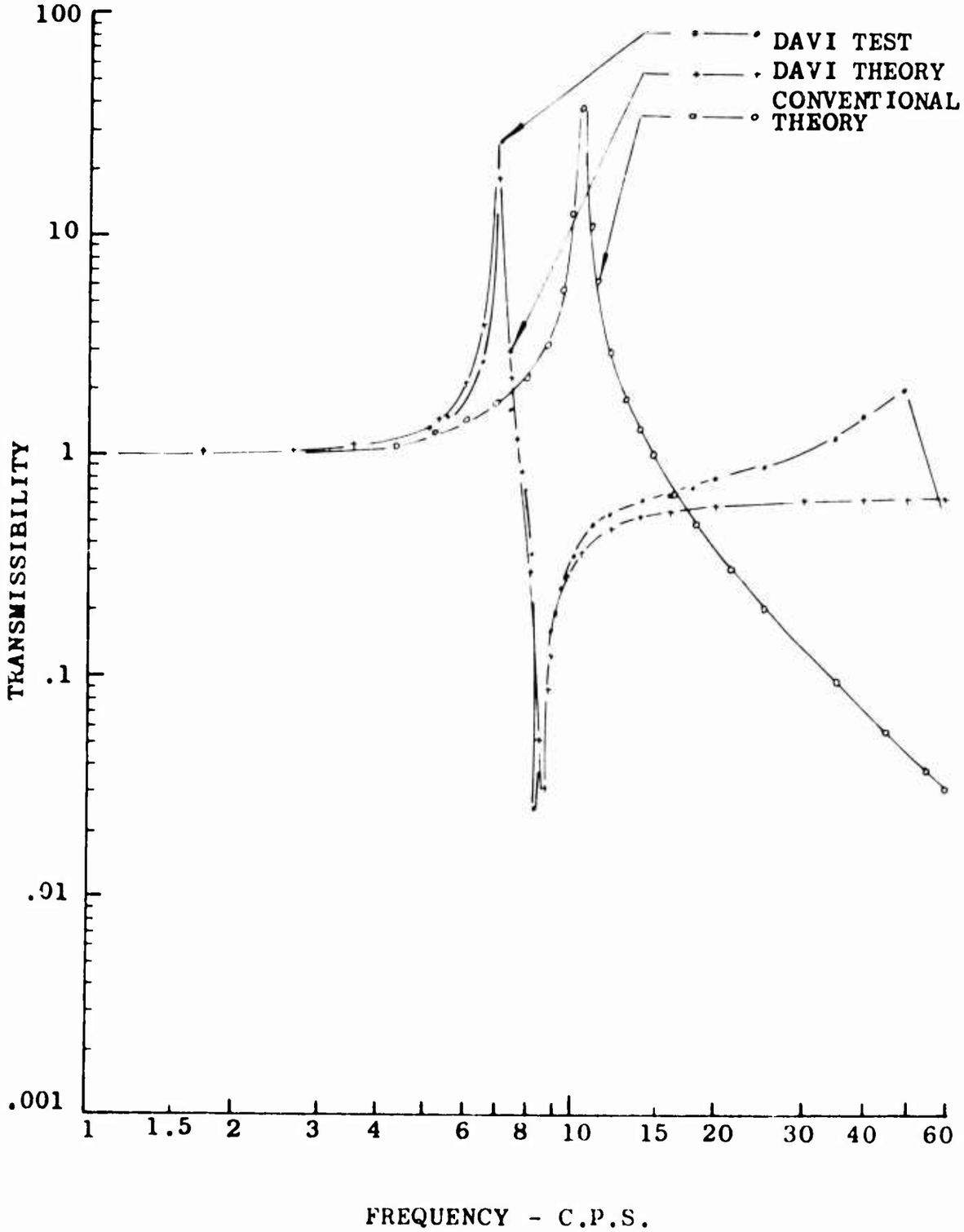

Figure 41. Analytical and Experimental Response Curves of the Unidirectional DAVI Alpha for Isolated Weight of 42 Pounds and $\frac{R}{r} = 4.872$

TWO-DIMENSIONAL DAVI ALPHA

Analysis

Below is a schematic of the two-dimensional DAVI Alpha.

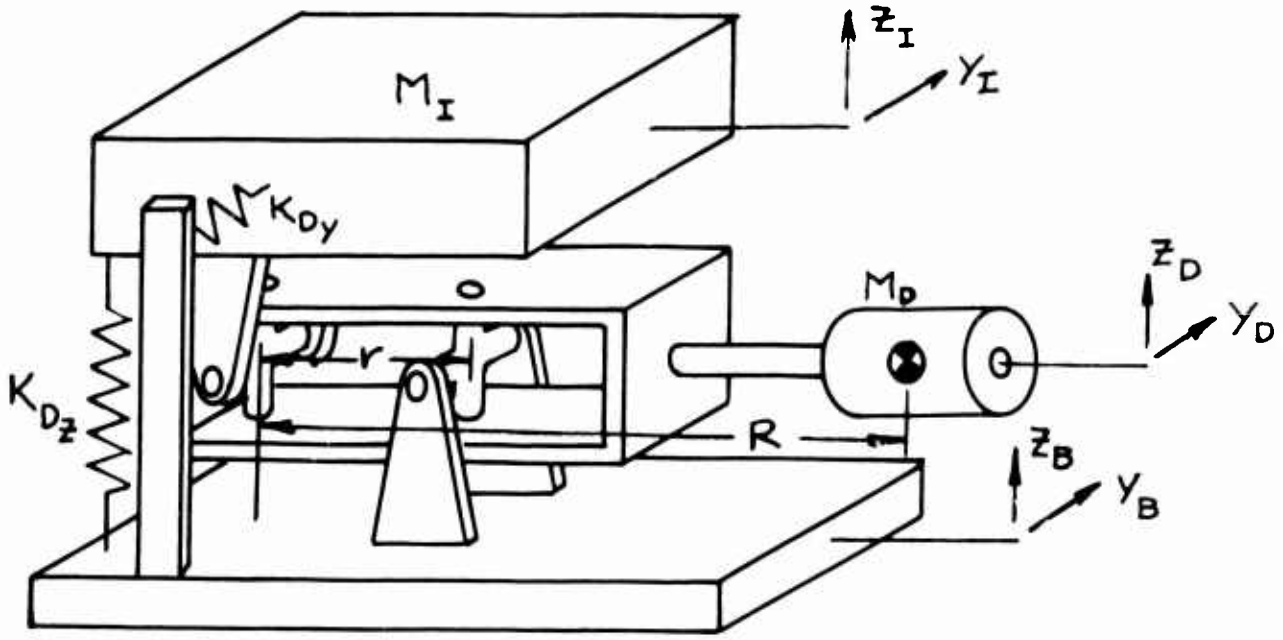

Figure 42. Schematic of Two-Dimensional DAVI Alpha

From the above schematic, the energies of the system may be written

$$T = \frac{1}{2} M_I (\dot{z}_I^2 + \dot{y}_I^2) + \frac{1}{2} M_D (\dot{z}_D^2 + \dot{y}_D^2) + \frac{1}{2} I_z \dot{\theta}_z^2 + \frac{1}{2} I_y \dot{\theta}_y^2 \qquad (52)$$

$$V = \frac{1}{2} K_{D_z} (z_I - z_B)^2 + \frac{1}{2} K_{D_y} (y_I - y_B)^2 \qquad (53)$$

In order to obtain the proper coupling terms and geometric relationships of the inertia bar, the principal axes of the inertia bar were rotated to the axis of the system shown in Figure 43.

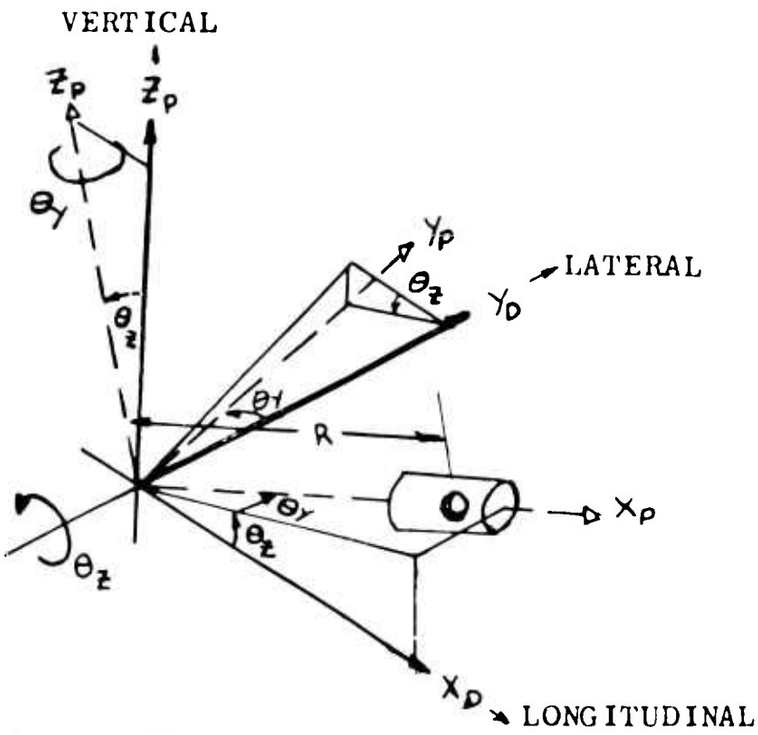

Figure 43. Axes of Inertia Bar

In the above schematic, Z_p , X_p , and Y_p are the principal axes of the inertia bar in which

$$Z_p = 0$$

$$Y_p = 0$$

$$X_p = R$$

First rotating the axes about Z_p results in the following relationship

$$Y' = R \sin\theta_y$$

$$X' = R \cos\theta_y$$

and then rotating the axes about the Y' axis gives

$$Y_D = R \sin\theta_y$$

$$Z_D = R \cos\theta_y \sin\theta_z$$

As in the unidirectional DAVI Alpha, it is seen that

$$\theta_z = \frac{z_B - z_I}{r} \tag{54}$$

$$z_D = z_B \frac{R}{r} - z_I\left(\frac{R}{r}-1\right) \tag{55}$$

$$\theta_y = \frac{y_B - y_I}{r} \tag{56}$$

$$y_D = y_B \frac{R}{r} - y_I\left(\frac{R}{r}-1\right) \tag{57}$$

Substituting the above in the Kinetic Energy Equation (52) results in

$$T = \frac{1}{2}M_I(\dot{y}_I^2+\dot{z}_I^2)+\frac{1}{2}M_D\left\{\left[\dot{y}_B\frac{R}{r}-\dot{y}_I\left(\frac{R}{r}-1\right)\right]^2 + \left[\dot{z}_B\frac{R}{r}-\dot{z}_I\left(\frac{R}{r}-1\right)\right]^2\right\}+\frac{1}{2}\frac{I_y}{r^2}\left(\dot{y}_B-\dot{y}_I\right)^2+\frac{1}{2}\frac{I_z}{r^2}\left(\dot{z}_B-\dot{z}_I\right)^2 \tag{58}$$

Using Lagrange's equation, the equations of motion are

$$\left[M_I+M_D\left(\frac{R}{r}-1\right)^2+\frac{I_y}{r^2}\right]\ddot{y}_I+K_{D_y}y_I-\left[M_D\left(\frac{R}{r}-1\right)\frac{R}{r}+\frac{I_y}{r^2}\right]\ddot{y}_B-K_{D_y}y_B=0 \tag{59}$$

$$\left[M_I+M_D\left(\frac{R}{r}-1\right)^2+\frac{I_z}{r^2}\right]\ddot{z}_I+K_{D_z}z_I-\left[M_D\left(\frac{R}{r}-1\right)\frac{R}{r}+\frac{I_z}{r^2}\right]\ddot{z}_B-K_{D_z}z_B=0 \tag{60}$$

Assuming a steady-state solution of the form $e^{i\omega t}$, the transmissibility equations of the two-dimensional DAVI Alpha are

$$T_{\alpha_Y} = \frac{Y_I}{Y_B} = \frac{K_{DY} - \omega^2\left[M_D \frac{R}{r}\left(\frac{R}{r}-1\right) + \frac{I_Y}{r^2}\right]}{K_{DY} - \omega^2\left[M_I + M_D\left(\frac{R}{r}-1\right)^2 + \frac{I_Y}{r^2}\right]} \tag{61}$$

$$T_{\alpha_Z} = \frac{Z_I}{Z_B} = \frac{K_{DZ} - \omega^2\left[M_D \frac{R}{r}\left(\frac{R}{r}-1\right) + \frac{I_Z}{r^2}\right]}{K_{DZ} - \omega^2\left[M_I + M_D\left(\frac{R}{r}-1\right)^2 + \frac{I_Z}{r^2}\right]} \tag{62}$$

Substituting Equations (9) and (10) into the above two equations, Equations (61) and (62) become

$$T_{\alpha_Y} = \frac{K_{DY} - M_{AY}\omega^2}{K_{DY} - M_{RY}\omega^2} \tag{63}$$

$$T_{\alpha_Z} = \frac{K_{DZ} - M_{AZ}\omega^2}{K_{DZ} - M_{RZ}\omega^2} \tag{64}$$

It is seen from the above expressions that the two-dimensional DAVI Alpha is completely decoupled. However, for motions of the base that are not along the principal axes of the DAVI, installation will result in both Y and Z motions.

In order to determine this effect, a change in coordinates is necessary. Figure 44 shows the coordinate system.

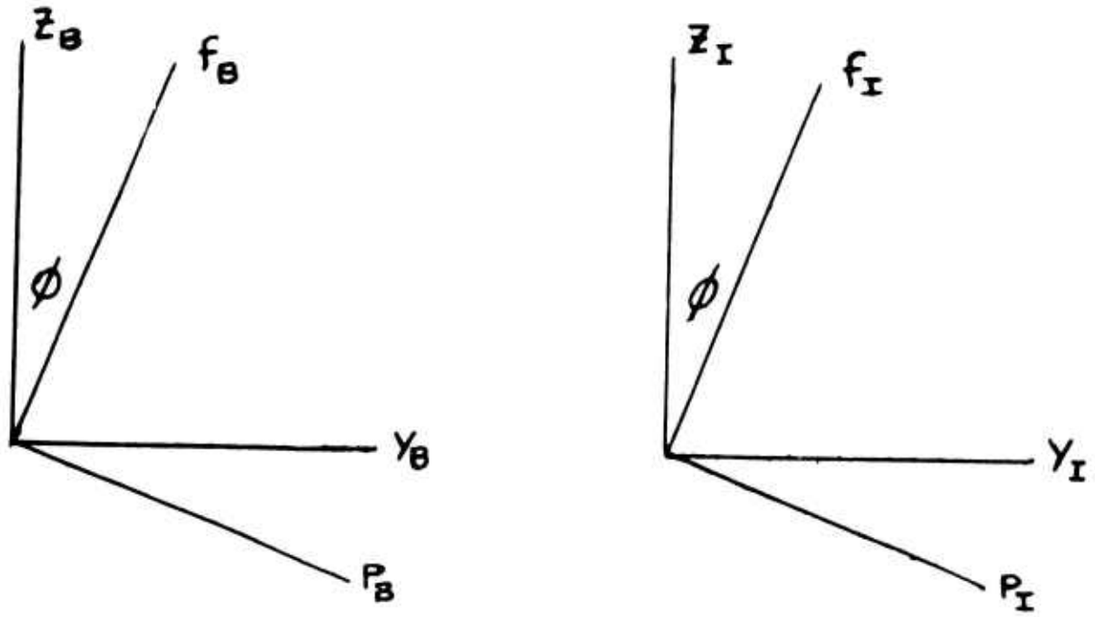

A - Lower Body

B - Isolated Body

Figure 44. Coordinate System of Two-Dimensional DAVI Alpha

In the above coordinate system, Z_B, Y_B, Z_I, and Y_I are the principal axes of the DAVI Alpha, and f_B, P_B, and f_I, P_I are the axes of the motion of the base and isolated body, respectively.

From Figure 44, it is seen that

$$Z_B = f_B \cos\phi - P_B \sin\phi \tag{65}$$

$$Y_B = P_B \cos\phi + f_B \sin\phi \tag{66}$$

$$\ddot{Z}_B = \ddot{f}_B \cos\phi - \ddot{P}_B \sin\phi \tag{67}$$

$$\ddot{Y}_B = \ddot{P}_B \cos\phi + \ddot{f}_B \sin\phi \tag{68}$$

$$Z_I = f_I \cos\phi - P_I \sin\phi \tag{69}$$

$$Y_I = P_I \cos\phi + f_I \sin\phi \tag{70}$$

$$\ddot{z}_I = \ddot{f}_I \cos\phi - \ddot{P}_I \sin\phi \tag{71}$$

$$\ddot{y}_I = \ddot{P}_I \cos\phi + \ddot{f}_I \sin\phi \tag{72}$$

Substituting the above expressions in Equations (59) and (60) results in the following equations of motion:

$$M_{R_Z}\left(\ddot{f}_I \cos\phi - \ddot{P}_I \sin\phi\right) + K_{D_Z}\left(f_I \cos\phi - P_I \sin\phi\right) =$$
$$M_{A_Z}\left(\ddot{f}_B \cos\phi - P_B \sin\phi\right) + K_{D_Z}\left(f_B \cos\phi - P_B \sin\phi\right) \tag{73}$$

$$M_{R_Y}\left(\ddot{f}_I \sin\phi + \ddot{P}_I \cos\phi\right) + K_{D_Y}\left(f_I \sin\phi + P_I \cos\phi\right) =$$
$$M_{A_Y}\left(\ddot{f}_B \sin\phi + P_B \cos\phi\right) + K_{D_Y}\left(f_B \sin\phi + P_B \cos\phi\right) \tag{74}$$

Assuming a solution of the form $q = q_o e^{i\omega t}$, and letting $P_B = 0$, since the motion of the base is along the f_B axis, the equations in matrix form are for convenience, where

$$C_\phi = \cos\phi$$

$$S_\phi = \sin\phi$$

Then

$$\begin{bmatrix} (K_{D_Z} - \omega^2 M_{R_Z}) C_\phi & -(K_{D_Z} - \omega^2 M_{R_Z}) S_\phi \\ (K_{D_Y} - \omega^2 M_{R_Y}) S_\phi & (K_{D_Y} - \omega^2 M_{R_Y}) C_\phi \end{bmatrix} \begin{bmatrix} f_{I_o} \\ P_{I_o} \end{bmatrix} = \begin{bmatrix} (K_{D_Z} - \omega^2 M_{A_Z}) C_\phi f_B \\ (K_{D_Y} - \omega^2 M_{A_Y}) S_\phi f_B \end{bmatrix} \tag{75}$$

Applying Cramer's rule to the above matrix results in the following expressions of transmissibility in the f_I and P_I directions:

$$\frac{f_I}{f_B} = \left[\frac{K_{DY} - \omega^2 M_{AY}}{K_{DY} - \omega^2 M_{RY}}\right] S_\phi^2 + \left[\frac{K_{DZ} - \omega^2 M_{AZ}}{K_{DZ} - \omega^2 M_{RZ}}\right] C_\phi^2 \tag{76}$$

$$\frac{P_I}{f_B} = \left[\frac{K_{DY} - \omega^2 M_{AY}}{K_{DY} - \omega^2 M_{RY}} - \frac{K_{DZ} - \omega^2 M_{AZ}}{K_{DZ} - \omega^2 M_{RZ}}\right] S_\phi C_\phi \tag{77}$$

However, from Equation (11), it is seen that the above equations can be rewritten as

$$\frac{f_I}{f_B} = T_{\alpha Y} S_\phi^2 + T_{\alpha Z} C_\phi^2 \tag{78}$$

$$\frac{P_I}{f_B} = (T_{\alpha Y} - T_{\alpha Z}) S_\phi C_\phi \tag{79}$$

It is seen from the above expressions that the transmissibility in the f_I and P_I directions is a function of the transmissibilities of the two-dimensional DAVI along the DAVI's principal axes. It is also seen that motion of the isolated body occurs at 90^o to the input as well as in the direction of the input.

The effective absolute amplitude and phasing can be determined from the following diagram.

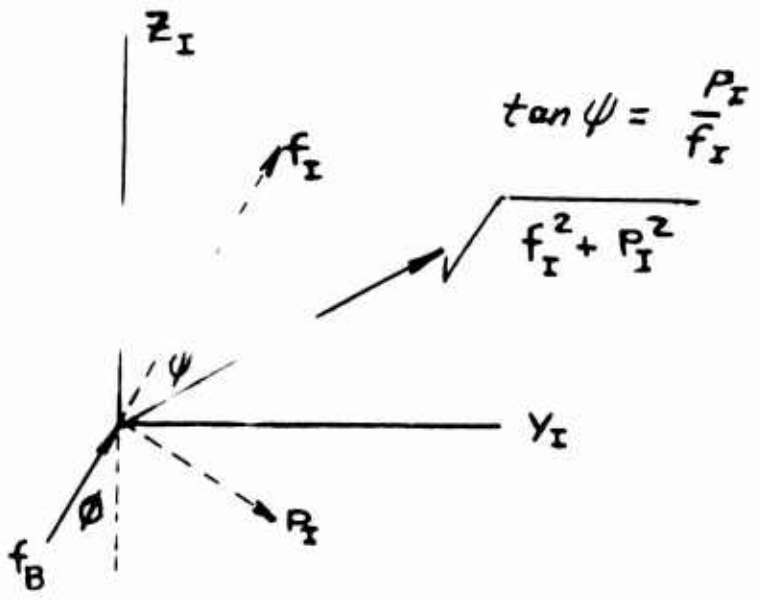

Figure 45. Phasing and Absolute Amplitude of the Two-Dimensional Transmissibility

Calculations were done to obtain the transmissibility of the two-dimensional DAVI Alpha. Figures 46 through 50 show the result of these calculations, in which the absolute transmissibility is plotted versus the angle of input, resulting in the polar plot. Table III gives the physical parameters used in the calculations of the nonisotropic two-dimensional DAVI.

TABLE III

PHYSICAL PARAMETERS OF TWO-DIMENSIONAL DAVI ALPHA

Frequency Of Input (c.p.s.)	Natural Frequency (c.p.s.)		Antiresonant Frequency (c.p.s.)		Figure Number
ω	ω_{Rz}	ω_{RY}	ω_{Az}	ω_{AY}	
8	9.3	6.5	25	17.7	46
17.7	9.3	6.5	25	17.7	47
25	9.3	6.5	25	17.7	48
30	9.3	6.5	25	17.7	49
25	16.0	6.5	25	17.7	50

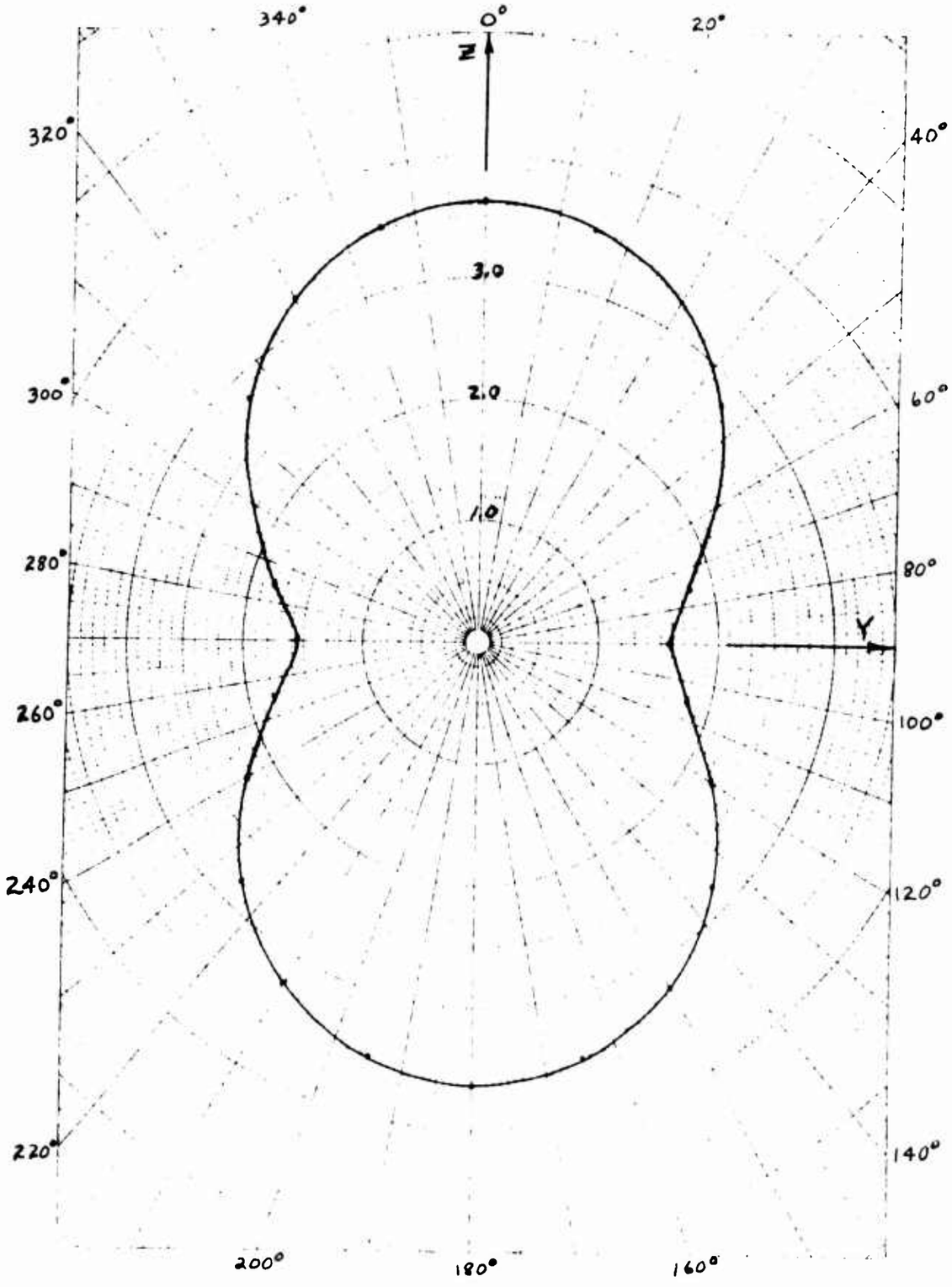

Figure 46. Transmissibility of the Two-Dimensional DAVI Alpha Around the Azimuth for a Frequency Input of 8 C.P.S.

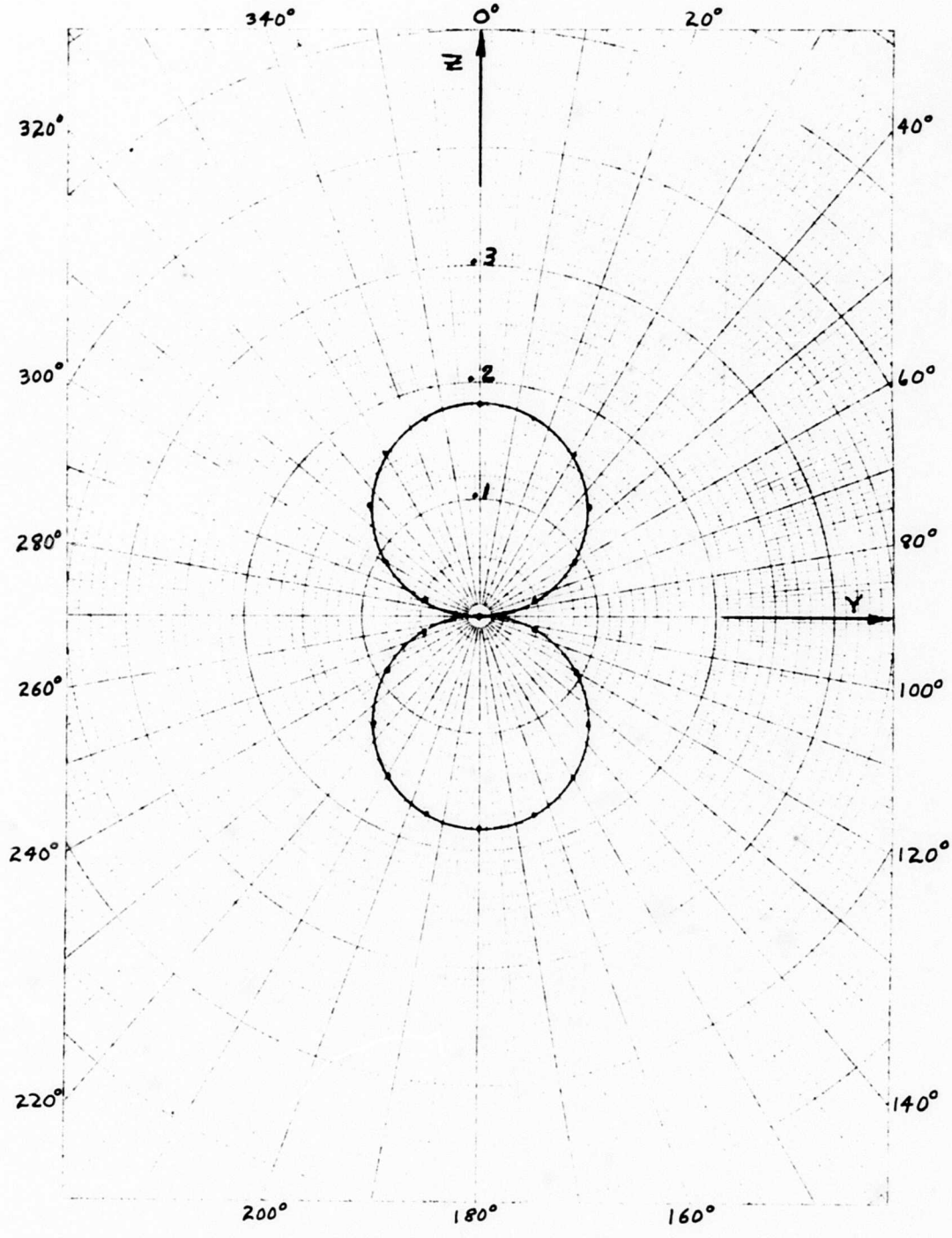

Figure 47. Transmissibility of the Two-Dimensional DAVI Alpha Around the Azimuth for a Frequency Input of 17.7 C.P.S.

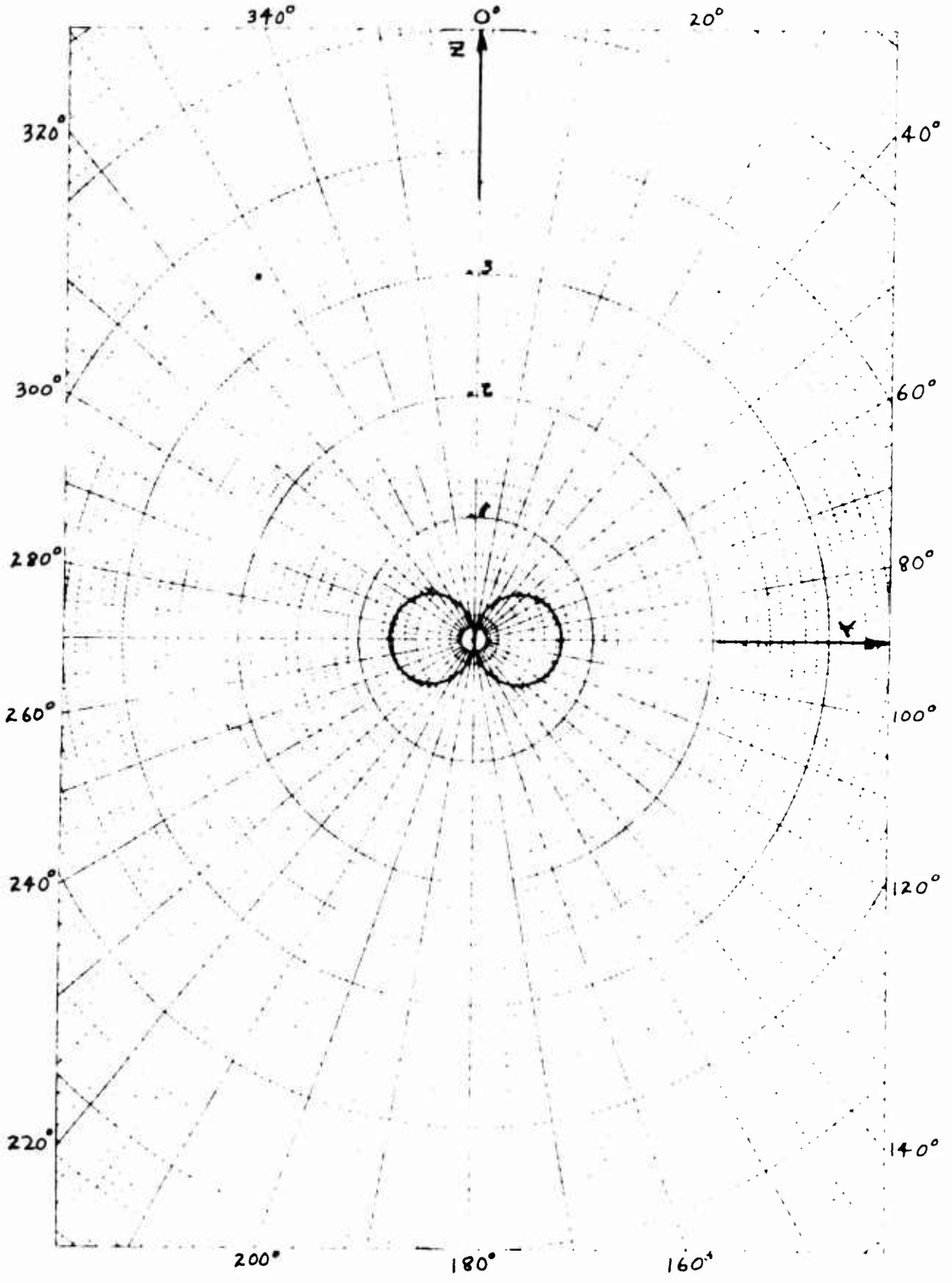

Figure 48. Transmissibility of the Two-Dimensional DAVI Alpha Around the Azimuth for a Frequency Input of 25 C.P.S.

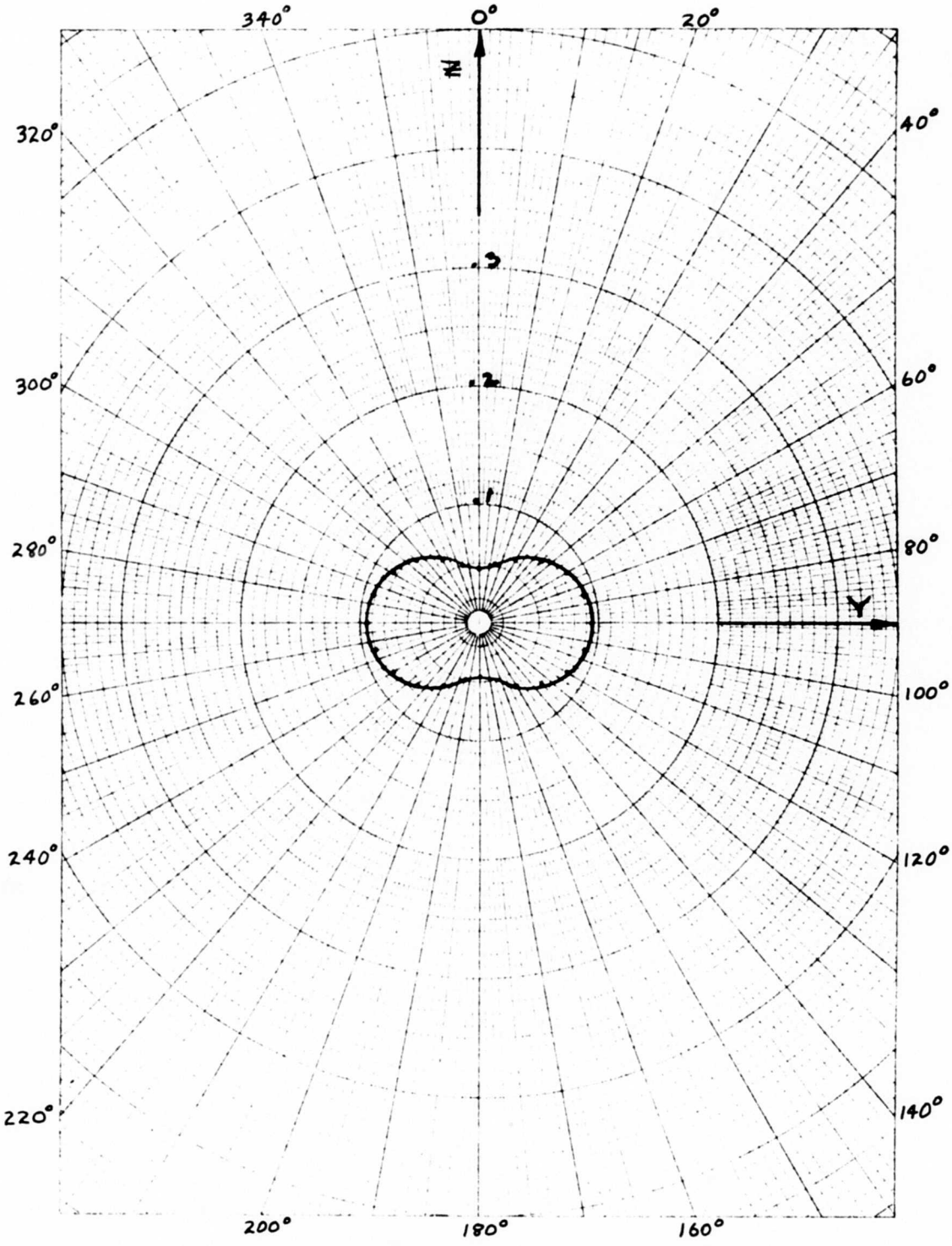

Figure 49. Transmissibility of the Two-Dimensional DAVI Alpha Around the Azimuth for a Frequency Input of 30 C.P.S.

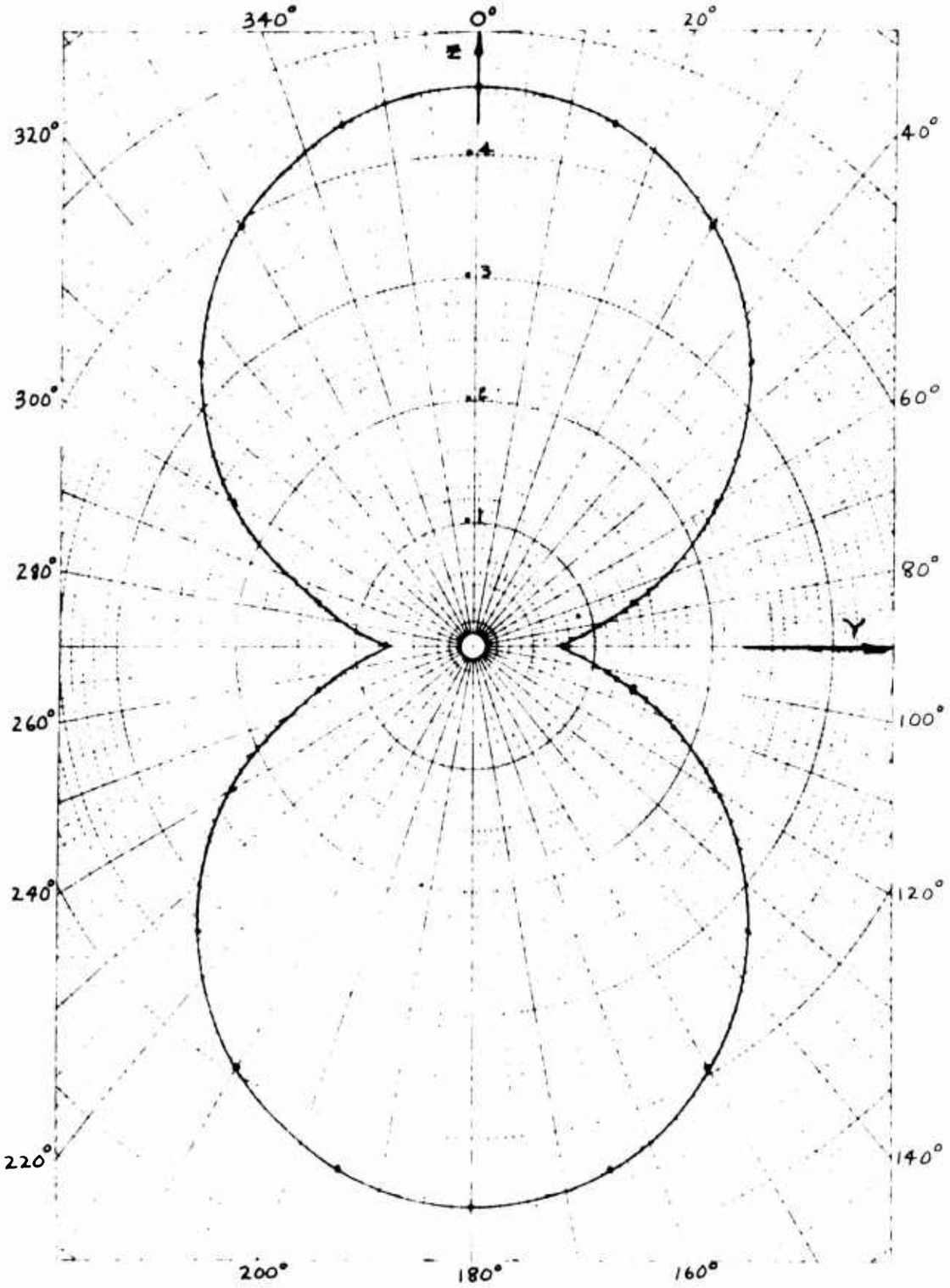

Figure 50. Transmissibility of the Two-Dimensional DAVI Alpha Around the Azimuth for a Frequency Input of 25 C.P.S.

It is seen in Figures 45 through 49 that a figure eight-type lissajous pattern is obtained and that the magnitude of the transmissibility depends upon the angular orientation of the two-dimensional DAVI Alpha to the input.

Design Criteria

In many applications it will be desirable to so design a two-dimensional DAVI that the dynamic properties in one direction will be different from those in an orthogonal direction; that is, for example, a vertical antiresonant frequency different from the lateral antiresonant frequency. This can be physically accomplished in three ways: first, the pivots can be Hooke's joints with non-intersecting crossarms giving different pivot separations (r) in the two principal directions; secondly, the two principal spring rates can be different; and thirdly, the principal mass moments of inertia of the bar can be made different. Any combination of these three methods can also be used.

The analyses have considered a DAVI in which the principal elastic axes, the principal inertial axes, and the pivot axes are parallel. The transmissibility of the DAVI in a principal direction is given by the equations for a unidirectional DAVI Alpha as the principal axes are decoupled. However, the transmissibility in a direction oblique to the principal axes is a function of the principal transmissibilities and the angle between the principal axes and the direction under consideration. Further, there is a response (vibration) of the isolated body in a direction perpendicular to the direction of excitation when the excitation is obliquely applied in a nonisotropic DAVI. The response of the isolated body to excitations of different frequencies and applied at various oblique angles is obtained by summation of the individual responses as the Principle of Superposition applies.

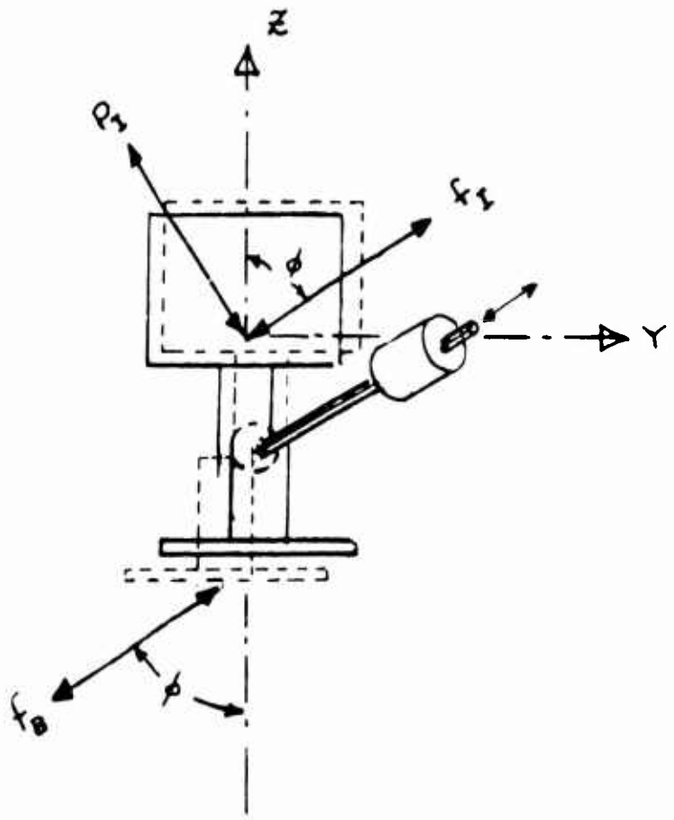

Figure 51. Two-Dimensional DAVI Alpha With Base Excitation Applied To Angle ϕ To Principal Axis

In Figure 51, Z is either one of the two principal DAVI axes. The base excitation of amplitude f_B is applied at angle ϕ to the Z axis. The isolated body responds with amplitude f_I in a direction parallel to f_B, the excitation, and with amplitude P_I in a direction perpendicular to the direction of the base excitation. The designer, using the basic unidirectional DAVI equations or the design charts - Figures 5A through 10C - will have determined the principal axes' transmissibilities, $T_{\alpha Z}$ and $T_{\alpha Y}$, at the frequency under consideration. He can determine the transmissibility in an oblique direction using Equation (80), and he can find the "orthogonal transmissibility" (P_I/f_B) using Equation (81). Equations (80) and (81) are simply nondimensionalized forms of Equations (78) and (79).

$$\frac{f_I/f_B}{T_{\alpha Z}} = 1 + \left(\frac{T_{\alpha Y}}{T_{\alpha Z}} - 1\right) S_\phi^2 \qquad (80)$$

$$\frac{P_I/f_B}{T_{\alpha_Z}} = \left(\frac{T_{\alpha_Y}}{T_{\alpha_Z}} - 1\right) S_\phi C_\phi \qquad (81)$$

Equation (80) is plotted in Figure 52, and Equation (81) is plotted in Figure 53.

To illustrate the use of these curves, consider a two-dimensional nonisotropic DAVI with a transmissibility of .40 in the principal direction called Z and a transmissibility of .80 in the orthogonal direction at the frequency in question. This gives $T_{\alpha_Y}/T_{\alpha_Z} = 2.0$. First, let the excitation at this frequency be applied at an angle of 0° or along the Z axis. From Figure 52, following the $T_{\alpha_Y}/T_{\alpha_Z} = 2.0$ branch of the curve to the angle of 0°, it is seen that the transmissibility in the direction of the excitation is $1.0\ T_{\alpha_Z}$ or .40. From Figure 53, following the $T_{\alpha_Y}/T_{\alpha_Z} = 2.0$ branch of the curve to the angle of 0°, it is seen that the transmissibility in the orthogonal direction or the Y axis is zero.

Now let the excitation at this frequency be applied at an angle of 30° to axis Z. From Figure 52, following the $T_{\alpha_Y}/T_{\alpha_Z} = 2.0$ branch of the curve to an angle of 30°, it is seen that the transmissibility in the direction of the excitation is $1.25\ T_{\alpha_Z}$ or .5. From Figure 53, following the $T_{\alpha_Y}/T_{\alpha_Z} = 2.0$ branch of the curve to the angle 30°, it is seen that the transmissibility in the orthogonal direction is approximately $.43\ T_{\alpha_Z}$ or .172.

If the excitation at this frequency is applied at an angle of 90° to the axis Z, then from Figure 52 following the $T_{\alpha_Y}/T_{\alpha_Z} = 2.0$ branch of the curve to the angle of 90°, it is seen that the transmissibility in the direction of the excitation is $2.0\ T_{\alpha_Z}$ or .80. This is the transmissibility of the principal axis along the Y direction. From Figure 53, following the $T_{\alpha_Y}/T_{\alpha_Z} = 2.0$ branch of the curve to the angle 90°, it is seen that the transmissibility in the orthogonal direction or Z axis is zero.

These examples illustrate that in Figure 52, the transmissibility in the direction of excitation varies between the values of transmissibilities of the principal axes (T_{α_Y} & T_{α_Z}) and reaches these values at the four cardinal angles of excitation. In Figure 53, the orthogonal transmissibilities reach zero at the four cardinal angles of excitation; this rosette plot results from the fact that the principal directions are uncoupled in the equations of motion.

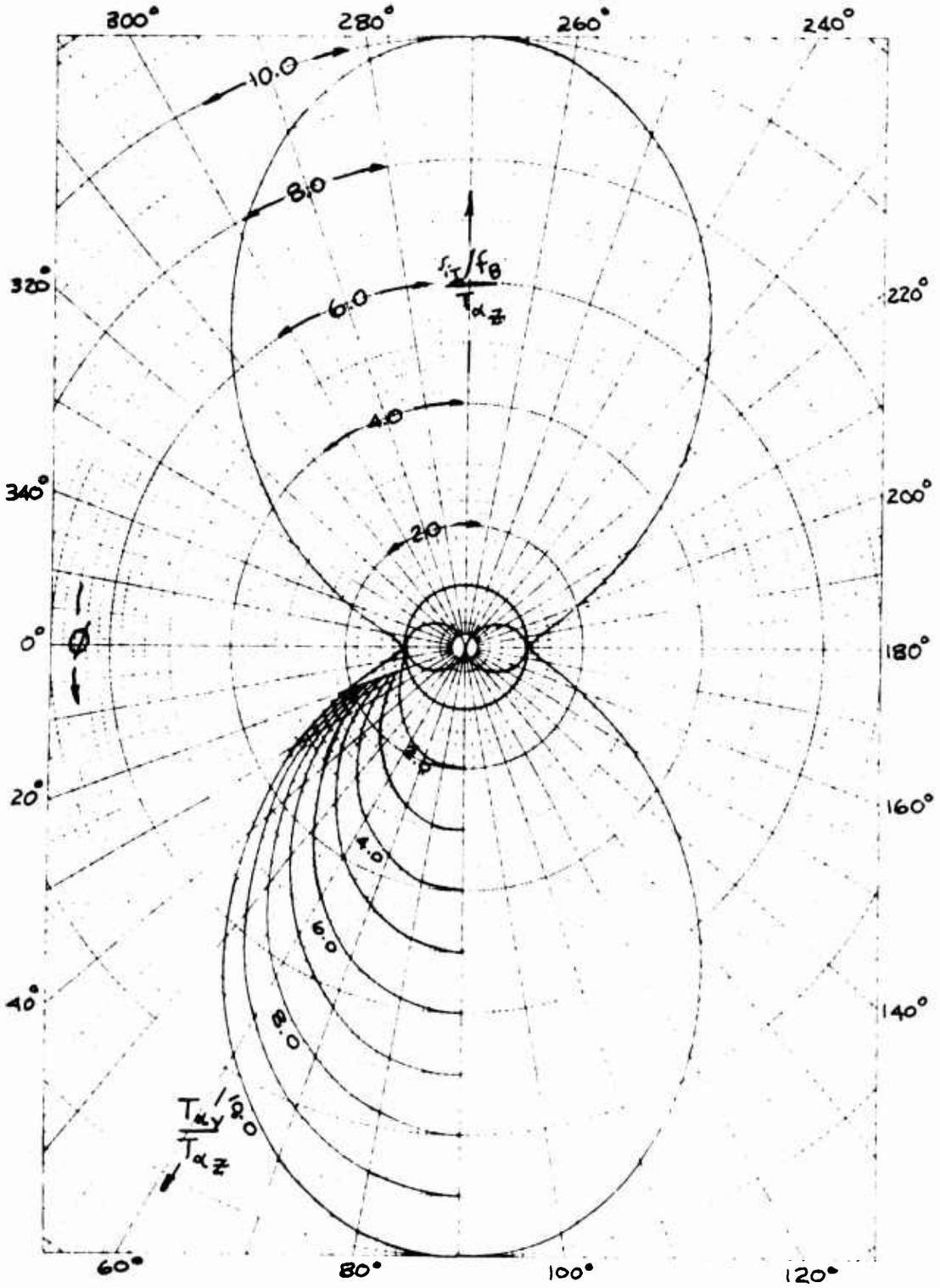

Figure 52. Design Chart for Two-Dimensional DAVI Alpha

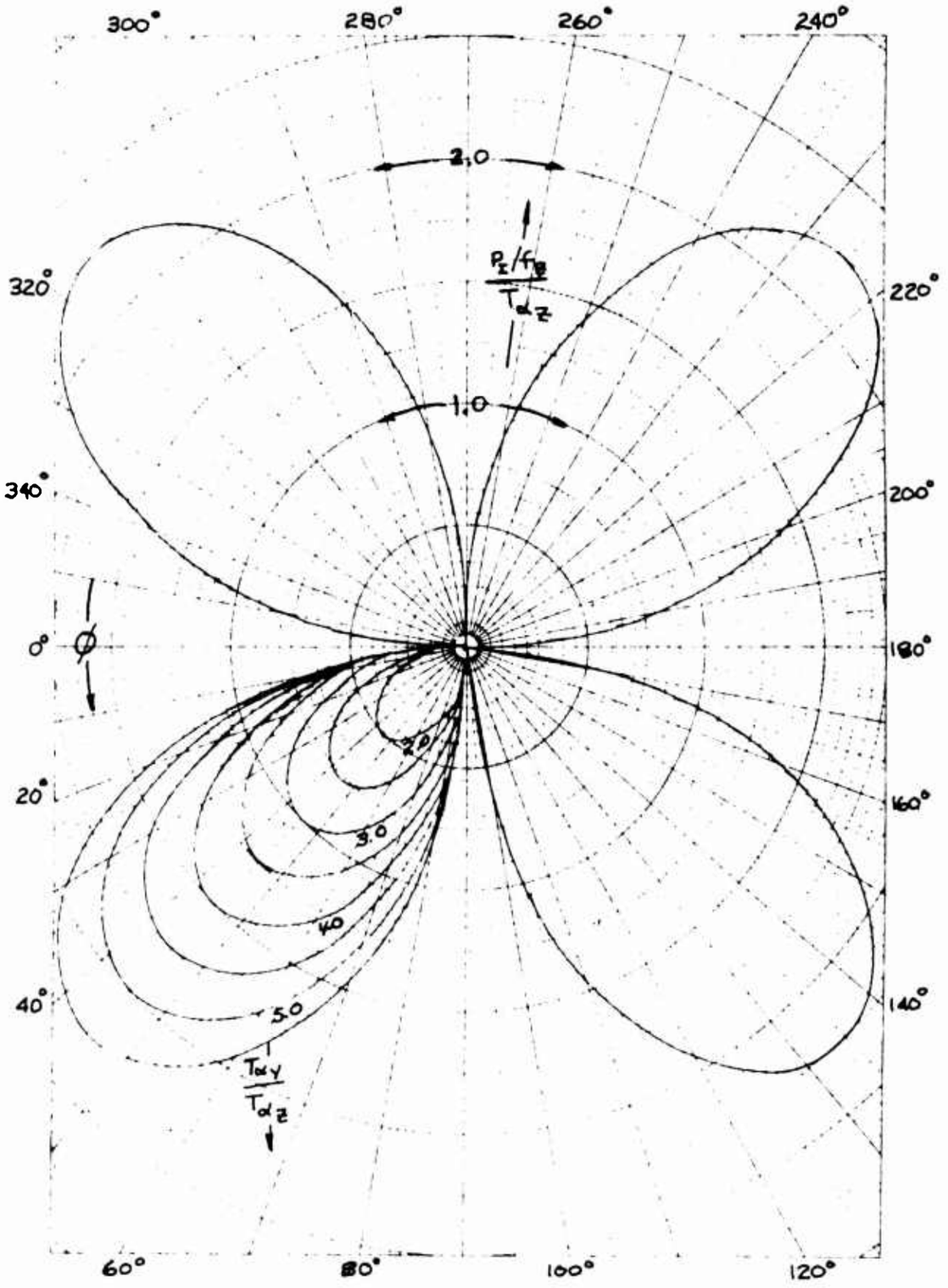

Figure 53. Design Chart for Two-Dimensional DAVI Alpha

Test Fixture

The test fixture used for these tests is essentially the same as that shown in Figures 13 and 14. However, the bronze bushings on the base and isolated weight were changed to allow for lateral translation as well as longitudinal translation. This change is shown in the following schematic.

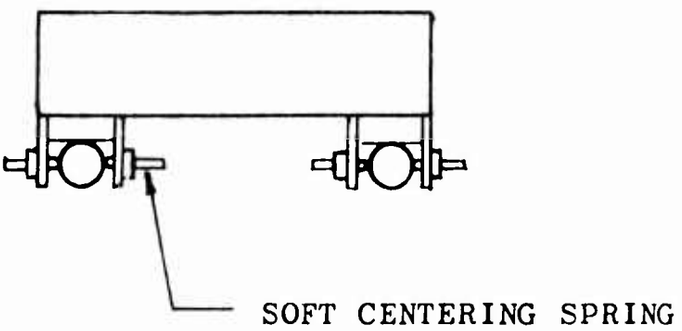

Figure 54. Schematic of Weight on Test Fixture Allowing Lateral Translation

Lateral motions of $\pm$1/8 inch were obtainable before the stops were hit.

Equipment and Procedure

Figure 55 is a photograph of the test setup showing the installation of the two shakers. In this test, an MB Model C-11 electromagnetic shaker with a force capability of 50 pounds was connected to the base weight to excite the longitudinal response.

An MB Model S-DA electromegnetic shaker with a force capability of 10 pounds was connected to the base weight to excite the lateral response. Both shakers were connected to a common oscillator so that an exact frequency input could be obtained. In one test, the 10-pound shaker was disconnected, and the 50-pound shaker was connected at an angle of 29^{o} to the longitudinal axis. Test results were also obtained by shaking in the longitudinal direction with the lateral shaker disconnected, and then by shaking in the lateral direction with the longitudinal shaker disconnected. Four MB velocity pickups were used. Two were attached longitudinally and laterally to the base weight to obtain the input. Two pickups were attached longitudinally and laterally to the isolated weight to obtain the output. The output of the pickups was fed through filters to reduce the inherent noise level from the test fixture and then to a Hewlett Packard Model Scope for visual display. Data were recorded manually from the scope, and the transmissibility was obtained by dividing the output readings by the input readings.

The two-dimensional DAVI Alpha model tested is shown in the test fixture (Figure 55). This two-dimensional model was of similar design to the unidirectional DAVI Alpha tested. The pivots were the ball and socket type, allowing complete freedom of the inertia bar in a plane perpendicular to the bar. Lateral restraint was provided by two metal coil springs giving approximately three-fourths spring rate as obtained in the longitudinal direction. It was realized that friction in the bearings could be a problem. However, if good results could be obtained from this type of configuration, this could be an ideal configuration for isolation of large packages.

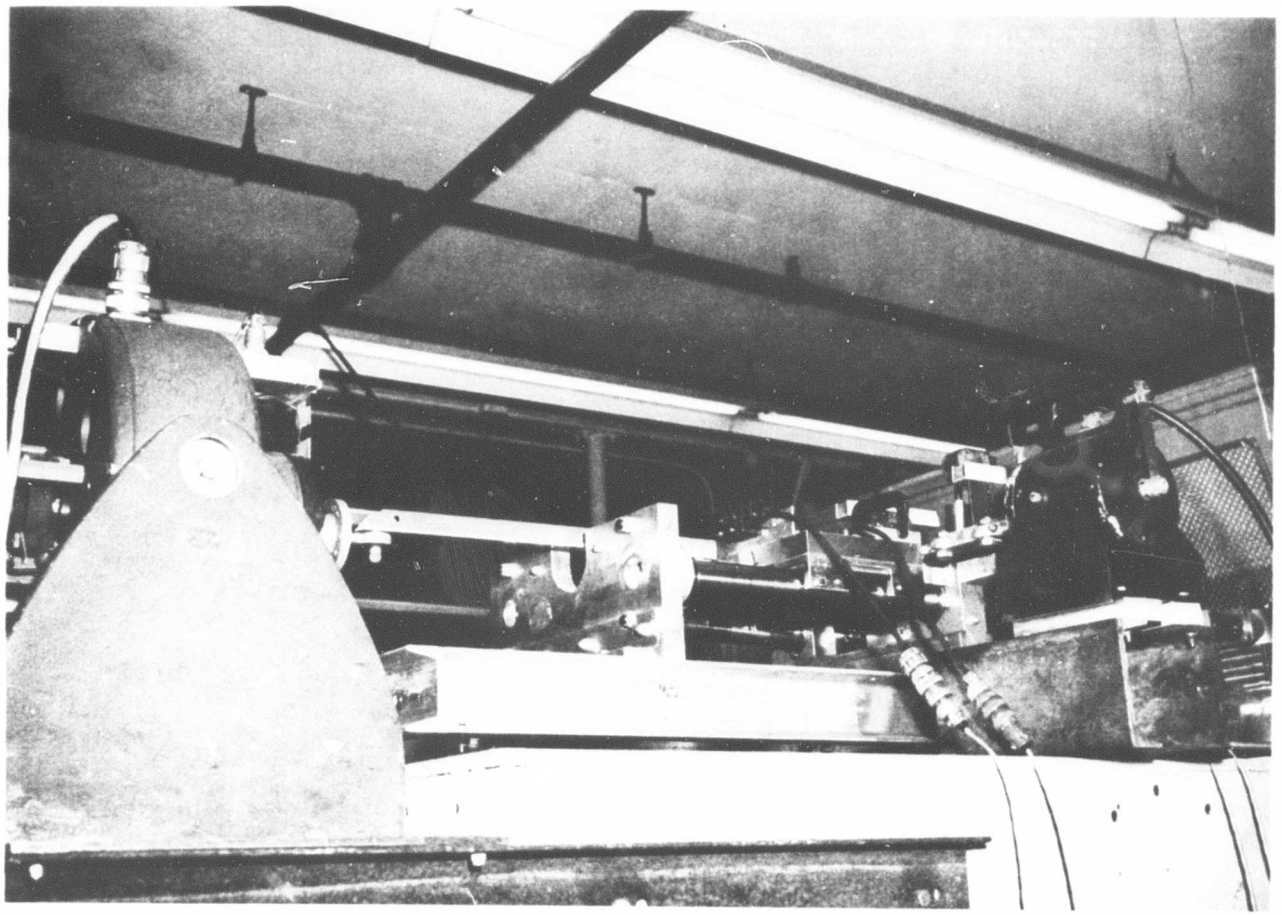

Figure 55. Installation of Two Shakers for Two-Dimensional DAVI Alpha Testing

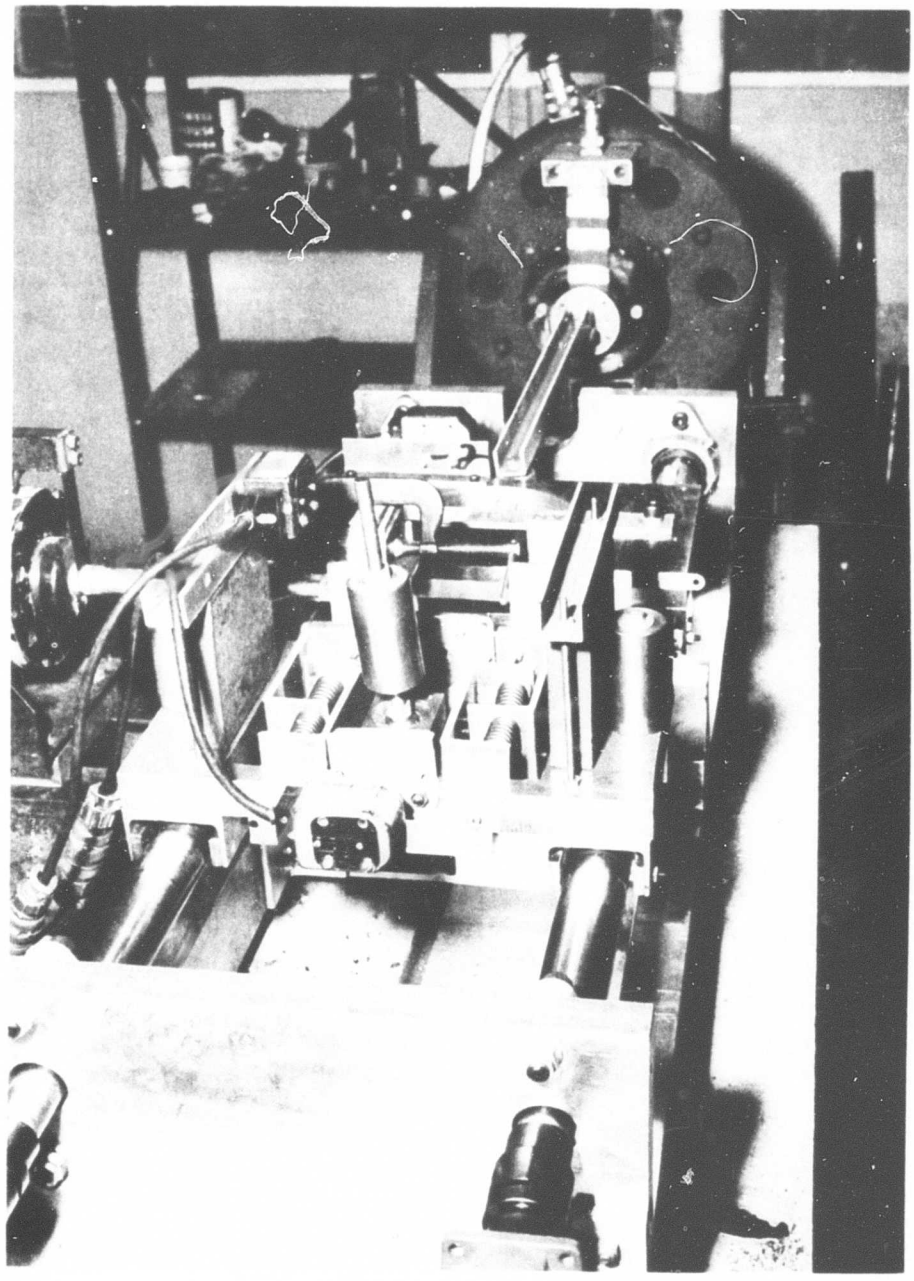

Figure 56. Installation of the Two-Dimensional DAVI Alpha Model in Test Rig

Results

Figures 57 through 60 show the results of the tests. The table below gives the configurations tested.

TABLE IV

TWO-DIMENSIONAL DAVI ALPHA TESTS

Isolated Weight (Lb)	DAVI Inertia Bar Weight (Lb)	R/r	ρ/r	Spring Rate Longitudinal (Lb/In.)	Spring Rate Lateral (Lb/In.)	Direction of Excitation	Figure Number
27	2.25	2.0	2.1	396	273	Long. only	57
27	2.25	2.0	2.1	396	273	Lat. only	58
27	2.25	2.0	2.1	396	273	Long. and Lat.	59
27	2.25	2.0	2.1	396	273	29° from Long.	60

It is seen from Figure 57 that with longitudinal excitation only, the two-dimensional DAVI Alpha exhibits the expected results, in that a distinct resonance and antiresonance are obtained. At the antiresonant frequency, the 93-percent isolation obtained did not compare with the over 98-percent isolation obtained with the unidirectional DAVI model. However, this was due to the spherical bearings used in the two-dimensional model which provided more damping.

The lateral response of the two-dimensional DAVI Alpha with lateral excitation only, as shown in Figure 58, is much more erratic, and a distinct natural frequency was not obtained. The reason for this erratic response is that the lateral shaker not only introduced a force in the system but also moments about base and isolated weight center of gravity, producing angular and translational motions, thus, pure lateral translation was not obtained. However, the data show a distinct antiresonance. This lateral antiresonant frequency is lower than that obtained

for the longitudinal direction because of the difference of spring rates in these directions.

Figure 59 shows the results of the simultaneous longitudinal and lateral excitation, and Figure 60 shows the results of the single excitation at 29° to the longitudinal axis.

Comparing these figures with those showing the longitudinal and lateral directions only, it is seen that in the longitudinal direction, almost identical results were obtained; thus, the transmissibility of the two-dimensional DAVI Alpha, along its longitudinal principal axis, was not affected by the type of input.

In the lateral direction, the antiresonant frequency was not affected by the type of input which is to be expected. However, the transmissibility along the lateral principal axis of the two-dimensional DAVI Alpha, above the antiresonant frequency, was erratic. This is attributed to angular motion of the system introduced by the lateral forcing and the 29° offset excitation producing moments about the base and isolated weight center of gravity.

Correlation

Since the transmissibilities were obtained about the longitudinal and lateral principal axes of the two-dimensional DAVI Alpha, it is only necessary to calculate the transmissibility along the principal axes of the two-dimensional DAVI Alpha. The physical parameters used in the theoretical analysis are shown in Table IV. The amount of damping used in the analysis is $\zeta_A = .055$. The analytical results obtained are shown in Figures 57 and 58. It is seen that the test and analytical results of two-dimensional DAVI Alpha agree quite well along the longitudinal principal axis. However, in the lateral direction, there are discrepancies between the analytical and test results. This discrepancy is possibly due to the rotation of the system which occurred in testing but was not accounted for in the theoretical results.

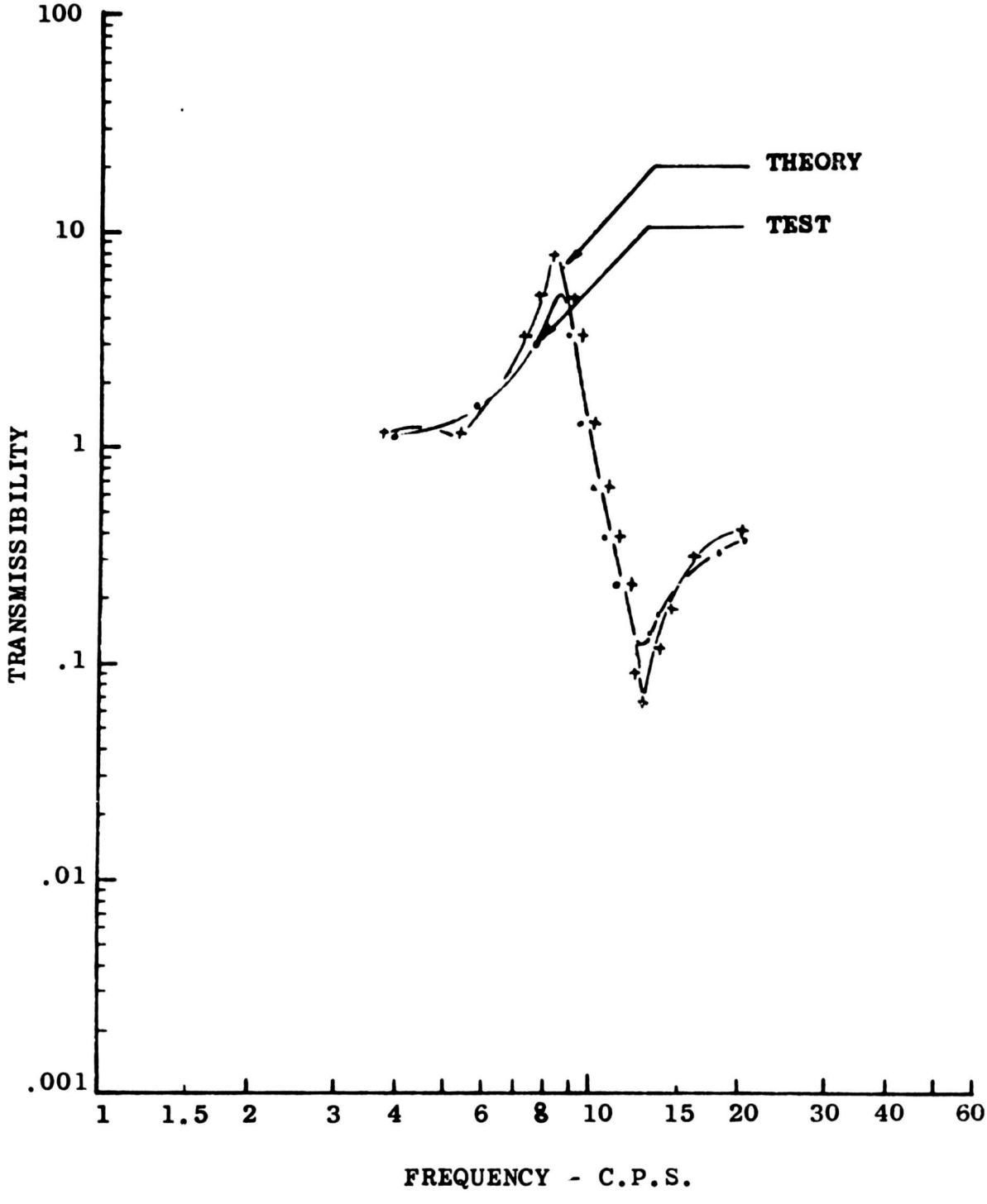

Figure 57. Longitudinal Response of Two-Dimensional DAVI Alpha With Longitudinal Excitation Only

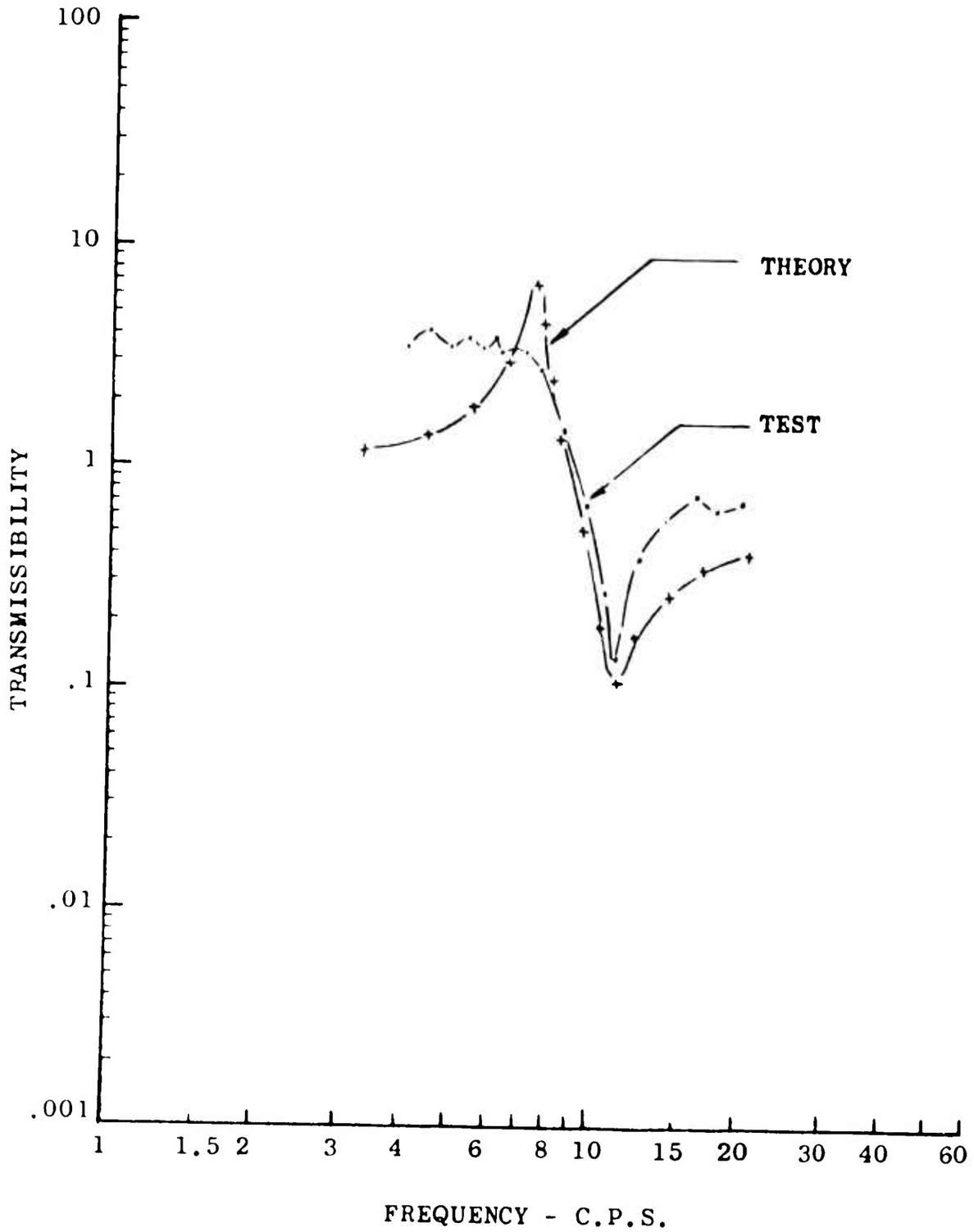

Figure 58. Lateral Response of Two-Dimensional DAVI Alpha With Lateral Excitation Only

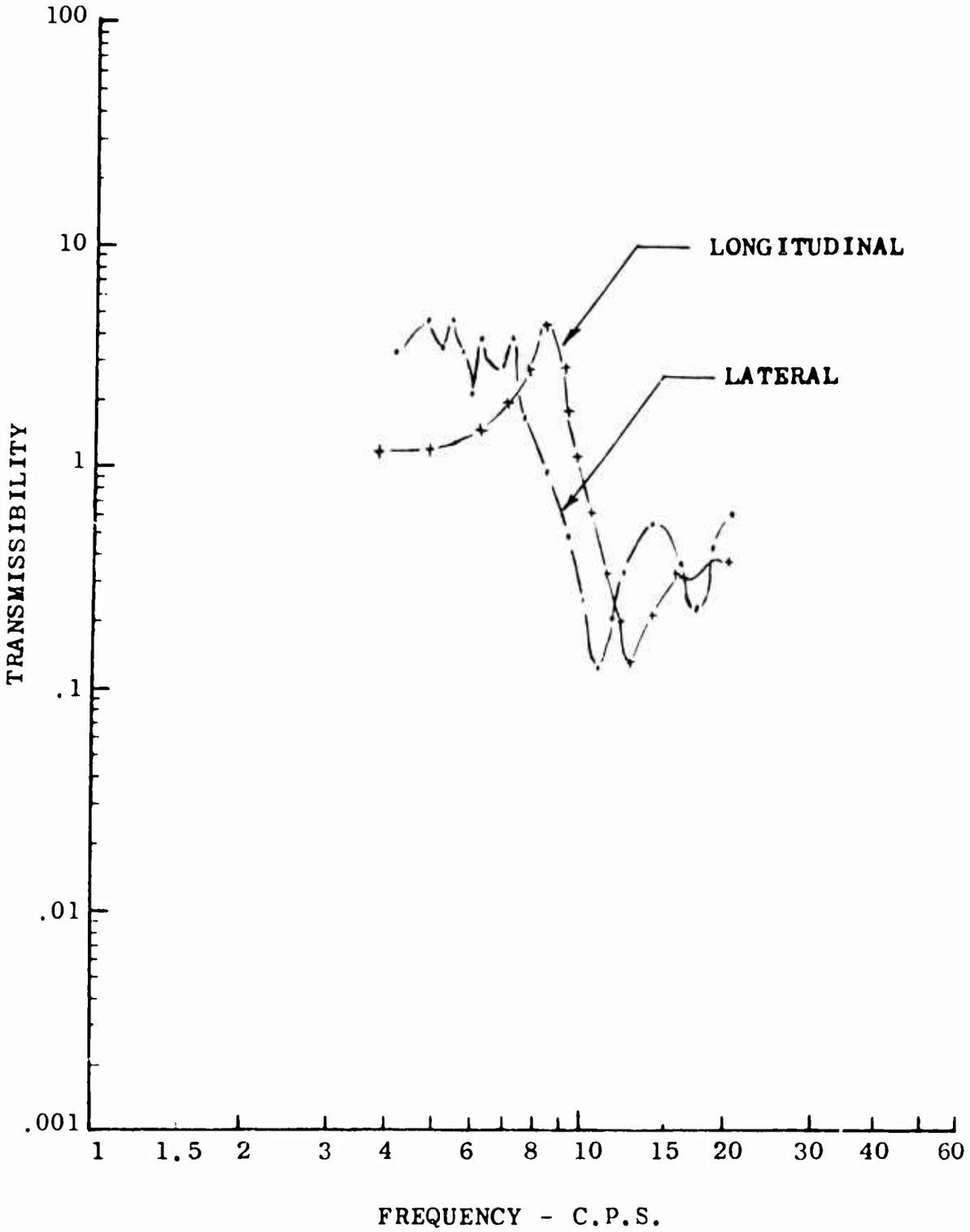

Figure 59. Response of Two-Dimensional DAVI Alpha With Longitudinal and Lateral Excitation

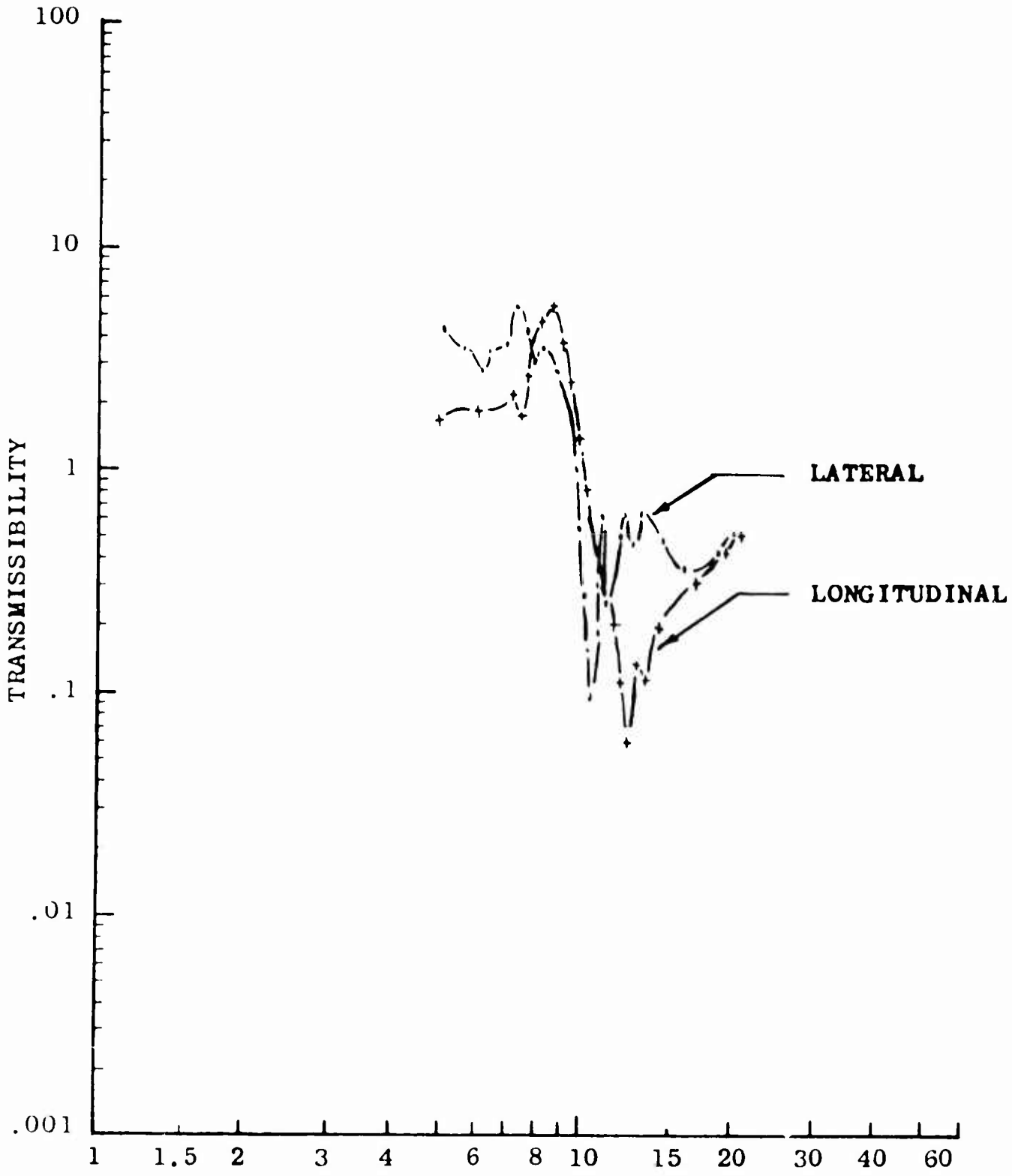

Figure 60. Response of Two-Dimensional DAVI Alpha With Excitation at 29 Degrees to the Longitudinal Axis

SERIES-TYPE DAVI

The analysis and tests on the unidirectional and two-dimensional DAVI Alphas have shown the capability of low-frequency isolation and of obtaining an antiresonant frequency that is not affected by the weight of the isolated item. However, this system approaches a finite value of isolation at high frequency which could be a disadvantage for some applications. A series system can be designed to obtain high-frequency isolation approaching zero and retain the advantages of the DAVI Alpha. These series DAVI's are shown in the following schematics.

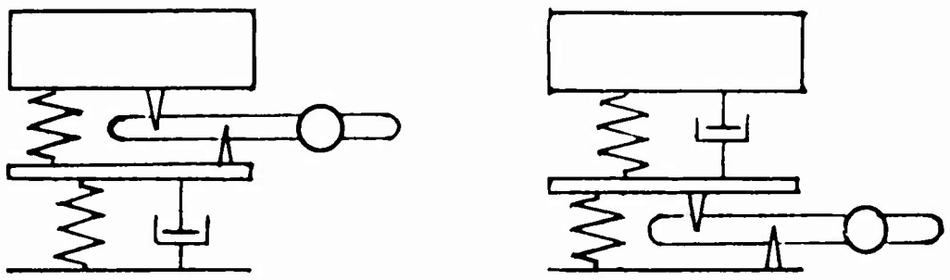

A - DAVI Beta

B - DAVI Gamma

Figure 61. Series-Damped DAVI

ANALYSIS

DAVI Beta

The DAVI Beta is an incorporation of the DAVI Alpha and conventional isolation systems. The mass to be isolated is supported by the DAVI Alpha part of the system which, in turn, is supported by the base-connected conventional isolator. A schematic of the DAVI Beta is shown in Figure 62.

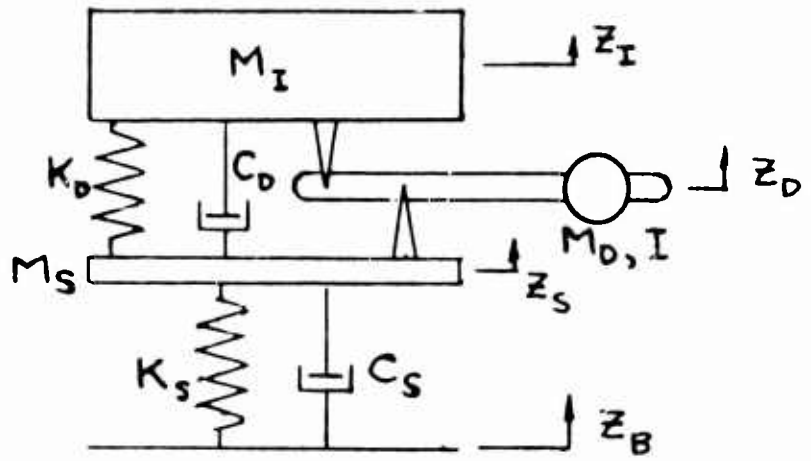

Figure 62. DAVI Beta

From the above figure, the following energy equations can be derived:

$$T = \frac{1}{2} M_I \dot{z}_I^2 + \frac{1}{2} M_D \dot{z}_D^2 + \frac{1}{2} M_S \dot{z}_S^2 + \frac{1}{2} I \dot{\theta}^2 \tag{82}$$

$$V = \frac{1}{2} K_D (z_I - z_S)^2 + \frac{1}{2} K_S (z_S - z_B)^2 \tag{83}$$

$$D = \frac{1}{2} C_D (\dot{z}_I - \dot{z}_S)^2 + \frac{1}{2} C_S (\dot{z}_S - \dot{z}_B)^2 \tag{84}$$

Substituting Equations (4) and (5) into Equation (82), Equation (82) becomes

$$T = \frac{1}{2} M_I \dot{z}_I^2 + \frac{1}{2} M_D \left[\dot{z}_S \left(\frac{R}{r}\right) - \dot{z}_I \left(\frac{R}{r} - 1\right) \right]^2 + \frac{1}{2} M_S \dot{z}_S^2 + \frac{1}{2} \frac{I}{r^2} (\dot{z}_I - \dot{z}_S)^2 \tag{85}$$

Applying Lagrange's equation, the equations of motion become

$$\left[M_I + M_D \left(\frac{R}{r} - 1\right)^2 + \frac{I}{r^2} \right] \ddot{z}_I + C_D \dot{z}_I + K_D z_I - \left[M_D \left(\frac{R}{r}\right)\left(\frac{R}{r} - 1\right) + \frac{I}{r^2} \right] \ddot{z}_S - C_D \dot{z}_S - K_D z_S = 0 \tag{86}$$

$$-\left[M_D\left(\frac{R}{r}\right)\left(\frac{R}{r}-1\right)+\frac{I}{r^2}\right]\ddot{z}_I - C_D\dot{z}_I - K_D z_I + \left[M_S + M_D\left(\frac{R}{r}\right)^2 + \frac{I}{r^2}\right]\ddot{z}_S + (C_D+C_S)\dot{z}_S + (K_D+K_S)z_S = C_S\dot{z}_B + K_S z_B \quad (87)$$

Assuming a solution of the form $z = z_0 e^{i\omega t}$, and letting

$$M_A = M_D\left(\frac{R}{r}\right)\left(\frac{R}{r}-1\right) + \frac{I}{r^2}$$

$$M_R = M_I + M_D\left(\frac{R}{r}-1\right)^2 + \frac{I}{r^2}$$

$$M_T = M_S + M_D\left(\frac{R}{r}\right)^2 + \frac{I}{r^2}$$

the equations may be written in matrix form as follows:

$$\begin{bmatrix} (K_D+i\omega C_D-M_R\omega^2) & -(K_D+i\omega C_D-M_A\omega^2 \\ -(K_D+i\omega C_D-M_A\omega^2) & \left[(K_D+K_S)+i\omega(C_D+C_S)-M_T\omega^2\right] \end{bmatrix} \begin{bmatrix} z_I \\ z_S \end{bmatrix} = \begin{bmatrix} 0 \\ (K_S+i\omega C_S)z_B \end{bmatrix} \quad (88)$$

Using Cramer's rule, and solving the above matrix for z_I, the DAVI Beta transmissibility equation is

$$T_\beta = \frac{z_I}{z_B} = \frac{\left[K_S(K_D-\omega^2 M_A)-\omega^2 C_S C_D\right] + i\omega\left[(K_D-M_A\omega^2)C_S + C_D K_S\right]}{\Delta} \quad (89)$$

where

$$\Delta = \{(M_T M_R - M_A^2)\omega^4 - [M_R(K_S+K_D) - 2M_A K_D + M_T K_D + C_D C_S]\omega^2 + K_D K_S\} - i\{[M_R(C_S+C_D) + M_T C_D - 2M_A C_D]\omega^3 - [C_D K_S + C_S K_D]\omega\} \quad (90)$$

Equation (90) is the characteristic frequency equation of the DAVI Beta.

The transmissibility equation of the DAVI Beta can be nondimensionalized by letting

$\omega_A^2 = \frac{K_D}{M_A}$ (antiresonant frequency of the DAVI)

$\omega_S^2 = \frac{K_S}{M_I}$ (natural frequency of the conventional system)

$f_A = \frac{C_D}{C_A}$ (% damping at antiresonance)

$f_S = \frac{C_S}{C_C}$ (% critical damping of the conventional system)

where

$C_A = 2M_A\omega_A$

$C_C = 2M_I\omega_S$

$\mu_D = \frac{M_D}{M_I}$ (mass ratio of DAVI inertia bar mass to isolated mass)

$\mu_S = \frac{M_S}{M_I}$ (ratio of intermediate mass to isolated mass)

Substituting the above in Equation (89), the transmissibility of the DAVI Beta can be written in the following form:

$$T_\beta = \frac{A + iB}{C + iD} \tag{91}$$

and the absolute magnitude of the transmissibility is

$$T_\beta = \sqrt{\frac{A^2 + B^2}{C^2 + D^2}} \tag{92}$$

where

$$A = \left\{ \frac{\omega_s^2}{\omega_A^2}\left(1 - \frac{\omega^2}{\omega_A^2}\right) - 4 f_A f_S \frac{\omega_s}{\omega_A} \frac{\omega^2}{\omega_A^2} \right\} \tag{93}$$

$$B = 2\frac{\omega}{\omega_A}\left\{ f_S \frac{\omega_s}{\omega_A}\left(1 - \frac{\omega^2}{\omega_A^2}\right) + \frac{\omega_s^2}{\omega_A^2} f_A \right\} \tag{94}$$

$$C = \left\{ \frac{\mu_D\left[\left(\frac{R}{r}\right)^2 + \left(\frac{e}{r}\right)^2\right]}{M_A/M_I} + \mu_s \frac{M_R}{M_A} + \frac{\mu_D^2 \left(\frac{e}{r}\right)^2}{M_A/M_I} \right\} \frac{\omega^4}{\omega_A^4}$$
$$- \left[\frac{\omega_s^2}{\omega_A^2} \frac{M_R}{M_A} + (1 + \mu_D + \mu_s) + 4 \frac{\omega_s}{\omega_A} f_A f_S \right] \frac{\omega^2}{\omega_A^2} + \frac{\omega_s^2}{\omega_A^2} \tag{95}$$

$$D = 2\frac{\omega}{\omega_A}\left\{ f_S \frac{\omega_s}{\omega_A} + f_A \frac{\omega_s^2}{\omega_A^2} \right) - \left[\frac{M_R}{M_A} \frac{\omega_s}{\omega_A} f_S + (1 + \mu_s + \mu_D) f_A \right] \frac{\omega^2}{\omega_A^2} \Bigg\} \tag{96}$$

The denominator of the transmissibility equation is the damped natural frequency equation of the DAVI Beta. It is seen that if $\zeta_A = 0$ (zero damping across the DAVI), damped natural frequencies still occur, and the amplitude at resonance can be controlled. However, in the numerator with $\zeta_A = 0$, 100-percent isolation can be obtained. Also, when $\omega/\omega_A \rightarrow \infty$, the transmissibility approaches zero. Thus, a DAVI Beta can be designed to give approximately 100-percent isolation at a discrete frequency, to have controlled resonant amplitudes, and to give high-frequency isolation.

Since the DAVI Beta can be designed to give high-frequency isolation, a comparison is made of the high-frequency isolation of the DAVI Beta and a conventional system. This comparison is made on the undamped transmissibility equations. The undamped transmissibility equation of the DAVI Beta is

$$T_\beta = \frac{\frac{\omega_s^2}{\omega_A^2}\left(1 - \frac{\omega^2}{\omega_A^2}\right)}{\left\{\frac{\mu_D\left[\left(\frac{R}{r}\right)^2 + \left(\frac{\rho}{r}\right)^2\right]}{M_A/M_I} + \mu_S\frac{M_R}{M_A} + \frac{\mu_D^2\frac{\rho^2}{r^2}}{M_A/M_I}\right\}\frac{\omega^4}{\omega_A^4} - \left[\frac{\omega_s^2}{\omega_A^2}\frac{M_R}{M_A} + (1+\mu_D+\mu_S)\right]\frac{\omega^2}{\omega_A^2} + \frac{\omega_s^2}{\omega_A^2}} \qquad (97)$$

However,

$$\frac{M_A}{M_I} = \mu_D\left[\left(\frac{R}{r}\right)\left(\frac{R}{r} - 1\right) + \frac{\rho^2}{r^2}\right]$$

$$\frac{M_R}{M_I} = 1 + \mu_D\left[\left(\frac{R}{r} - 1\right)^2 + \frac{\rho^2}{r^2}\right]$$

Therefore, the transmissibility equation can be rewritten as

$$T_\beta = \left\{\mu_D\left[\left(\frac{R}{r}\right)\left(\frac{R}{r}-1\right) + \frac{\rho^2}{r^2}\right]\left(1 - \frac{\omega^2}{\omega_A^2}\right)\frac{\omega_s^2}{\omega_A^2}\right\} \Bigg/ \left\{\left[\mu_D\left(\frac{R^2}{r^2} + \frac{\rho^2}{r^2}\right) + \mu_S\left[1 + \mu_D\left/\left(\frac{R}{r}-1\right)^2 + \frac{\rho^2}{r^2}\right.\right]\right] + \mu_D^2\frac{\rho^2}{r^2}\right]\frac{\omega^4}{\omega_A^4}$$

$$- \left[\frac{\omega_s^2}{\omega_A^2}\left(1 + \mu_D\left/\left(\frac{R}{r}-1\right)^2 + \frac{\rho^2}{r^2}\right.\right) + \mu_D\left/\frac{R}{r}\left(\frac{R}{r}-1\right) + \frac{\rho^2}{r^2}\right/(1+\mu_D+\mu_S)\right]\frac{\omega^2}{\omega_A^2}$$

$$+ \mu_D\left[\frac{R}{r}\left(\frac{R}{r}-1\right) + \frac{\rho^2}{r^2}\right]\frac{\omega_s^2}{\omega_A^2}\Bigg\} \qquad (98)$$

The undamped transmissibility equation of a conventional system is

$$T_C = \frac{1}{\left(1 - \frac{\omega^2}{\omega_N^2}\right)} \tag{99}$$

For an equivalent conventional system having the same overall spring rate as the DAVI Beta, the natural frequency is

$$\omega_N^2 = \frac{K_S K_D}{(K_S + K_D) M_I} = \frac{K_D}{K_S + K_D} \omega_S^2 \tag{100}$$

Using the above relationship, Equation (99) can be rewritten as

$$T_C = \frac{\frac{\omega_S^2}{\omega_A^2}}{\frac{\omega_S^2}{\omega_A^2} - \left(1 + \frac{K_S}{K_D}\right)\frac{\omega^2}{\omega_A^2}} \tag{101}$$

A ratio of the transmissibilities is then obtained by dividing the DAVI Beta transmissibility Equation (98) by the equivalent conventional transmissibility Equation (101), resulting in the following equation:

$$\frac{T_\beta}{T_C} = \frac{\mu_D\left[\left(\frac{R}{r}\right)\left(\frac{R}{r} - 1\right) + \frac{\rho^2}{r^2}\right]\left[\frac{\omega^2}{\omega_A^2} - \left(1 + \frac{K_S}{K_D}\right)\frac{\omega^2}{\omega_A^2}\right]\left(1 - \frac{\omega^2}{\omega_A^2}\right)}{E\,\frac{\omega^4}{\omega_A^4} - F\,\frac{\omega^2}{\omega_A^2} + G} \tag{102}$$

where

$$E = \mu_D\left[\left(\frac{R}{r}\right)^2 + \left(\frac{\rho}{r}\right)^2\right] + \mu_S\left\{1 + \mu_D\left[\left(\frac{R}{r} - 1\right)^2 + \frac{\rho^2}{r^2}\right]\right\} + \mu_D^2\frac{\rho^2}{r^2}$$

$$F = \left\{1+\mu_D\left[\left(\frac{R}{r}-1\right)^2+\frac{\rho^2}{r^2}\right]\right\}\frac{\omega_S^2}{\omega_A^2}+\mu_D\left[\frac{R}{r}\left(\frac{R}{r}-1\right)+\frac{\rho^2}{r^2}\right](1+\mu_D+\mu_S)$$

$$G = \left\{\mu_D\left[\frac{R}{r}\left(\frac{R}{r}-1\right)+\frac{\rho^2}{r^2}\right]\frac{\omega_S^2}{\omega_A^2}\right\}$$

To compare at very high frequency, divide the numerator and denominator by ω^4/ω_A^4 and let $\omega/\omega_A \longrightarrow \infty$; the ratio then becomes

$$\frac{T_{\theta VHF}}{T_{CVHF}} = \frac{\left(1+\frac{K_S}{K_D}\right)\left[\frac{R}{r}\left(\frac{R}{r}-1\right)+\frac{\rho^2}{r^2}\right]}{\left[\left(\frac{R}{r}\right)^2+\left(\frac{\rho}{r}\right)^2\right]+\mu_S\left[\left(\frac{R}{r}-1\right)^2+\frac{\rho^2}{r^2}\right]+\frac{\mu_S}{\mu_D}+\mu_D\frac{\rho^2}{r^2}} \qquad (103)$$

For comparison and approximate design purposes, let the inertia of the bar be that of a straight rod, as shown in Figure 63.

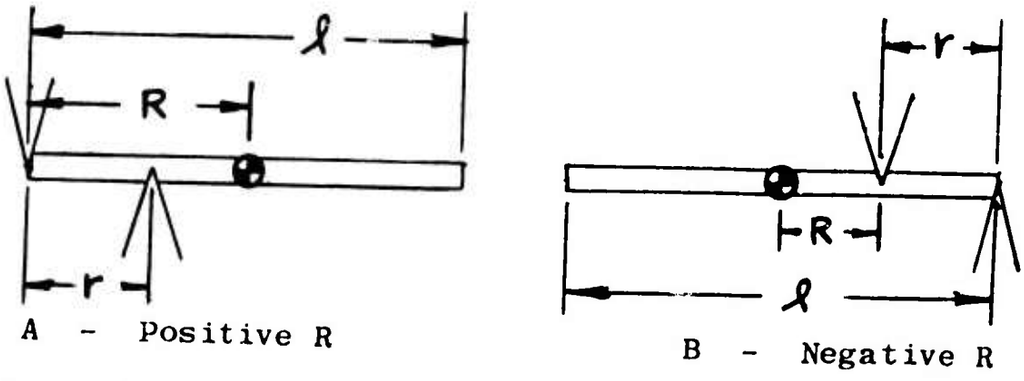

Figure 63. Schematic of Thin Rod Inertia Bar

From Figure 63A, it is seen that for a positive R that gives a value of $R/r \geq 0.5$, $\ell = 2R$, and since for a straight rod $\rho^2 = \frac{\ell^2}{12}$, then for the DAVI bar with a positive R , $\rho^2/r^2 = R^2/3r^2$.

From Figure 63B , it is seen that for a positive R that gives a value less than .5 or for a negative R, $\ell = 2(r-R)$ and, therefore, $\rho^2/r^2 = \frac{1}{3}\left(1-\frac{R}{r}\right)^2$, in which the actual value and not the absolute amplitude of $\frac{R}{r}$ should be used. Therefore, two equations are obtained from Equation (103).

For values of $\frac{R}{r} \geq 0.5$, then

$$\frac{T_{B_{VHF}}}{T_{C_{VHF}}} = \frac{\left(1+\frac{K_S}{K_D}\right)\left(\frac{4}{3}\frac{R}{r}-1\right)\frac{R}{r}}{\frac{4}{3}\frac{R^2}{r^2}+\mu_S\left[\left(\frac{R}{r}-1\right)^2+\frac{1}{3}\frac{R^2}{r^2}\right]+\frac{\mu_S}{\mu_D}+\frac{\mu_D}{3}\frac{R^2}{r^2}} \qquad (104)$$

and for values of $\frac{R}{r} < 0.5$, then

$$\frac{T_{B_{VHF}}}{T_{C_{VHF}}} = \frac{\left(1+\frac{K_S}{K_D}\right)\left(\frac{4}{3}\frac{R}{r}-1\right)\left(\frac{R}{r}-1\right)}{\left[\left(\frac{R}{r}\right)^2+\frac{\left(1-\frac{R}{r}\right)^2}{3}\right]+\mu_S\left[\left(\frac{R}{r}-1\right)^2+\frac{\left(1-\frac{R}{r}\right)^2}{3}\right]+\frac{\mu_S}{\mu_D}+\frac{\mu_D}{3}\left(1-\frac{R}{r}\right)^2} \qquad (105)$$

It is seen from the above equations that a conservative approximation can be obtained by letting $\mu_S = 0$; and since $\frac{\mu_D}{3}\left(\frac{R}{r}\right)^2 \ll \frac{4}{3}\left(\frac{R}{r}\right)^2$ and $\frac{\mu_D}{3}\left(1-\frac{R}{r}\right)^2 \ll \left[\left(\frac{R}{r}\right)^2+\frac{\left(1-\frac{R}{r}\right)^2}{3}\right]$, the equations can be rewritten as

$$\frac{T_{B_{VHF}}}{T_{C_{VHF}}} = \left(1+\frac{K_S}{K_D}\right)\left(1-\frac{1}{\frac{4}{3}\frac{R}{r}}\right) \qquad (106)$$

for $\frac{R}{r} \geq 0.5$ and

$$\frac{T_{\beta_{VHF}}}{T_{C_{VHF}}} = \frac{\left(1+\frac{K_S}{K_D}\right)\left(\frac{4}{3}\frac{R}{r}-\frac{1}{3}\right)\left(\frac{R}{r}-1\right)}{\left(\frac{4}{3}\frac{R}{r}-\frac{1}{3}\right)\frac{R}{r}-\frac{1}{3}\left(\frac{R}{r}-1\right)} \qquad (107)$$

for $\frac{R}{r} < 0.5$.

It is seen from the above equations that at very high frequency, the comparison of the DAVI Beta with an equivalent system is primarily a function of the R/r and K_S/K_D ratios. Calculations were done varying R/r from +10 to -10 and varying the spring rate ratio (K_S/K_D) from .2 to 5. The results of these calculations are shown in Figure 65.

It is seen from this figure that a DAVI Beta can be designed to give much better high-frequency isolation than a conventional system of equivalent stiffness. However, a positive R/r is required, which should be as small as possible, and the spring ratio K_S/K_D should also be as small as possible; that is, the spring rate across the DAVI should be much stiffer than the spring rate in the series system. A negative R/r will always give high-frequency isolation that is less than the conventional system.

DAVI Gamma

As in the DAVI Beta, the DAVI Gamma is a combination of the DAVI Alpha and a conventional isolation system. However, in the DAVI Gamma, the mass to be isolated is supported by the conventional system which, in turn, is supported by the DAVI Alpha part of the system. A schematic of the DAVI Gamma is shown in Figure 64.

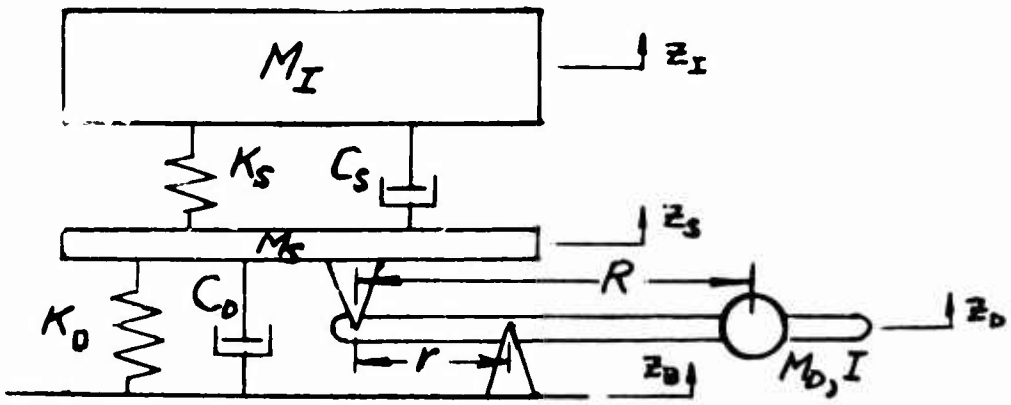

Figure 64. DAVI Gamma

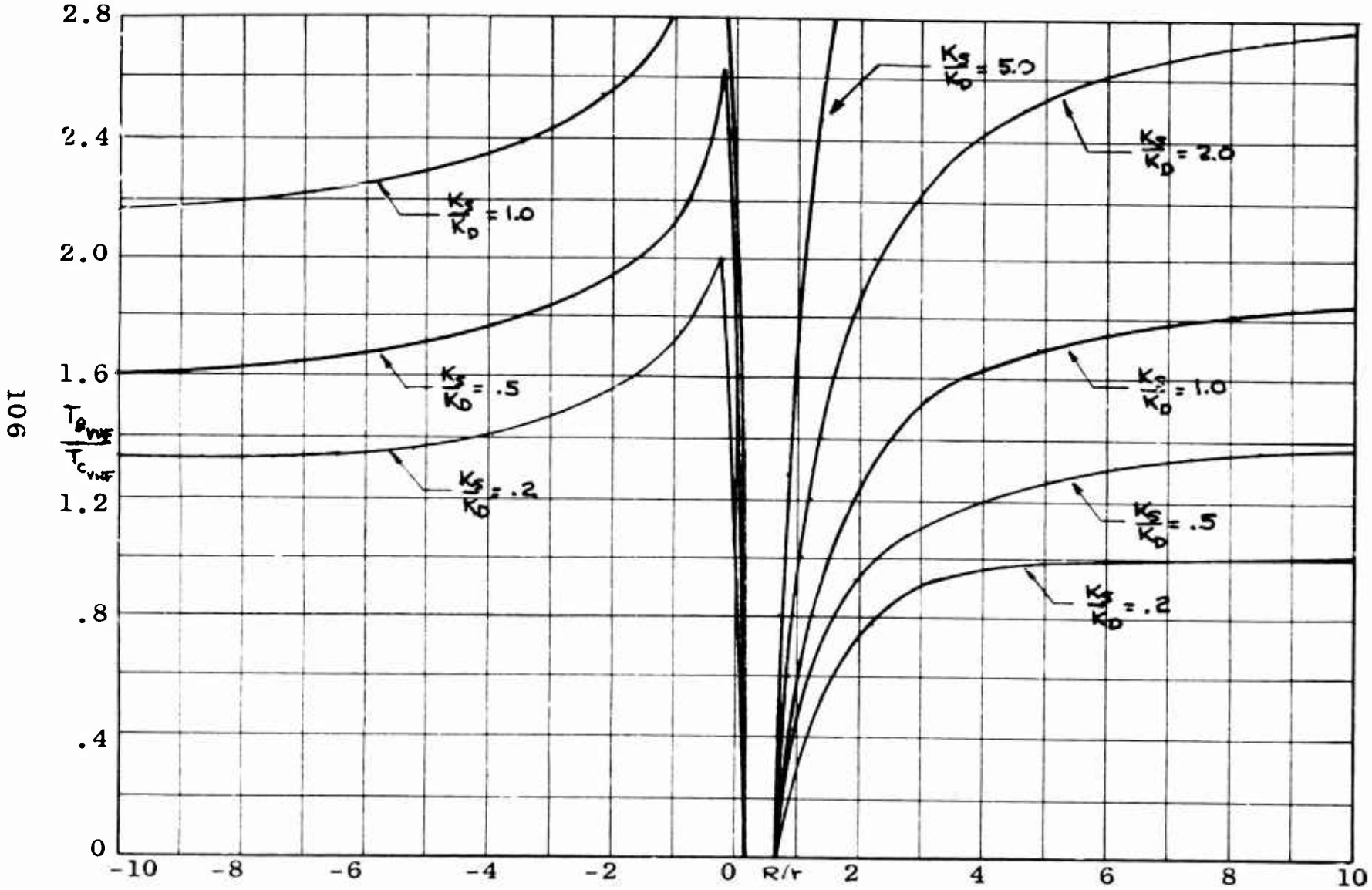

Figure 65. Comparison of the DAVI Beta With a Conventional Isolator for High-Frequency Isolation

From Figure 64, the following energy equations can be derived:

$$T = \frac{1}{2} M_I \dot{z}_I^2 + \frac{1}{2} M_D \dot{z}_D^2 + \frac{1}{2} M_S \dot{z}_S^2 + \frac{1}{2} I \dot{\theta}^2 \tag{108}$$

$$V = \frac{1}{2} K_D (z_S - z_B)^2 + \frac{1}{2} K_S (z_I - z_S)^2 \tag{109}$$

$$D = \frac{1}{2} C_D (\dot{z}_S - \dot{z}_B)^2 + \frac{1}{2} C_S (\dot{z}_I - \dot{z}_S)^2 \tag{110}$$

Substituting Equations (4) and (5) into Equation (108), Equation (108) becomes

$$T = \frac{1}{2} M_I \dot{z}_I^2 + \frac{1}{2} M_D \left[\frac{R}{r} \dot{z}_B - \left(\frac{R}{r} - 1 \right) \dot{z}_S \right]^2 + \frac{1}{2} M_S \dot{z}_S^2 + \frac{1}{2} \frac{I}{r^2} (\dot{z}_S - \dot{z}_B)^2 \tag{111}$$

Applying Lagrange's equation to the energy equations, the equations of motion are

$$M_I \ddot{z}_I + C_S \dot{z}_I + K_S z_I - C_S \dot{z}_S - K_S z_S = 0 \tag{112}$$

$$\left[M_S + M_D \left(\frac{R}{r} - 1 \right)^2 + \frac{I}{r^2} \right] \ddot{z}_S + (C_S + C_D) \dot{z}_S + (K_S + K_D) z_S$$

$$- C_S \dot{z}_I - K_S z_I = \left[M_D \frac{R}{r} \left(\frac{R}{r} - 1 \right) + \frac{I}{r^2} \right] \ddot{z}_B + C_D \dot{z}_B + K_D z_B \tag{113}$$

Assuming a solution of the form $z = Z e^{i\omega t}$ and letting

$$M_A = M_D \frac{R}{r} \left(\frac{R}{r} - 1 \right) + \frac{I}{r^2}$$

$$M_R' = M_S + M_D \left(\frac{R}{r} - 1 \right)^2 + \frac{I}{r^2}$$

the equations may be written in matrix form as

$$\begin{bmatrix} (K_S+i\omega C_S-M_I\omega^2) & -(K_S+i\omega C_S) \\ -(K_S+i\omega C_S) & [K_S+K_D+i\omega(C_S+C_D)-M'_R\omega^2] \end{bmatrix} \begin{bmatrix} Z_I \\ Z_S \end{bmatrix} = \begin{bmatrix} 0 \\ (K_D+i\omega C_D-M_A\omega^2)Z_B \end{bmatrix} \quad (114)$$

Using Cramer's rule and solving the above matrix for Z_I, the DAVI Gamma transmissibility is

$$T_\gamma = \frac{Z_I}{Z_B} = \left\{\left[K_S(K_D-M_A\omega^2)-C_DC_S\omega^2\right]+i\omega\left[C_S(K_D-M_A\omega^2)+K_SC_D\right]\right\} \Big/ \left\{\left[M_IM'_R\omega^4 - (M'_RK_S+M_IK_S+K_DM_I+C_DC_S)\omega^2+K_DK_S\right]+i\omega\left[-(C_SM_S+C_DM_S+C_SM'_R)\omega^2+(C_SK_D+C_DK_S)\right]\right\} \quad (115)$$

Substituting the relationships found on page 99 into Equation (115), the transmissibility of the DAVI Gamma can be written in the following form:

$$T_\gamma = \frac{A+iB}{C+iD} \quad (116)$$

and the absolute magnitude of the transmissibility is

$$\left|T_\gamma\right| = \sqrt{\frac{A^2+B^2}{C^2+D^2}} \quad (117)$$

where

$$A = \frac{\omega_S^2}{\omega_A^2}\left(1-\frac{\omega}{\omega_A^2}\right)-4\zeta_A\zeta_S\frac{\omega_S}{\omega_A}\frac{\omega^2}{\omega_A^2} \quad (118)$$

$$B = 2\frac{\omega}{\omega_A}\left[\zeta_S\frac{\omega_S}{\omega_A}\left(1-\frac{\omega^2}{\omega_A^2}\right)+\zeta_A\frac{\omega_S^2}{\omega_A^2}\right] \quad (119)$$

$$C = \frac{M'_R}{M_A}\frac{\omega^4}{\omega_A^4}-\left[\frac{\omega_S^2}{\omega_A^2}\left(\frac{M'_R}{M_A}+\frac{1}{M_A/M_I}\right)+1+4\zeta_A\zeta_S\frac{\omega_S}{\omega_A}\right]\frac{\omega^2}{\omega_A^2}+\frac{\omega_S^2}{\omega_A^2} \quad (120)$$

$$D = 2\frac{\omega}{\omega_A}\left\{\left(\zeta_S\frac{\omega_S}{\omega_A}+\zeta_A\frac{\omega_S^2}{\omega_A^2}\right)-\left[\zeta_S\frac{\omega_S}{\omega_A}\left(\frac{M'_R}{M_A}+\frac{1}{M_A/M_I}\right)+\zeta_A\right]\frac{\omega^2}{\omega_A^2}\right\} \quad (121)$$

The denominator of the transmissibility equation is the damped natural frequency equation of the DAVI Gamma. As in the DAVI Beta, it is seen that if $\zeta_A = 0$, damped natural frequencies still occur and the amplitude at resonance can be controlled. However, in the numerator with $\zeta_A = 0$, 100-percent isolation can be obtained. When $\omega/\omega_A \longrightarrow \infty$, the transmissibility approaches zero. Therefore, as in the DAVI Beta, the DAVI Gamma can be designed to give approximately 100-percent isolation at a discrete frequency, to have controlled resonant amplitudes, and to give high-frequency isolation.

A comparison is made of the high-frequency isolation of the DAVI Gamma and an equivalent conventional system. This comparison is made on the undamped transmissibility equations. The undamped transmissibility equation of the DAVI Gamma is

$$T_\gamma = \frac{\frac{\omega_S^2}{\omega_A^2}\left(1-\frac{\omega^2}{\omega_A^2}\right)}{\frac{M'_R}{M_A}\frac{\omega^4}{\omega_A^4}-\left[\frac{\omega_S^2}{\omega_A^2}\left(\frac{M'_R}{M_A}+\frac{1}{M_A/M_I}\right)+1\right]\frac{\omega^2}{\omega_A^2}+\frac{\omega_S^2}{\omega_A^2}} \quad (122)$$

However,

$$\frac{M_A}{M_I} = \mu_D\left[\frac{R}{r}\left(\frac{R}{r}-1\right)+\frac{\rho^2}{r^2}\right]$$

$$\frac{M'_R}{M_I} = \mu_S+\mu_D\left[\left(\frac{R}{r}-1\right)^2+\frac{\rho^2}{r^2}\right]$$

Therefore, the undamped transmissibility equation of the DAVI Gamma can be rewritten as

$$T_\gamma = \left\{\mu_D\left[\frac{R}{r}\left(\frac{R}{r}-1\right)+\frac{\rho^2}{r^2}\right]\left(1-\frac{\omega^2}{\omega_A^2}\right)\frac{\omega_S^2}{\omega_A^2}\right\}\Bigg/\left\{\left[\mu_S+\mu_D\left(\left|\frac{R}{r}-1\right|^2+\frac{\rho^2}{r^2}\right)\right]\frac{\omega^4}{\omega_A^4}\right.$$
$$-\left[\frac{\omega_S^2}{\omega_A^2}\left(\mu_S+\mu_D\left|\frac{R}{r}-1\right|^2+\mu_D\frac{\rho^2}{r^2}+1\right)\right.$$
$$\left.\left.+\mu_D\left(\frac{R}{r}\left|\frac{R}{r}-1\right|+\frac{\rho^2}{r^2}\right)\right]\frac{\omega^2}{\omega_A^2}+\frac{\omega_S^2}{\omega_A^2}\right\} \quad (123)$$

A ratio of the transmissibilities is obtained by dividing the DAVI Gamma transmissibility by the equivalent conventional transmissibility, Equation (101). This results in

$$\frac{T_\gamma}{T_c} = \frac{\mu_D\left[\frac{R}{r}\left(\frac{R}{r}-1\right)+\frac{\rho^2}{r^2}\right]\left[\frac{\omega_s^2}{\omega_A^2}-\left(1+\frac{K_s}{K_D}\right)\frac{\omega^2}{\omega_A^2}\right]\left(1-\frac{\omega^2}{\omega_A^2}\right)}{\cdot E\,\frac{\omega^4}{\omega_A^4}-F\,\frac{\omega^2}{\omega_A^2}+G} \qquad (124)$$

where

$$E = \mu_s + \mu_D\left[\left(\frac{R}{r}-1\right)^2+\frac{\rho^2}{r^2}\right]$$

$$F = \frac{\omega_s^2}{\omega_A^2}\left\{\mu_s+\mu_D\left[\left(\frac{R}{r}-1\right)^2+\frac{\rho^2}{r^2}\right]+1\right\}+\mu_D\left[\frac{R}{r}\left(\frac{R}{r}-1\right)+\frac{\rho^2}{r^2}\right]$$

$$G = \mu_D\left[\frac{R}{r}\left(\frac{R}{r}-1\right)+\frac{\rho^2}{r^2}\right]\frac{\omega_s^2}{\omega_A^2}$$

To compare at very high frequency, divide the numerator and denominator by ω^4/ω_A^4 and let $\omega/\omega_A \longrightarrow \infty$; the ratio then becomes

$$\frac{T_{\gamma_{VHF}}}{T_{C_{VHF}}} = \frac{\left(1+\frac{K_s}{K_D}\right)\left[\frac{R}{r}\left(\frac{R}{r}-1\right)+\frac{\rho^2}{r^2}\right]}{\left[\left(\frac{R}{r}-1\right)^2+\frac{\rho^2}{r^2}\right]+\frac{\mu_s}{\mu_D}} \qquad (125)$$

It is seen from the above equation that at very high frequency, the comparison of the DAVI Gamma is a function of K_S/K_D and R/r ratios; and since $\left[\frac{R}{r}\left(\frac{R}{r}-1\right)+\frac{\rho^2}{r^2}\right]/\left[\left(\frac{R}{r}-1\right)^2+\frac{\rho^2}{r^2}\right]=M_A/M'_R$, it is also seen to be a function of the high-frequency isolation of the DAVI Alpha without the isolated mass.

In order to make a similar comparison as in the DAVI Beta, let $\mu_S = 0$ and make the inertia of the bar the same as that given on pages 103 and 104. Therefore, Equation (125) is, for $\frac{R}{r} \geq 0.5$,

$$\frac{T_{\delta VHF}}{T_{C VHF}} = \frac{\left(1+\frac{K_S}{K_D}\right)\left[\frac{R}{r}\left(\frac{R}{r}-1\right)+\frac{R^2}{3r^2}\right]}{\left[\left(\frac{R}{r}-1\right)^2+\frac{R^2}{3r^2}\right]} \qquad (126)$$

and, for $\frac{R}{r} < 0.5$,

$$\frac{T_{\delta VHF}}{T_{C VHF}} = \frac{\left(1+\frac{K_S}{K_D}\right)\left[\frac{R}{r}\left(\frac{R}{r}-1\right)+\frac{1}{3}\left(1-\frac{R}{r}\right)^2\right]}{\left[\left(\frac{R}{r}-1\right)^2+\frac{1}{3}\left(1-\frac{R}{r}\right)^2\right]} \qquad (127)$$

Calculations were done varying R/r from +10 to -10 and varying the spring rate ratio (K_S/K_D) from .2 to 5. The results of these calculations are shown in Figure 66. It is seen from this figure that a DAVI Gamma can be designed to give much better high-frequency isolation than a conventional system of equivalent stiffness. However, an $R/r \leq 0.2$ is required, and the spring ratio, K_S/K_D, should be as small as possible; a positive $R/r \geq 1.0$ will always give high-frequency isolation that is less than a conventional isolator of the same stiffness.

DAVI Delta

Another type of DAVI that can obtain high-frequency isolation approaching zero and retain the advantage of the simple DAVI Alpha in having an antiresonant frequency is the DAVI Delta. Figure 67 gives a schematic of the DAVI Delta.

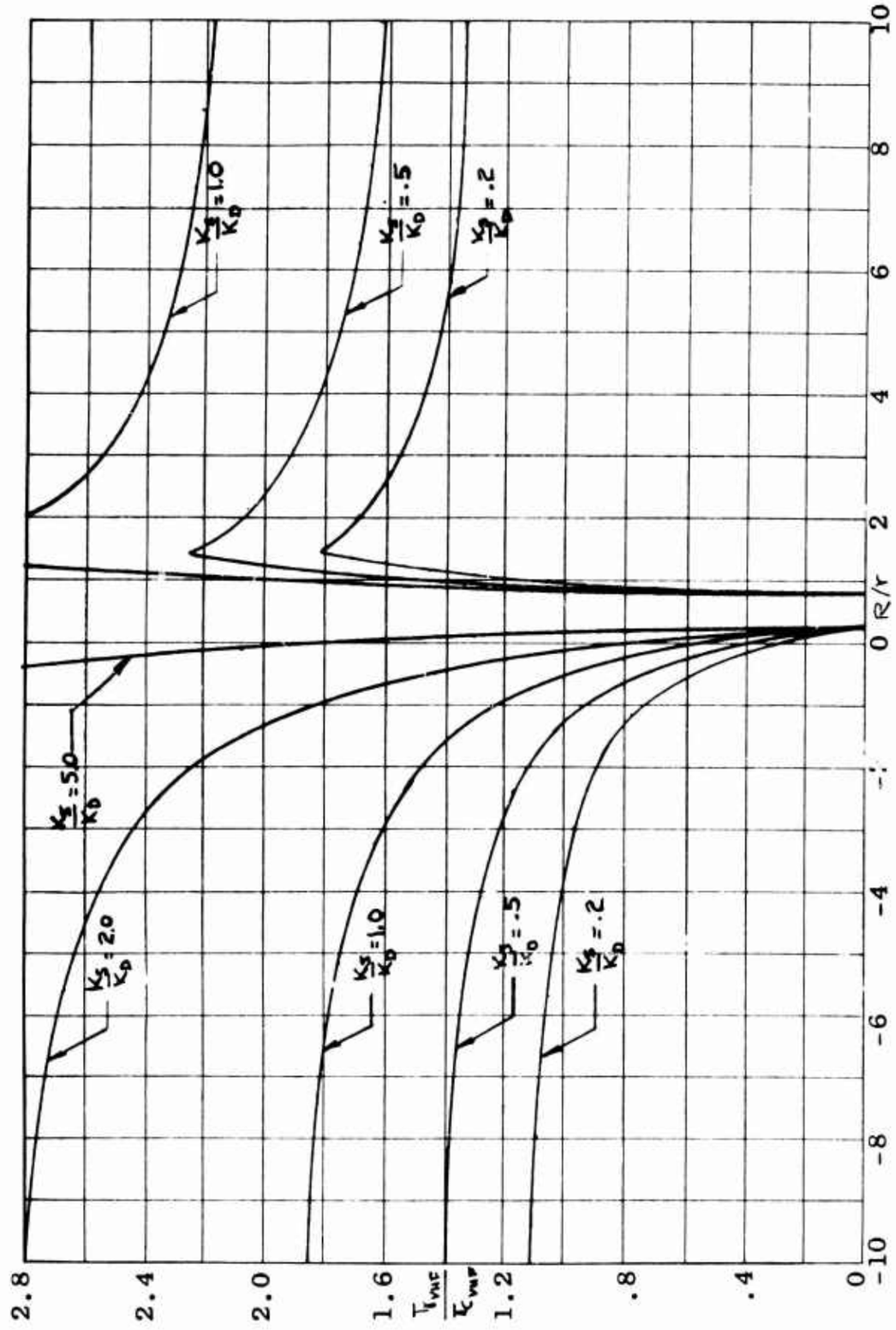

Figure 66. Comparison of the DAVI Gamma With a Conventional Isolator for High-Frequency Isolation

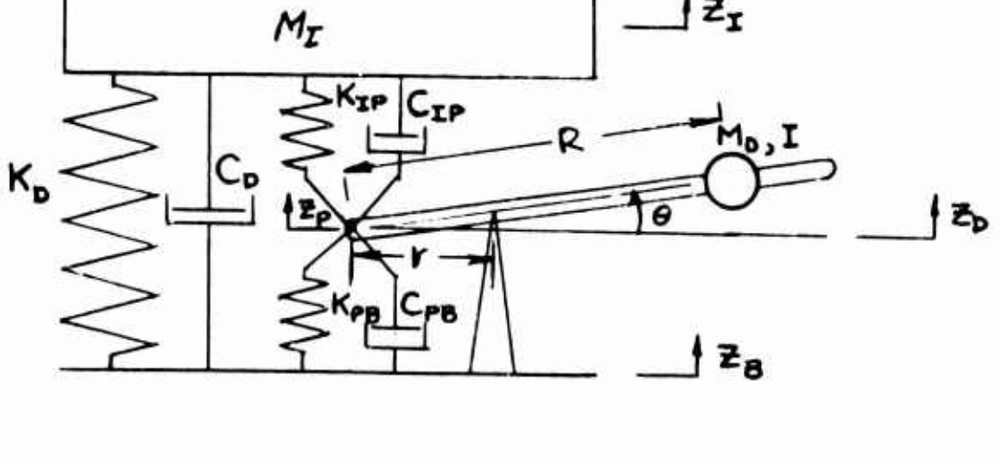

Figure 67. Schematic of DAVI Delta

From Figure 67, the energy equations can be derived:

$$T = \tfrac{1}{2} M_I \dot{z}_I^2 + \tfrac{1}{2} I\dot{\theta}^2 + \tfrac{1}{2} M_D \dot{z}_D^2 \tag{128}$$

$$V = \tfrac{1}{2} K_D (z_I - z_B)^2 + \tfrac{1}{2} K_{IP} (z_I - z_P)^2 + \tfrac{1}{2} K_{PB} (z_P - z_B)^2 \tag{129}$$

$$D = \tfrac{1}{2} C_D (\dot{z}_I - \dot{z}_B)^2 + \tfrac{1}{2} C_{IP} (\dot{z}_I - \dot{z}_P)^2 + \tfrac{1}{2} C_{PB} (\dot{z}_P - \dot{z}_B)^2 \tag{130}$$

However,

$$z_P = z_B - r\theta \quad ; \quad z_D = z_B + (R-r)\theta$$

Therefore, the above energy equations may be rewritten as

$$T = \tfrac{1}{2} M_I \dot{z}_I^2 + \tfrac{1}{2} I\dot{\theta}^2 + \tfrac{1}{2} M_D \left[\dot{z}_B + (R-r)\dot{\theta}\right]^2 \tag{131}$$

$$V = \tfrac{1}{2} K_D (z_I - z_B)^2 + \tfrac{1}{2} K_{IP} (z_I + r\theta - z_B)^2 + \tfrac{1}{2} K_{PB} r^2\theta^2 \tag{132}$$

$$D = \tfrac{1}{2} C_D (\dot{z}_I - \dot{z}_B)^2 + \tfrac{1}{2} C_{IP} (\dot{z}_I + r\dot{\theta} - \dot{z}_B)^2 + \tfrac{1}{2} C_{PB} r^2\dot{\theta}^2 \tag{133}$$

Applying Lagrange's equation, the equations of motion become

$$M_I \ddot{z}_I + (C_D + C_{IP})\dot{z}_I + (K_D + K_{IP}) z_I + C_{IP} r\dot{\theta} + K_{IP} r\theta = \tag{134}$$

$$(K_D + K_{IP}) z_B + (C_D + C_{IP}) \dot{z}_B$$

$$\left[I+M_D(R-r)^2\right]\ddot{\theta}+(C_{IP}r^2+C_{PB}r^2)\dot{\theta}+(K_{IP}r^2+K_{PB}r^2)\theta$$

$$+C_{IP}r\dot{z}_I+K_{IP}r z_I=K_{IP}r z_B+C_{IP}r\dot{z}_B-M_D(R-r)\ddot{z}_B \tag{135}$$

Assuming a steady-state solution of the form $z = Z e^{i\omega t}$, the equations become, in matrix form,

$$\begin{bmatrix} \left[K_D+K_{IP}-M_I\omega^2+i\omega(C_D+C_{IP})\right] & (K_{IP}+iC_{IP})r\omega \\ (K_{IP}+iC_{IP})r\omega & \left\{(K_{IP}+K_{PB})r^2-\left[I+M_D(R-r)^2\right]\omega^2+i\omega(C_{IP}+C_{PB})r^2\right\} \end{bmatrix} \begin{bmatrix} Z_I \\ \theta \end{bmatrix} = \begin{bmatrix} \left[K_D+K_{IP}+i\omega(C_D+C_{IP})\right]Z_B \\ \left[K_{IP}r+M_D(R-r)^2\omega^2+i\omega C_{IP}r\right]Z_B \end{bmatrix} \tag{136}$$

Using Cramer's rule, the transmissibility of the DAVI Delta becomes

$$T_\delta = \frac{Z_I}{Z_B} = \frac{A+i\omega B}{C+i\omega D} \tag{137}$$

where

$$A=\left[K_{PB}(K_D+K_{IP})+K_DK_{IP}\right]-\left[K_DM_R''+K_{IP}M_A+C_{PB}(C_D+C_{IP})+C_DC_{IP}\right]\omega^2 \tag{138}$$

$$B=\left[C_{PB}(K_D+K_{IP})+C_D(K_{IP}+K_{PB})+C_{IP}(K_D+K_{PB})\right]-\left[C_DM_R''+C_{IP}M_A\right]\omega^2 \tag{139}$$

$$C=\left[K_{PB}(K_D+K_{IP})+K_DK_{IP}\right]-\left\{(K_D+K_{IP})M_R''+(K_{IP}+K_{PB})M_I+\left[C_{PB}(C_D+C_{IP})+C_DC_{IP}\right]\right\}\omega^2+M_R''M_I\omega^4 \tag{140}$$

$$D=\left[C_{PB}(K_D+K_{IP})+C_D(K_{IP}+K_{PB})+C_{IP}(K_D+K_{PB})\right]-\left[C_{IP}(M_I+M_R'')+C_{PB}M_I+C_DM_R''\right]\omega^2 \tag{141}$$

where

$$M_A=M_D\left[\left(\frac{R}{r}-1\right)\frac{R}{r}+\frac{\rho^2}{r^2}\right]$$

$$M_R''=M_D\left[\left(\frac{R}{r}-1\right)^2+\frac{\rho^2}{r^2}\right]$$

It is seen from the above equations that the numerator is not a function of the mass of the isolated item. It is also seen from the above equations that it is difficult to obtain an antiresonant frequency by making the values of A and B zero at a discrete frequency because of the many variables involved. However, one possible advantage of the DAVI Delta is that zero deflection of the inertia bar is obtained under static load. This can be accomplished by letting $K_{IP} = 0$. Therefore, there is no spring connection between the isolated weight and the inertia bar; thus, there will be no deflection in the bar under a static load. Further, let $C_D = 0$ and $C_{PB} = 0$. The transmissibility equation (137) reduces to

$$T_S = \frac{K_D\left[K_{PB} - M_R''\omega^2\right] + i\omega C_{IP}\left[(K_D + K_{PB}) - M_A\omega^2\right]}{(K_{PB} - M_R''\omega^2)(K_D - M_I\omega^2) + i\omega C_{IP}\left[K_D + K_{PB} - (M_I + M_R'')\omega^2\right]} \qquad (142)$$

It is seen from the above equation that if the damping is zero, the above equation reduces to

$$T_S = \frac{K_D}{K_D - M_I\omega^2} \qquad (143)$$

which is the transmissibility equation of an undamped conventional isolator.

When the damping is infinite, the equation reduces to

$$T_S = \frac{(K_D + K_{PB}) - M_A\omega^2}{(K_D + K_{PB}) - (M_I + M_R'')\omega^2} \qquad (144)$$

which is the transmissibility of the DAVI Alpha system.

It is also seen from Equation (142) that with damping, an antiresonant frequency can be obtained that is not a function of isolated mass, and that damped resonances are obtained. In order to obtain the antiresonant frequency, the real and imaginary parts of the numerator must become zero at the same frequency. The real part of the numerator is zero when

$$\omega^2 = \frac{K_{PB}}{M_R''} \qquad (145)$$

and the imaginary part becomes zero when

$$\omega^2 = \frac{K_D + K_{PB}}{M_A} \tag{146}$$

Therefore, to obtain the antiresonance,

$$\frac{K_{PB}}{M_R''} = \frac{K_D + K_{PB}}{M_A}$$

and solving for K_{PB} ,

$$K_{PB} = \frac{M_R'' K_D}{M_A - M_R''} \tag{147}$$

Substituting the values of M_A and M_R'' in Equation (147), it becomes

$$\frac{K_{PB}}{K_D} = \frac{\left(\frac{R}{r}-1\right)^2 + \frac{\rho^2}{r^2}}{\left(\frac{R}{r}-1\right)} \tag{148}$$

It is seen that the above relationship must be maintained to obtain an antiresonant frequency. Although a zero static deflection can be maintained on the inertia bar of the DAVI Delta, the antiresonant frequency does not have the simple relationship that the DAVI Alpha, Beta, or Gamma has. In order to change the antiresonant frequency of the DAVI Delta, the ratio of the spring rates must also be changed. The DAVI Delta, therefore, does not have the versatility in simple tuning of the antiresonant frequency that the other DAVI configurations have.

COMPARISON OF DAVI BETA AND GAMMA

High-Frequency Comparison

As was done in the comparison of the DAVI Beta and Gamma with the high-frequency isolation of the conventional isolator, a similar comparison can be made of the DAVI Beta and Gamma at high frequency. Dividing the high-frequency transmissibility equation (103) of the DAVI Beta by the high-frequency transmissibility equation (125) of the DAVI Gamma results in the following:

$$\frac{T_{\beta VHF}}{T_{\gamma VHF}} = \frac{\left[\left(\frac{R}{r}-1\right)^2 + \frac{\rho^2}{r^2}\right] + \frac{\mu_S}{\mu_D}}{\left[\left(\frac{R}{r}\right)^2 + \frac{\rho^2}{r^2}\right] + \mu_S\left[\left(\frac{R}{r}-1\right)^2 + \frac{\rho^2}{r^2}\right] + \frac{\mu_S}{\mu_D} + \mu_D\frac{\rho^2}{r^2}} \qquad (149)$$

Assuming a straight, thin rod for the inertia bar as was done previously, then for $R/r \geq 0.5$, the above equation becomes

$$\frac{T_{\beta VHF}}{T_{\gamma VHF}} = \frac{\left[\left(\frac{R}{r}-1\right)^2 + \frac{1}{3}\left(\frac{R}{r}\right)^2\right] + \frac{\mu_S}{\mu_D}}{\frac{4}{3}\left(\frac{R}{r}\right)^2 + \mu_S\left[\left(\frac{R}{r}-1\right)^2 + \frac{R^2}{3r^2}\right] + \frac{\mu_S}{\mu_D} + \frac{\mu_D}{3}\left(\frac{R}{r}\right)^2} \qquad (150)$$

and for $R/r < 0.5$,

$$\frac{T_{\beta VHF}}{T_{\gamma VHF}} = \frac{\left[\left(\frac{R}{r}-1\right)^2 + \frac{1}{3}\left(\frac{R}{r}-1\right)^2\right] + \frac{\mu_S}{\mu_D}}{\left(\frac{R}{r}\right)^2 + \frac{1}{3}\left(\frac{R}{r}-1\right) + \mu_S\left[\left(\frac{R}{r}-1\right)^2 + \frac{1}{3}\left(\frac{R}{r}-1\right)^2\right] + \frac{\mu_S}{\mu_D} + \frac{\mu_D}{3}\left(\frac{R}{r}-1\right)^2} \qquad (151)$$

Calculations were done using the above two equations. Calculations were made for $\mu_S = 0$ and for $R/r = 10$ to -10. The results of these calculations are shown in Figure 68.

It is seen from Figure 68 that the DAVI Beta gives better high-frequency isolation than the DAVI Gamma for $R/r > 0.5$ and that the DAVI Gamma gives better high-frequency isolation than the DAVI Beta for $R/r < 0.5$.

Invariant Point

From Equation 91, it is seen that the DAVI Beta transmissibility equation can be written in the form of

$$(T_\beta)^2 = \frac{A^2}{C^2} + \frac{B^2}{D^2} \qquad (152)$$

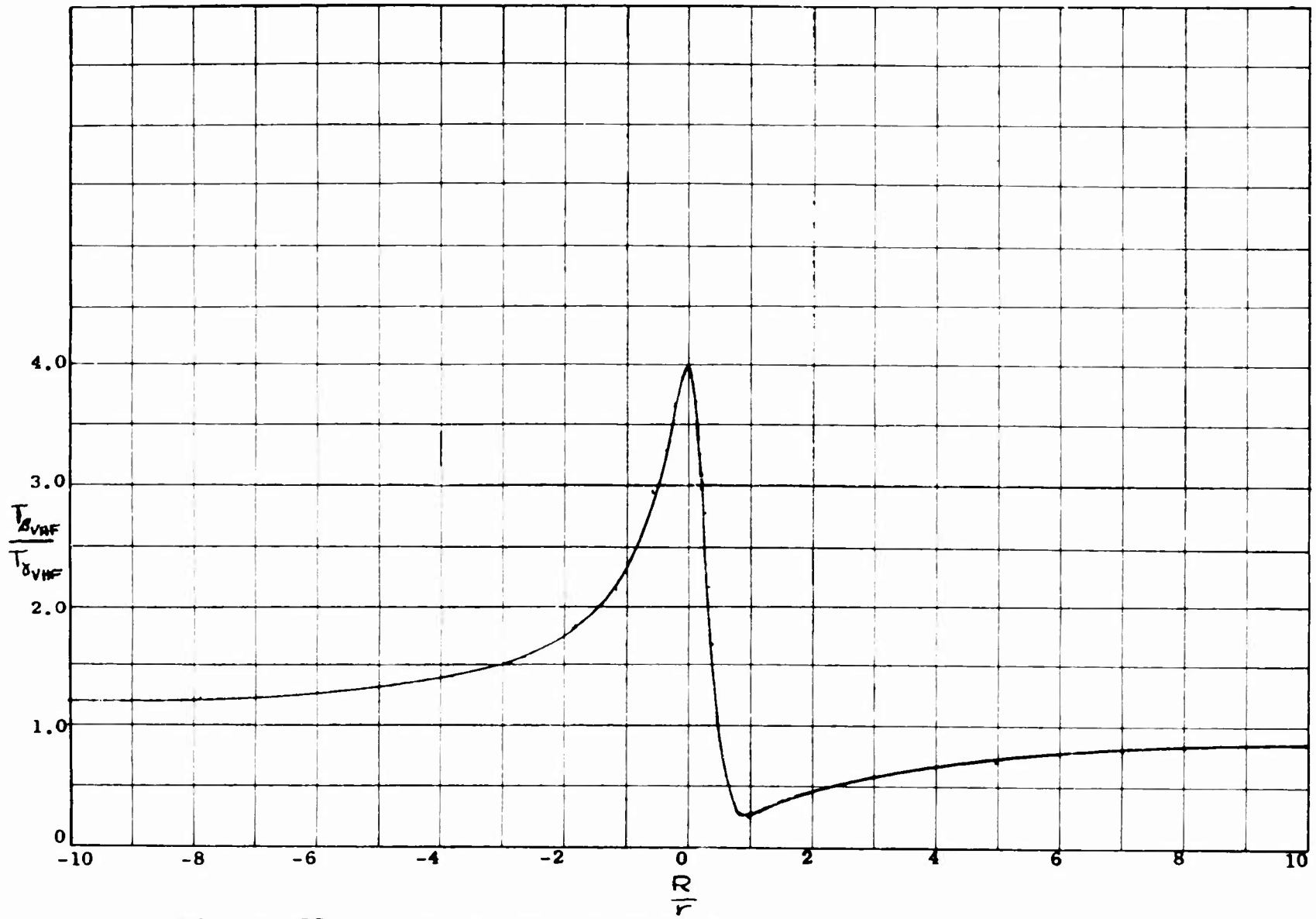

Figure 68. Comparison of DAVI Beta and Gamma at High Frequency

For $\mu_S = 0$ and $\varphi_A = 0$, the transmissibility may be rewritten as

$$(T_B)^2 = \frac{A^2}{C^2} + \frac{4 F_S B'^2}{4 F_S D'^2} \tag{153}$$

where

$$A = \frac{\omega_S^2}{\omega_A^2}\left(1 - \frac{\omega^2}{\omega_A^2}\right) \tag{154}$$

$$B' = \frac{\omega}{\omega_A}\frac{\omega_S}{\omega_A}\left(1 - \frac{\omega^2}{\omega_A^2}\right) \tag{155}$$

$$C = \left\{\frac{\mu_D\left[\left(\frac{R}{r}\right)^2 + \left(\frac{\rho}{r}\right)^2\right] + \mu_D^2\frac{\rho^2}{r^2}}{M_A/M_I}\right\}\frac{\omega^4}{\omega_A^4} - \left[\frac{\omega_S^2}{\omega_A^2}\frac{M_R}{M_I} + (1+\mu_D)\right]\frac{\omega^2}{\omega_A^2} + \frac{\omega_S^2}{\omega_A^2} \tag{156}$$

$$D' = \frac{\omega}{\omega_A}\frac{\omega_S}{\omega_A}\left(1 - \frac{M_R}{M_A}\frac{\omega^2}{\omega_A^2}\right) \tag{157}$$

and the transmissibility will be independent of the damping across the series element when $A/C = \pm B'/D'$, or

$$\frac{\frac{\omega_S^2}{\omega_A^2}\left(1 - \frac{\omega^2}{\omega_A^2}\right)}{\left\{\frac{\mu_D\left[\frac{R^2}{r^2} + \frac{\rho^2}{r^2}\right] + \mu_D\frac{\rho^2}{r^2}}{M_A/M_I}\right\}\frac{\omega^4}{\omega_A^4} - \left[\frac{\omega_S^2}{\omega_A^2}\frac{M_R}{M_A} + (1+\mu_D)\right]\frac{\omega^2}{\omega_A^2} + \frac{\omega_S^2}{\omega_A^2}} = \pm\frac{\left(1 - \frac{\omega^2}{\omega_A^2}\right)}{\left(1 - \frac{M_R}{M_A}\frac{\omega^2}{\omega_A^2}\right)} \tag{158}$$

It is seen from the above equation that one invariant point occurs at the antiresonant frequency of the DAVI Beta. Disregarding this trivial point, first using the negative sign, Equation (158) becomes

$$\left[\frac{\mu_D\left(\frac{R^2}{r^2} + \frac{\rho^2}{r^2}\right) + \mu_D^2\frac{\rho^2}{r^2}}{M_A/M_I}\right]\frac{\omega^4}{\omega_A^4} - \left[2\frac{\omega_S^2}{\omega_A^2}\frac{M_R}{M_A} + (1+\mu_D)\right]\frac{\omega^2}{\omega_A^2} + 2\frac{\omega_S^2}{\omega_A^2} = 0 \tag{159}$$

which gives two invariant points.

Using the positive sign of Equation (158), Equation (158) becomes

$$\left[\frac{\mu_D\left(\frac{R^2}{r^2} + \frac{\rho^2}{r^2}\right) + \mu_D^2\frac{\rho^2}{r^2}}{M_A/M_I}\right]\frac{\omega^4}{\omega_A^4} - (1+\mu_D)\frac{\omega^2}{\omega_A^2} = 0 \tag{160}$$

Disregarding the trivial case of $\omega^2/\omega_A^2 = 0$, one invariant point is obtained. Substituting that $M_A/M_I = \mu_D\left[\frac{R}{r}\left(\frac{R}{r}-1\right)+\frac{\rho^2}{r^2}\right]$ into Equation (160), Equation (160) becomes

$$\frac{\omega^2}{\omega_A^2} = \frac{(1+\mu_D)\left[\left(\frac{R}{r}-1\right)\frac{R}{r}+\frac{\rho^2}{r^2}\right]}{\left[\frac{R^2}{r^2}+\frac{\rho^2}{r^2}\right]+\mu_D\frac{\rho^2}{r^2}} \tag{161}$$

An inspection of Equation (103) shows that Equation (161) can be rewritten as

$$\frac{\omega^2}{\omega_A^2} = \frac{(1+\mu_D)\,T_{\theta VHF}}{\left(1+\frac{K_S}{K_D}\right)T_{C\,VHF}} \tag{162}$$

From this equation, it is seen that if an efficient DAVI Beta is designed, that is, if the high-frequency isolation of the DAVI Beta is much better than the conventional system, this invariant point will always be less than the antiresonant frequency.

As in the DAVI Beta, the transmissibility of the DAVI Gamma will be independent of the damping when $A/C = \pm B'/D'$, where for the DAVI Gamma, when $\alpha_S = 0$ and $\gamma_A = 0$,

$$A = \frac{\omega_S^2}{\omega_A^2}\left(1-\frac{\omega^2}{\omega_A^2}\right) \tag{163}$$

$$B' = \frac{\omega}{\omega_A}\frac{\omega_S}{\omega_A}\left(1-\frac{\omega^2}{\omega_A^2}\right) \tag{164}$$

$$C = \frac{M_R'}{M_A}\frac{\omega^4}{\omega_A^4} - \left[\frac{\omega_S^2}{\omega_A^2}\left(\frac{M_R'}{M_A}+\frac{1}{M_A/M_I}\right)+1\right]\frac{\omega^2}{\omega_A^2}+\frac{\omega^2}{\omega_A^2} \tag{165}$$

$$D' = \frac{\omega}{\omega_A}\frac{\omega_S}{\omega_A}\left[1-\left(\frac{M_R'}{M_A}+\frac{1}{M_A/M_I}\right)\frac{\omega^2}{\omega_A^2}\right] \tag{166}$$

Therefore, the invariant points may be obtained from

$$\frac{\frac{\omega_s^2}{\omega_A^2}\left(1-\frac{\omega^2}{\omega_A^2}\right)}{\frac{M_R'}{M_A}\frac{\omega^4}{\omega_A^4}-\left[\frac{\omega_s^2}{\omega_A^2}\left(\frac{M_R'}{M_A}+\frac{1}{M_A/M_I}\right)+1\right]\frac{\omega^2}{\omega_A^2}+\frac{\omega_s^2}{\omega_A^2}} = \pm \frac{\left(1-\frac{\omega^2}{\omega_A^2}\right)}{\left[1-\left(\frac{M_R'}{M_A}+\frac{1}{M_A/M_I}\right)\frac{\omega^2}{\omega_A^2}\right]} \quad (167)$$

It is seen from the above equation that one invariant point occurs at the antiresonant frequency of the DAVI Gamma. Disregarding this trivial point, first using the negative sign, Equation (167) becomes

$$\frac{M_R'}{M_A}\frac{\omega^4}{\omega_A^4}-\left[2\frac{\omega_s^2}{\omega_A^2}\left(\frac{M_R'}{M_A}+\frac{1}{M_A/M_I}\right)+1\right]\frac{\omega^2}{\omega_A^2}+2\frac{\omega_s^2}{\omega_A^2}=0 \quad (168)$$

which gives two invariant points.

Using the positive sign of Equation (167), Equation (167) becomes

$$\frac{M_R'}{M_A}\frac{\omega^4}{\omega_A^4}-\frac{\omega^2}{\omega_A^2}=0 \quad (169)$$

Disregarding the trivial case of $\omega^2/\omega_A^2 = 0$, one invariant point is obtained. Making the substitution in Equation (169) that $M_R'/M_I = \mu_D\left[\left(\frac{R}{r}-1\right)^2+\frac{\rho_1^2}{r^2}\right]$ with $\mu_s = 0$ and that $M_A/M_I = \mu_D\left[\frac{R}{r}\left(\frac{R}{r}-1\right)+\frac{\rho_2^2}{r^2}\right]$, then Equation (169) becomes

$$\frac{\omega^2}{\omega_A^2}=\frac{\left[\left(\frac{R}{r}\right)\left(\frac{R}{r}-1\right)+\frac{\rho^2}{r^2}\right]}{\left[\left(\frac{R}{r}-1\right)^2+\frac{\rho^2}{r^2}\right]} \quad (170)$$

An inspection of Equation (125) shows that Equation (170) can be rewritten as

$$\frac{\omega^2}{\omega_A^2}=\frac{T_{\gamma_{VHF}}}{T_{C_{VHF}}\left(1+\frac{K_s}{K_D}\right)} \quad (171)$$

From this equation, it is seen that if a DAVI Gamma is designed to give better high-frequency isolation than a conventional isolator, this invariant point will always be less than the antiresonant frequency.

In order to obtain the effects of damping, the transmissibility was obtained for both the DAVI Beta and the DAVI Gamma for the configurations given in Table V.

TABLE V

DAVI BETA AND GAMMA PARAMETERS

ω_S/ω_A	K_S/K_D	R/r	ρ^2/r^2	μ_D
.129	.5	1.0	.3333	.10
.129	.5	.0	.3333	.10

The calculations were done for a range of damping (f_S) from 0 to .10 in increments of .025. The results of these calculations are shown in Figures 69 through 72.

It is seen from these figures that damping is very effective in reducing the amplitude of the second resonance in both the DAVI Beta and the DAVI Gamma. With $f_S = .025$, isolation is obtained at the second resonance in all cases calculated. For the DAVI Beta and the DAVI Gamma in which the two resonances occur below the antiresonant frequency, the optimum damping is $f_S = .075$; and when the antiresonance occurs between the resonant conditions, the optimum damping is $f_S = .050$. It is also seen in both the DAVI Beta and the DAVI Gamma that when the two resonances are below the antiresonance, better high-frequency isolation is obtained than when the antiresonance is between the resonances.

TEST

DAVI Beta

Equipment and Procedure

The test fixture used for these tests is shown in Figures 13 and 14. Original testing for the DAVI Beta was done utilizing an MB Model S-DA electromagnetic shaker with a force capability of 10 pounds connected to the base weight. Two MB velocity pickups were attached to the input and isolated weights. The output of the pickups was fed to an MB vibration meter, and the results were manually recorded. Results using this procedure were very poor in that good correlation was obtained in the low-frequency range, but high-frequency isolation was very poor. It was determined that the cause of these results was an inherent

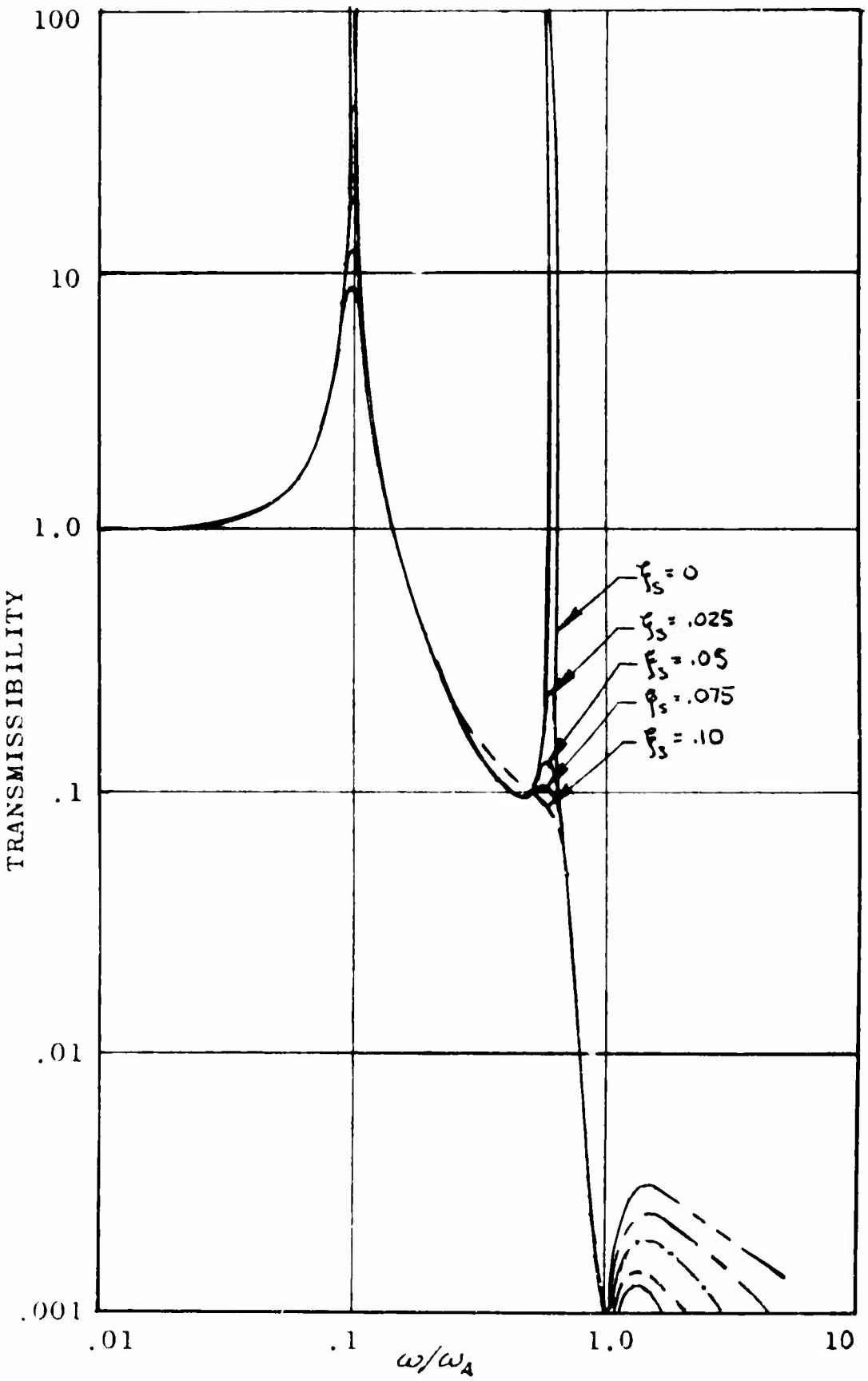

Figure 69. Damping of DAVI With Both Resonances Below the Antiresonance

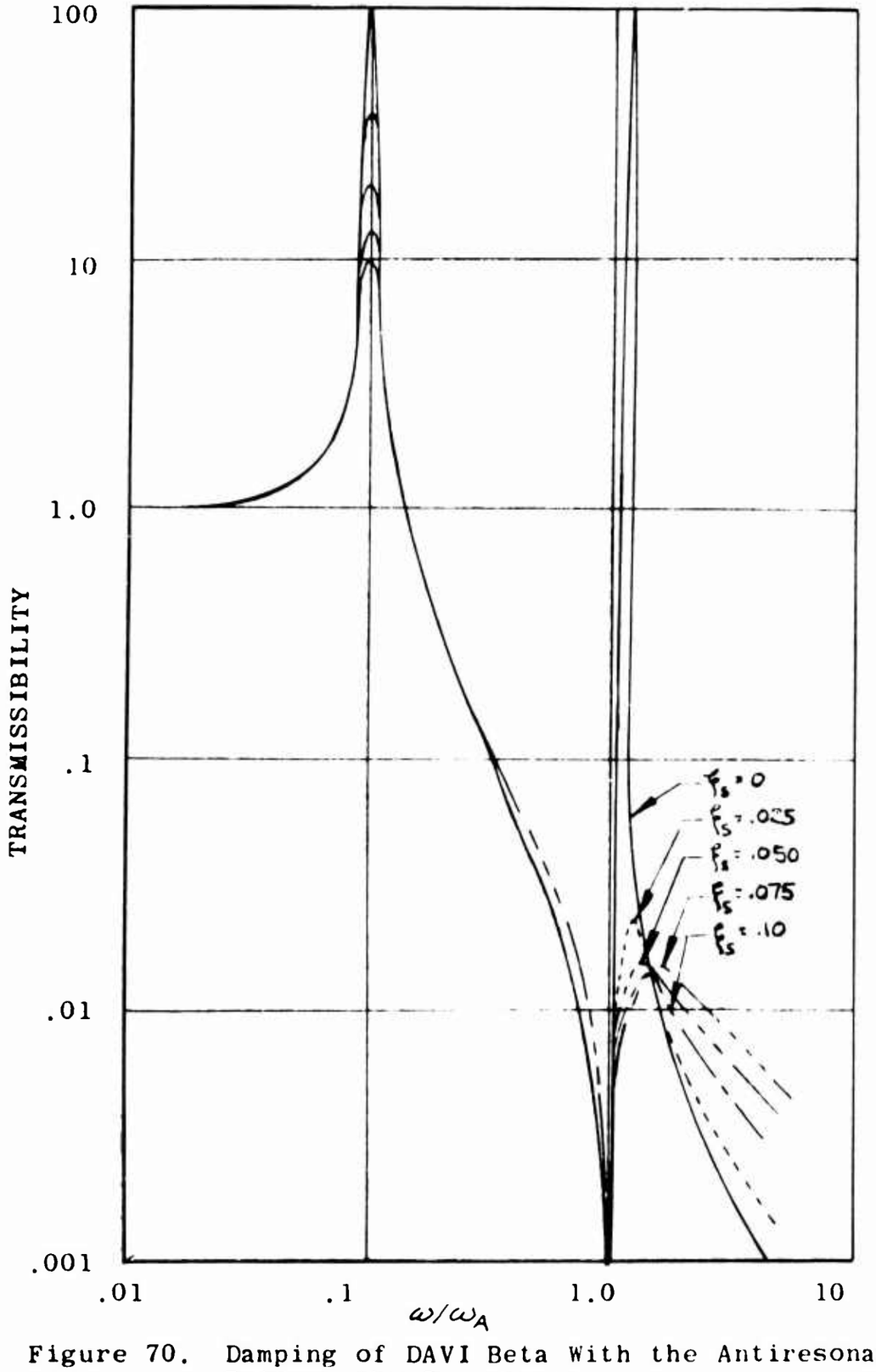

Figure 70. Damping of DAVI Beta With the Antiresonance Between the Resonances

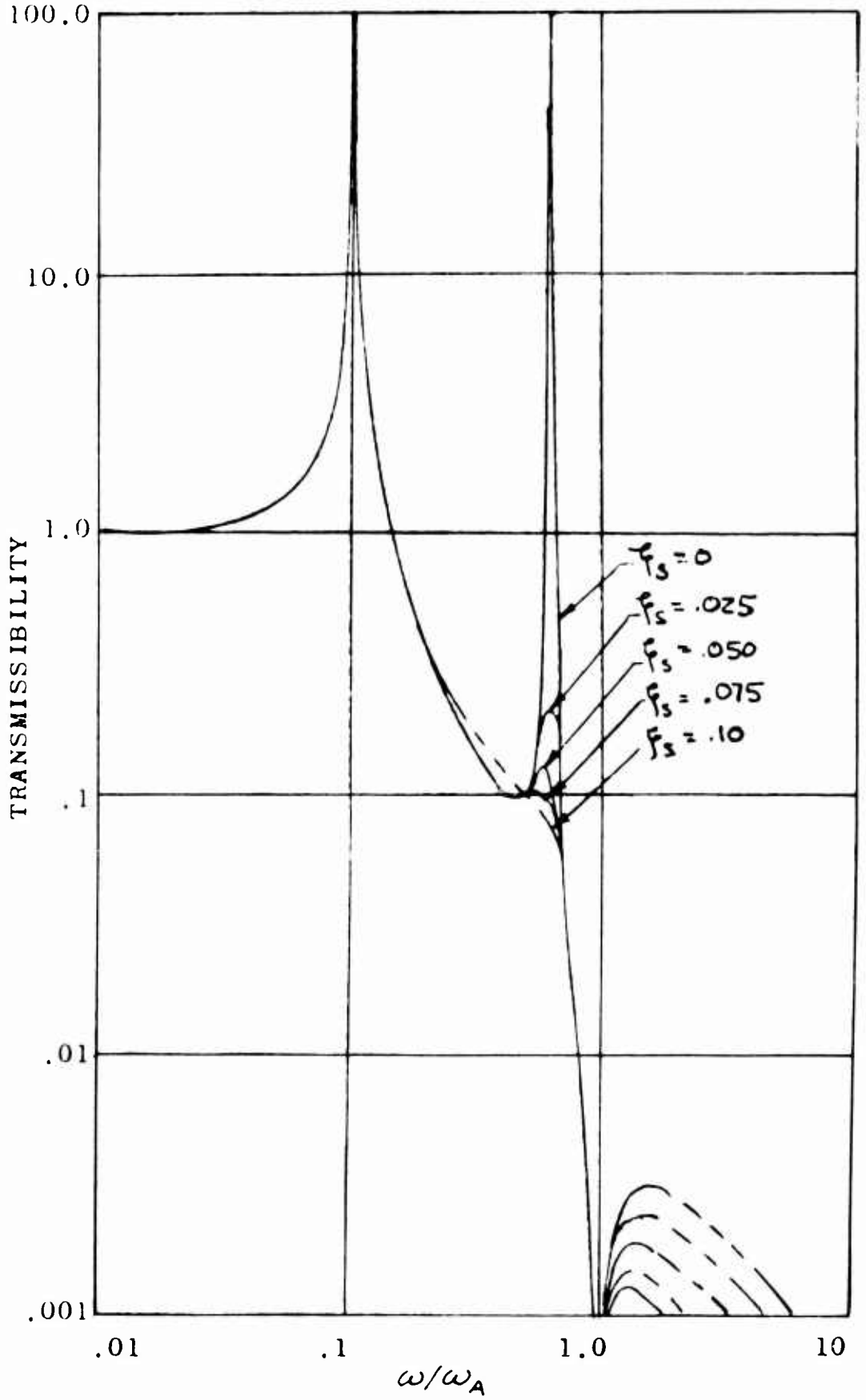

Figure 71. Damping of DAVI Gamma With Both Resonances Below the Antiresonance

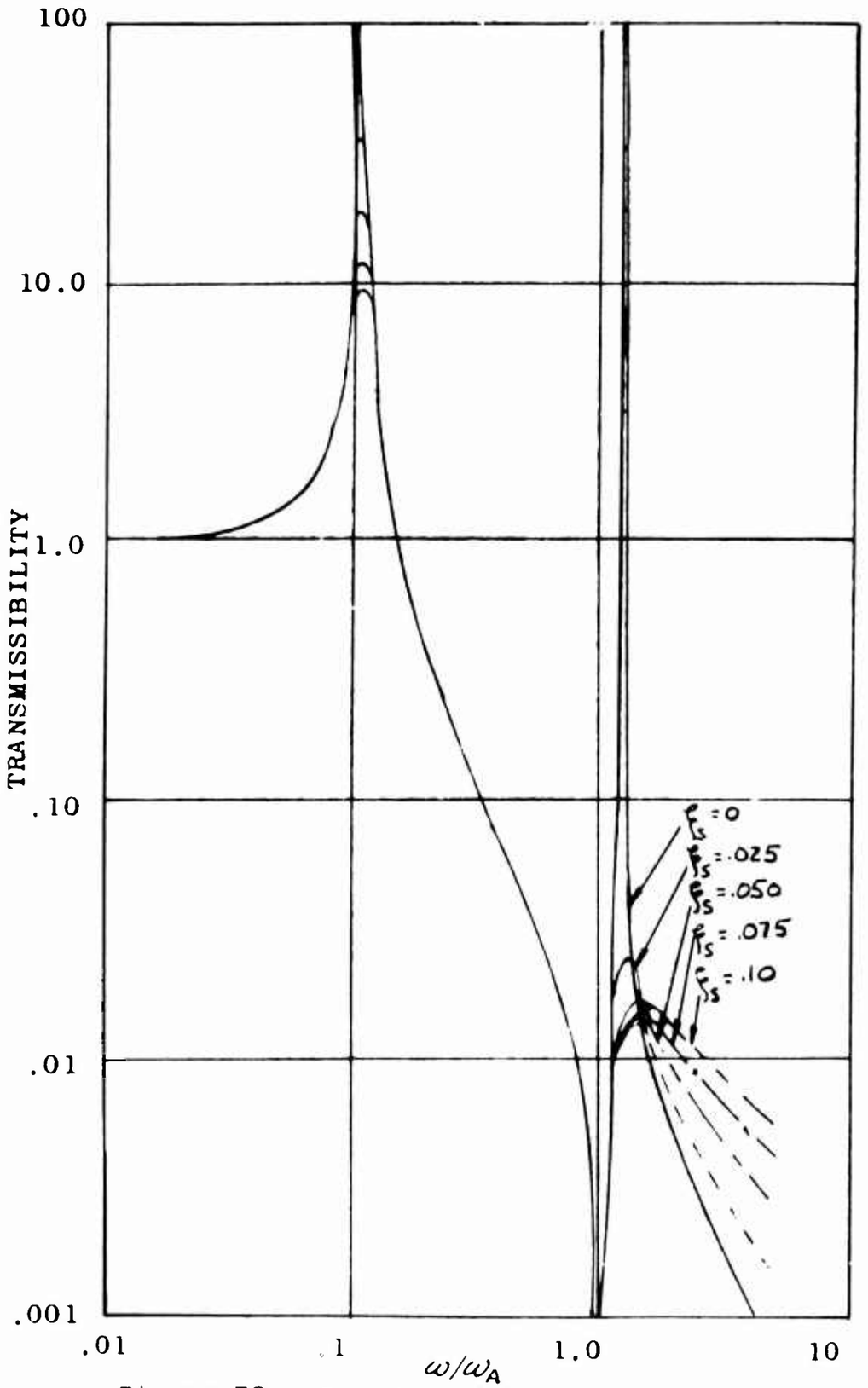

Figure 72. Damping of DAVI Gamma With the Antiresonance Between the Resonances

noise problem in the rig due to rotation of the shafts and gear noise. In order to eliminate this problem, an MB Model C-11 electromagnetic shaker with a force capability of 50 pounds was used to make the actual response to noise level larger. Filters were also designed to attenuate the noise level. Data were recorded manually from readings made on a Hewlett Packard Model Scope. The following table gives the configurations tested.

TABLE VI

DAVI BETA CONFIGURATIONS TESTED

Isolated Weight (Lb)	Percent Damping		DAVI Inertia Bar Weight (Lb)	Spring Rate (Lb/In.)		R (In.)	r (In.)	ρ (In.)	Fig. No.
	ζ_S	ζ_A		K_S	K_D				
27	.016	.01	.9	396	428	+3.0	2.0	2.58	75
27	.050	.01	.9	396	428	3.0	2.0	2.58	76
27	.117	.01	.9	396	428	3.0	2.0	2.58	77
27	.016	.01	2.25	396	428	4.20	2.00	2.435	78
27	.050	.01	2.25	396	428	4.20	2.00	2.435	79
27	.117	.01	2.25	396	428	4.20	2.00	2.435	80
27	.016	.01	2.25	396	450	2.95	1.00	1.92	81
27	.050	.01	2.25	396	450	2.95	1.00	1.92	82
27	.117	.01	2.25	396	450	2.95	1.00	1.92	83
27	.016	.01	2.25	396	484	3.68	.76	2.30	84
27	.050	.01	2.25	396	484	3.68	.76	2.30	85
27	.117	.01	2.25	396	484	3.68	.76	2.30	86

The DAVI Beta model that was used in the tests is shown in Figures 73 and 74. It is seen from these figures that the model used was the same DAVI used in the DAVI Alpha unidirectional testing. The series element was the spring rates of another DAVI unit with the inertia bar and pivots removed. Since compressive coil springs were used in the series element, these coil springs gave minimum damping. A Sesco Model Rotary Damper was used to control the amount of damping across the series element.

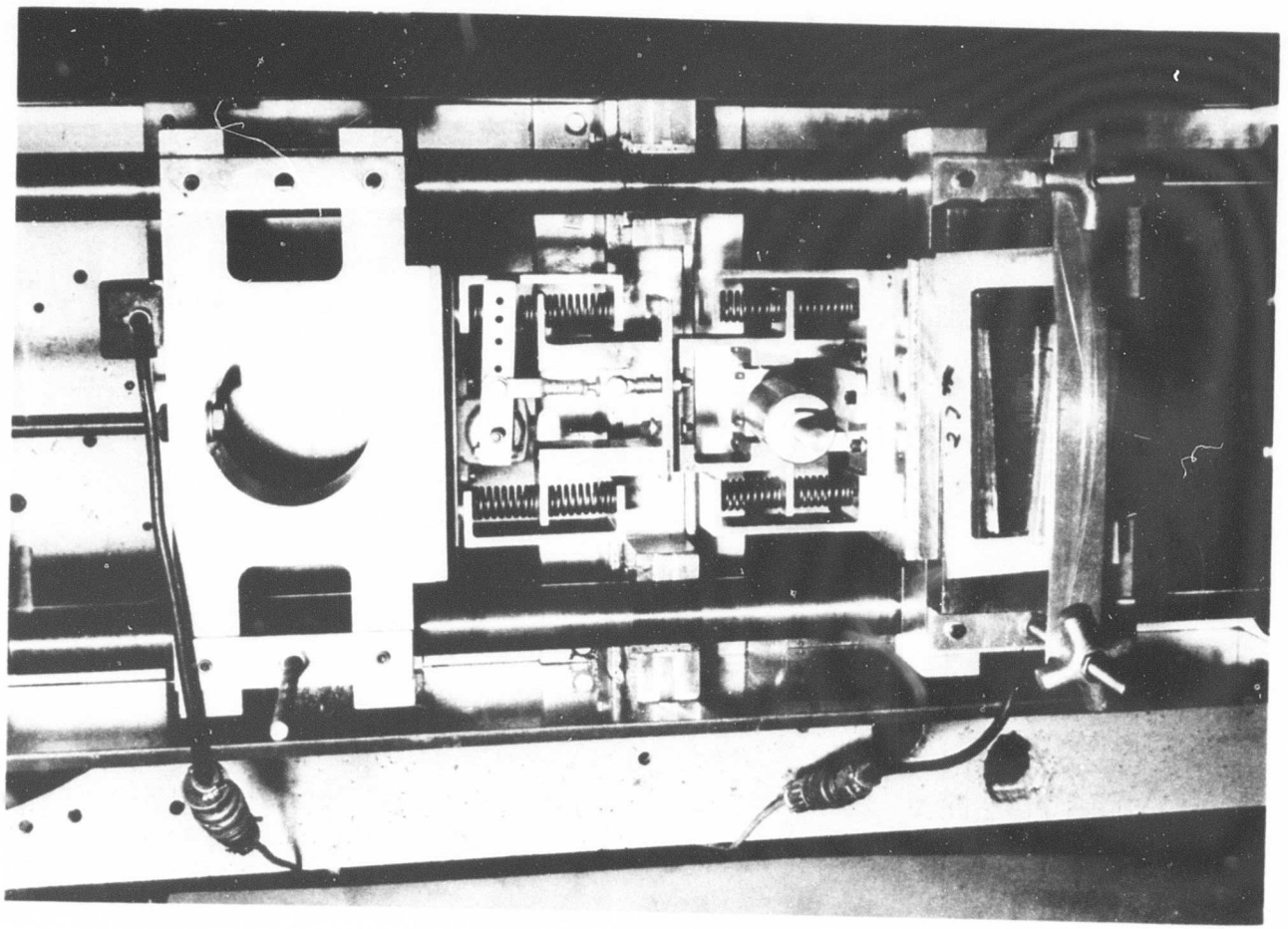

Figure 73. Top View of DAVI Beta Installed in the Test Rig

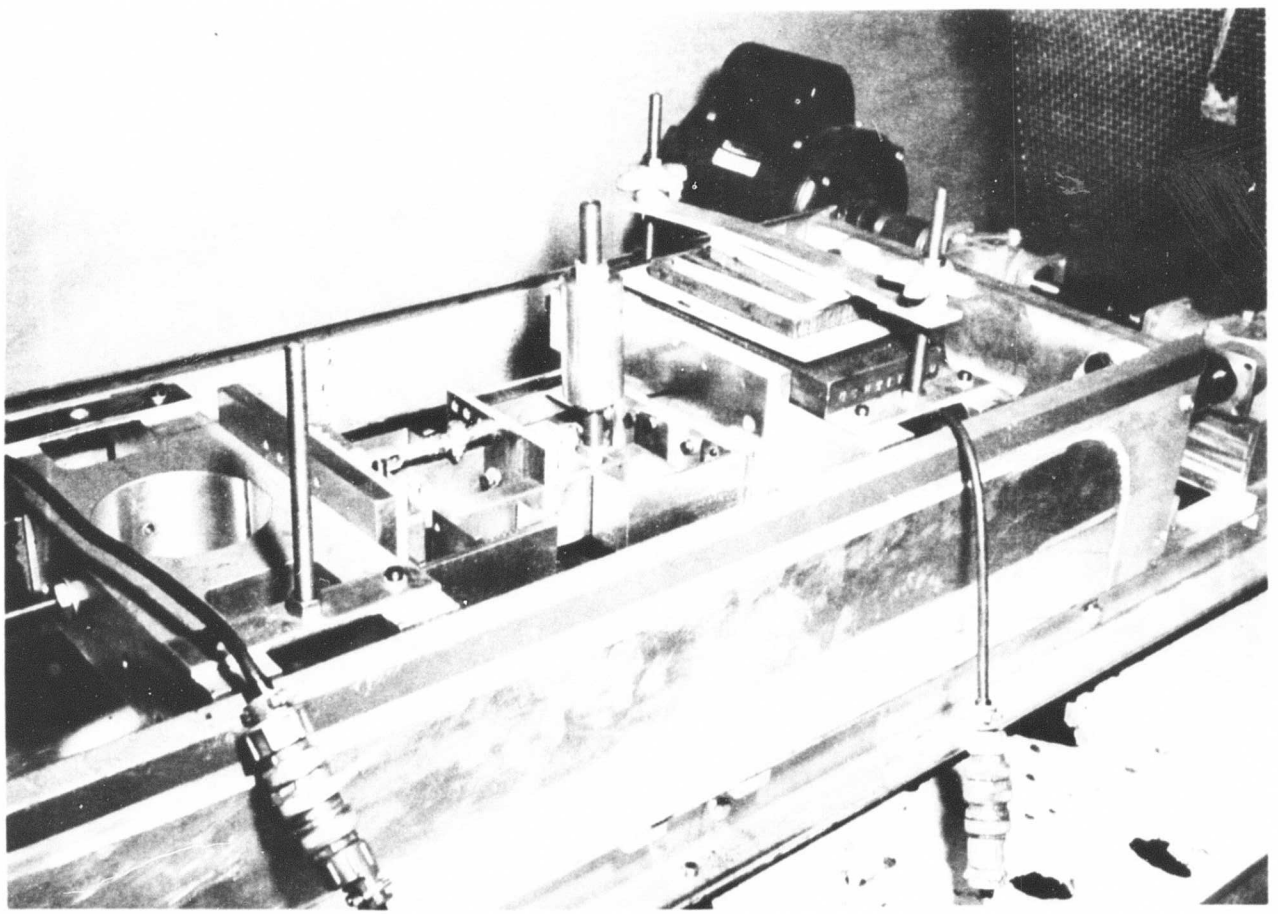

Figure 74. Side View of DAVI Beta Installed in the Test Rig

Results

In these series of tests, four different configurations were tested, each having three different values of damping across the series element. The main purpose of this testing was to determine the effects of damping, especially on the transmissibility of the upper natural frequency.

It is seen from the following table and Figures 75 through 86 that the results of the test were as expected - that the increased damping did reduce the transmissibilities at the natural frequencies, that the antiresonant frequency was not affected by the magnitude of damping, and that high-frequency isolation was obtained. It is seen in the first three figures that with only 1.6-percent critical damping, the transmissibility at the higher natural frequency was only .3. With the damping increased to 5 percent and 11.7 percent critical, the second natural frequency appears to be virtually eliminated.

TABLE VII

SUMMARY OF DAVI BETA TEST RESULTS

Mode				Antiresonance		
Natural Frequency (c.p.s.)	Trans.	Natural Frequency (c.p.s.)	Trans.	Frequency (c.p.s.)	Trans.	Fig. No.
8.0	55.0	37.0	.3	40.0	.015	75
11.0	26.0	-	-	41.0	.010	76
10.0	84.0	-	-	42.0	.005	77
8.0	30.0	22.0	.36	20.0	.037	78
9.8	7.5	26.0	.26	20.0	.010	79
10.0	9.0	25.0	.31	20.0	.0065	80
8.0	32.0	16.0	1.8	14.0	.003	81
9.4	5.0	19.0	1.7	14.0	.002	82
9.4	14.0	20.0	.95	14.0	.0065	83
7.2	10.7	12.0	22.0	8.6	.030	84
7.6	6.5	13.0	2.0	8.6	.010	85
7.6	5.6	12.2	1.7	8.6	.015	86

Correlation

The analytical and test results were correlated. The analytical results are plotted in Figures 75 through 86. It is seen that in all cases, the analytical predictions compare favorably with the test results. Excellent correlation is obtained with the minimum amount of critical damping. Poorer correlation is obtained with the higher amounts of critical damping, in that the natural frequencies are not predicted as well. This is apparently due to the fact that in testing for the lowest critical damping, the damper arm across the series element was not attached; whereas for the higher critical damping configuration, the damper arm was attached, and a higher effective spring rate in the series element was obtained. This apparent increase in spring rate was not taken into effect when the analytical results were calculated. It is interesting to note that this effective change in spring rate did not affect the antiresonant frequency as shown by the test results.

DAVI Gamma

Equipment and Procedure

The test equipment and procedure in this series of tests were identical to those used in the DAVI Beta testing. The model was identical to that used in the DAVI Beta except that the series element and DAVI element were reversed, such that the series element and damper were between the isolated weight and the DAVI Alpha.

Results

In this series of testing, four different configurations were tested, each having three different values of damping across the series element. The amount of damping was identical to that used in the DAVI Beta testing. As in the DAVI Beta testing, the main purpose of this testing was to determine the effects of damping, especially on the transmissibility of the upper natural frequency. Table VIII gives the configurations tested.

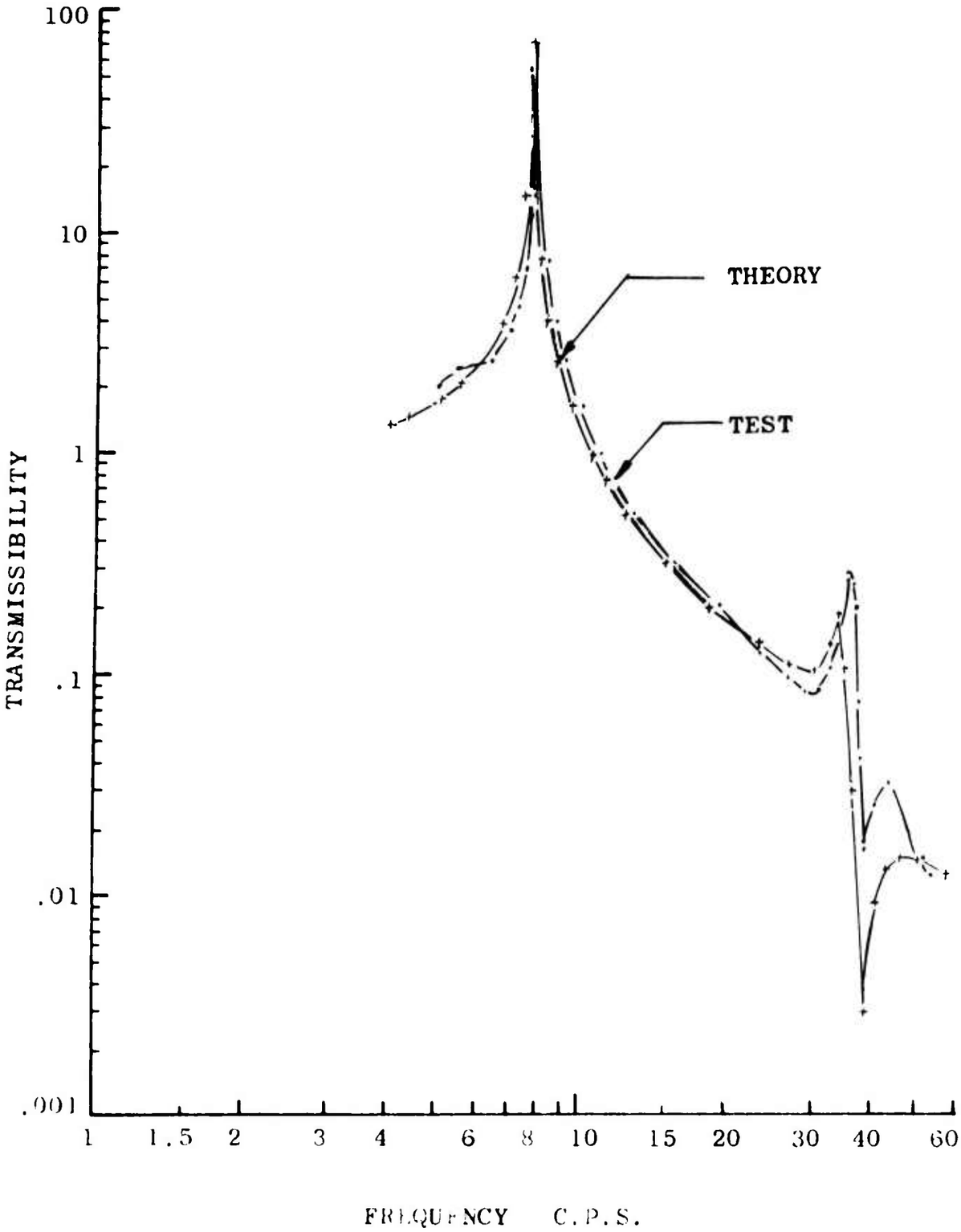

Figure 75. Analytical and Experimental Response Curves of the DAVI Beta With ζ_s = .016 and $\frac{R}{r}$ = 1.5

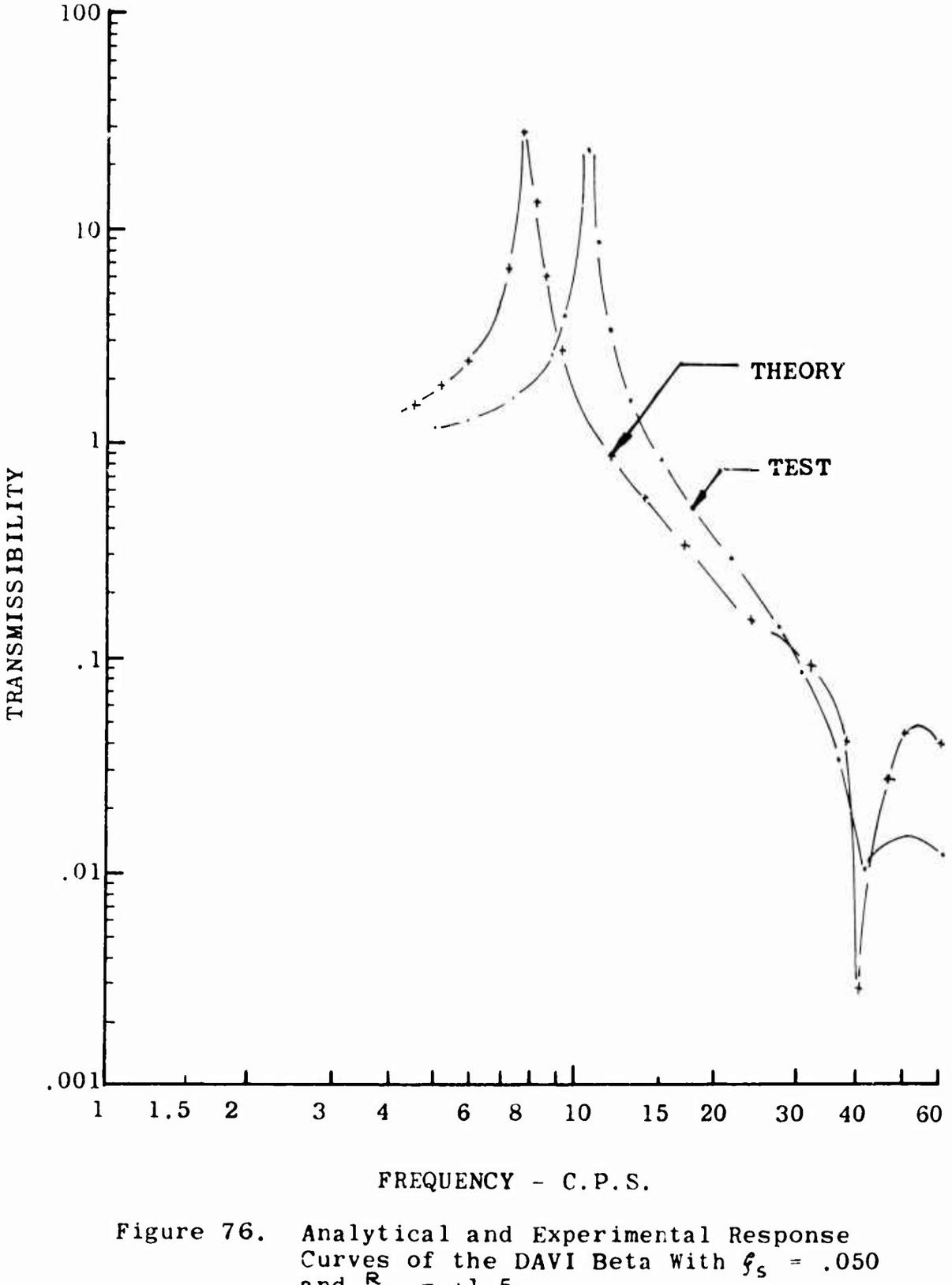

Figure 76. Analytical and Experimental Response Curves of the DAVI Beta With ζ_s = .050 and $\frac{R}{r}$ = +1.5

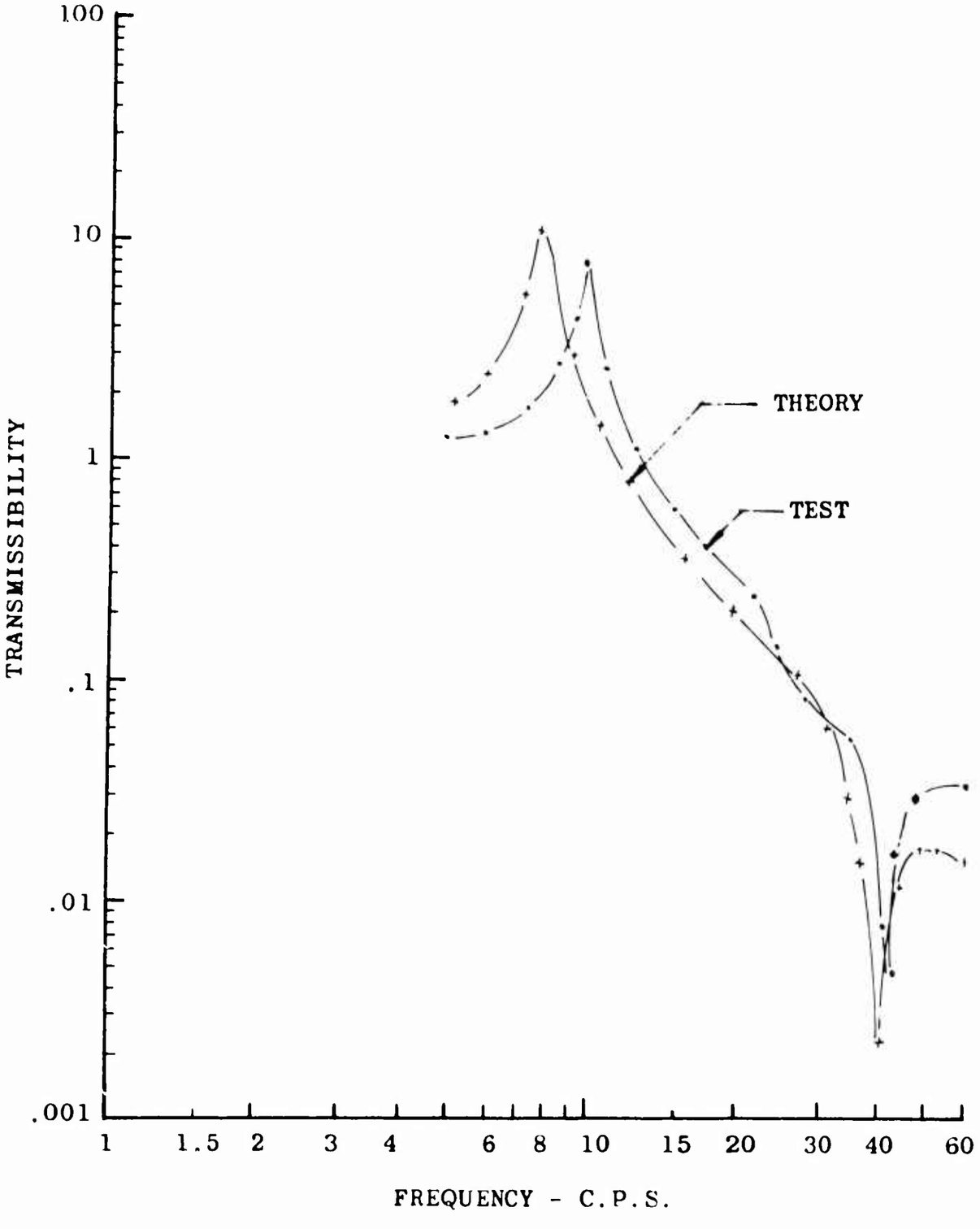

Figure 77. Analytical and Experimental Response Curves of the DAVI Beta With ζ_s = .117 and $\frac{R}{r}$ = +1.5

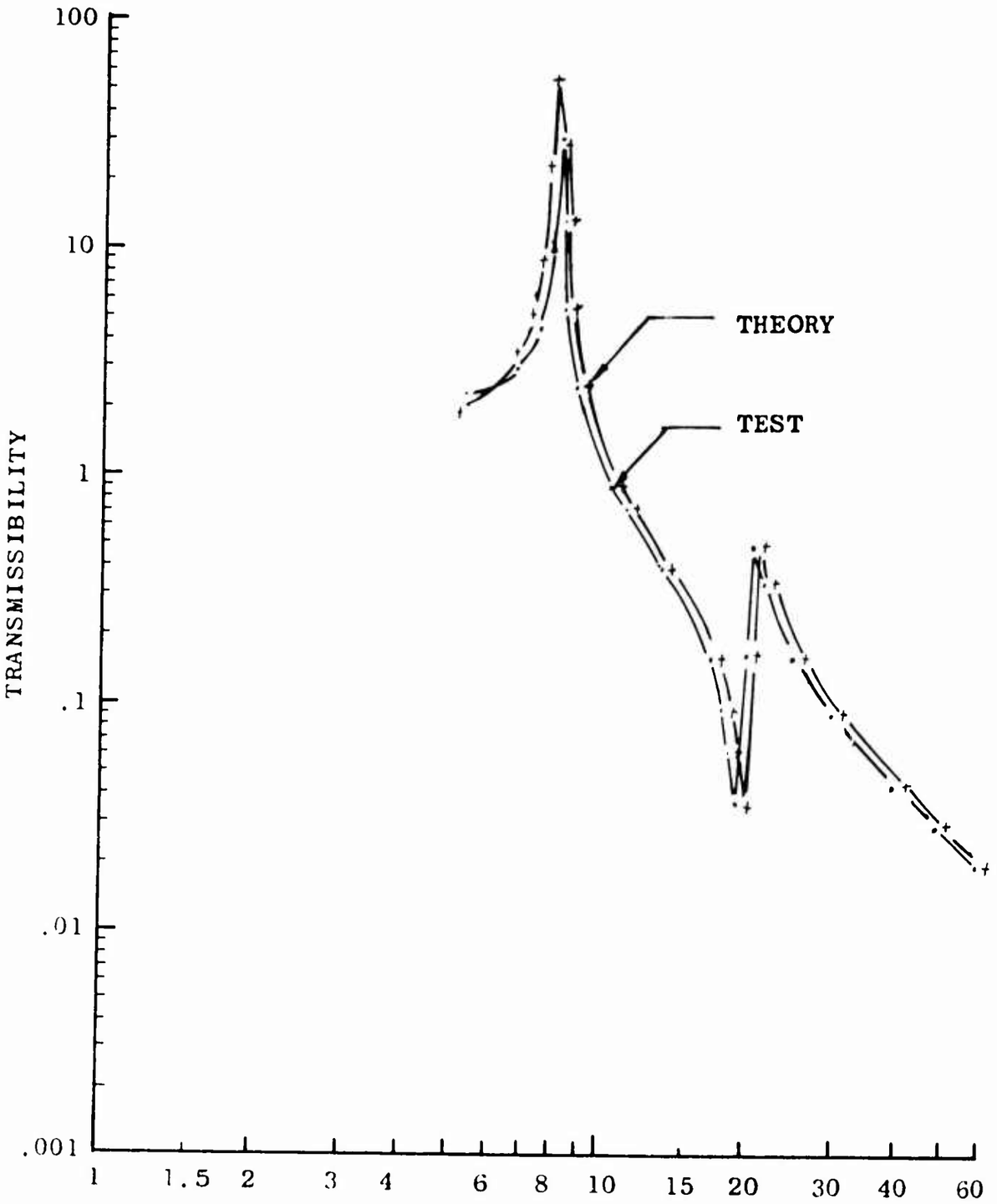

Figure 78. Analytical and Experimental Response Curves of the DAVI Beta With ζ_s = .016 and $\frac{R}{r}$ = 2.100

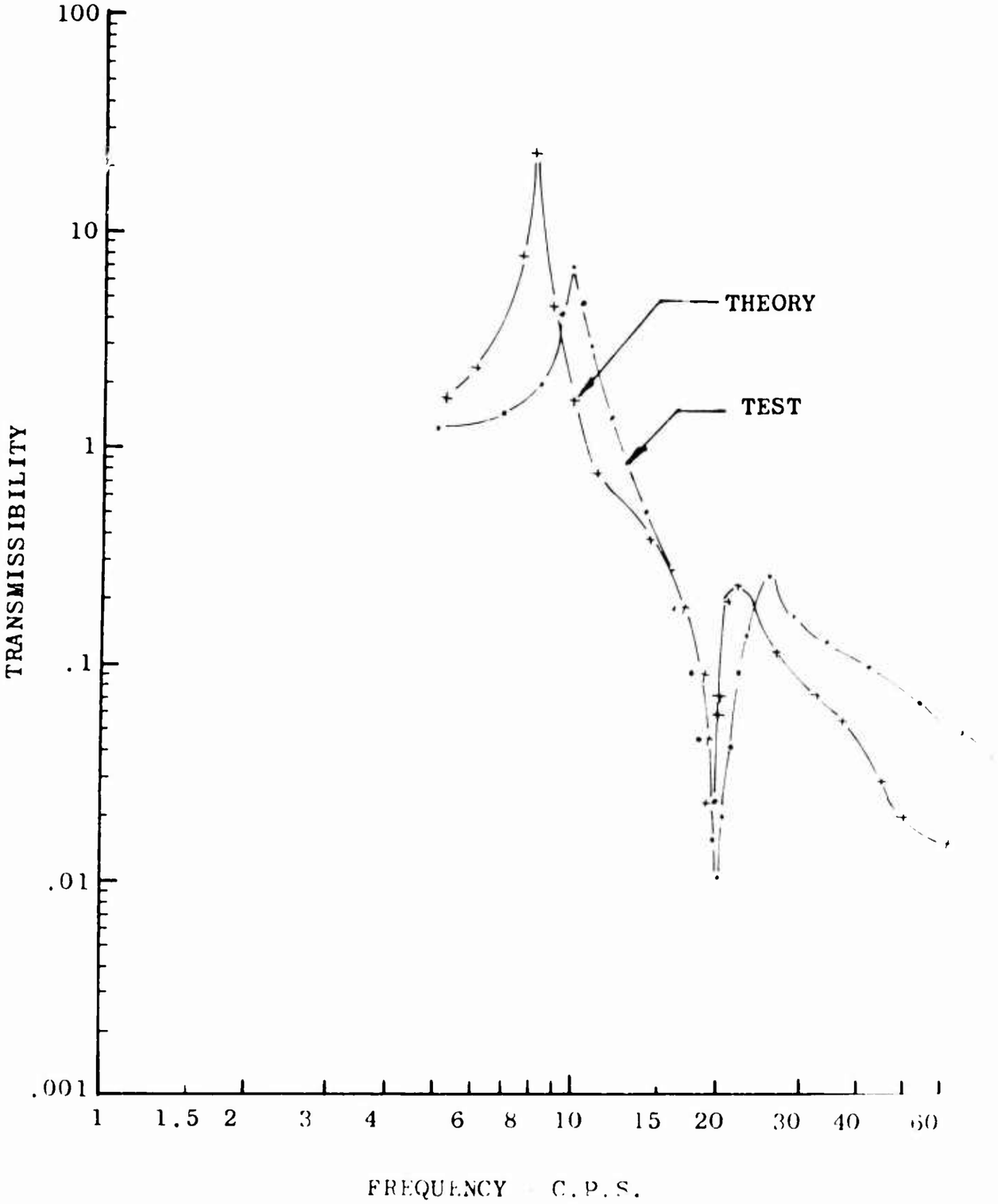

Figure 79. Analytical and Experimental Response Curves of the DAVI Beta With ζ_s = .050 and $\frac{R}{r}$ = 2.100

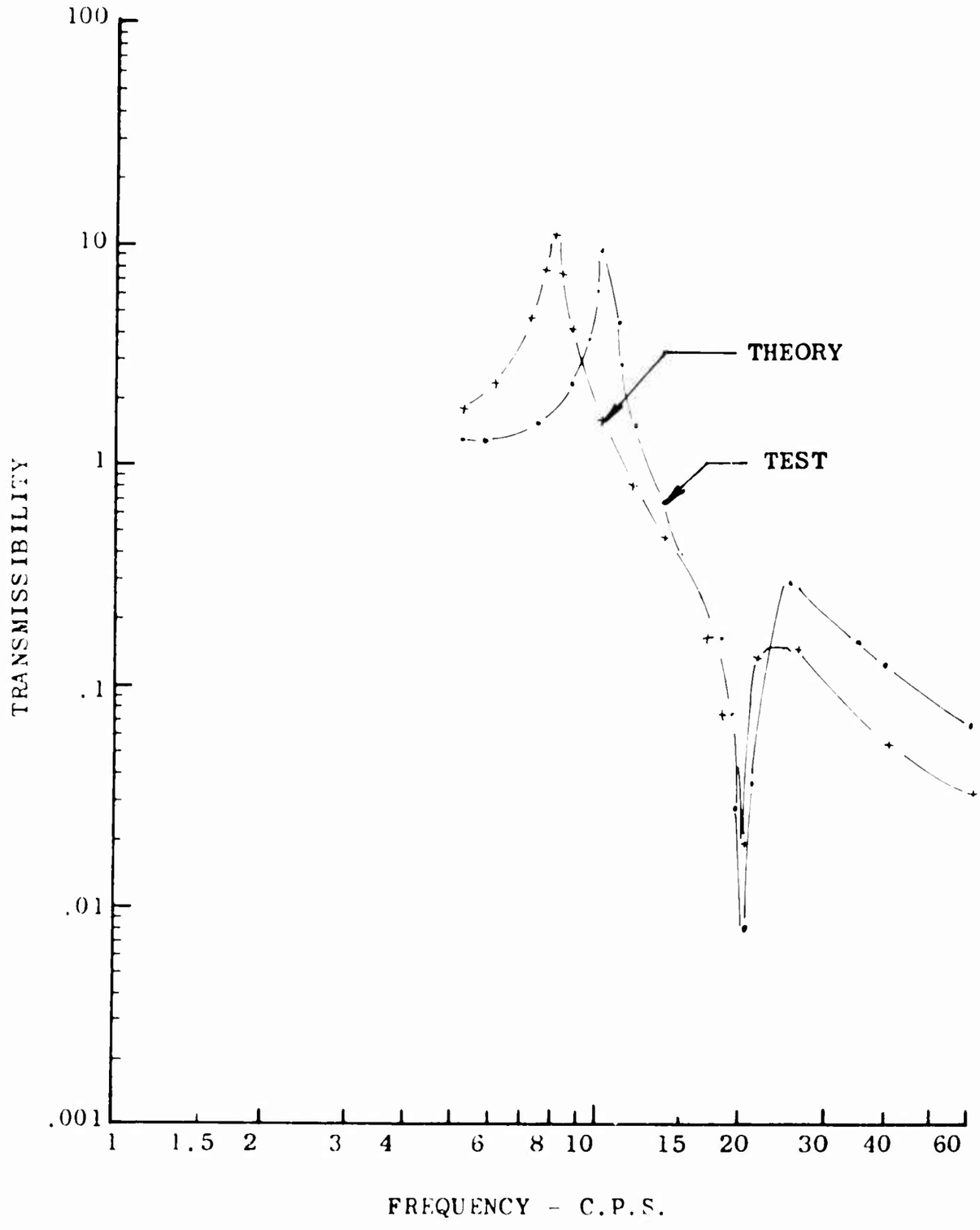

Figure 80. Analytical and Experimental Response Curves of the DAVI Beta With ζ_s = .117 and $\frac{R}{r}$ = 2.100

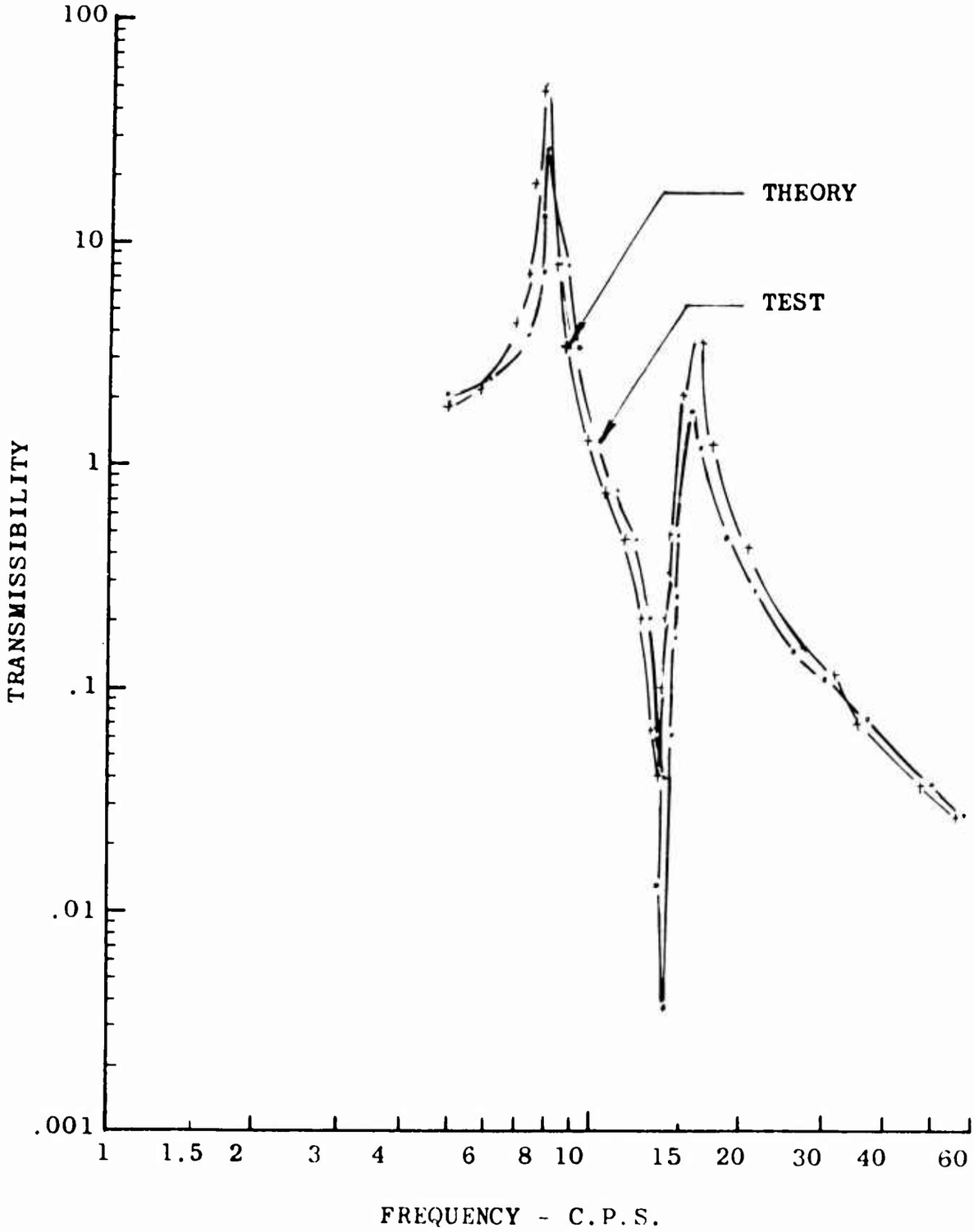

Figure 81. Analytical and Experimental Response Curves of the DAVI Beta With $\zeta_s = .016$ and $\frac{R}{r} = 2.95$

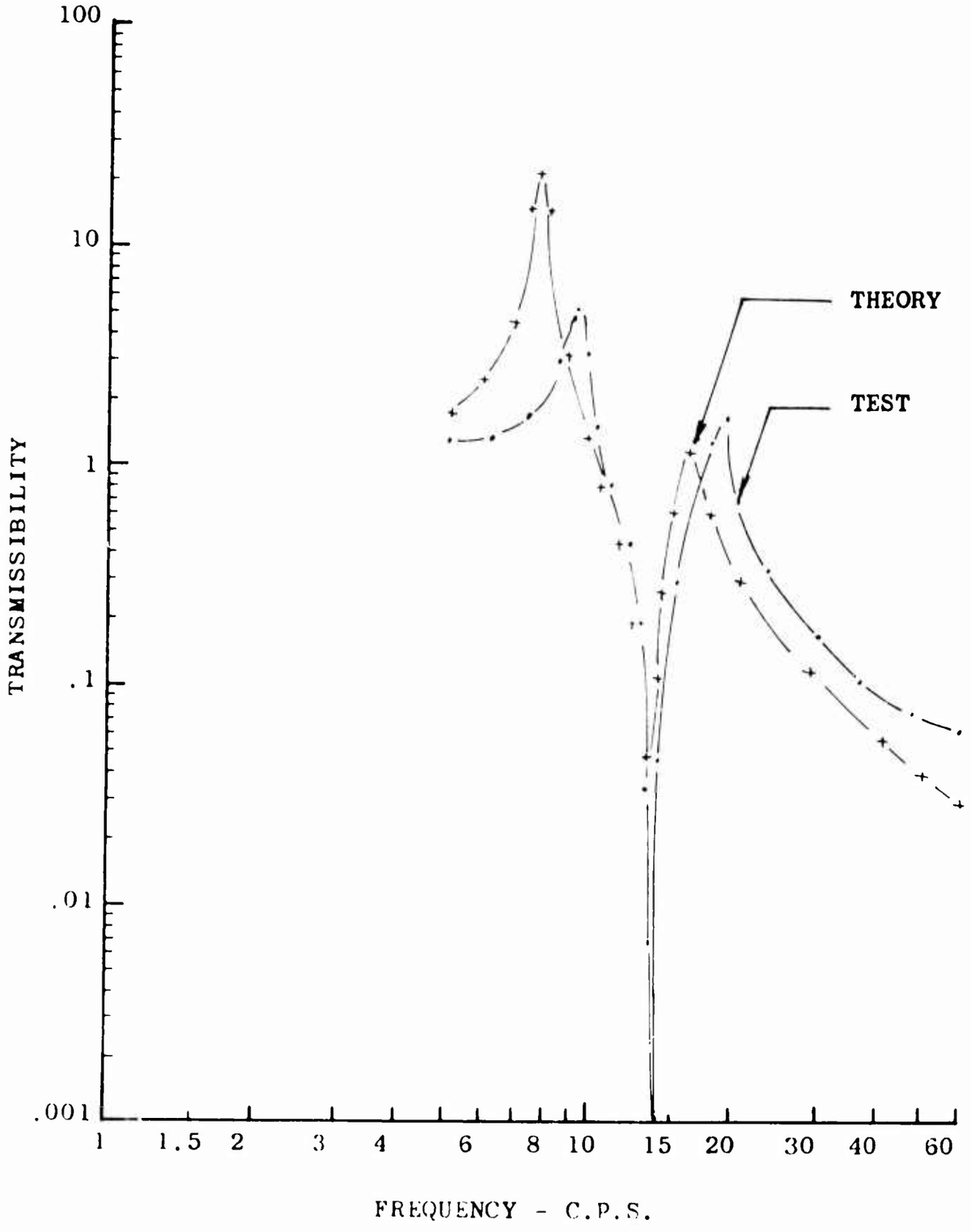

Figure 82. Analytical and Experimental Response Curves of the DAVI Beta With ζ_s = .050 and $\frac{R}{r}$ = 2.95

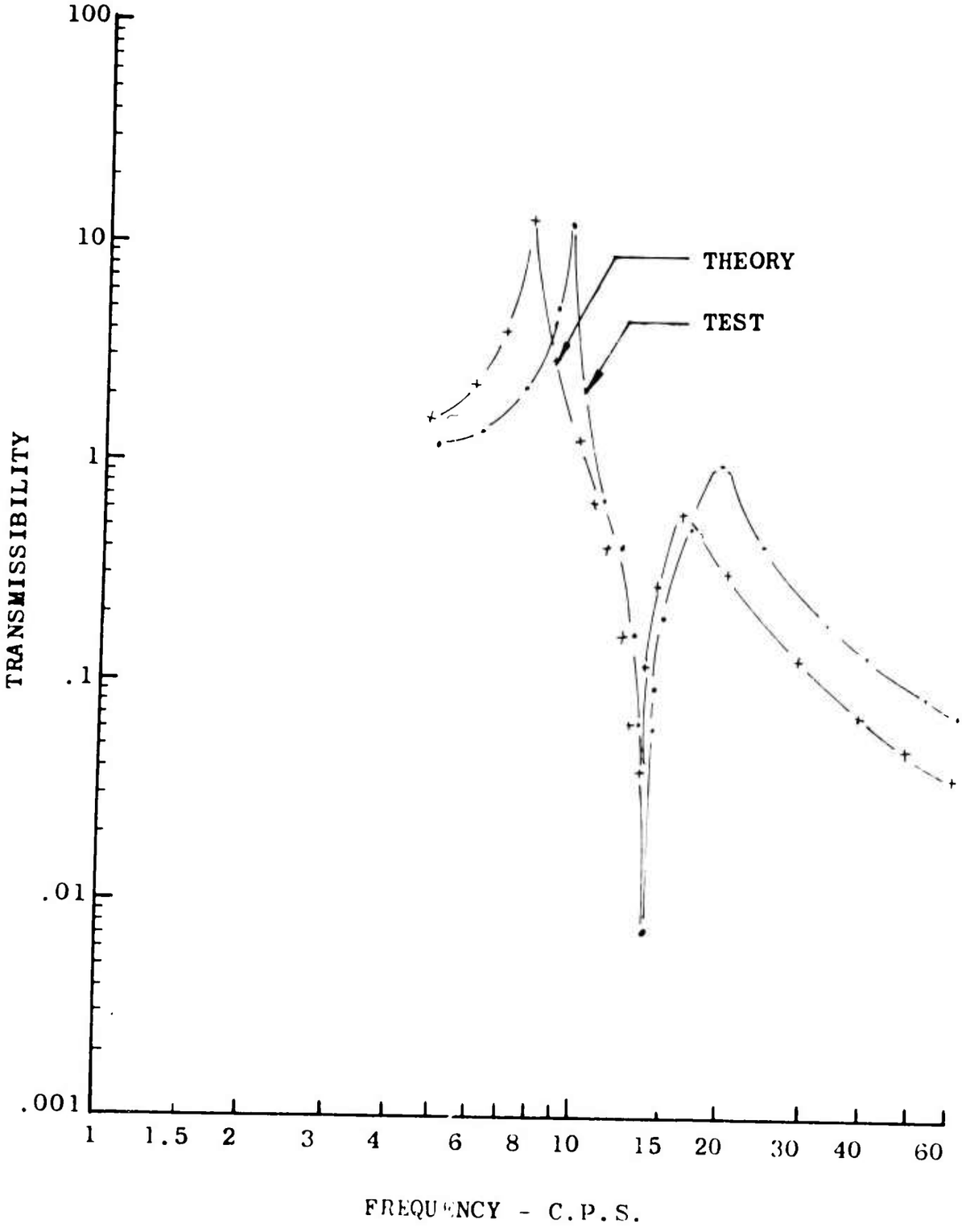

Figure 83. Analytical and Experimental Response Curves of the DAVI Beta With ζ_s = .117 and $\frac{R}{r}$ = 2.95

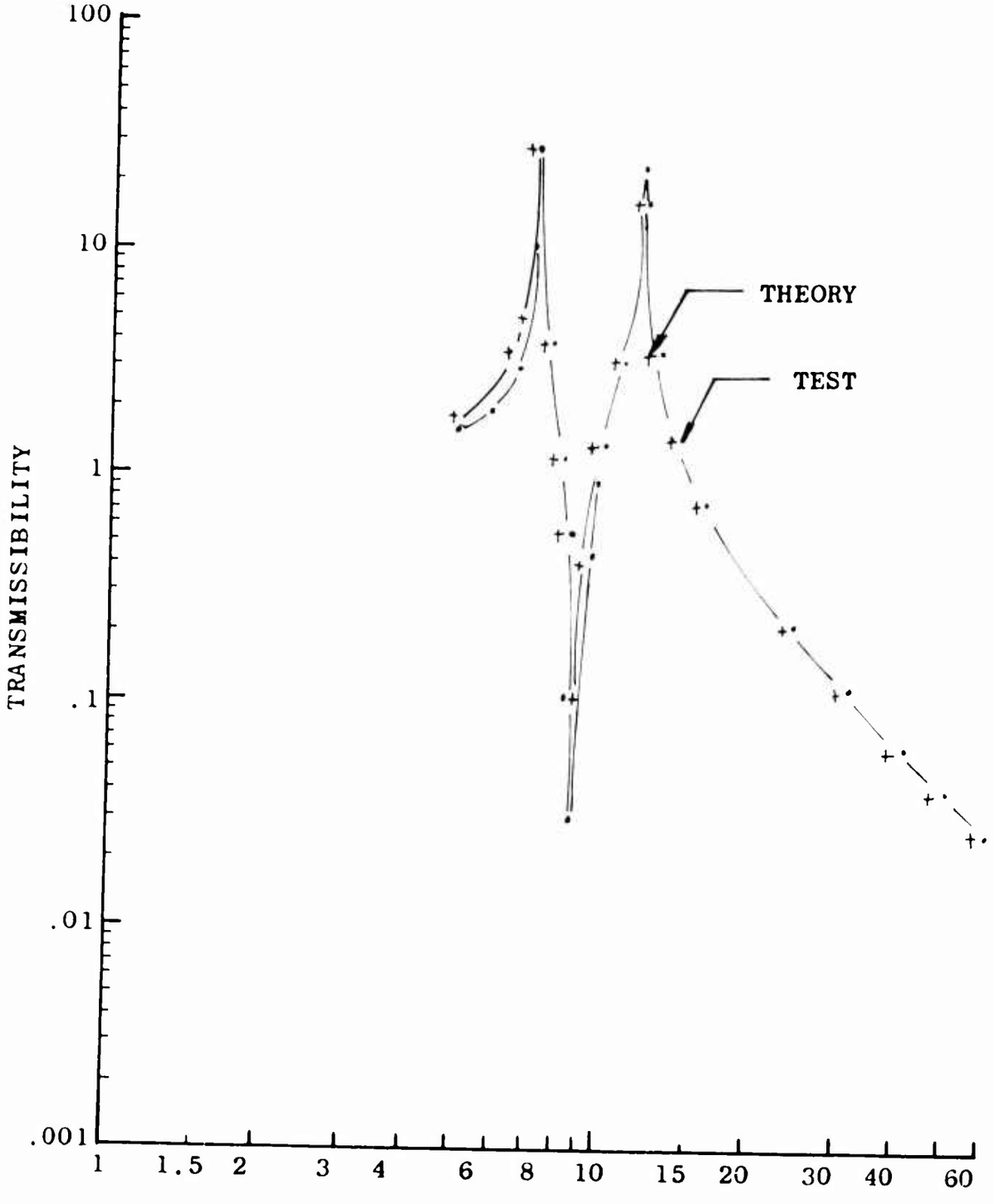

Figure 84. Analytical and Experimental Response Curves of the DAVI Beta With $\zeta_s = .016$ and $\frac{R}{r} = 4.82$

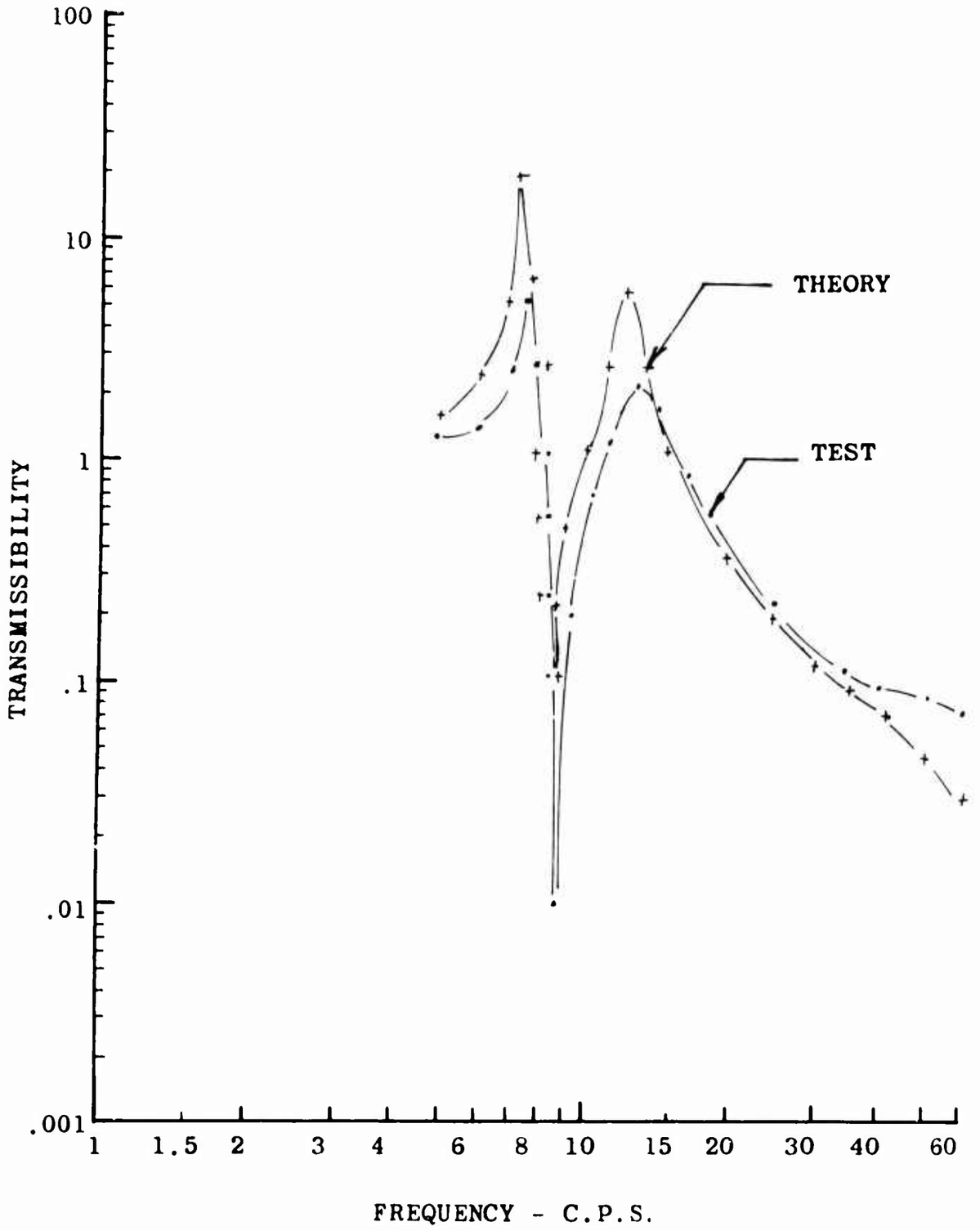

Figure 85. Analytical and Experimental Response Curves of the DAVI Beta With ζ_s = .050 and $\frac{R}{T}$ = 4.82

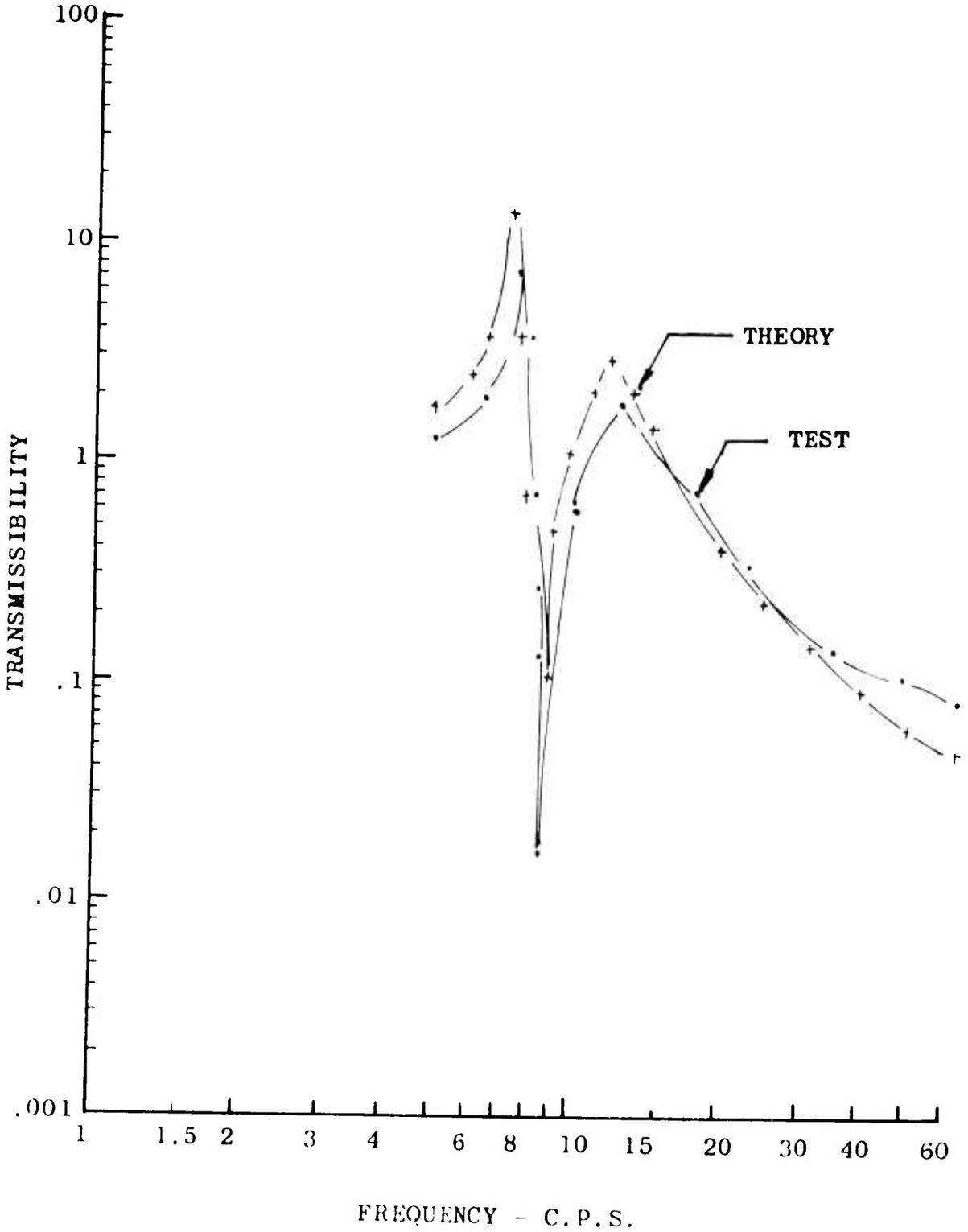

Figure 86. Analytical and Experimental Response Curves of the DAVI Beta With ζ_S = .117 and $\frac{R}{r}$ = 4.82

TABLE VIII

DAVI GAMMA CONFIGURATIONS TESTED

Fig. No.	Isolated Weight (Lb)	Percent Damping ζ_S	Percent Damping ζ_A	DAVI Inertia Bar Weight (Lb)	Spring Rate (Lb/In.) K_S	Spring Rate (Lb/In.) K_D	R (In.)	r (In.)	P (In.)
86	27	.016	.01	.9	396	428	-1.0	2.0	2.58
87	27	.050	.01	.9	396	428	-1.0	2.0	2.58
88	27	.117	.01	.9	396	428	-1.0	2.0	2.58
89	27	.016	.01	2.25	396	428	-2.27	2.0	2.405
90	27	.050	.01	2.25	396	428	-2.27	2.0	2.405
91	27	.117	.01	2.25	396	428	-2.27	2.0	2.405
92	27	.016	.01	2.25	396	450	-2.40	1.0	2.125
93	27	.050	.01	2.25	396	450	-2.40	1.0	2.125
94	27	.117	.01	2.25	396	450	-2.40	1.0	2.125
95	27	.016	.01	2.25	396	484	-4.66	.76	3.48
96	27	.050	.01	2.25	396	484	-4.66	.76	3.48
97	27	.117	.01	2.25	396	484	-4.66	.76	3.48

Figures 87 through 98 give the results of the tests, and Table IX shows a summary of the test results.

TABLE IX

SUMMARY OF DAVI GAMMA TEST RESULTS

Fig. No.	Mode: First Natural Frequency (c.p.s.)	Trans.	Second Natural Frequency (c.p.s.)	Trans.	Antiresonance: Frequency (c.p.s.)	Trans.
87	7.6	24.0	36.0	.20	40.0	.014
88	8.0	6.0	-	-	40.0	.010
89	8.0	8.0	-	-	40.0	.012
90	7.4	17.0	21.0	.45	20.0	.021
91	8.0	8.0	22.0	.25	20.0	.012
92	8.0	6.5	23.0	.19	20.0	.011
93	7.0	30.0	15.0	10.5	12.0	.013
94	7.0	11.0	15.0	1.9	12.0	.018
95	6.9	8.0	15.0	1.1	12.0	.010
96	-	-	12.0	19.0	5.1	.028
97	-	-	12.0	7.2	5.1	.028
98	-	-	11.0	3.2	5.1	.030

It is seen from the above table and Figures 87 through 98 that the test results were as expected. As in the DAVI Beta series of testing, these tests show that the increased damping did reduce the transmissibility at the natural frequencies, that the antiresonant frequencies were not affected by the magnitude of the damping, and that high-frequency isolation was obtained. In Figure 99, a test was done by completely removing the inertia bar; thus, a series spring system was tested and compared to the DAVI of the same static stiffness. It is seen in this test that at antiresonance of the DAVI, considerably greater isolation was obtained. The DAVI Gamma also achieved greater isolation at the higher frequencies than this series system. It is seen in Figures 87, 88, and 89 that with only 1.6 percent of critical damping, the transmissibility at the higher frequency resonance was only .2; and that at the higher magnitude of damping, the second natural frequency appears to be virtually eliminated. In Figures 96, 97, and 98, the lower natural frequencies could not be obtained due to the limitation of the test equipment, in which frequencies below 5 c.p.s. could not be obtained.

Correlation

The analytical and test results were correlated. The correlation, which is shown in Figures 87 through 98, is seen to be excellent. The natural frequencies of the system are predicted quite accurately, and the predicted transmissibilities of the DAVI Gamma agree with the test results.

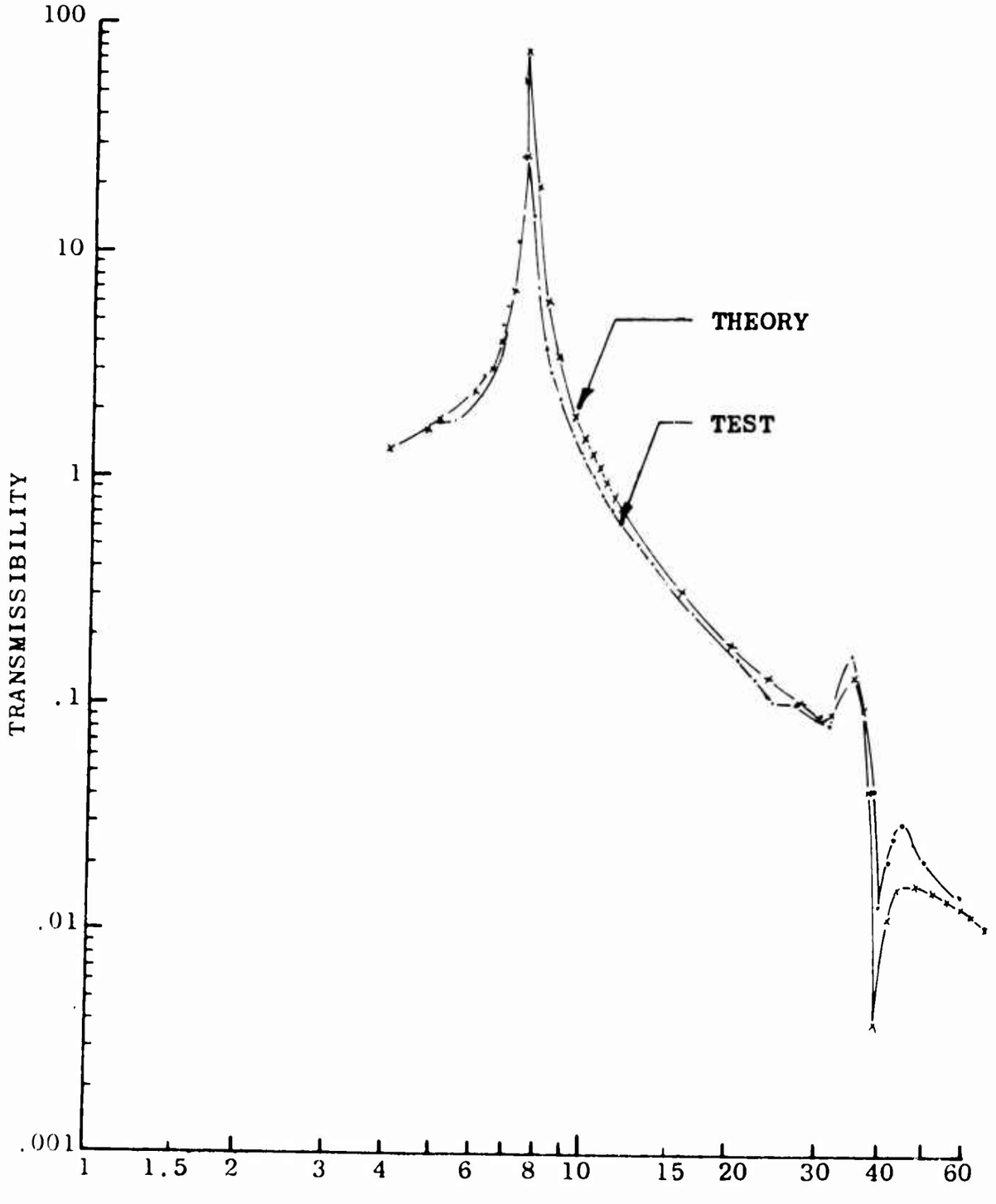

Figure 87. Analytical and Experimental Response Curves of the DAVI Gamma With $\zeta_s = .016$ and $\frac{R}{r} = -0.5$

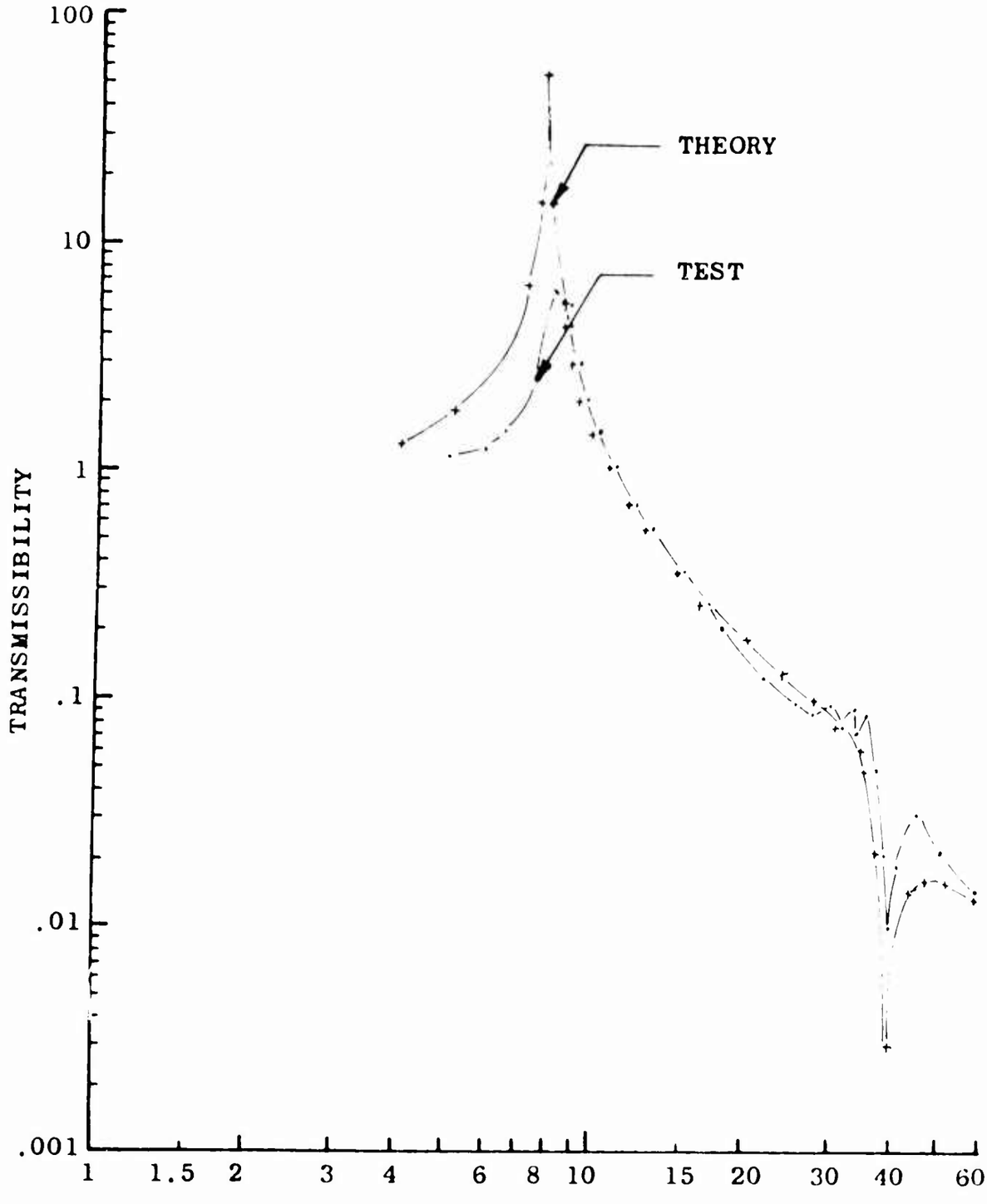

Figure 88. Analytical and Experimental Response Curves of the DAVI Gamma With ζ_s = .050 and $\frac{r}{R}$ = -0.5

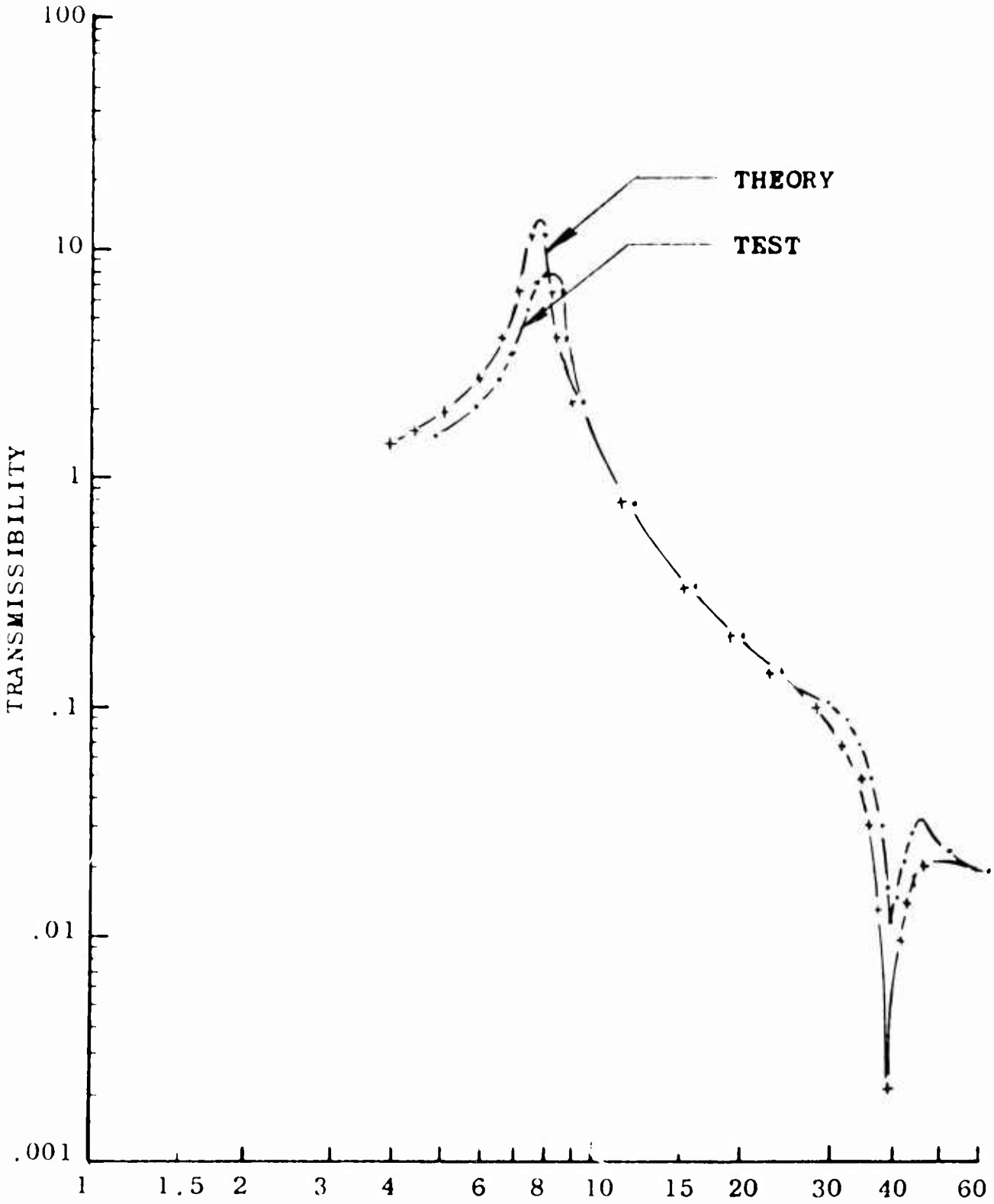

Figure 89. Analytical and Experimental Response Curves of the DAVI Gamma With $\zeta_s = .117$ and $\frac{R}{r} = -0.5$

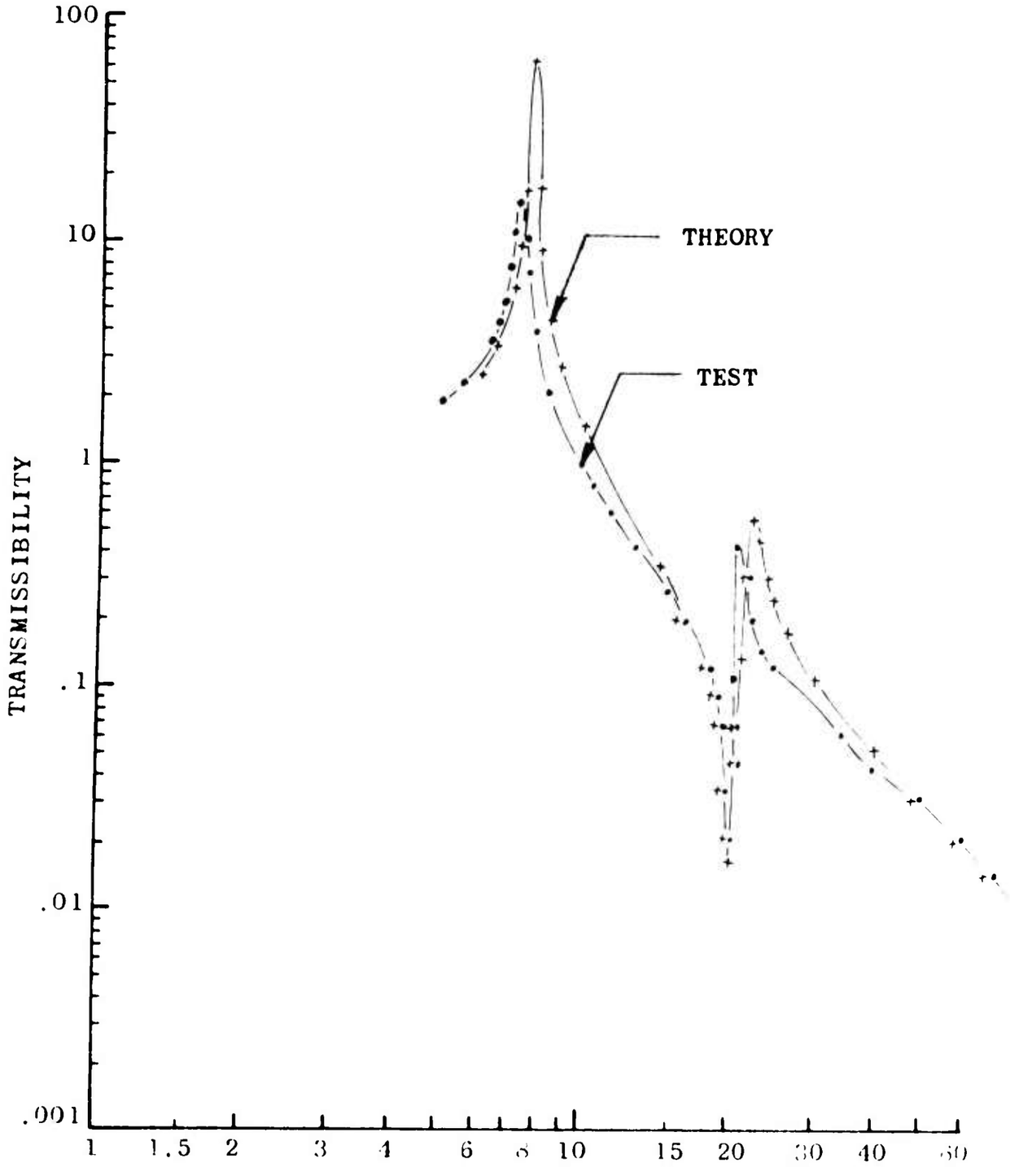

Figure 90. Analytical and Experimental Response Curves of the DAVI Gamma With ζ_s = .016 and $\frac{R}{r}$ = 1.135

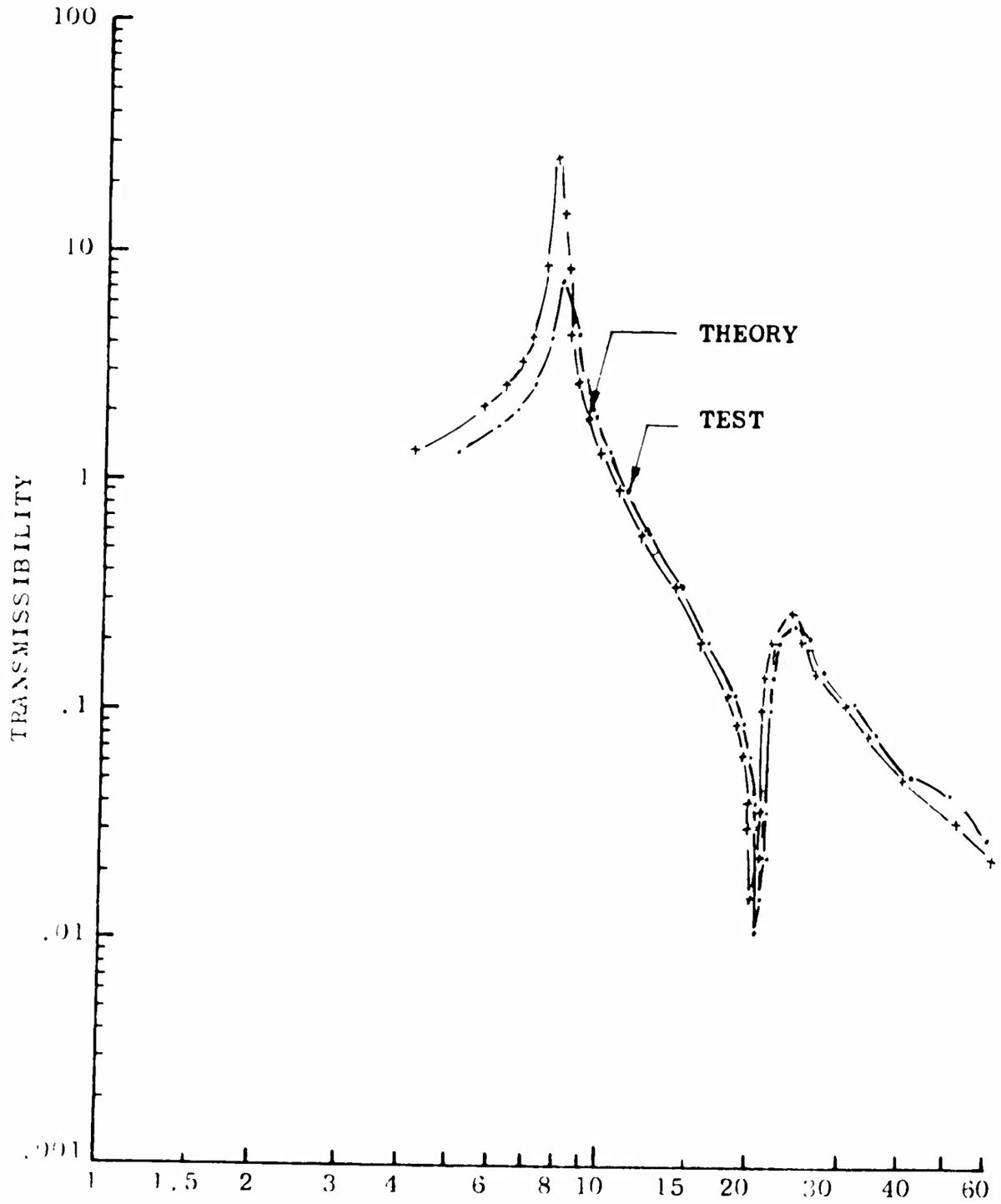

Figure 91. Analytical and Experimental Response Curves of the DAVI Gamma With ζ_s = .050 and $\frac{R}{r}$ = 1.135

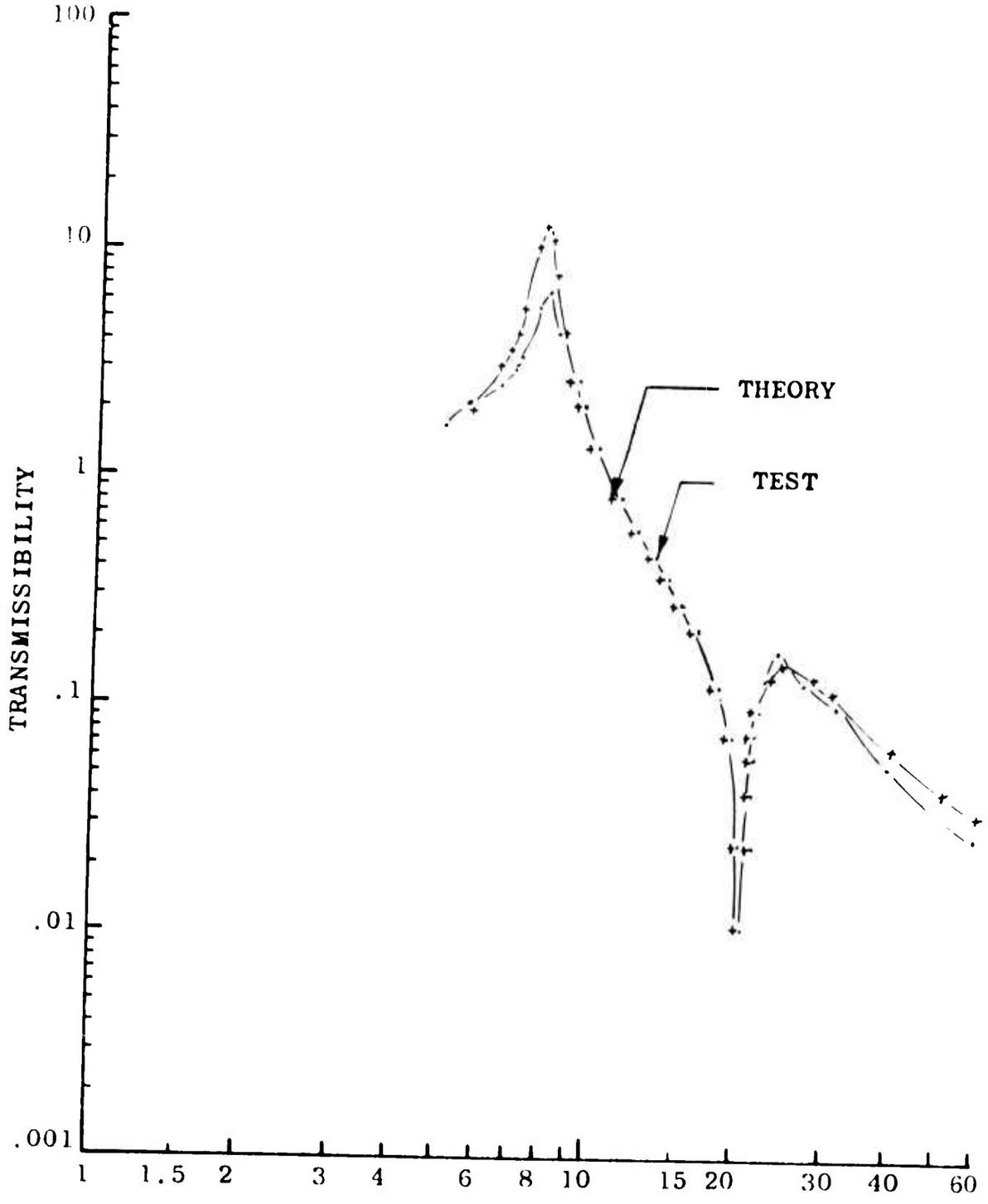

Figure 92. Analytical and Experimental Response Curves of the DAVI Gamma With $\zeta_s = .117$ and $\frac{R}{r} = -1.135$

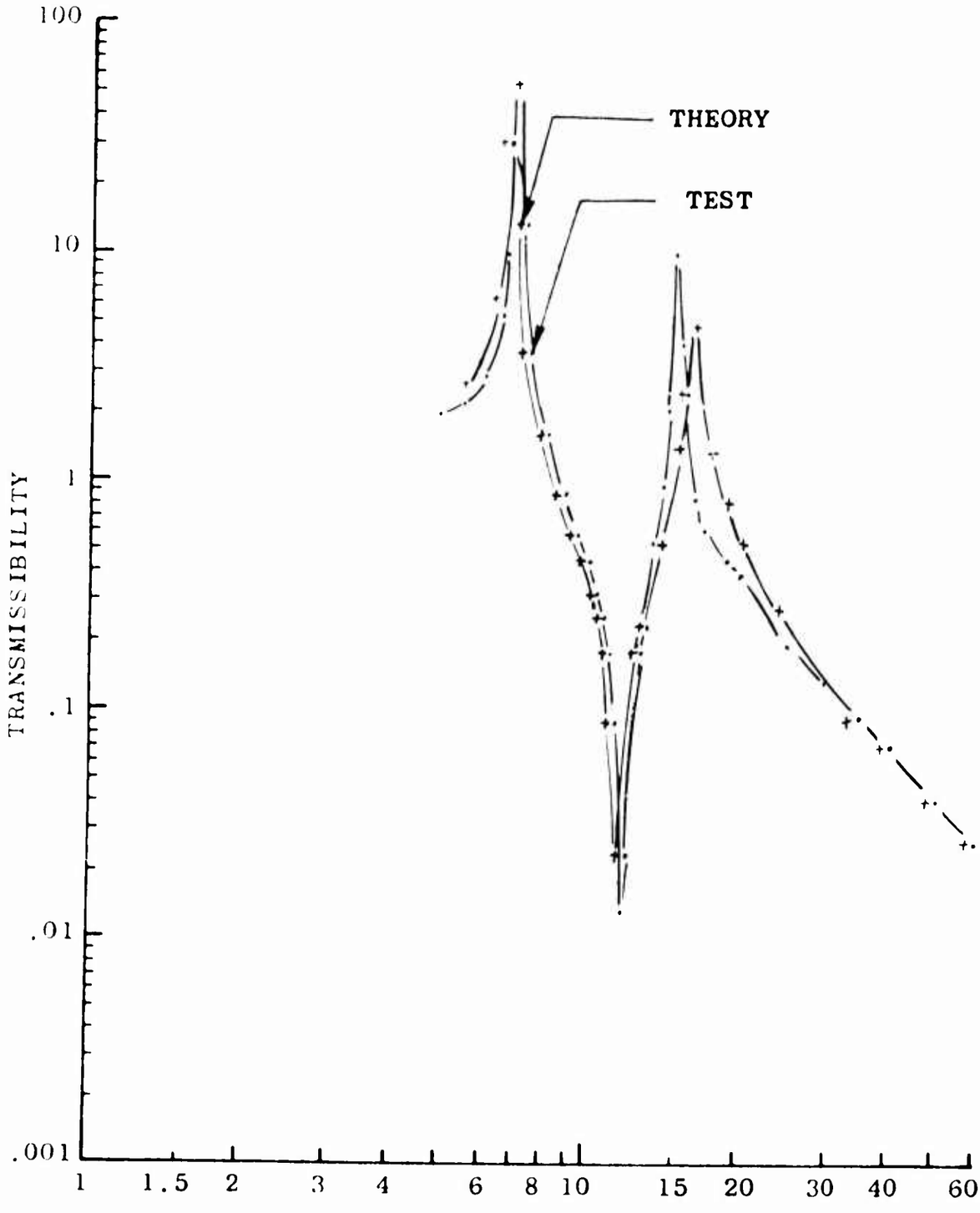

Figure 93. Analytical and Experimental Response Curves of the DAVI Gamma With ζ_s = 016 and $\frac{R}{r}$ = -2.40

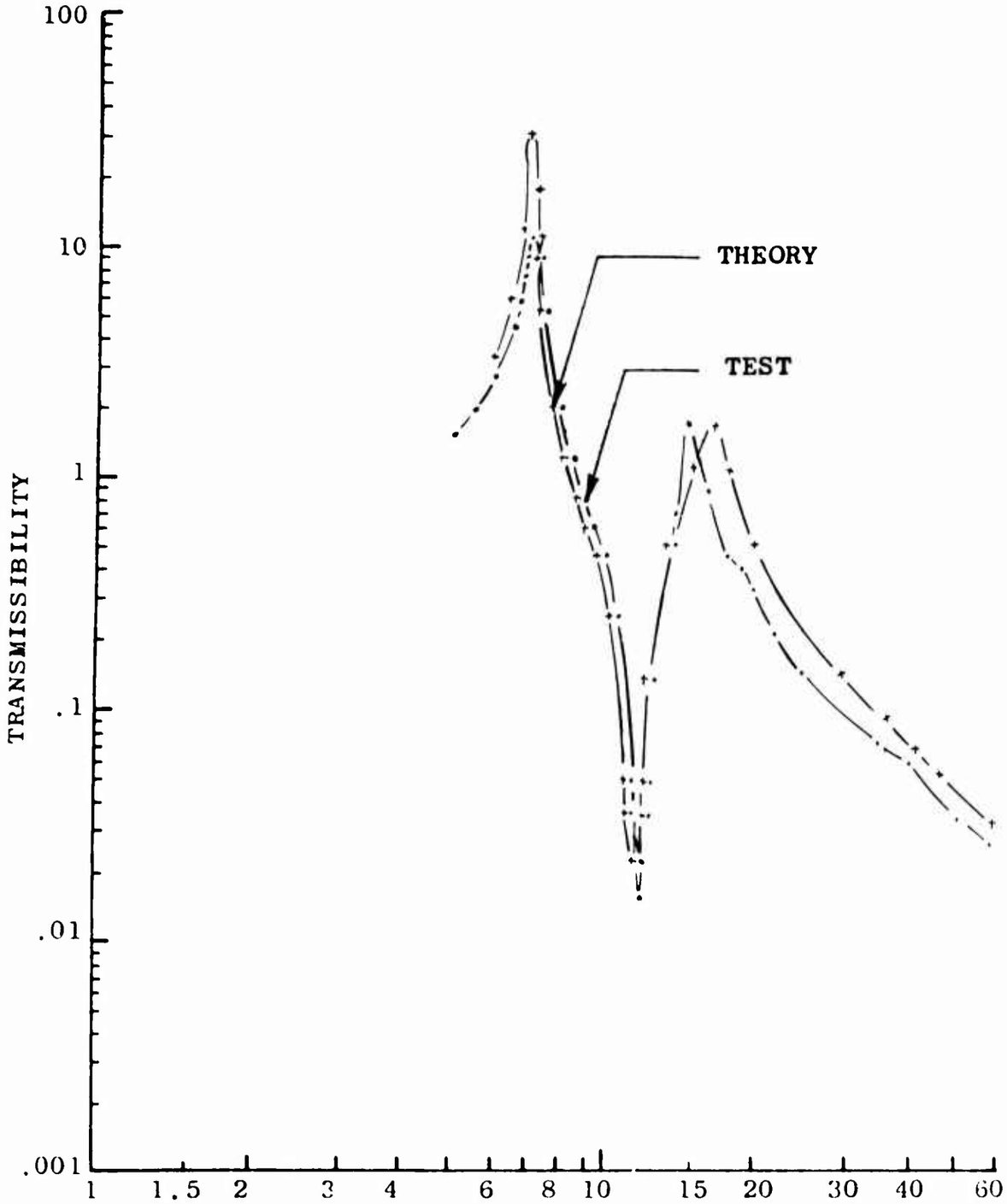

Figure 94. Analytical and Experimental Response Curves of the DAVI Gamma With ζ_s .050 and $\frac{R}{r^2}$ = -2.40

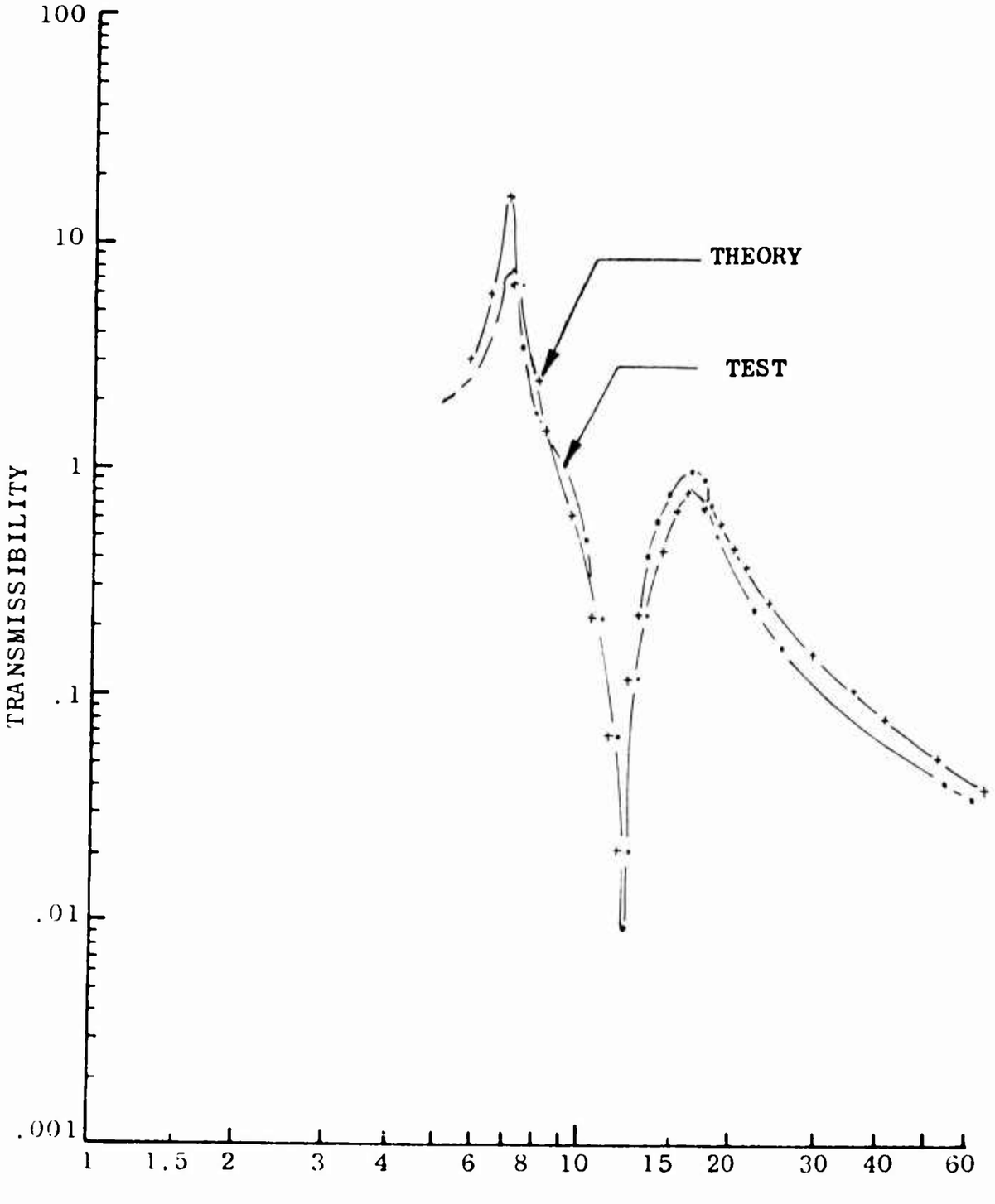

Figure 95. Analytical and Experimental Response Curves of the DAVI Gamma With ζ_s = .117 and $\frac{R}{r}$ = -2.40

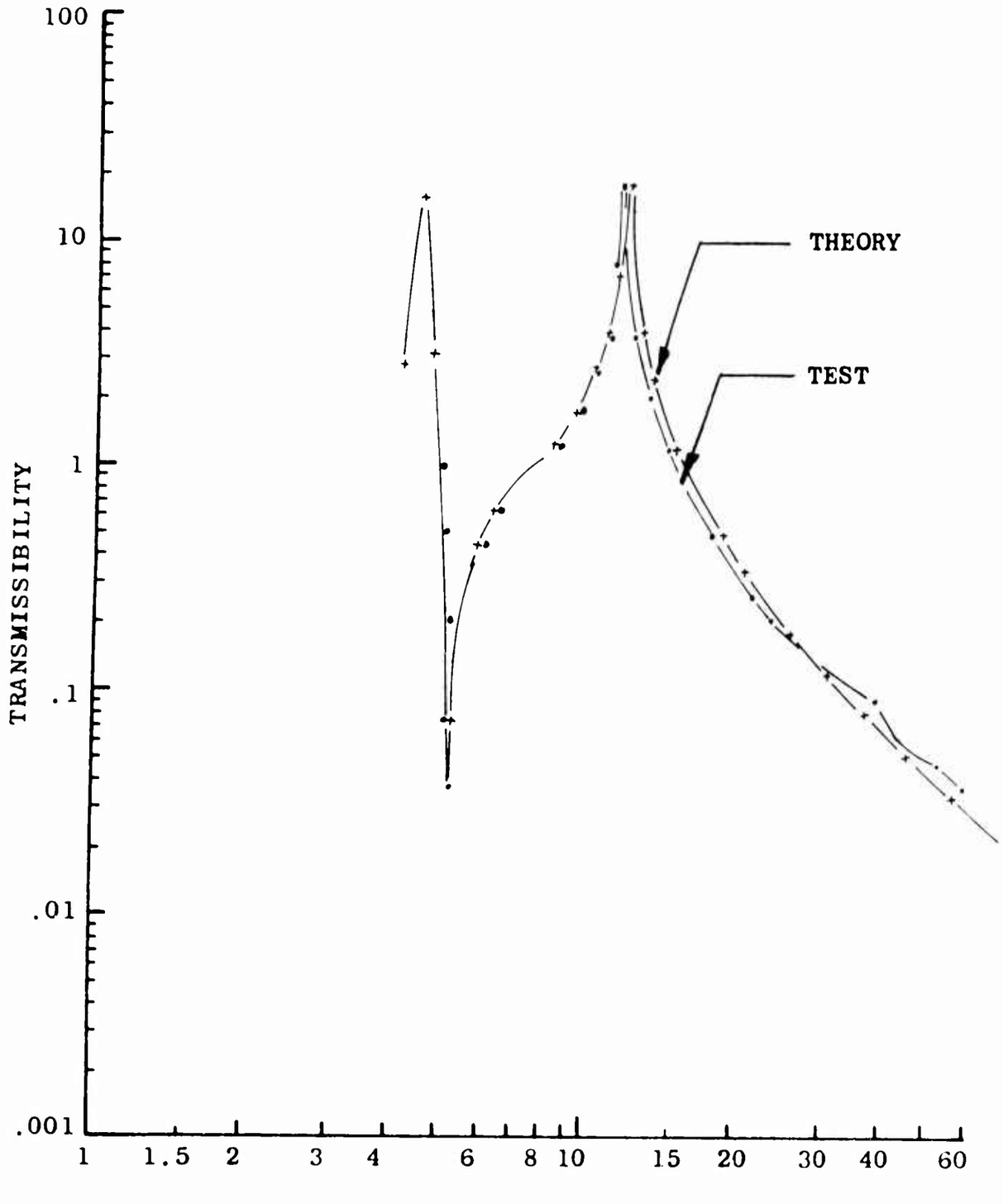

Figure 96. Analytical and Experimental Response Curves of the DAVI Gamma With $\zeta_s = .016$ and $\frac{R}{r} = -6.14$

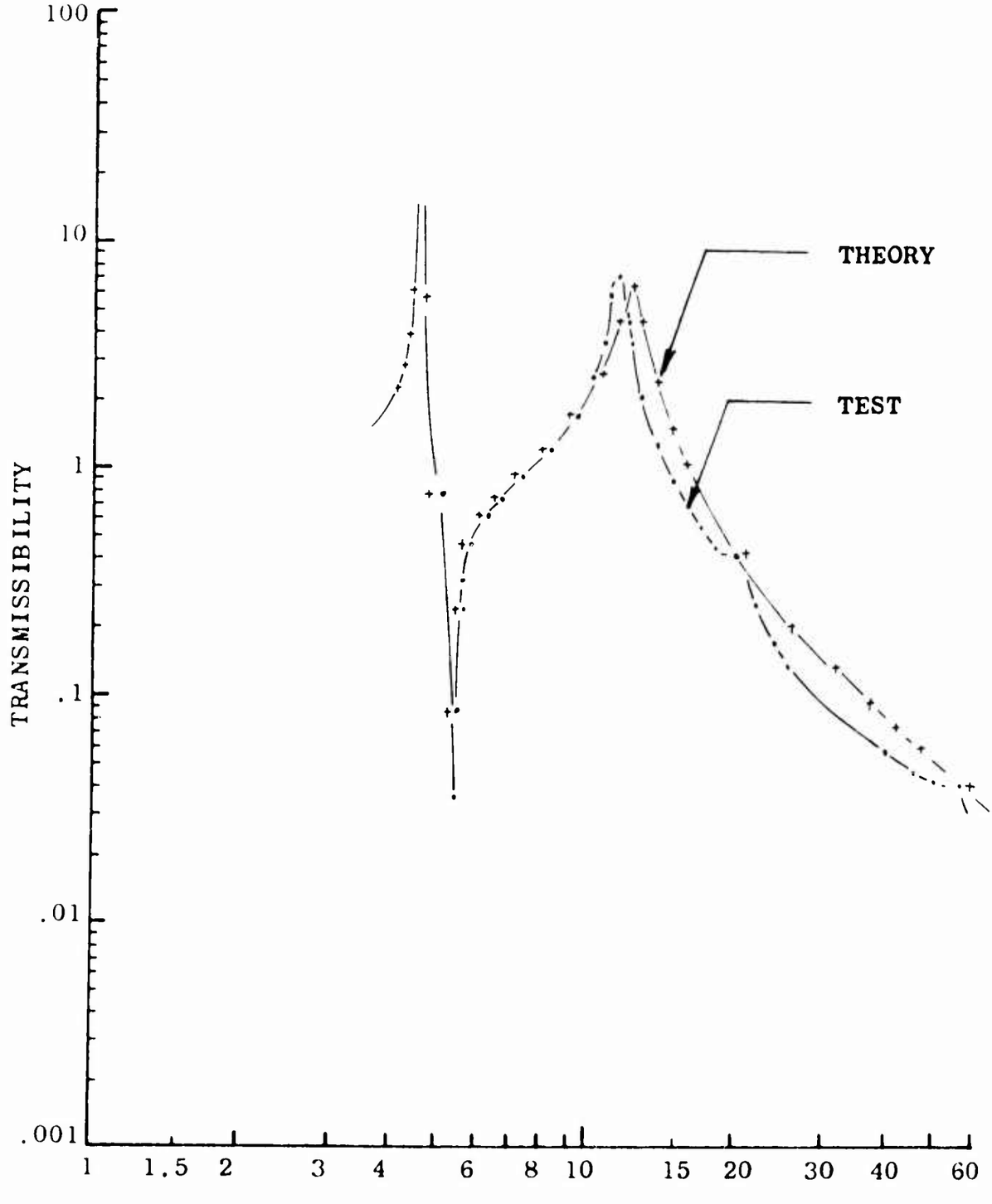

Figure 97. Analytical and Experimental Response Curves of the DAVI Gamma With $\zeta_s = .050$ and $\frac{R}{r} = -6.14$

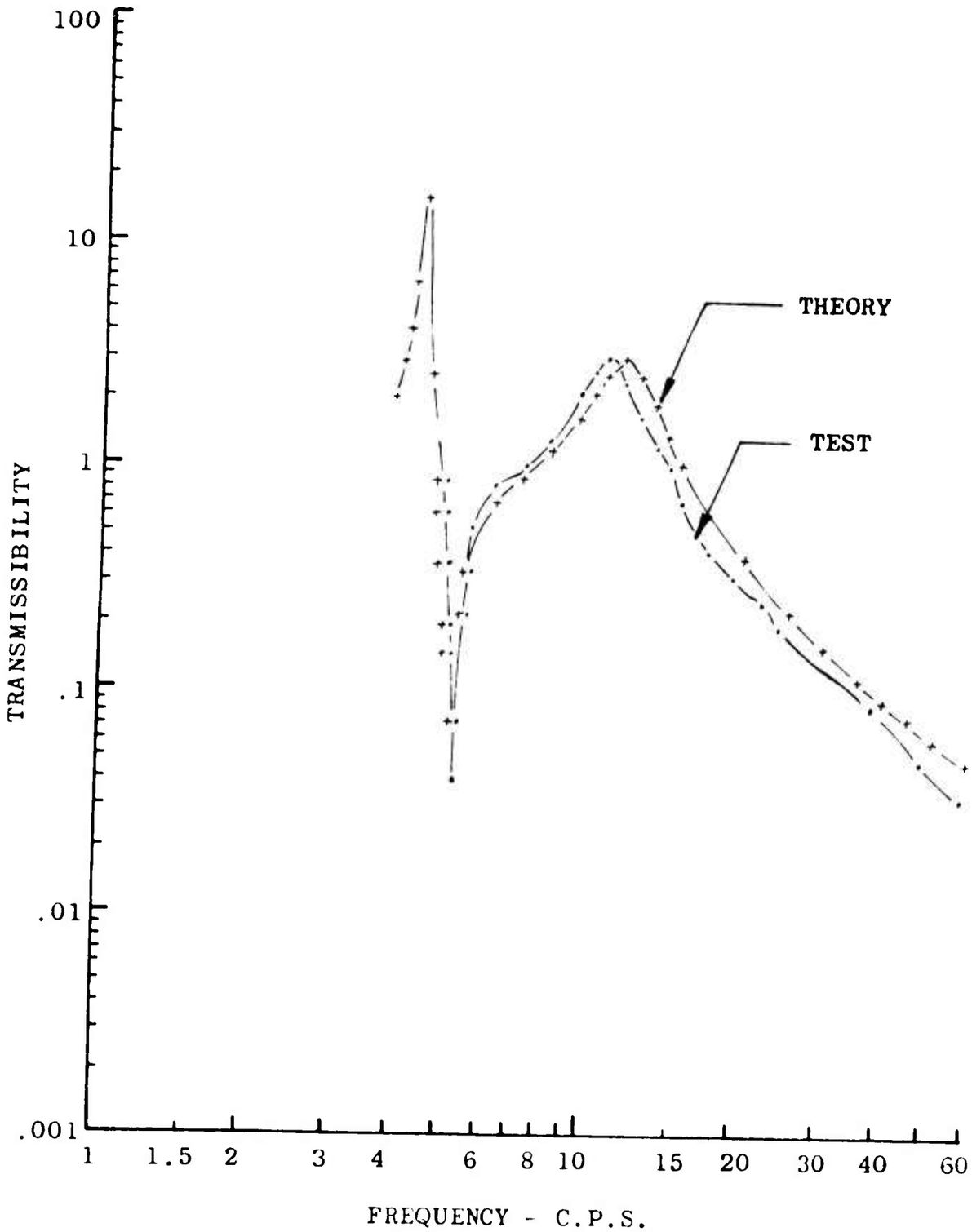

Figure 98. Analytical and Experimental Response Curves of the DAVI Gamma With $\zeta_s = .117$ and $\frac{R}{r} = -6.14$

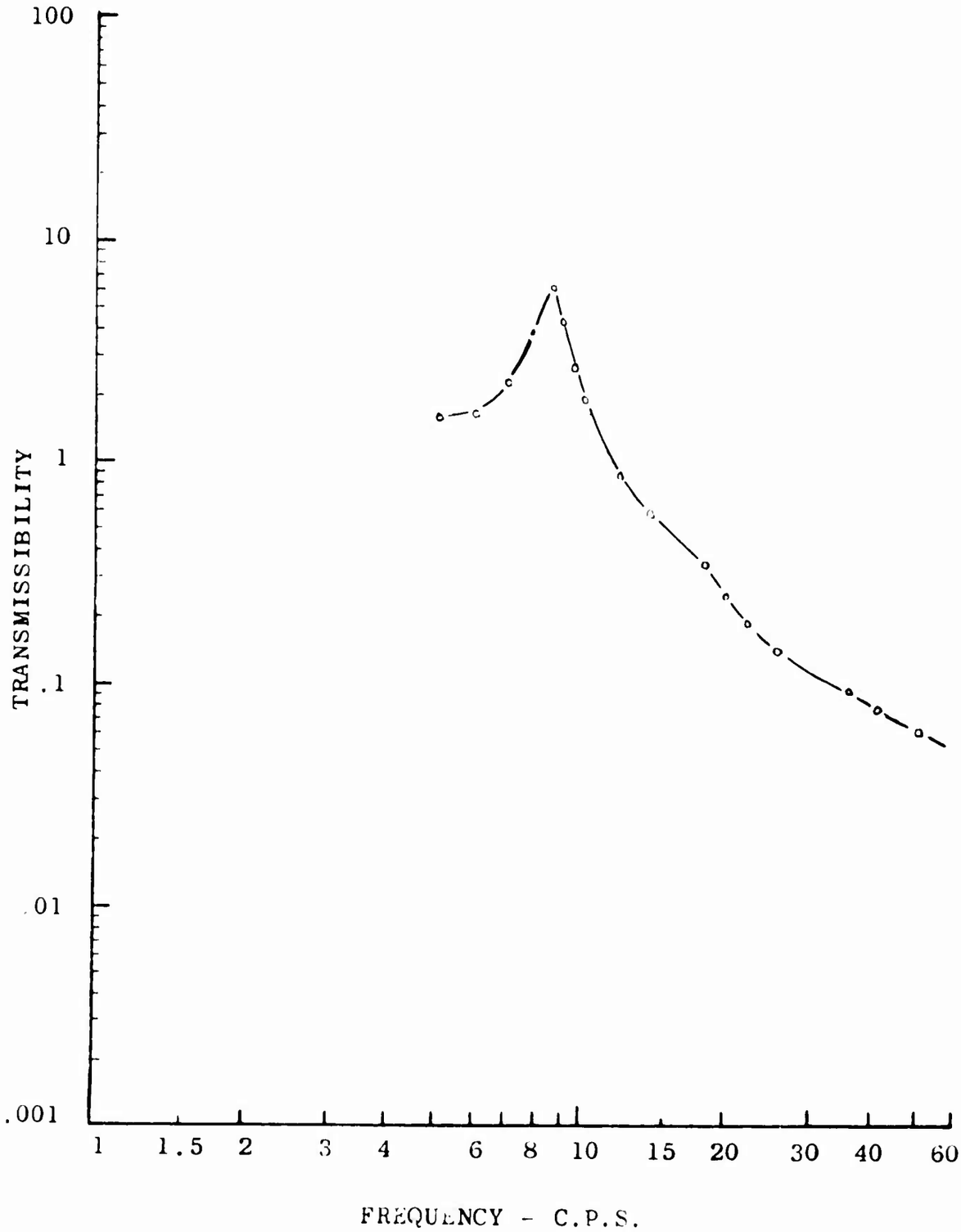

Figure 99. Experimental Response of the System With DAVI Element Removed

DAVI ALPHA SHOCK

ANALYSIS

This analysis determines the shock transmissibility of the DAVI Alpha. It does so with special emphasis on the problem of correlating theoretical results with the results of actual shock tests.

This analysis applies to two types of DAVI Alphas. One type is the conventional single-degree-of-freedom DAVI Alpha, where the DAVI pivots are assumed to be rigid except in rotation. The second type is the DAVI Alpha in which the pivots are allowed to have translational freedom as well as rotation, as is the case with elastomeric pivots. Since damping is inherently present in elastomers in amounts dependent on the particular material, it is included in the derivation.

In order that the response of the DAVI Alpha may be compared with the response of a conventional isolator, equations of motion for the conventional isolator are derived and solved in a similar fashion to those for the DAVI Alpha.

Three types of inputs are considered: half-sine, triangular, and square waves.

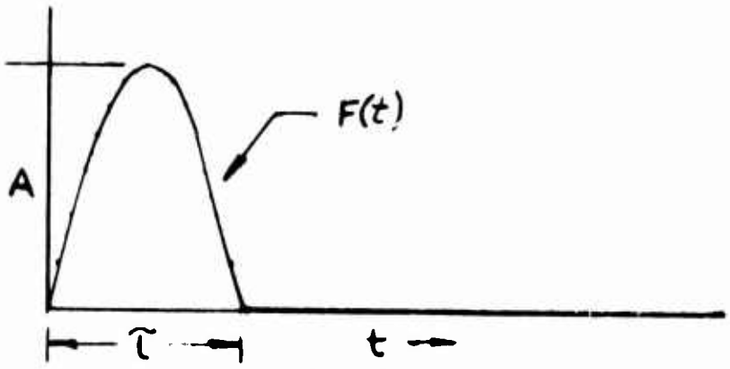

Figure 100. Half-Sine Wave Input

The equations for a half-sine pulse (Figure 100) can be written as

$$F(t) = A \sin \frac{\pi t}{\tau} \left[u(t) - u(t-\tau) \right] \qquad (172)$$

where $u(t)$ is the step function. The Laplace Transform of $F(t)$ is

$$F(s) = \frac{A \frac{\pi}{\tau}}{s^2 + \left(\frac{\pi}{\tau}\right)^2} \left[1 + e^{-s\tau} \right] \qquad (173)$$

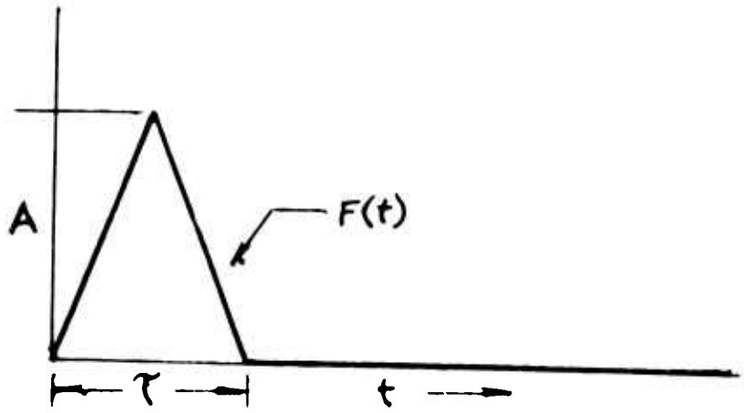

Figure 101. Triangular Input

The equations for a saw-tooth pulse (Figure 101) can be written as

$$F(t) = \frac{2A}{\tau} t\left[u(t) - u\left(t-\frac{\tau}{2}\right)\right] + 2A\left(1-\frac{t}{\tau}\right)\left[u\left(t-\frac{\tau}{2}\right) - u(t-\tau)\right] \tag{174}$$

and the Laplace Transform of $F(t)$ is

$$F(s) = \frac{2A}{\tau s^2}\left[1 - 2e^{-\frac{\tau}{2}s} + e^{-\tau s}\right] \tag{175}$$

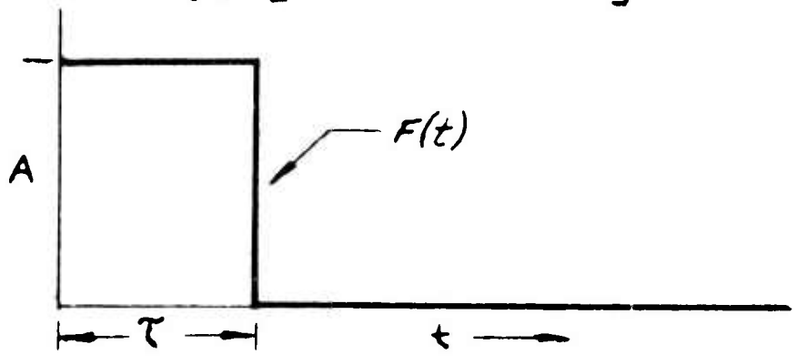

Figure 102. Square-Wave Input

The equations for a square-wave pulse (Figure 102) can be written

$$F(t) = A\left[u(t) - u(t-\tau)\right] \tag{176}$$

and the Laplace Transform of $F(t)$ is

$$F(s) = \frac{A}{s}\left(1 - e^{-\tau s}\right) \tag{177}$$

The equations of motion were derived in a manner that would give results similar to drop test results. The conventional method of shock-testing the spring mass (M_I, K_D), as shown in Figure 103, is to fix the equipment to the carriage (M_C) of a drop test machine, to place plastic material on the anvil of the machine which is known to give the desired shock impulse and to carry out a drop test. The procedure is well described in Reference 2, "Shock and Vibration Handbook", by Harris and Crede.

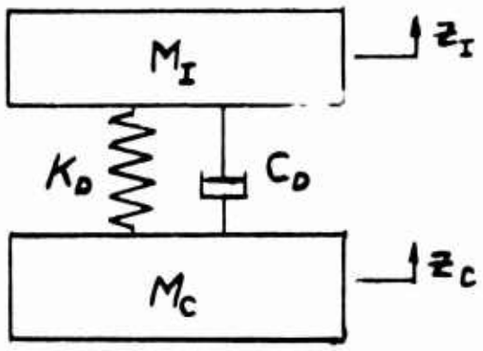

Figure 103. Schematic of Isolated Mass on Drop Test Carriage

The shock input is usually measured as an acceleration of the carriage, and the output is usually the measured acceleration of the isolated mass, M_I. Therefore, the system responses, as derived from the equations of motion, are expressed as the ratio of the accelerations of the carriage to the isolated mass.

From Figure 103, the energy equations of the conventional isolator, including the mass of the base, can be obtained. The kinetic energy is

$$T = \frac{1}{2} M_I \dot{z}_I^2 + \frac{1}{2} M_C \dot{z}_C^2 \qquad (178)$$

The potential energy is

$$V = \frac{1}{2} K_D (z_I - z_C)^2 \qquad (179)$$

The dissipation function is

$$D = \frac{1}{2} C_D (\dot{z}_I - \dot{z}_C)^2 \tag{180}$$

and

$$Q = F(t) z_C \tag{181}$$

Applying Lagrange's equation, the equations of motion for this two-mass system with a time-dependent force input are

$$M_I \ddot{z}_I + C_D (\dot{z}_I - \dot{z}_C) + K_D (z_I - z_C) = 0 \tag{182}$$

$$M_C \ddot{z}_C + C_D (\dot{z}_C - \dot{z}_I) + K_D (z_C - z_I) = F(t) \tag{183}$$

Now, since accelerations of the carriage, $\ddot{z}_C$, are determined in a drop test as described above, it is only necessary to consider Equation (182), or

$$M_I \ddot{z}_I + C_D \dot{z}_I + K_D z_I = K_D z_C + C_D \dot{z}_C \tag{184}$$

Equation (184) was then programmed for the digital computer for the three different inputs of half-sine, triangular, and square wave. Transients can also be solved for initial displacement and velocity. Equation (184) was solved by a step-by-step method utilizing the Runge Kutta method.

The computer program was checked for results by using the Laplace transformation of Equation (184), neglecting damping

$$(M_I s^2 + K_D) z_I(s) = K_D z_C(s) \tag{185}$$

Since $z_C(s)$ can be represented by the three inputs considered in the analysis, then the Laplace transformation, is, for the half-sine input,

$$\frac{s^2 z_I(s)}{A} = \frac{\frac{\pi}{t}}{s^2 + \left(\frac{\pi}{t}\right)^2} \left[1 + e^{-st}\right] \frac{\omega_N^2}{s^2 + \omega_N^2} \tag{186}$$

and for the triangular input,

$$\frac{s^2 z_I(s)}{A} = \frac{2}{\tau s^2} \left[1 - 2e^{-\frac{\tau}{2}s} + e^{-\tau s}\right] \frac{\omega_N^2}{s^2 + \omega_N^2} \tag{187}$$

and for the square wave,

$$\frac{S^2 Z_I(S)}{A} = \left(1 - e^{-S\tau}\right) \frac{\omega_N^2}{S^2 + \omega_N^2} \tag{188}$$

The inverse transformation of the above three equations gives the acceleration of the isolated mass versus time, or, for the half-sine input,

$$\frac{\ddot{Z}_I}{A} = \frac{\omega_N^2 \frac{\pi}{\tau}}{\omega_N^2 - \left(\frac{\pi}{\tau}\right)^2} \left\{\left[\frac{1}{\pi} \sin\frac{\pi}{\tau} t - \omega_N \sin\omega_N t\right] u(t) + \left[\frac{1}{\pi} \sin\frac{\pi}{\tau}(t-\tau) - \omega_N \sin\omega_N (t-\tau)\right] u(t-\tau)\right\} \tag{189}$$

for the triangular input,

$$\frac{\ddot{Z}_I}{A} = \frac{2}{\tau}\left\{\left[t - \omega_N \sin\omega_N t\right] u(t) - 2\left[\left(t - \frac{\tau}{2}\right) - \omega_N \sin\omega_N \left(t - \frac{\tau}{2}\right)\right] u\left(t - \frac{\tau}{2}\right) + \left[(t-\tau) - \omega_N \sin\omega_N (t-\tau)\right] u(t-\tau)\right\} \tag{190}$$

and for the square wave,

$$\frac{\ddot{Z}_I}{A} = \omega_N \left\{\left[1 - \cos\omega_N t\right] u(t) - \left[1 - \cos\omega_N (t-\tau)\right] u(t-\tau)\right\} \tag{191}$$

From Figure 104, the equations of motion of the DAVI shock analysis can be derived.

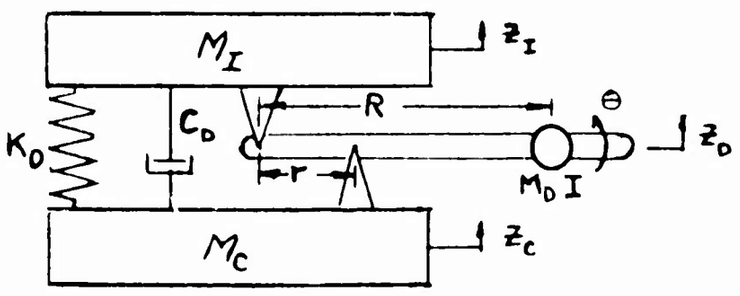

Figure 104. Schematic of DAVI Alpha Isolated Mass on Drop Test Carriage

The kinetic energy of the system is

$$T = \frac{1}{2} M_I \dot{z}_I^2 + \frac{1}{2} M_C \dot{z}_C^2 + \frac{1}{2} M_D \dot{z}_D^2 + \frac{1}{2} I \dot{\theta}^2 \tag{192}$$

The potential energy of the system is

$$V = \frac{1}{2} K_D (z_I - z_C)^2 \tag{193}$$

The dissipation function is

$$D = \frac{1}{2} C_D (\dot{z}_I - \dot{z}_C)^2 \tag{194}$$

and

$$Q = \frac{1}{2} F(t) z_C \tag{195}$$

Substituting the geometric relationships

$$\theta = \frac{z_I - z_C}{r} \quad \text{and} \quad z_D = \frac{R}{r} z_C - \left(\frac{R}{r} - 1\right) z_I$$

into the kinetic energy equation, Equation (192) becomes

$$T = \frac{1}{2} M_I \dot{z}_I^2 + \frac{1}{2} M_C \dot{z}_C^2 + \frac{1}{2} M_D \left[\frac{R}{r} \dot{z}_C - \left(\frac{R}{r} - 1\right) \dot{z}_I\right]^2 + \frac{1}{2} I \left(\frac{\dot{z}_I - \dot{z}_C}{r}\right)^2 \tag{196}$$

Applying Lagrange's equation, the equations of motion become

$$\left[M_I + M_D \left(1 - \frac{R}{r}\right)^2 + \frac{I}{r^2}\right] \ddot{z}_I + C_D \dot{z}_I + K_D z_I + \left[M_D \frac{R}{r} \left(1 - \frac{R}{r}\right) - \frac{I}{r^2}\right] \ddot{z}_C - C_D \dot{z}_C - K_D z_C = 0 \tag{197}$$

$$\left[M_D \frac{R}{r} \left(1 - \frac{R}{r}\right) - \frac{I}{r^2}\right] \ddot{z}_I - C_D \dot{z}_I - K_D z_I + \left[M_C + M_D \left(\frac{R}{r}\right)^2 + \frac{I}{r^2}\right] \ddot{z}_C + C_D \dot{z}_C + K_D z_C = F(t) \tag{198}$$

However, since the input $\ddot{z}_c$ is the acceleration of the carriage, it is only necessary to consider Equation (197), which can be rewritten as

$$M_R \ddot{z}_I + C_D \dot{z}_I + K_D z_I = M_A \ddot{z}_C + C_D \dot{z}_C + K_D z_C \qquad (199)$$

Equation (199) was then programmed for the digital computer in a similar manner as the equation(s) for the conventional system for the three different types of inputs and initial conditions of displacement and velocity.

From Figure 105, the equations of motion for the DAVI Alpha with flexible pivots can be derived.

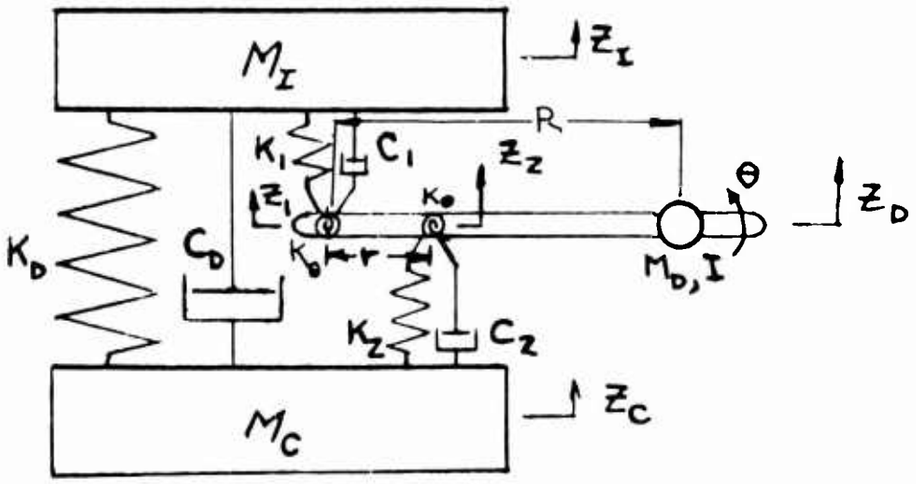

Figure 105. Schematic of DAVI Alpha With Flexible Pivots on Drop Test Carriage

The energies of this system are

$$T = \frac{1}{2} M_I \dot{z}_I^2 + \frac{1}{2} M_D \dot{z}_D^2 + \frac{1}{2} M_C \dot{z}_C^2 + \frac{1}{2} I \dot{\theta}^2 \qquad (200)$$

$$V = \frac{1}{2} K_D (z_I - z_C)^2 + \frac{1}{2} K_1 (z_I - z_1)^2 + \frac{1}{2} K_2 (z_2 - z_C)^2 + K_\theta \theta^2 \qquad (201)$$

$$D = \frac{1}{2} C_D (\dot{z}_I - \dot{z}_C)^2 + \frac{1}{2} C_1 (\dot{z}_I - \dot{z}_1)^2 + \frac{1}{2} C_2 (\dot{z}_2 - \dot{z}_C) + C_\theta \dot{\theta}^2 \qquad (202)$$

$$Q = F(t) z_C \qquad (203)$$

Substituting the geometric relationships

$$\theta = \frac{z_1 - z_2}{r} \qquad \text{and} \qquad z_D = \frac{R}{r} z_2 - \left(\frac{R}{r} - 1\right) z_1$$

into the energy equations and applying Lagrange's equation, the equations of motion are

$$M_I \ddot{z}_I + (C_D + C_1)\dot{z}_I + (K_D + K_1) z_I - C_1 \dot{z}_1 - C_D \dot{z}_C - K_1 z_1 - K_D z_C = 0 \quad (204)$$

$$- C_1 \dot{z}_I - K_1 z_I + \left[M_D (1 - \frac{R}{r})^2 + \frac{I}{r^2}\right] \ddot{z}_1 + C_1 \dot{z}_1 + \frac{2C_\theta}{r^2} \dot{z}_1 + \frac{2K_\theta}{r^2} z_1 + \left[M_D (1 - \frac{R}{r}) \frac{R}{r} - \frac{I}{r^2}\right] \ddot{z}_2 - \frac{2K_\theta}{r^2} z_2 - \frac{2C_\theta}{r^2} \dot{z}_2 = 0 \quad (205)$$

$$\left[M_D \frac{R}{r} (1 - \frac{R}{r}) - \frac{I}{r^2}\right] \ddot{z}_1 - \frac{2C_\theta}{r^2} \dot{z}_1 - \frac{2K_\theta}{r^2} z_1 + \left[M_D \left(\frac{R}{r}\right)^2 + \frac{I}{r^2}\right] \ddot{z}_2 + \left(C_2 + \frac{2C_\theta}{r^2}\right) \dot{z}_2 + \left(K_2 + \frac{2K_\theta}{r^2}\right) z_2 - C_2 \dot{z}_C - K_2 z_C = 0 \quad (206)$$

$$- C_D \dot{z}_I - K_D z_I - C_2 \dot{z}_2 - K_2 z_2 + M_C \ddot{z}_C + (C_D + C_2) \dot{z}_C + (K_D + K_2) z_C = F(t) \quad (207)$$

Since $\ddot{z}_C$ for the three types of inputs considered is known, Equations (204), (205), and (206) were programmed for a numerical solution on the digital computer.

NUMERICAL SOLUTIONS

Utilizing the digital programs, the shock transmissibility for the DAVI Alpha was calculated for three different inputs of square, triangular, and half-sine waves. The period of the inputs was .01 second. The results are compared to a conventional isolator having the same static spring rate. The range of R/r considered was -10 to +10.

Figures 106 through 110 show a typical time history of the DAVI Alpha for the three types of inputs. It is seen from these figures that the DAVI Alpha response differs from that of a conventional isolator. The DAVI Alpha has an initial peak, the amplitude of which is primarily a function of its high-frequency isolation; thus, a DAVI having a high-frequency isolation of .7 transmits approximately .7 of the applied shock, then oscillates at its natural frequency. Since the natural frequency of the DAVI is less than that of the conventional isolator for the same static frequency for the period of inputs considered, the DAVI always gave

better shock isolation in its fundamental mode of oscillation than the conventional isolator.

Figures 111 through 115 are carpet plots of the calculations in which R/r and $T_{\alpha VHF}$ (high-frequency isolation of the DAVI) are plotted versus peak values of shock transmissibility. It is seen from these carpet plots that it is the high-frequency isolation that primarily determines the shock transmissibility characteristics of the DAVI Alpha. The higher the $T_{\alpha VHF}$ value, the higher the initial transmitted peak and the lower the transmissibility for the long-period oscillation. The lower the value of $T_{\alpha VHF}$, the closer the DAVI Alpha approaches the shock characteristics of the conventional isolator. However, in the cases calculated, the DAVI Alpha had better shock isolation than the conventional isolator in the long-period oscillation.

Calculations were done to determine the effects of radial flexible pivots in the DAVI Alpha on velocity shock, and were compared to velocity shock calculations of the DAVI Alpha and conventional isolator. However, to determine the proper ratio of torsional flexibility to radial flexibility to use in the calculations, torsional and radial spring rates of 15 commercial bushings were calculated. These calculations are based upon the methods shown in Reference 3, pages 229 through 232. Figure 116 shows the results of these calculations, in which the ratio of radial spring rate is plotted versus torsional spring rate. It is seen from this figure that there is large scatter in the results; this is due to the fact that the calculations of the radial spring rate are based upon empirical relationships to determine the stiffness. This involves the creation of a hypothetical bonded compression pad whose stiffness is equivalent to the stiffness of the bushing. Therefore, only approximate results can be obtained. The method of least squares was used to determine the best straight-line fit, as shown in Figure 116.

Calculations were done for velocity shock for the DAVI Alpha with radial flexible pivots, and were compared to the calculations of velocity shock of the DAVI Alpha and conventional isolator. Table X gives the physical parameters used in the calculations.

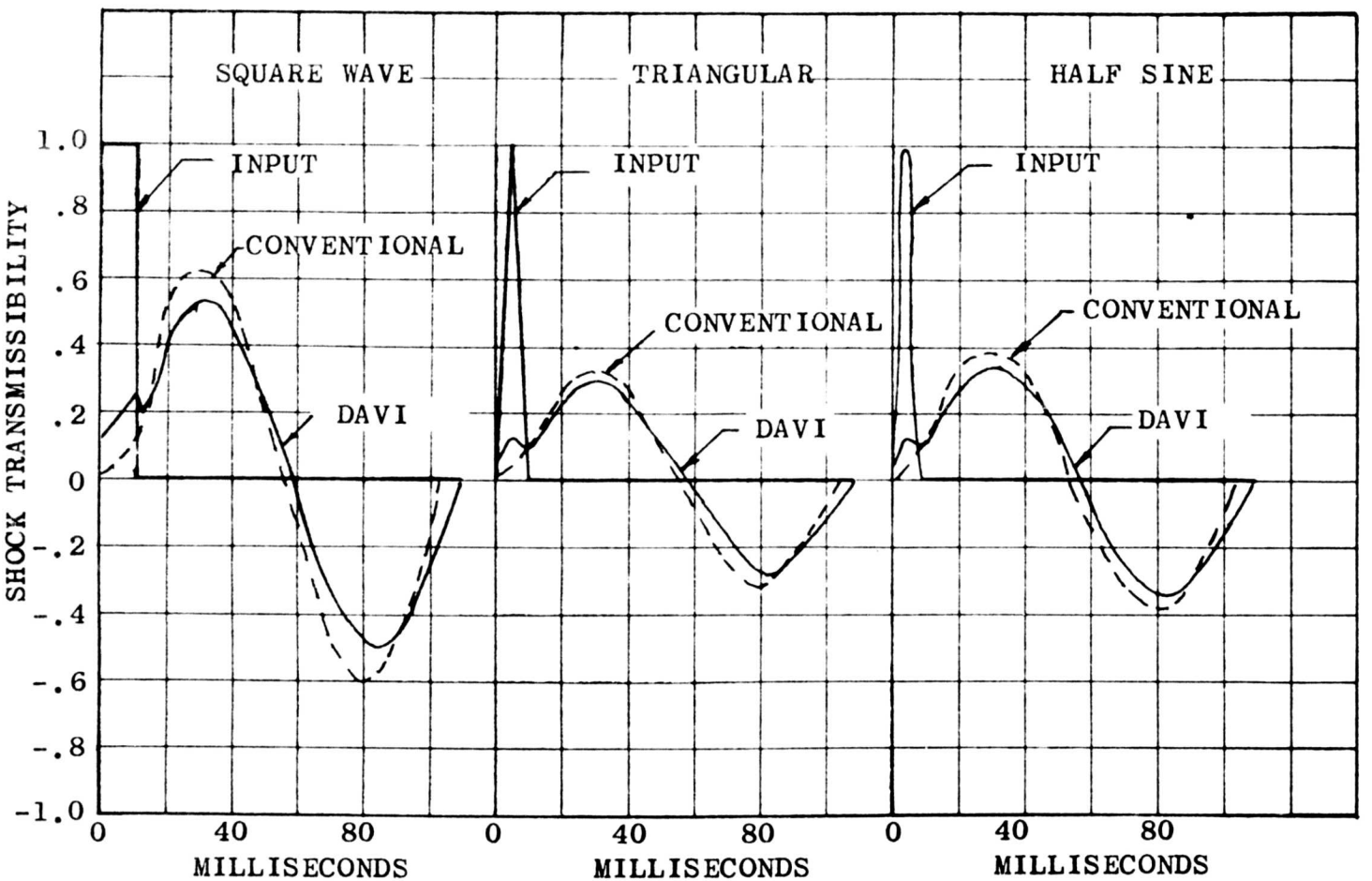

Figure 106. Time History of the DAVI Alpha With $T_{\alpha_{VHF}}$ =0.1

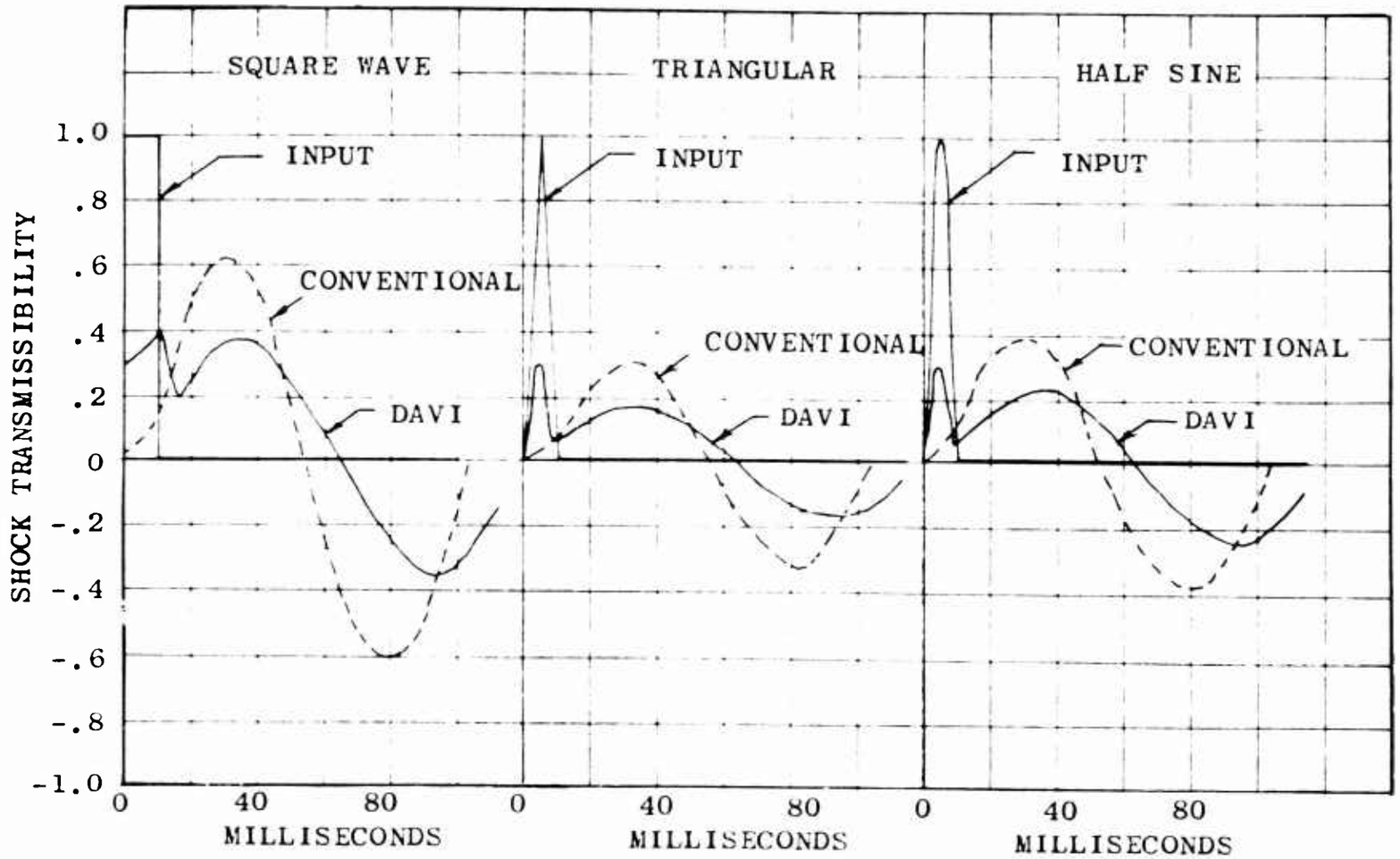

Figure 107. Time History of the DAVI Alpha With $T_{\alpha_{VHF}} = 0.3$

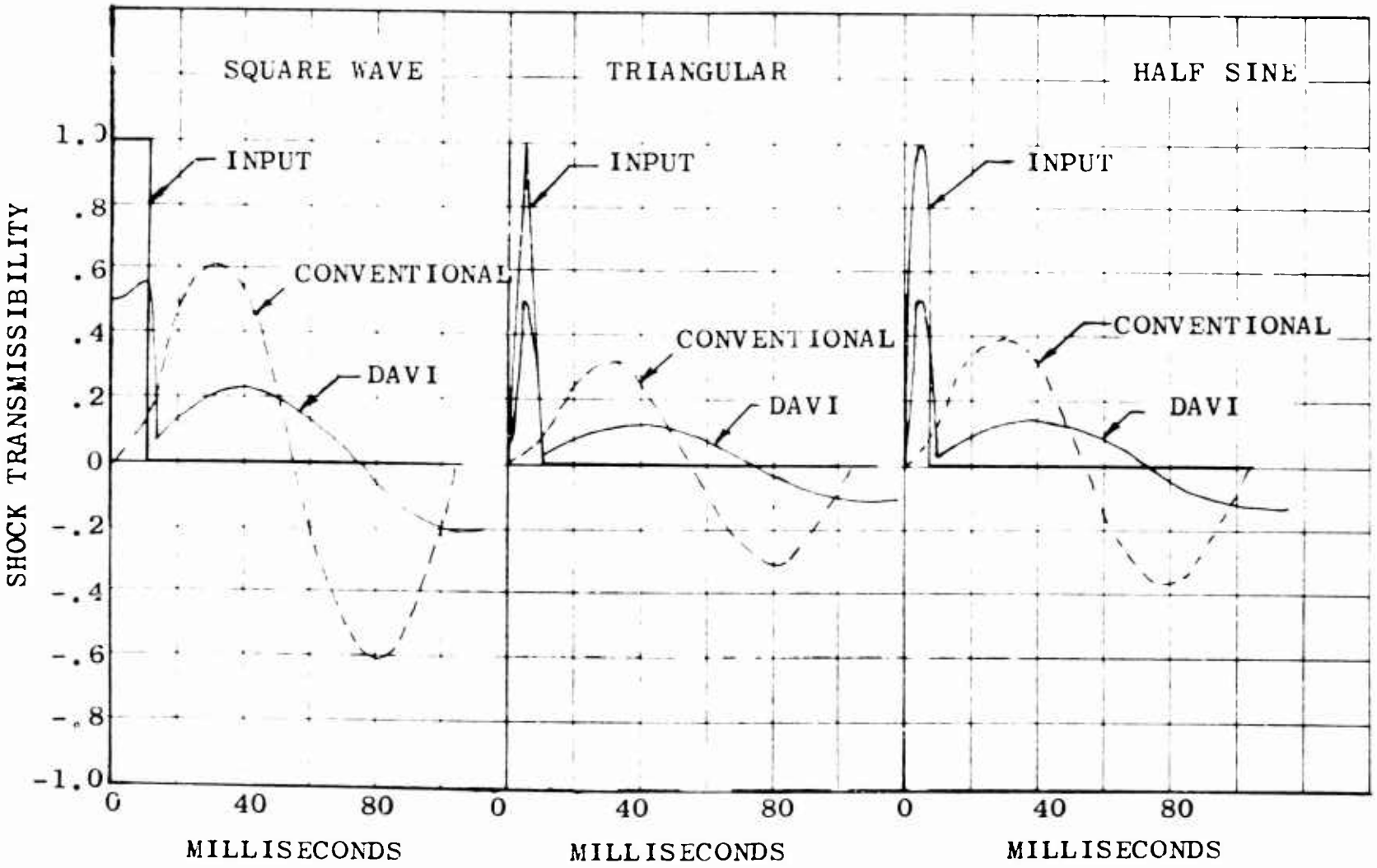

Figure 108. Time History of the DAVI Alpha With $T_{RAMP} = 0.5$

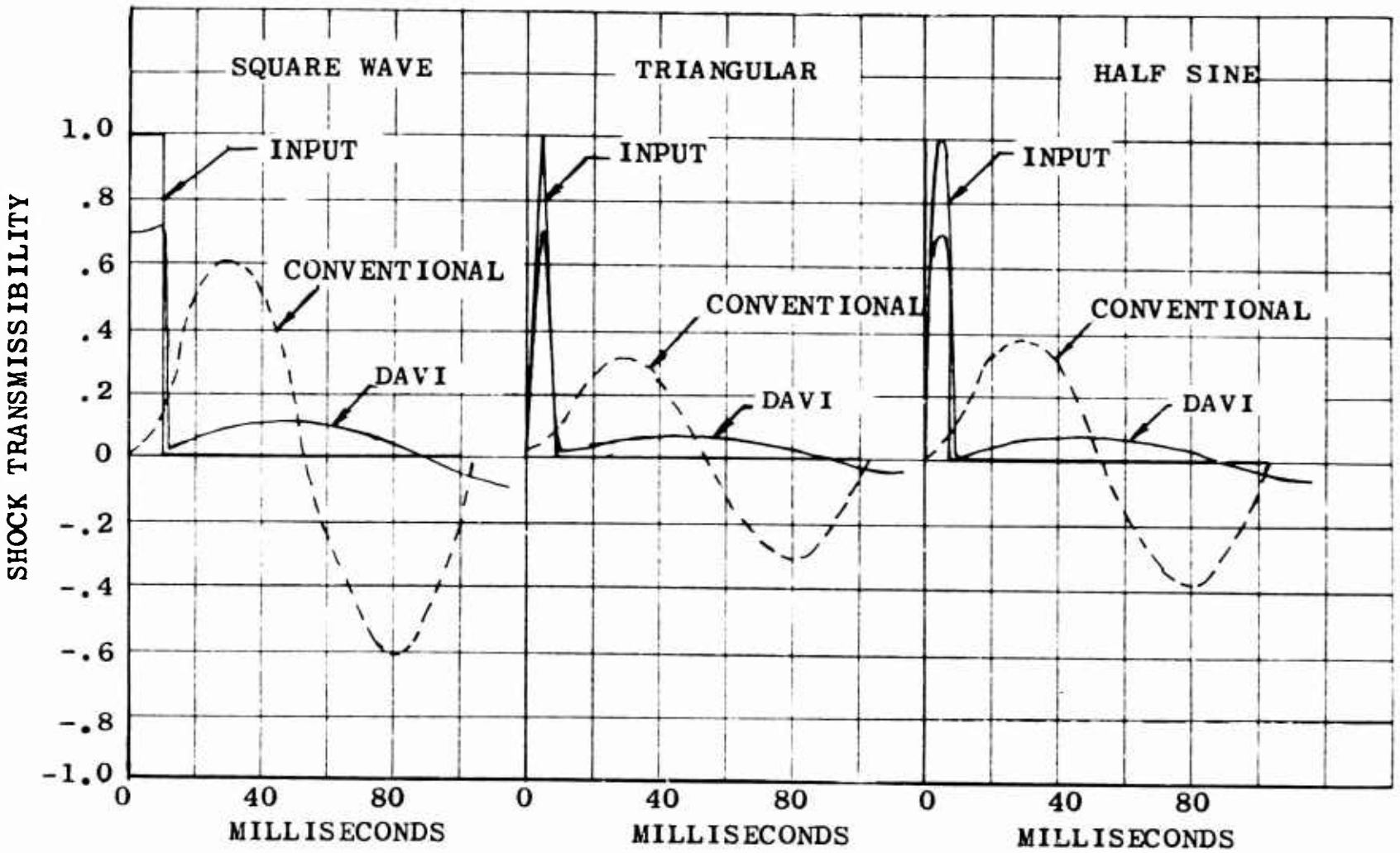

Figure 109. Time History of the DAVI Alpha With $T_{\alpha_{VHF}} = 0.7$

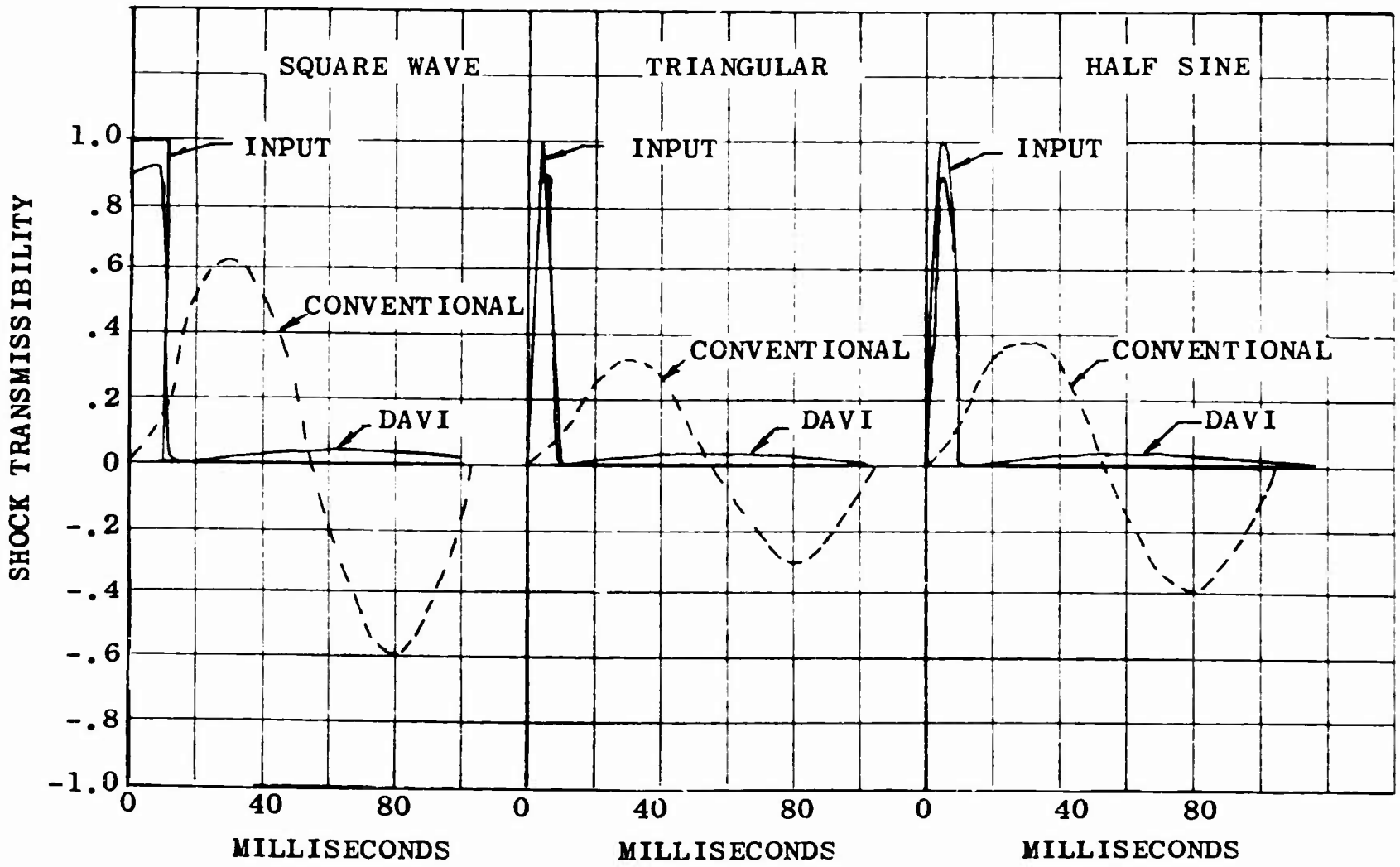

Figure 110. Time History of the DAVI Alpha With $T_{\alpha_{VHF}} = 0.9$

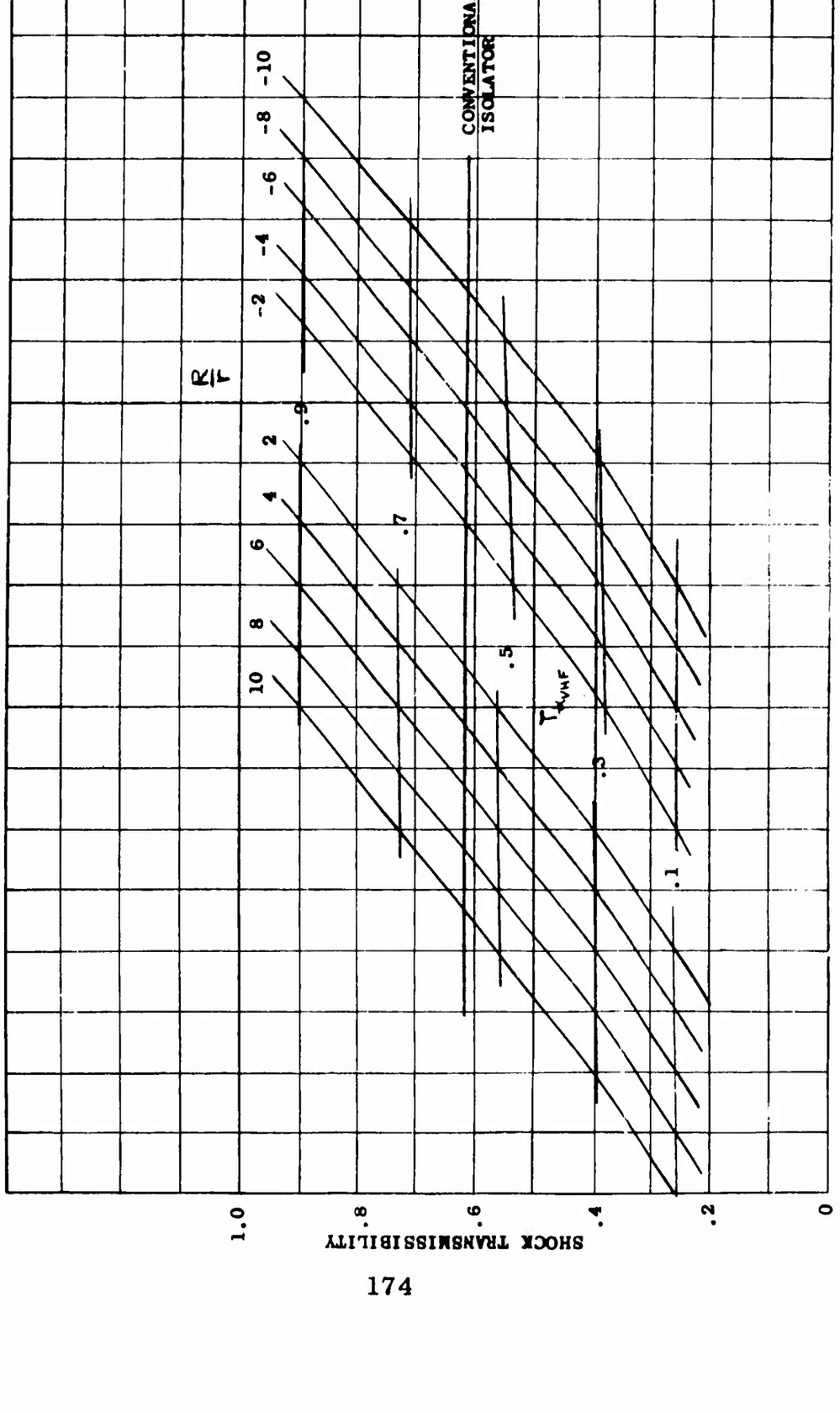

Figure 111. Initial Peak Shock Transmissibility of the DAVI Alpha for a Square-Wave Input

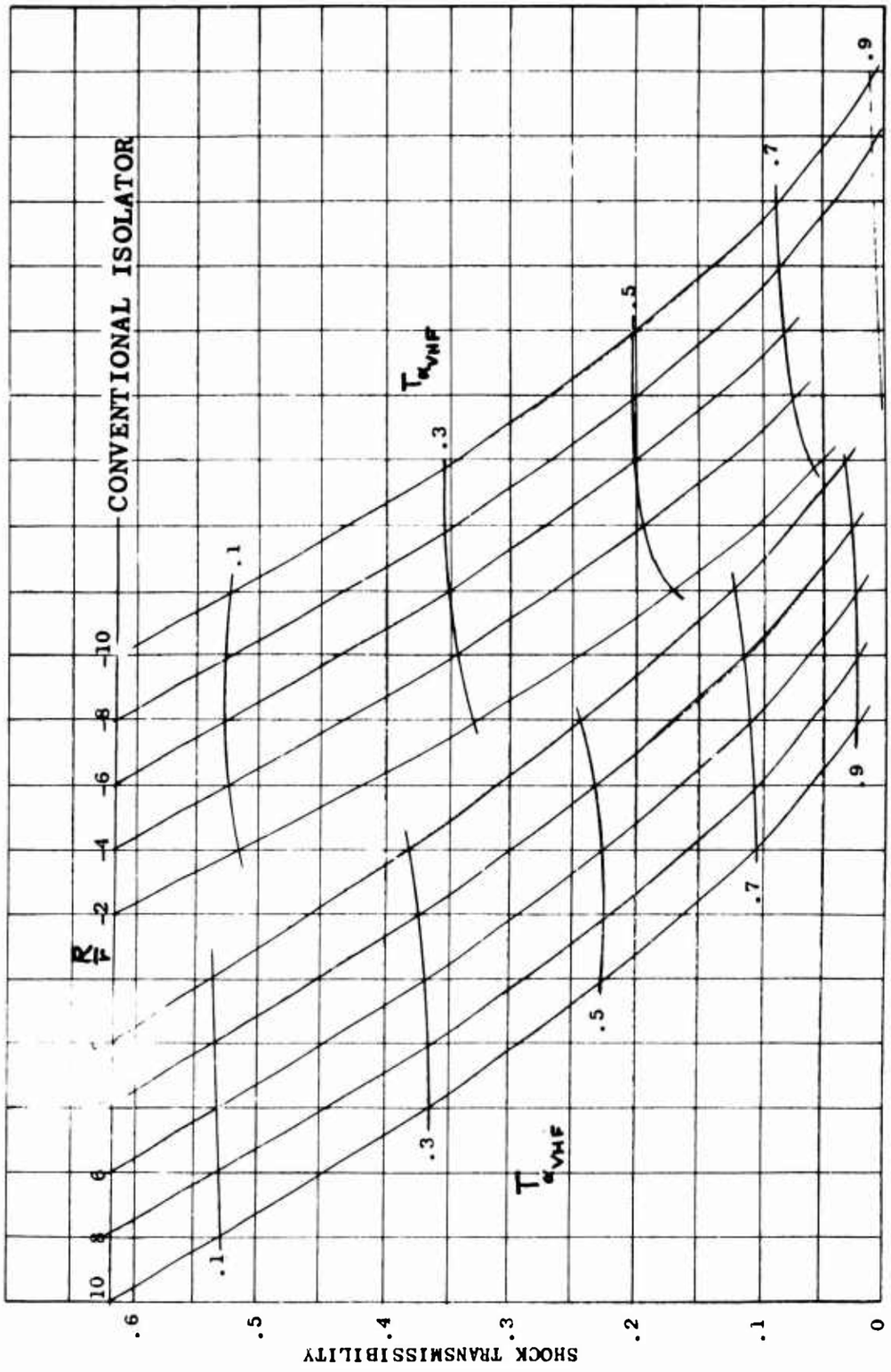

Figure 112. Fundamental Peak Shock Transmissibility of the DAVI Alpha for a Square-Wave Input

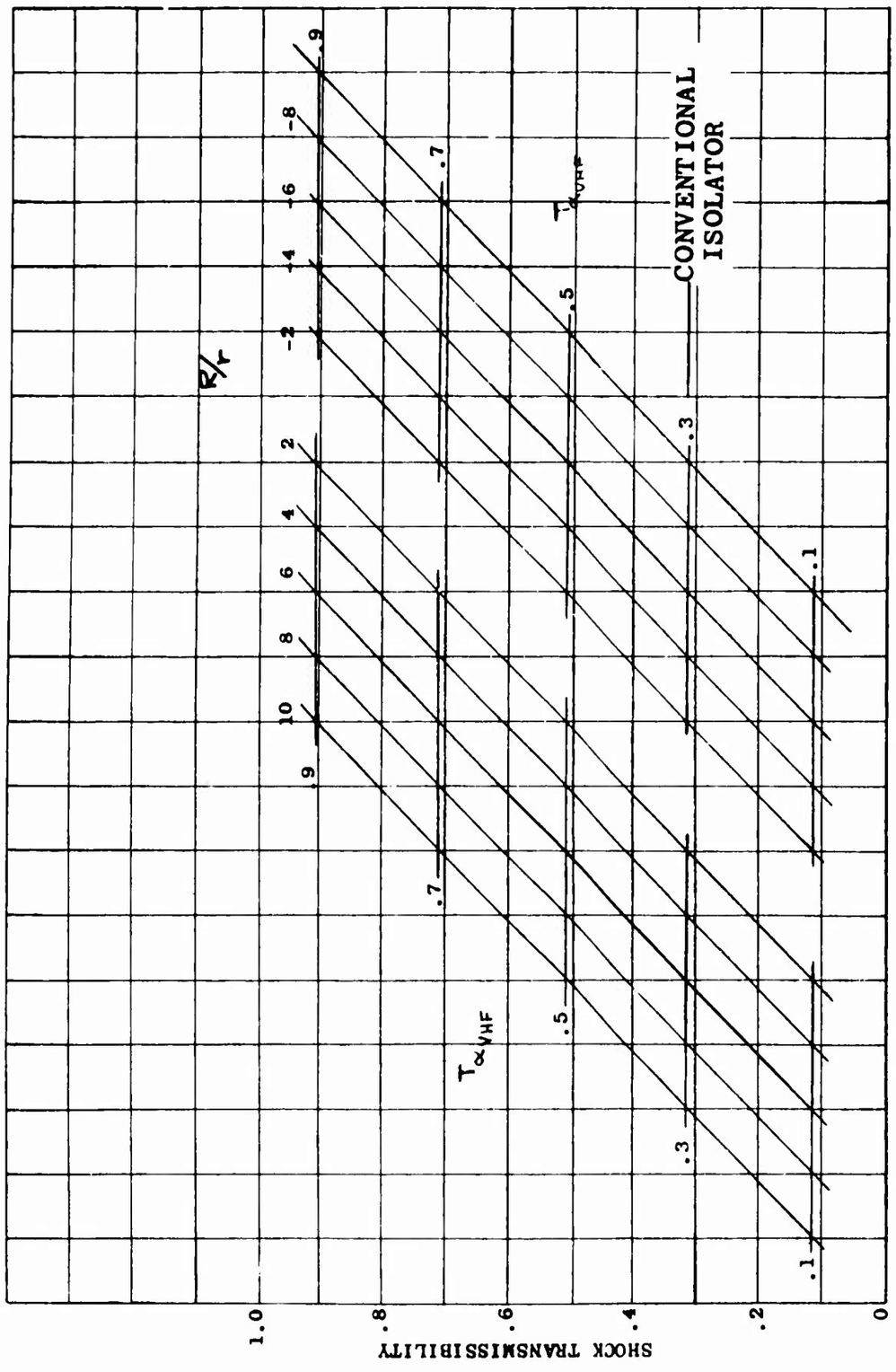

Figure 113. Initial Peak Shock Transmissibility of the DAVI Alpha for a Triangular and Half-Sine Input

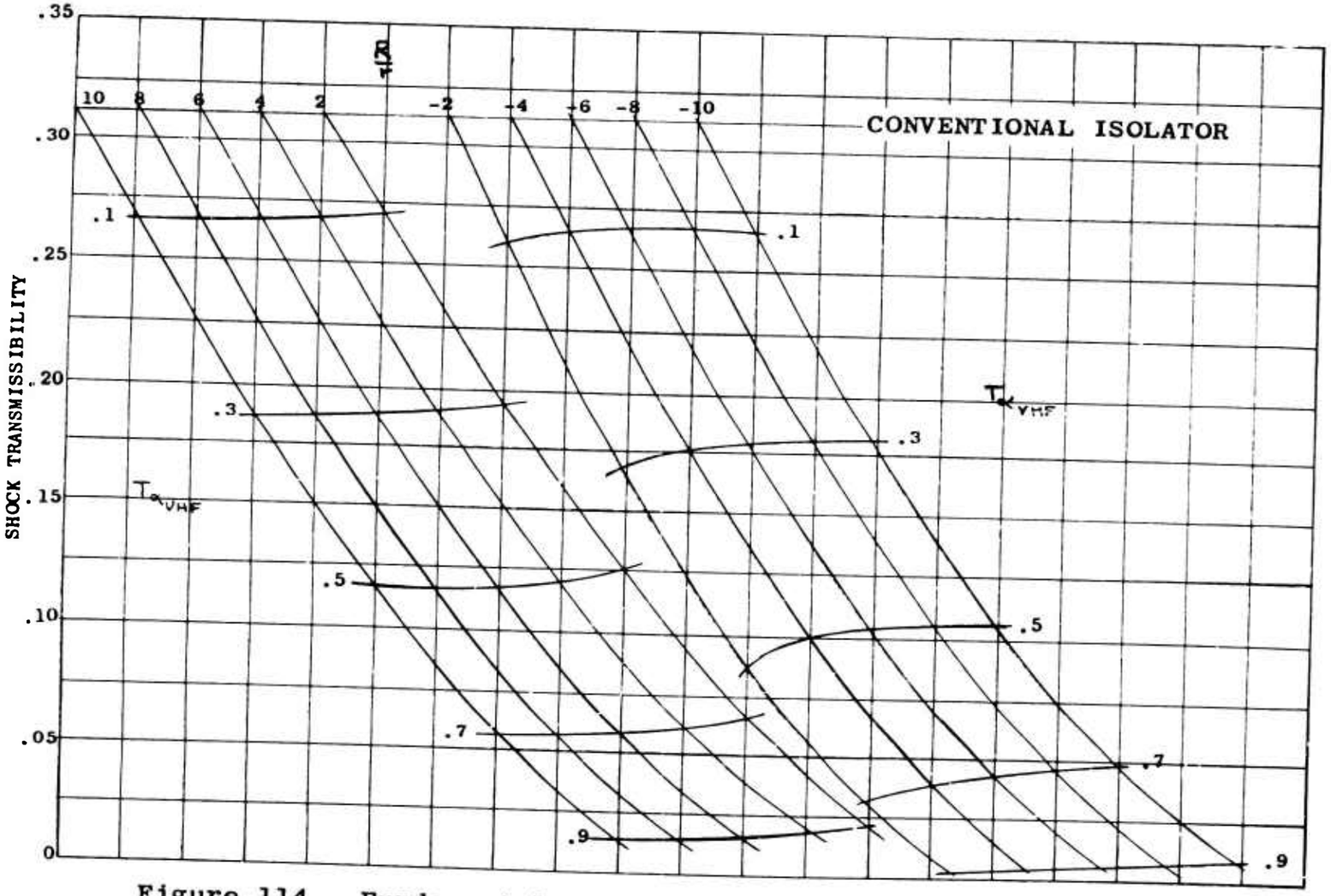

Figure 114. Fundamental Peak Shock Transmissibility of the DAVI Alpha for a Triangular Input

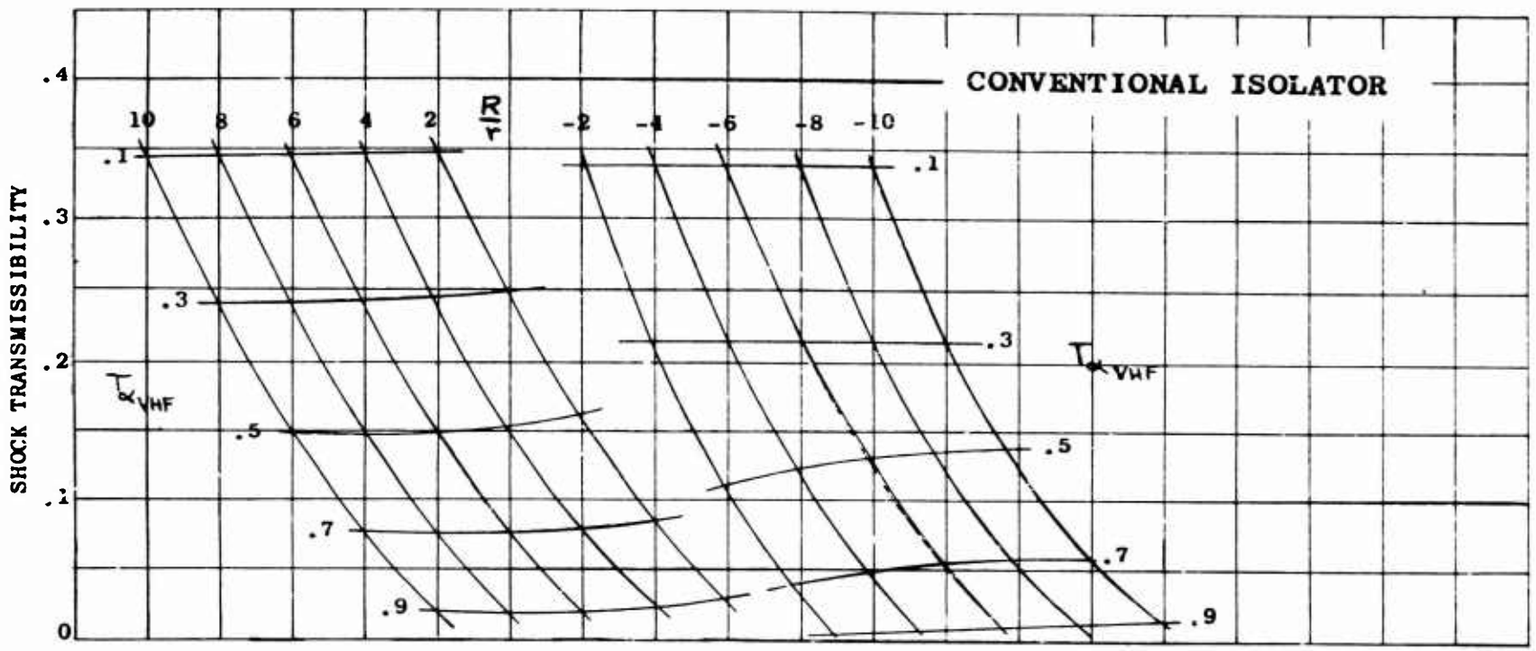

Figure 115. Fundamental Peak Shock Transmissibility of the DAVI Alpha for a Half-Sine Wave Input

TABLE X

PHYSICAL PARAMETERS OF DAVI ALPHA FOR VELOCITY SHOCK

Isolated Weight (Lb)	R/r	$2K_\theta$ (In.-Lb/Rad)	$K_{1,2}$ (Lb/In.)	K_D (Lb/In.)	μ_D	ω_R (c.p.s.)
39.1	10	400	7800	0	.01629	5.88
39.1	10	300	6750	100	.01629	5.91
39.1	10	200	5600	200	.01629	5.90
39.1	10	100	4200	300	.01629	5.83
39.1	10	0	∞	400	.01629	5.92
39.1	-	-	-	400	-	10.01

It is seen from the above table that physical parameters of the DAVI Alpha, with flexible pivots, were chosen such that the fundamental natural frequency was the same as in the DAVI Alpha with rigid pivots. The value of K_1 and K_2 used in the analysis was determined from Figure 116.

Figures 116 and 117 show the time histories versus g's of the isolated mass for a 10-inch/second initial velocity. The results show that in all the cases calculated, the DAVI Alpha with flexible pivots had a higher response than either the conventional or the simple DAVI Alpha. This high response is due to the fact that the DAVI Alpha with flexible pivots has three degrees of freedom. The high response, as seen from the figures, is the second mode of motion. The small variation in the envelope of this response is the motion due to the fundamental or low frequency. This fundamental frequency response is as low as the simple DAVI. Because the DAVI Alpha with flexible pivots has three degrees of freedom and will respond in all three modes for a transient excitation, it usually will have a higher response than the simple DAVI Alpha. It also is seen in these figures that the simple DAVI Alpha had a much lower response to the velocity shock than the conventional isolator with the same spring rate.

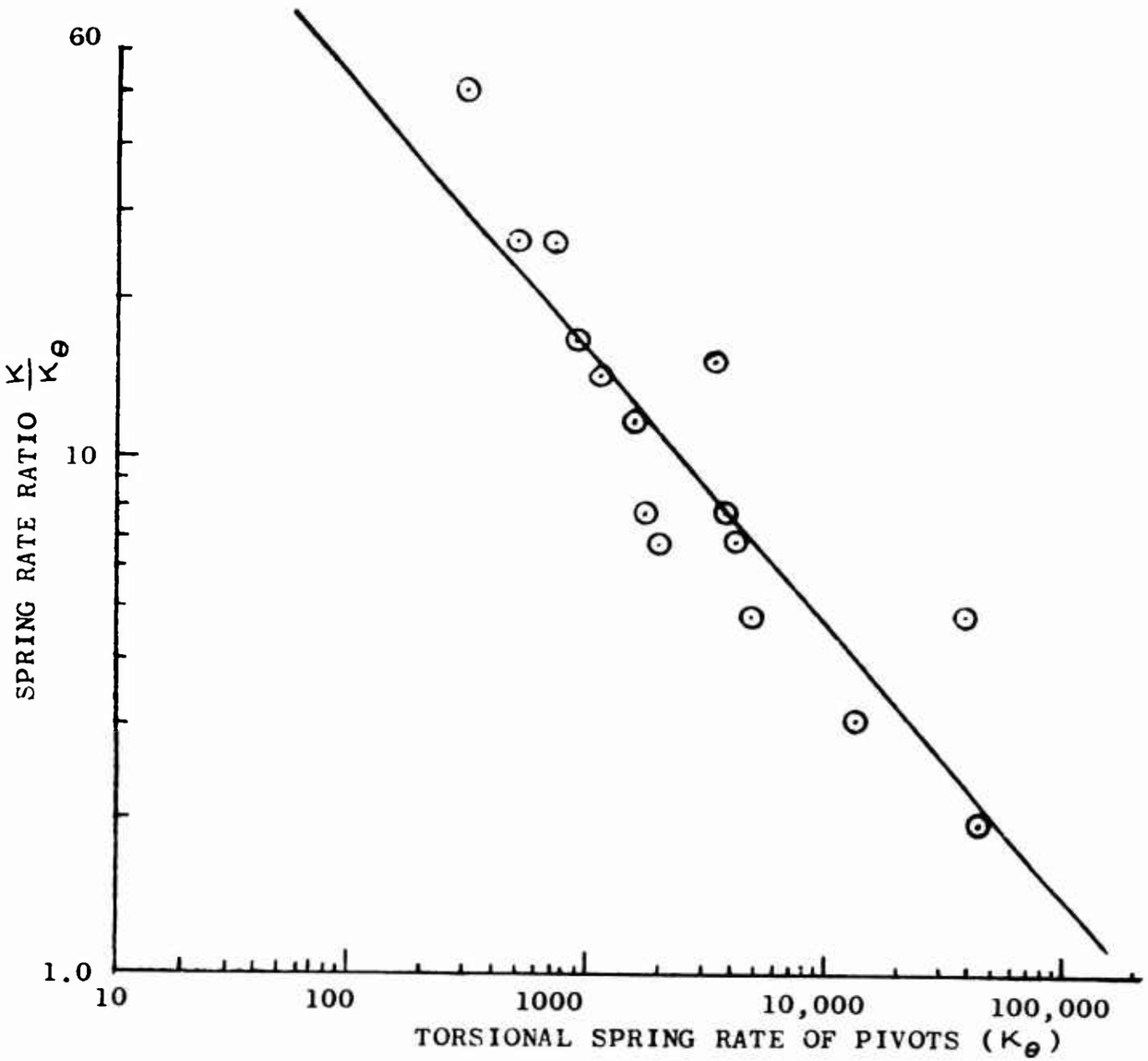

Figure 116. Torsional Flexibility Versus Radial Flexibility

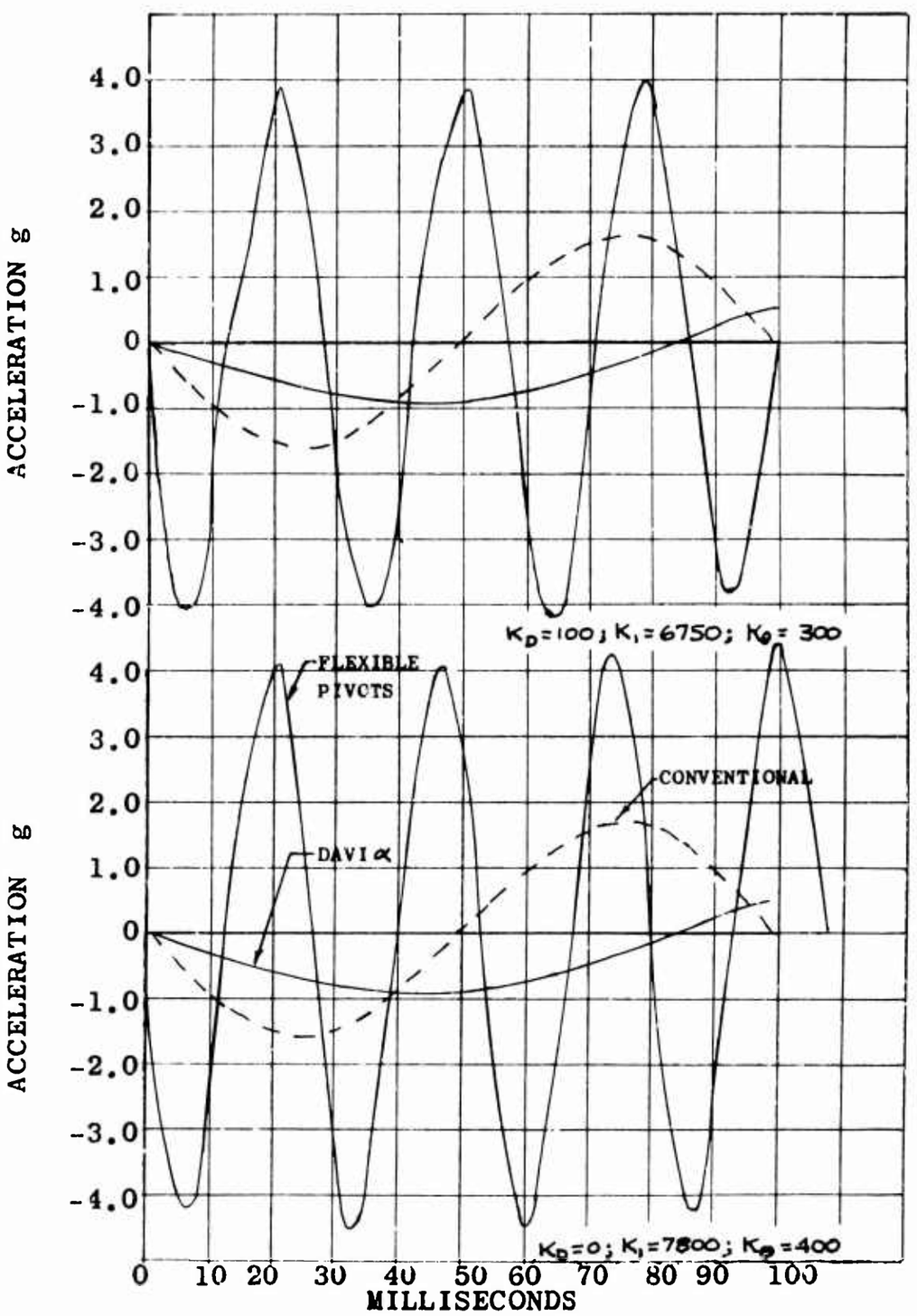

Figure 117. Time History of the DAVI Alpha With Flexible Pivots

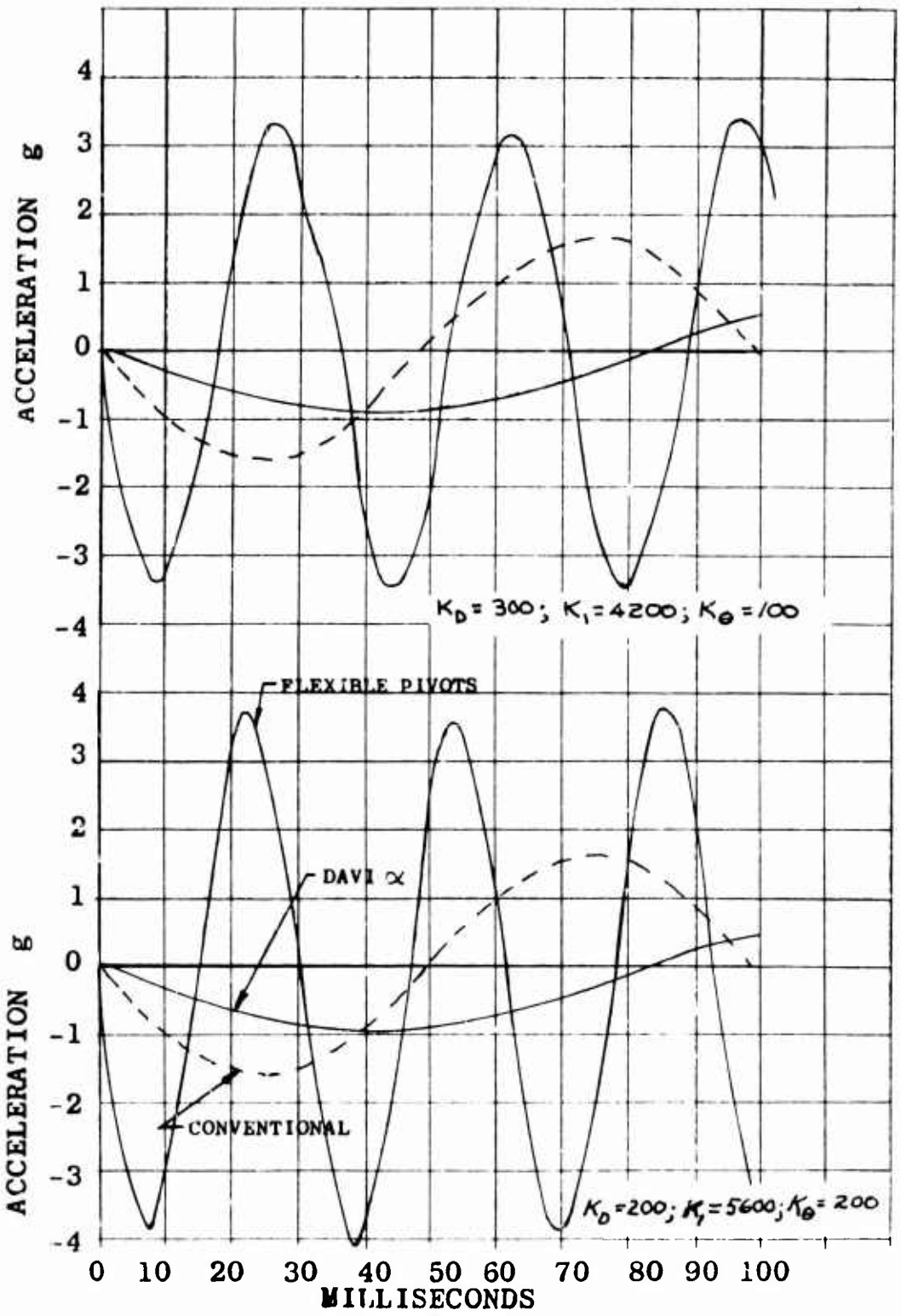

Figure 118. Time History of the DAVI Alpha With Flexible Pivots

TEST

Drop tests of the DAVI Alpha used in steady-state vibration surveys were done in December 1966 at Barry Controls, Watertown, Massachusetts, utilizing their drop test equipment and instrumentation.

The DAVI isolated platform used in the drop tests was the same as that used in the previous DAVI contract and is described in Reference 1. The test equipment used was the VP-400 varipulse machine, which is a free-fall type of mechanical shock test machine in which peak "g" values are obtained by varying the height of the drop. Three basic configurations were tested, as shown in Figures 119, 120, and 121. Figure 119 shows the DAVI Alpha isolated platform installed on the drop test machine. Figure 120 shows the platform isolated by the DAVI Alpha with molded rubber pivots installed on the drop test machine, and Figure 121 shows the conventional mounted platform. The conventional system was obtained by removing the DAVI Alpha with the molded rubber pivots.

The three configurations were subjected to three different types of inputs. Figure 122 shows the means of obtaining the one-half sine input. Figure 123 shows the means of obtaining the saw tooth, and Figure 124 shows the means of obtaining the square-wave input. Sixty-one drops were made; Table XI shows the forty-two drop tests that were reported.

Figures 125 through 166 give the results of the tests. In these figures, the bottom response is the input and the top response is of the isolated platform. The time scale is 20 milliseconds per major division, and the amplitude scale is 5 g's per major division.

Table XII gives a summary of the results obtained.

TABLE XI

DROP TEST CONFIGURATIONS

Platform Wt. (Lb)	DAVI Bar Wt. (Lb)	R/r	Input Type	Input Period Msec.	Input Mag. "g"	Fig. No.
41	2.25	-6.31	1/2 sine	20	10.0	124
41	2.25	-2.40	1/2 sine	20	10.0	125
41	2.25	-2.40(Rubber)	1/2 sine	20	12.0	126
41	2.25	-1.135	1/2 sine	20	10.0	127
41	0.90	-0.5	1/2 sine	20	10.0	128
41	2.25	+4.82	1/2 sine	20	9.0	129
41	2.25	+2.95	1/2 sine	20	9.0	130
41	2.25	+2.95(Rubber)	1/2 sine	20	12.0	131
41	2.25	+2.10	1/2 sine	20	10.0	132
41	0.90	+1.50	1/2 sine	20	10.0	133
41	-	Conventional	1/2 sine	20	12.0	134
41	2.25	-2.40	1/2 sine	60	2.5	135
41	2.25	-2.40(Rubber)	1/2 sine	60	3.5	136
41	2.25	-1.135	1/2 sine	60	3.0	137
41	2.25	+2.95	1/2 sine	60	2.5	138
41	2.25	+2.95(Rubber)	1/2 sine	60	5.0	139
41	2.25	+2.10	1/2 sine	60	5.0	140
41	-	Conventional	1/2 sine	60	6.0	141
41	2.25	-6.131	Saw-tooth	20	10.0	142
41	2.25	-2.40	Saw-tooth	20	10.0	143
41	2.25	-2.40(Rubber)	Saw-tooth	20	10.0	144
41	2.25	-1.135	Saw-tooth	20	10.0	145
41	0.90	-0.5	Saw-tooth	20	8.0	146
41	2.25	+4.842	Saw-tooth	20	10.0	147
41	2.25	+2.95	Saw-tooth	20	10.0	148
41	2.25	+2.95(Rubber)	Saw-tooth	20	10.0	149
41	2.25	+2.10	Saw-tooth	20	8.0	150
41	0.90	+1.50	Saw-tooth	20	8.0	151
41	-	Conventional	Saw-tooth	20	11.0	152
100	2.25	-6.131	Saw-tooth	20	8.0	153
100	+2.25	-2.40	Saw-tooth	20	10.0	154
100	2.25	-2.40(Rubber)	Saw-tooth	20	10.0	155
100	2.25	-1.135	Saw-tooth	20	12.0	156
100	2.25	+4.842	Saw-tooth	20	9.0	157
100	2.25	+2.95	Saw-tooth	20	8.0	158
100	2.25	+2 95(Rubber)	Saw-tooth	20	9.0	159
100	-	Conventional	Saw-tooth	20	11.0	160
41	2.25	-2.40	Square	20	13.0	161
41	2.25	-2.40(Rubber)	Square	20	14.0	162
41	2.25	+2.95	Square	20	10.0	163
41	2.25	+2.95(Rubber)	Square	20	12.0	164
41	-	Conventional	Square	20	12.0	165

TABLE XII

SUMMARY OF DROP TEST RESULTS

Fig. No.	Platform Wt. (Lb)	R/r	$T_{\alpha_{HF}}$	Trans. (Output/Input) Fundamental	Trans. (Output/Input) High Frequency
124	41	-6.131	.865	.111	1.335
125	41	-2.40	.595	.167	.834
126	41	-2.40(Rubber)	.595	.167	1.000
127	41	-1.135	.355	.500	.600
128	41	-0.5	.140	.723	-
129	41	4.842	.950	.1178	1.414
130	41	2.95	.744	.235	1.060
131	41	2.95(Rubber)	.744	-	1.25
132	41	2.10	.518	.526	.834
133	41	1.50	.140	.700	.25
134	41	Conventional	-	.834	-
135	41	-2.40	.595	1.00	-
136	41	-2.40(Rubber)	.595	1.00	-
137	41	-1.135	.355	1.33	-
138	41	+2.95	.744	1.00	-
139	41	+2.95(Rubber)	.744	1.20	-
140	41	+2.10	.518	.80	-
141	41	Conventional	-	1.68	-
142	41	-6.131	.865	.100	1.00
143	41	-2.40	.595	.227	.635
144	41	-2.40(Rubber)	.595	.200	1.10
145	41	-1.135	.355	.444	.555
146	41	-0.5	.140	.555	-
147	41	4.842	.950	.100	1.20
148	41	+2.950	.744	.200	.890
149	41	+2.95(Rubber)	.744	.200	1.60
150	41	+2.10	.518	.333	.625
151	41	+1.50	.140	.750	-
152	41	Conventional	-	.835	-
153	100	-6.131	.774	.11	1.111
154	100	-2.40	.665	.333	.777
155	100	-2.40(Rubber)	.665	.200	.900
156	100	-1.135	.485	.333	.333
157	100	+4.842	.770	.1875	1.125
158	100	2.95	.478	.333	.777
159	100	2.95(Rubber)	.478	.200	1.20
160	100	Conventional	-	.636	-
161	41	-2.40	.595	.333	1.412
162	41	-2.40(Rubber)	.595	-	1.230
163	41	+2.95	.744	.182	1.545
164	41	+2.95(Rubber)	.744	-	1.665
165	41	Conventional	-	1.083	-

The transmissibilities in Table XII were obtained from the first cycle of the time histories of the isolated platform. The first cycle was used to obtain the transmissibilities to minimize the feedback to the drop test table. It should be noted that for the one-half sine input, there was rebound. This was due to the low drop height to minimize the "g" loading, and the catch mechanism could not operate at this height. The transmissibility of the fundamental response was obtained by fairing out the high-frequency response. Because of this fairing and the scale factor on the figures, the transmissibilities are not precise.

Although theoretical calculations were not done to correlate the drop test results, the inspections of Figures 119 through 166 and of Table XII show that the test results definitely followed the theory as predicted in Figures 106 through 115. In every test case, the transmissibility of the DAVI Alpha in its fundamental frequency was lower than that of the equivalent conventional isolator. In most cases, the higher the high-frequency isolation of the DAVI Alpha, the lower the transmissibility obtained in the fundamental frequency response and the higher the transmissibility obtained in the initial response. The high response of the DAVI Alpha with molded rubber pivots appeared to be due to its second degree of freedom. It should be noted that with the higher period of 60-millisecond input of the one-half sine wave (Figures 136 through 142), no initial high response was obtained and, in every case, DAVI Alpha had lower transmissibility than the conventional isolator.

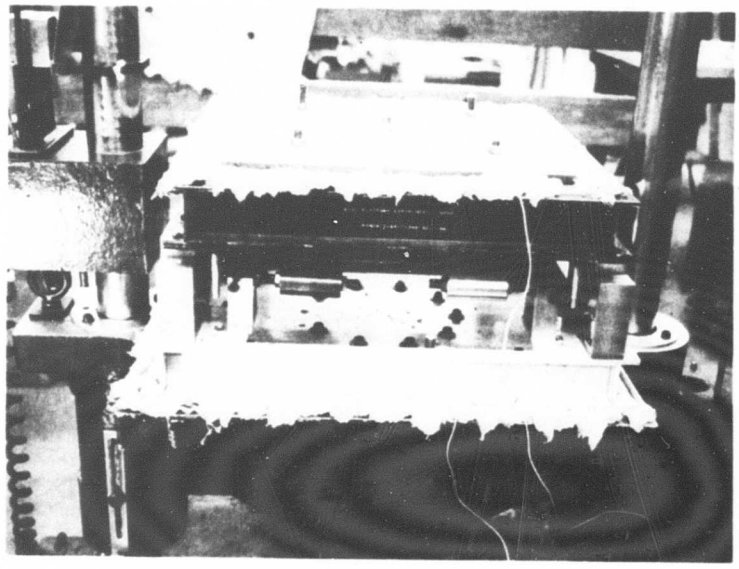

Figure 119. DAVI Alpha Installed on the Drop Test Fixture

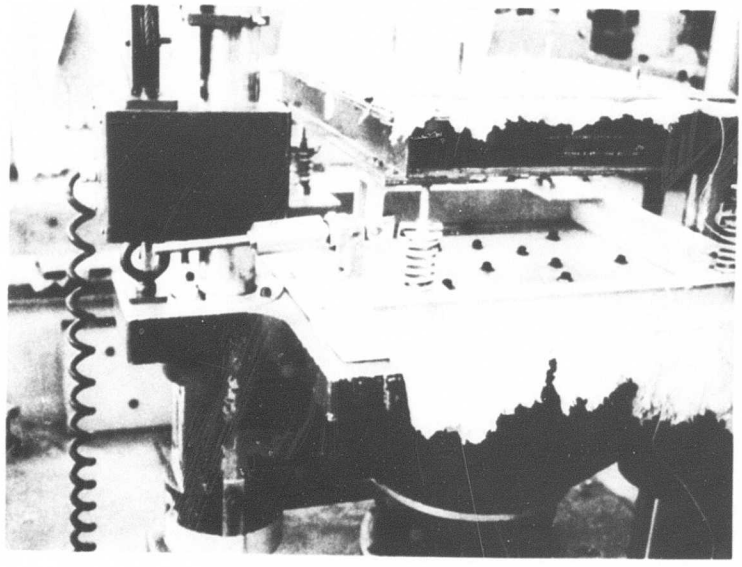

Figure 120. DAVI Alpha With Molded Rubber Pivots Installed on the Drop Test Fixture

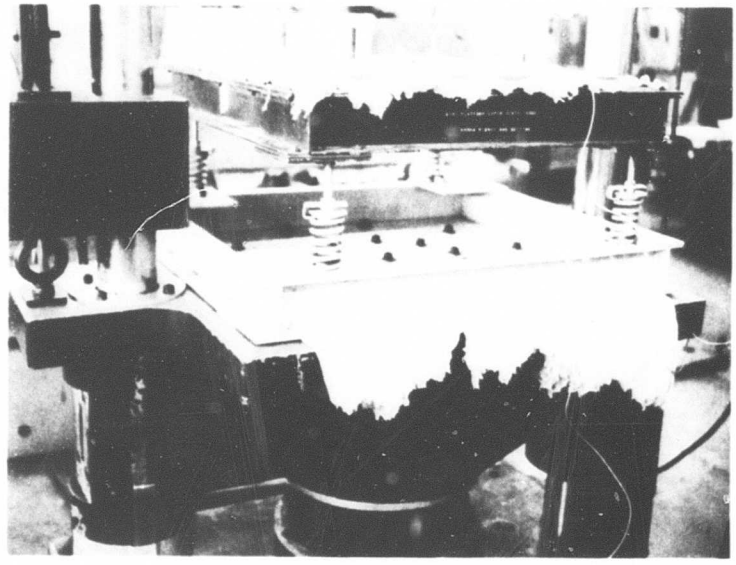

Figure 121. Conventional Isolator on Drop Test Machine

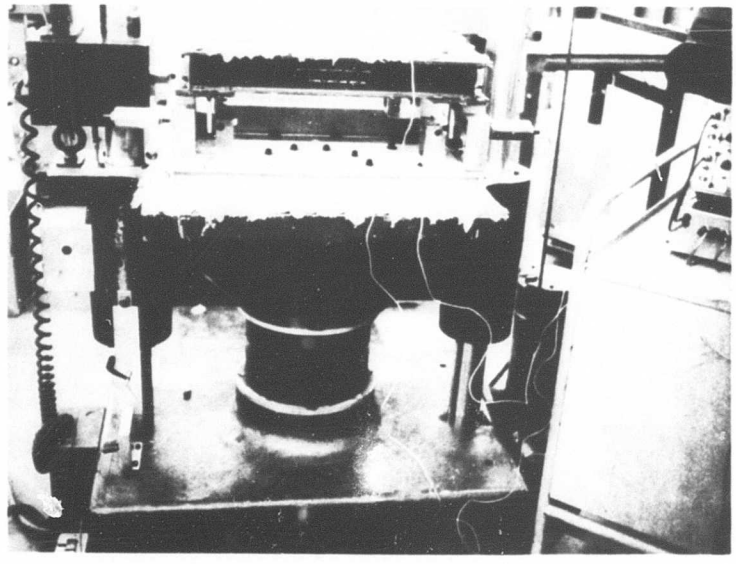

Figure 122. Half-Sine Input Installation

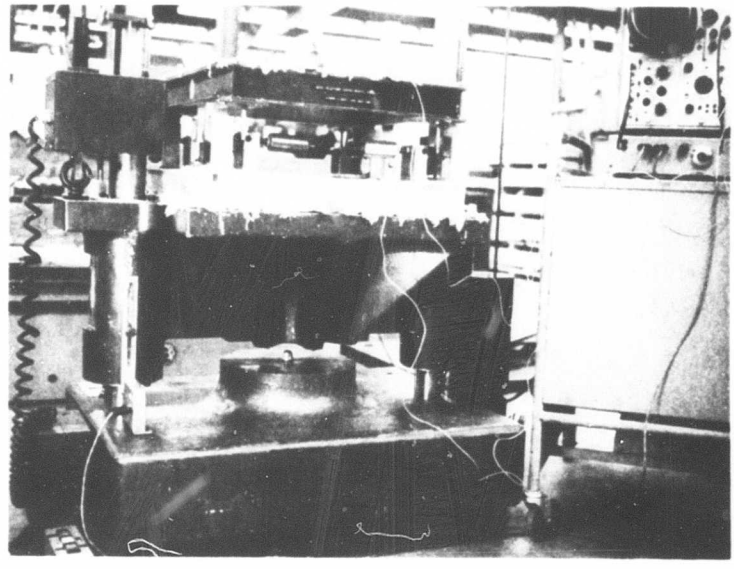

Figure 123. Saw-Tooth Input Installation

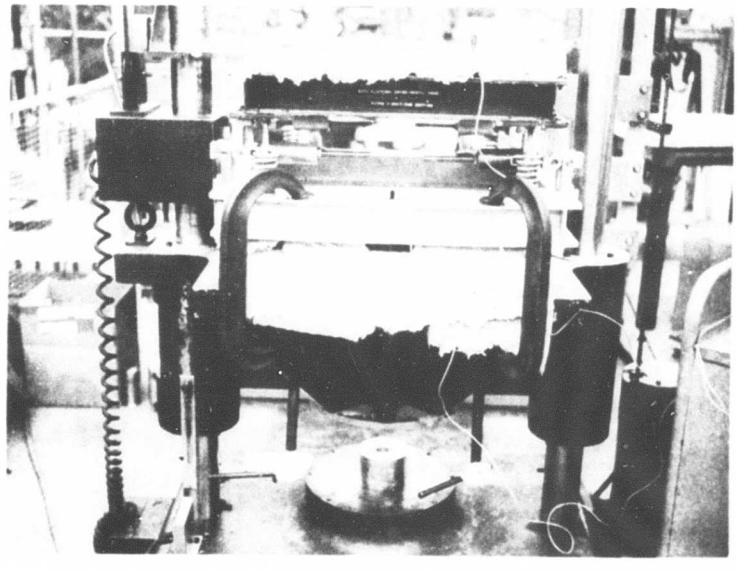

Figure 124. Square-Wave Input Installation

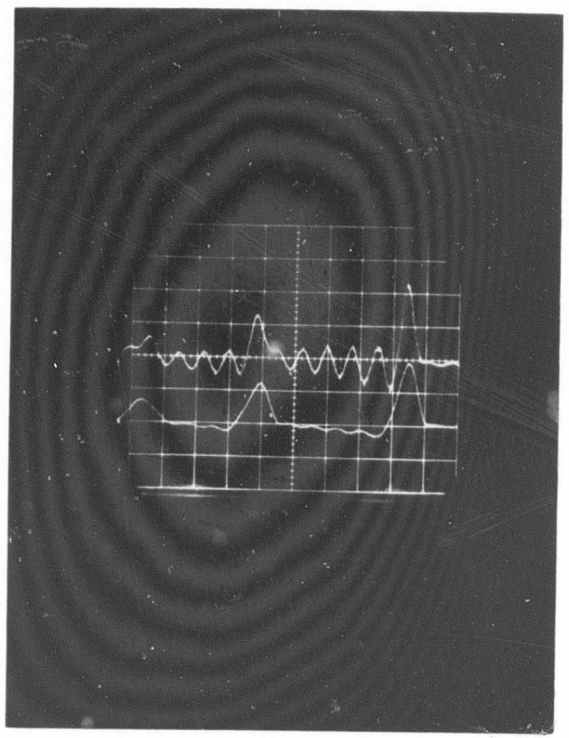

41# PLATFORM, $\frac{R}{r} = -6.131$

Figure 125. Time History of Experimental Drop Test

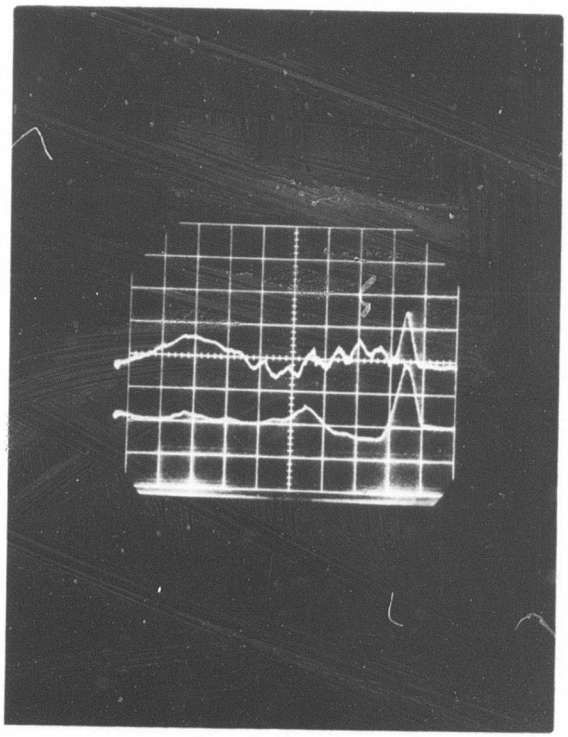

41# PLATFORM, $\frac{R}{r} = -2.40$

Figure 126. Time History of Experimental Drop Test

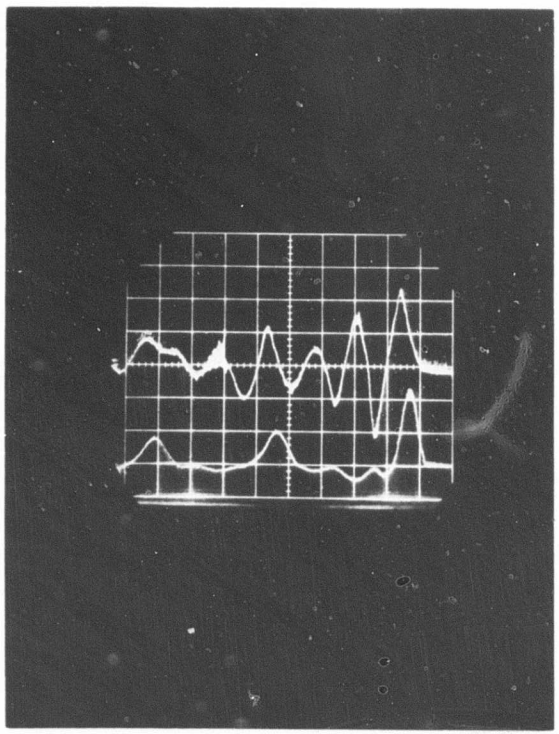

41# PLATFORM, $\frac{R}{r}$ = -2.40 (RUBBER)

Figure 127. Time History of Experimental Drop Test

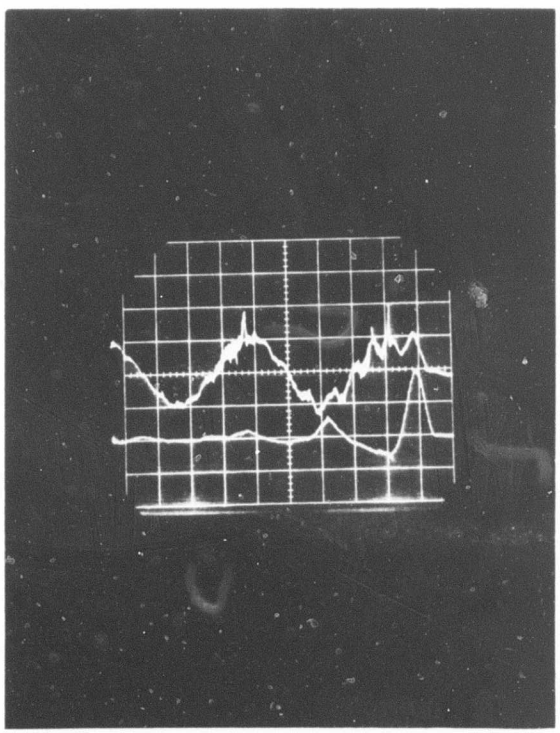

41# PLATFORM, $\frac{R}{r}$ = -1.135

Figure 128. Time History of Experimental Drop Test

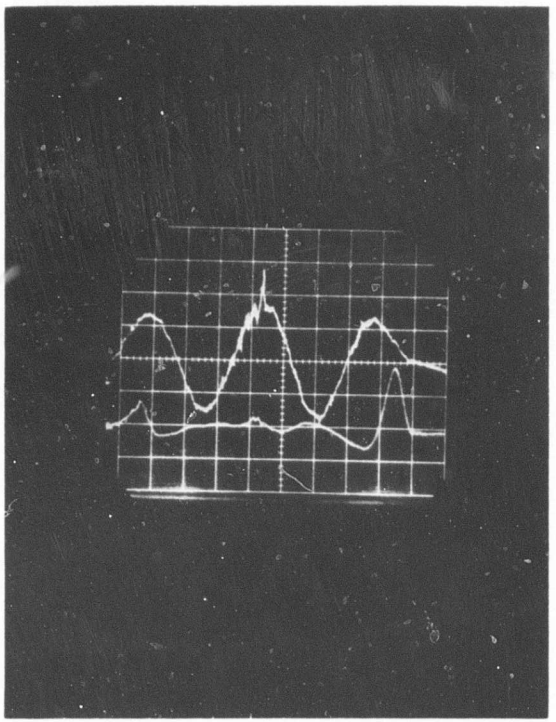

41# PLATFORM, $\frac{R}{r}$ = -0.5 (NO WT)

Figure 129. Time History of Experimental Drop Test

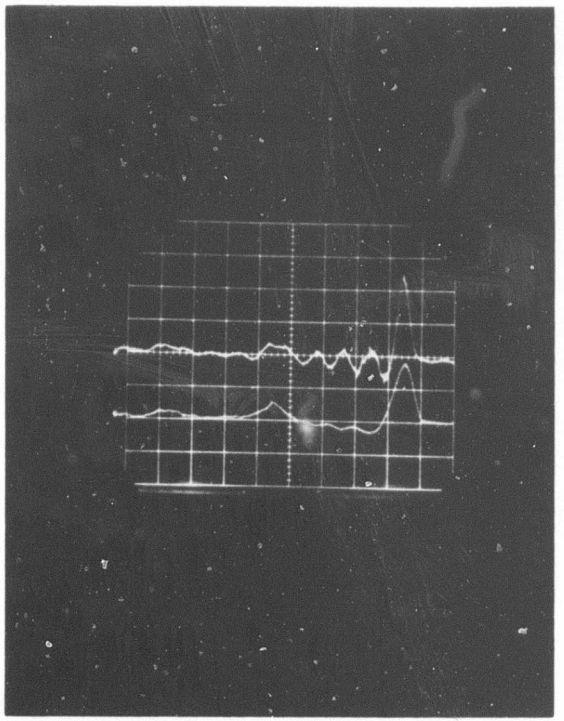

41# PLATFORM, $\frac{R}{r}$ = 4.842

Figure 130. Time History of Experimental Drop Test

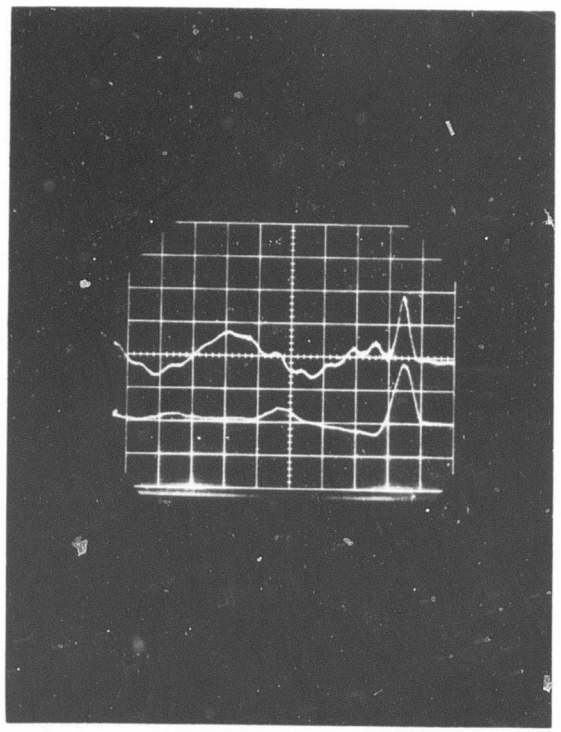

41# PLATFORM, $\frac{R}{r} = 2.95$

Figure 131. Time History of Experimental Drop Test

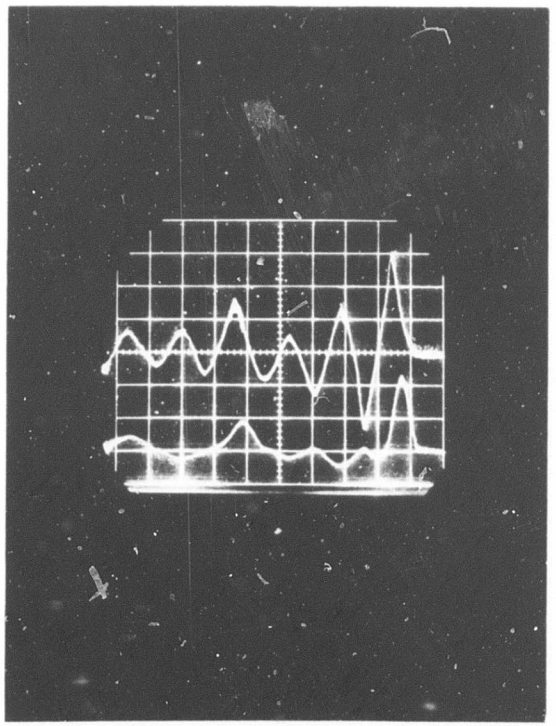

41# PLATFORM, $\frac{R}{r} = 2.95$ (RUBBER)

Figure 132. Time History of Experimental Drop Test

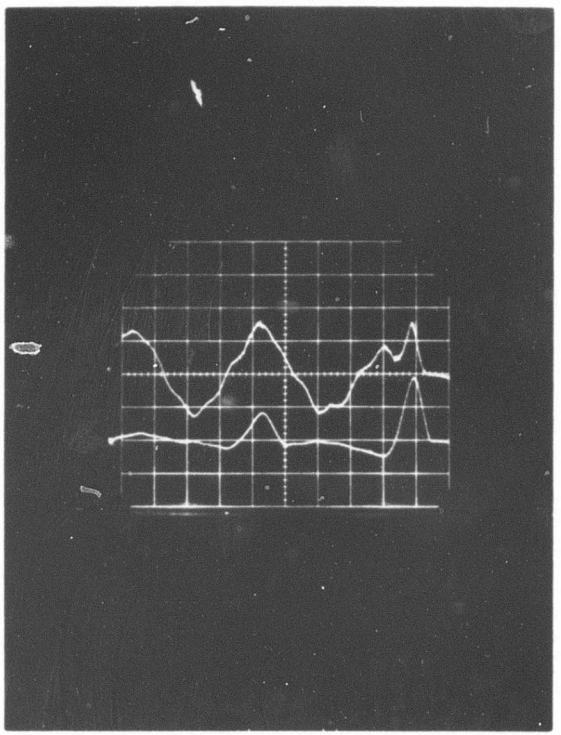

41# PLATFORM, $\frac{T}{R} = 2.10$

Figure 133. Time History of Experimental Drop Test

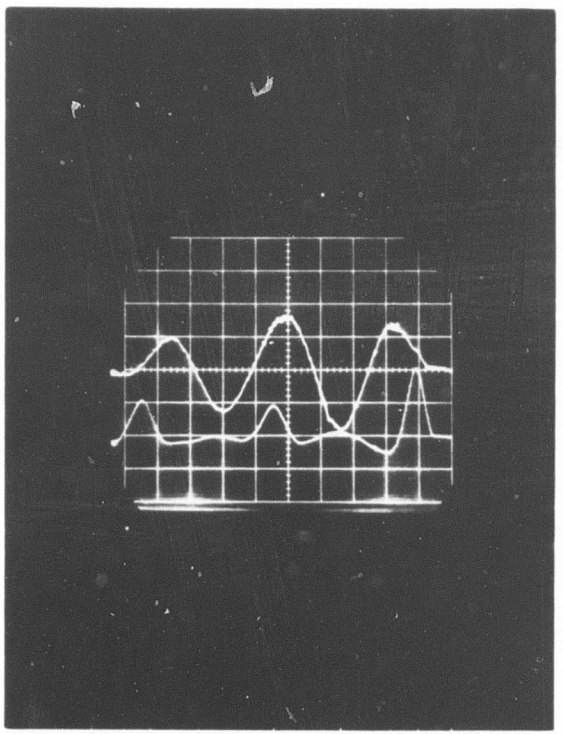

41# PLATFORM, $\frac{T}{R} = 1.50$ (NO WT)

Figure 134. Time History of Experimental Drop Test

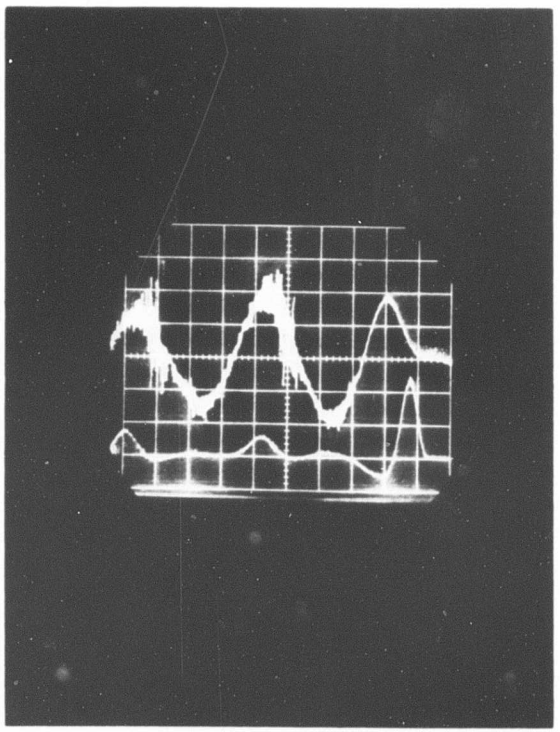

41# PLATFORM, CONVENTIONAL

Figure 135. Time History of Experimental Drop Test

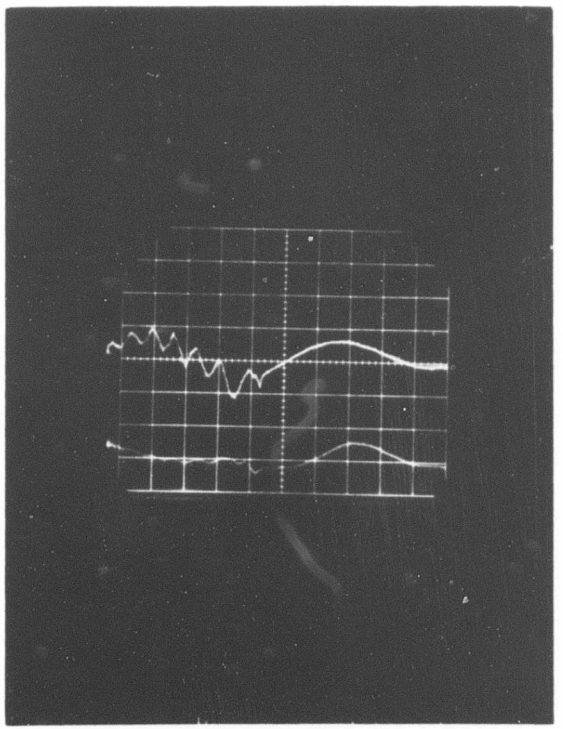

41# PLATFORM, $\frac{R}{r} = -2.40$

Figure 136. Time History of Experimental Drop Test

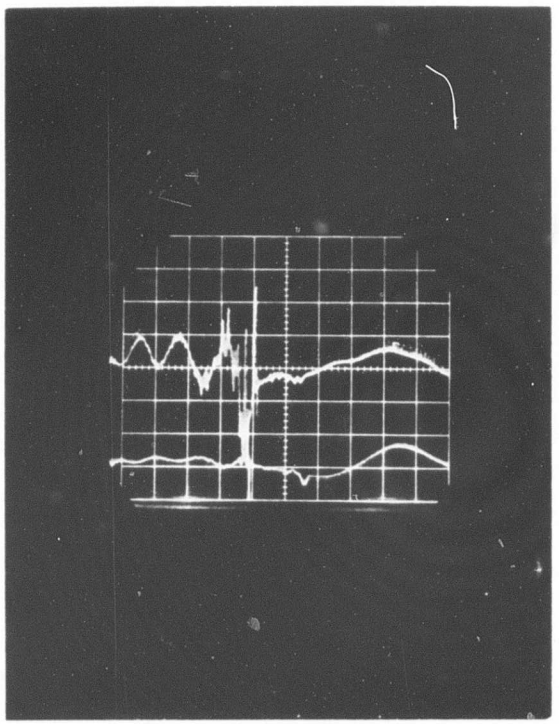

41# PLATFORM, $\frac{R}{T} = -2.40$ (RUBBER)

Figure 137. Time History of Experimental Drop Test

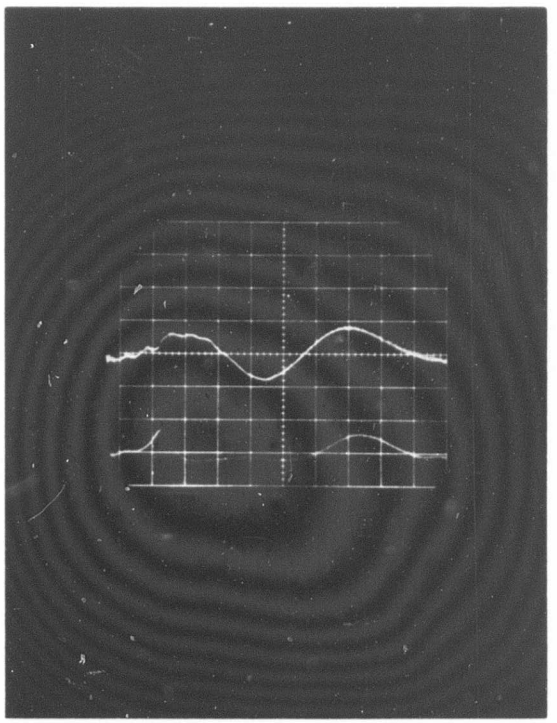

42# PLATFORM, $\frac{R}{T} = -1.135$

Figure 138. Time History of Experimental Drop Test

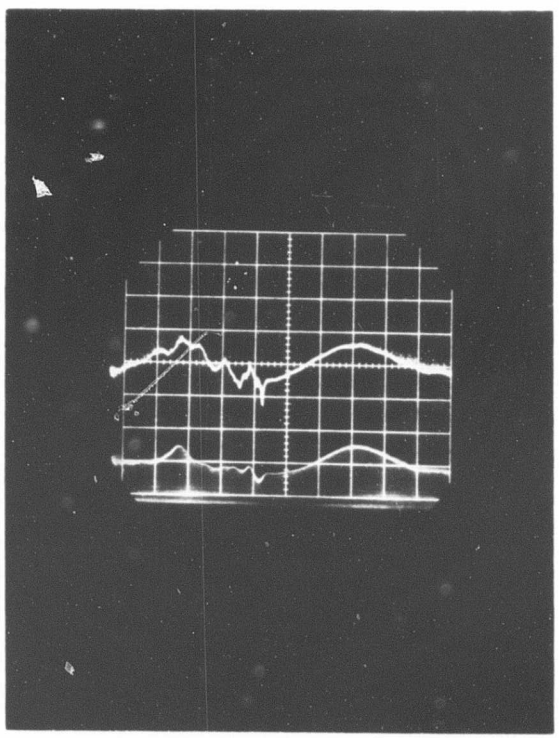

41# PLATFORM, $\frac{\tau}{R} = 2.95$

Figure 139. Time History of Experimental Drop Test

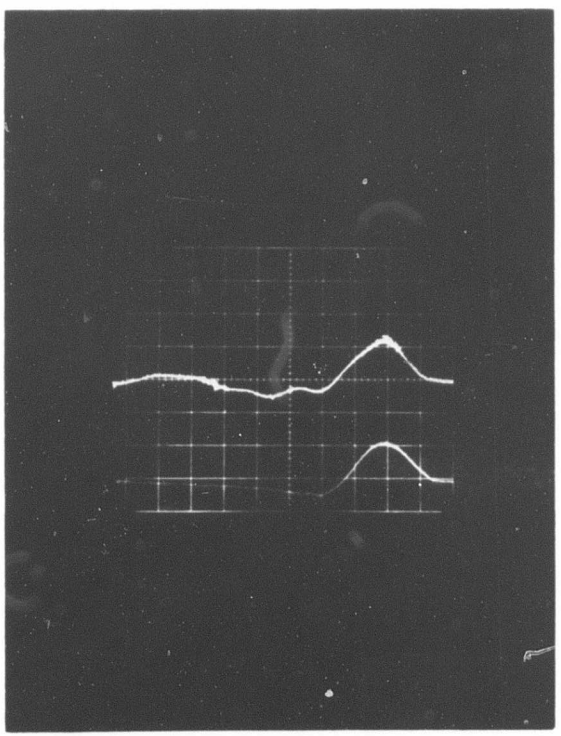

41# PLATFORM, $\frac{\tau}{R} = 2.95$ (RUBBER PIVOTS)

Figure 140. Time History of Experimental Drop Test

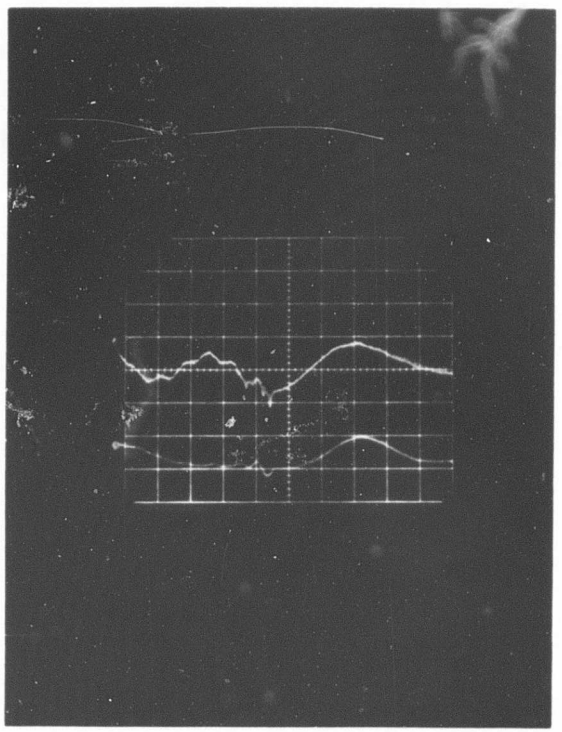

41# PLATFORM, $\frac{R}{r}$ = 2.10

Figure 141. Time History of Experimental Drop Test

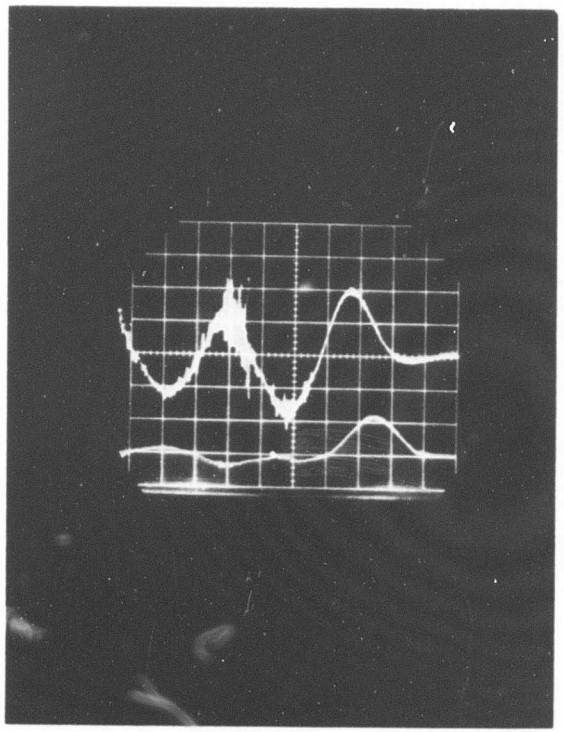

41# PLATFORM, CONVENTIONAL

Figure 142. Time History of Experimental Drop Test

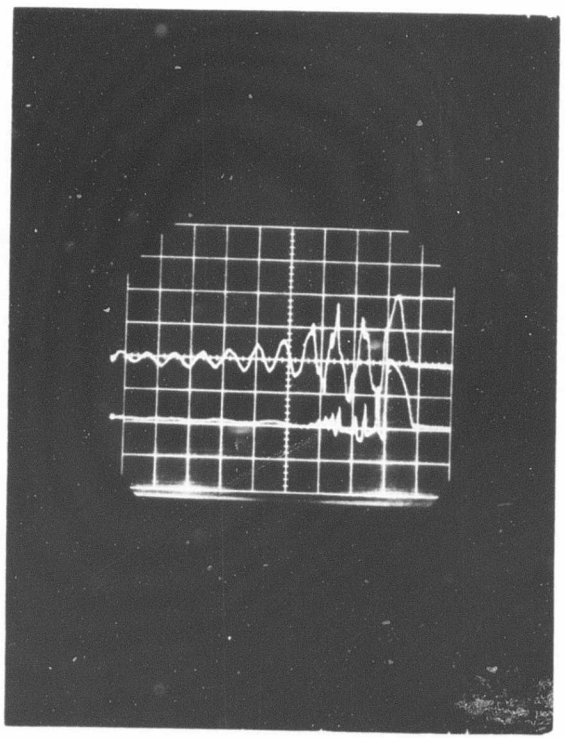

SAW-TOOTH

41# PLATFORM, $\frac{R}{r}$ = -6.131

Figure 143. Time History of Experimental Drop Test

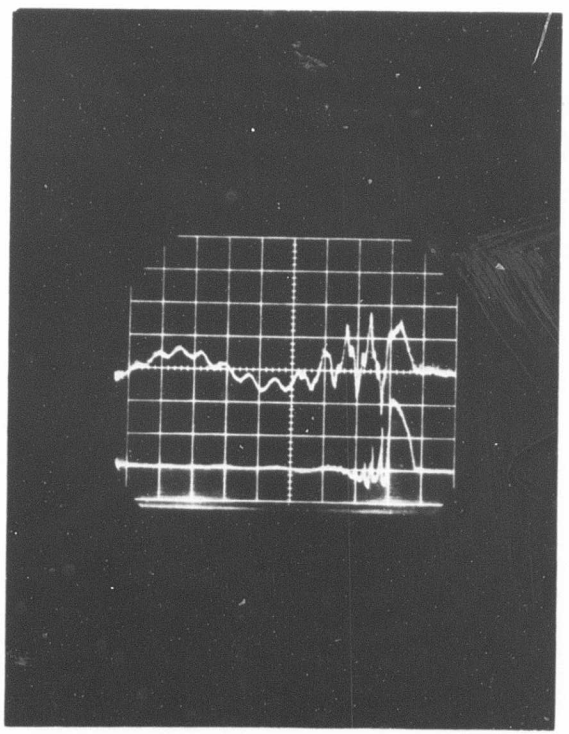

SAW-TOOTH

41# PLATFORM, $\frac{R}{r}$ = -2.40

Figure 144. Time History of Experimental Drop Test

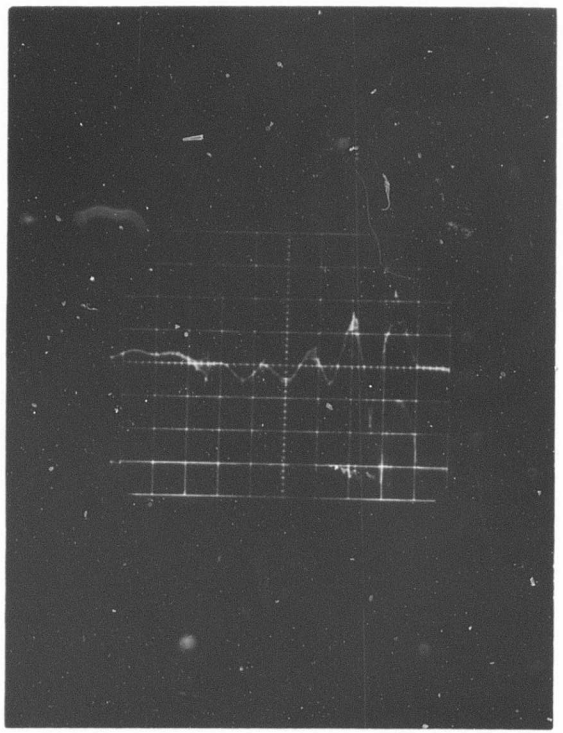

41# PLATFORM, $\frac{R}{r}$ = -2.40 (RUBBER)

Figure 145. Time History of Experimental Drop Test

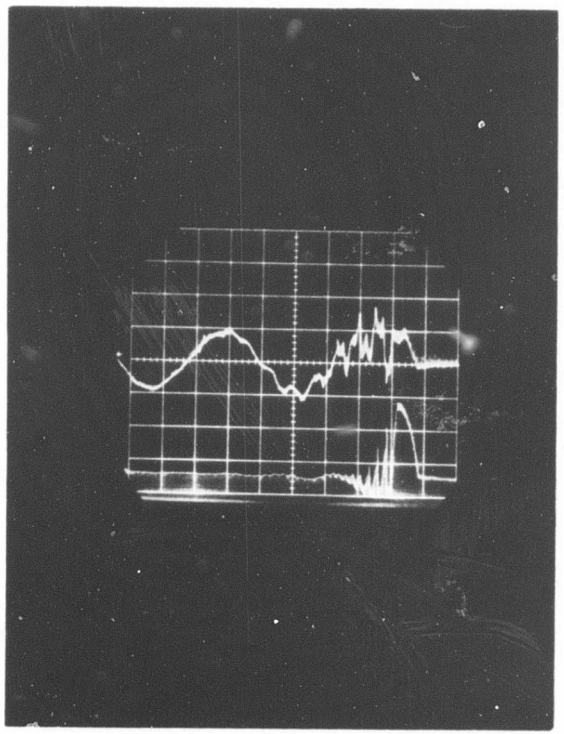

41# PLATFORM, $\frac{R}{r}$ = -1.135

Figure 146. Time History of Experimental Drop Test

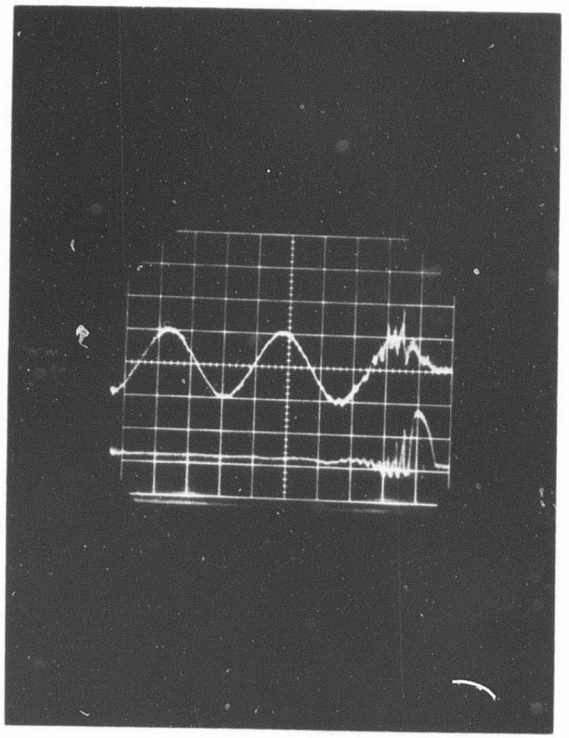

SAW-TOOTH

41# PLATFORM, $\frac{R}{r} = -0.5$

Figure 147. Time History of Experimental Drop Test

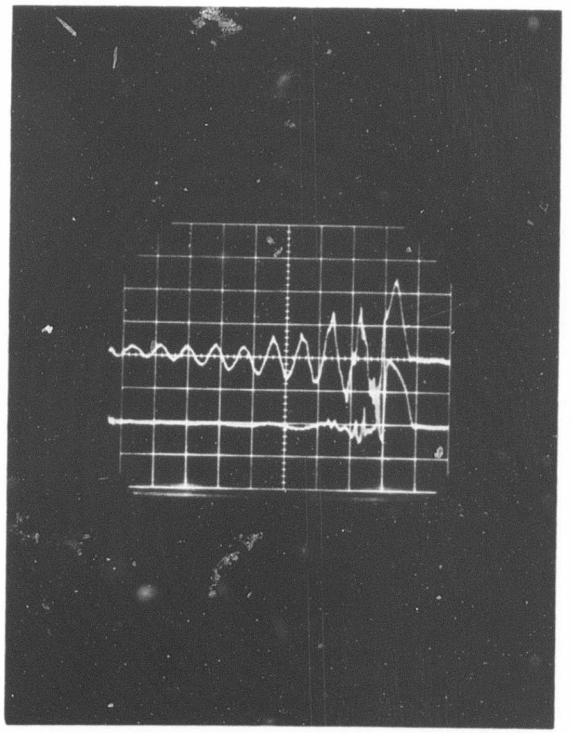

SAW-TOOTH

41# PLATFORM, $\frac{R}{r} = 4.842$

Figure 148. Time History of Experimental Drop Test

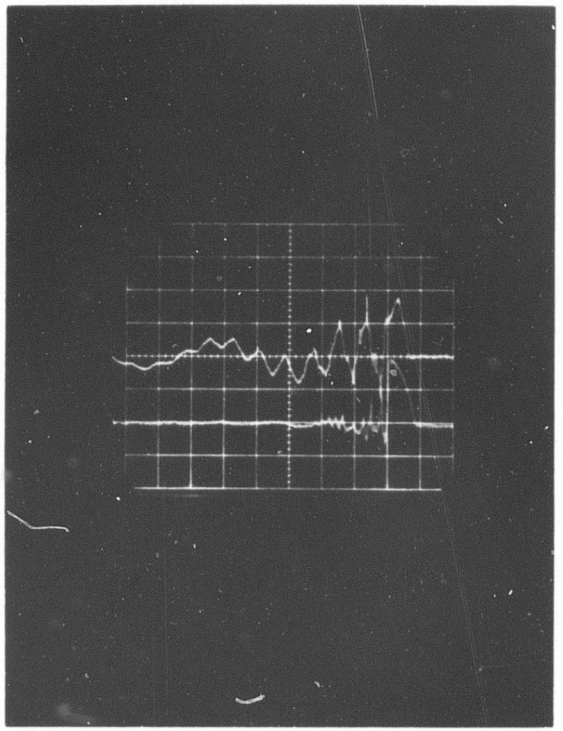

SAW-TOOTH

41# PLATFORM, $\frac{R}{r} = 2.95$

Figure 149. Time History of Experimental Drop Test

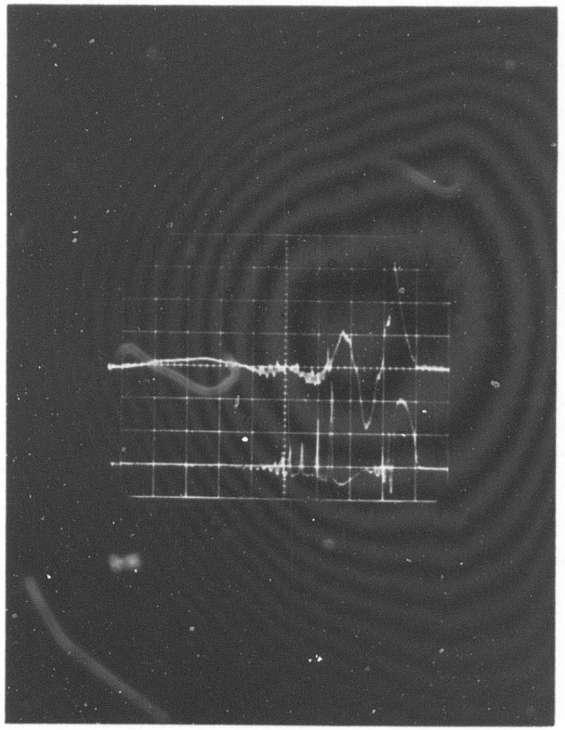

SAW-TOOTH

41# PLATFORM, $\frac{R}{r} = 2.95$ (RUBBER)

Figure 150. Time History of Experimental Drop Test

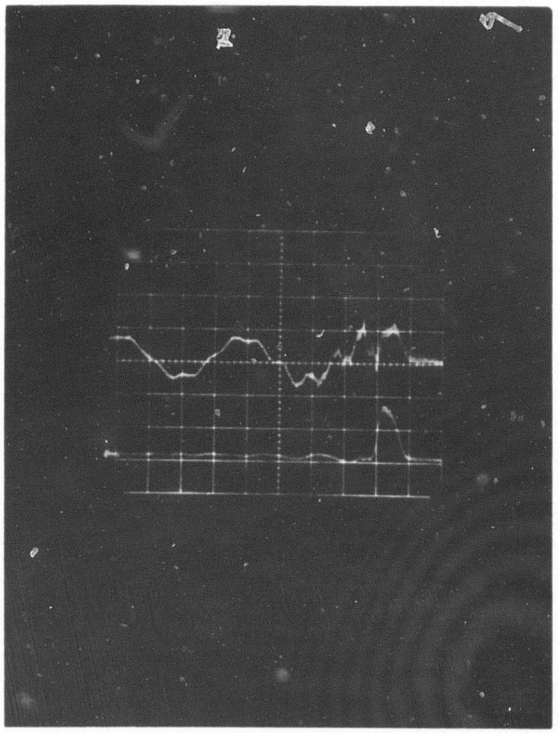

SAW-TOOTH

41# PLATFORM, $\frac{T}{T_1} = 2.10$

Figure 151. Time History of Experimental Drop Test

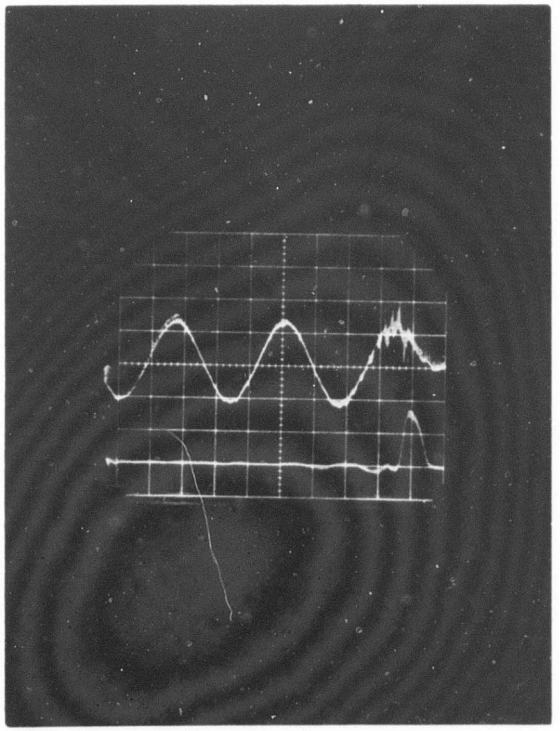

SAW-TOOTH

41# PLATFORM, $\frac{T}{T_1} = 1.50$

Figure 152. Time History of Experimental Drop Test

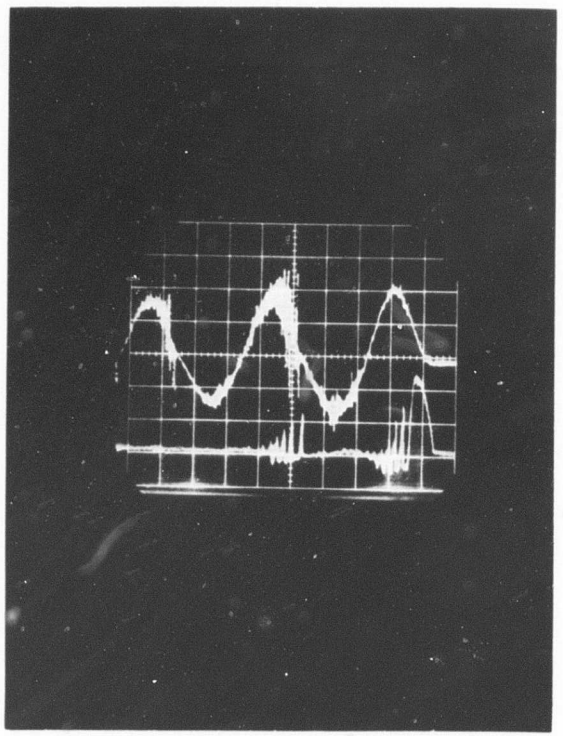

SAW-TOOTH

41# PLATFORM, CONVENTIONAL

Figure 153. Time History of Experimental Drop Test

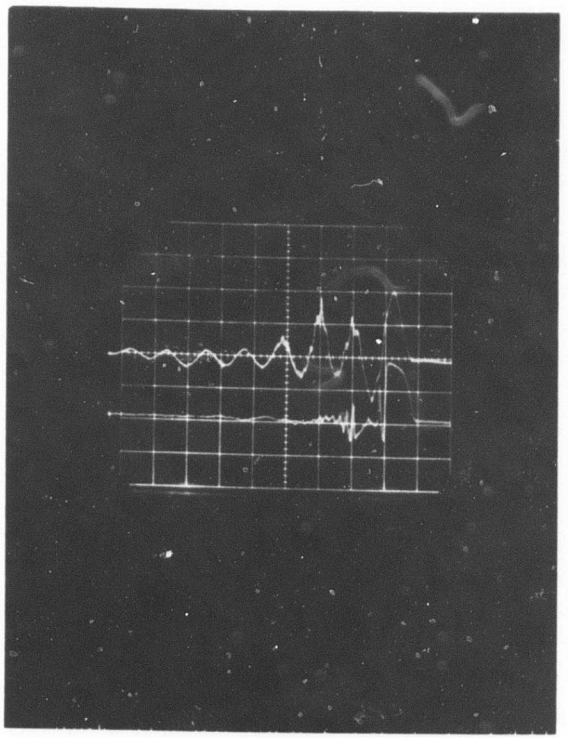

SAW-TOOTH

100# PLATFORM, $\frac{r}{R}$ = -6.131

Figure 154. Time History of Experimental Drop Test

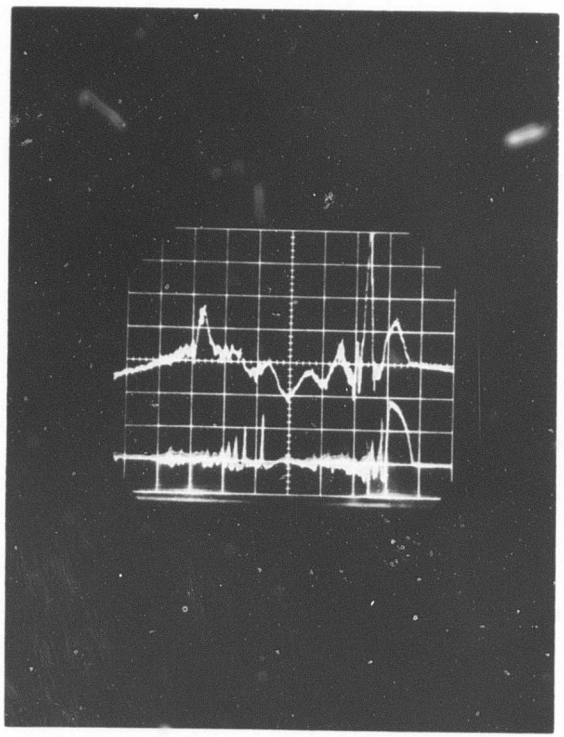

SAW-TOOTH

100# PLATFORM, $\frac{R}{r}$ = -2.40

Figure 155. Time History of Experimental Drop Test

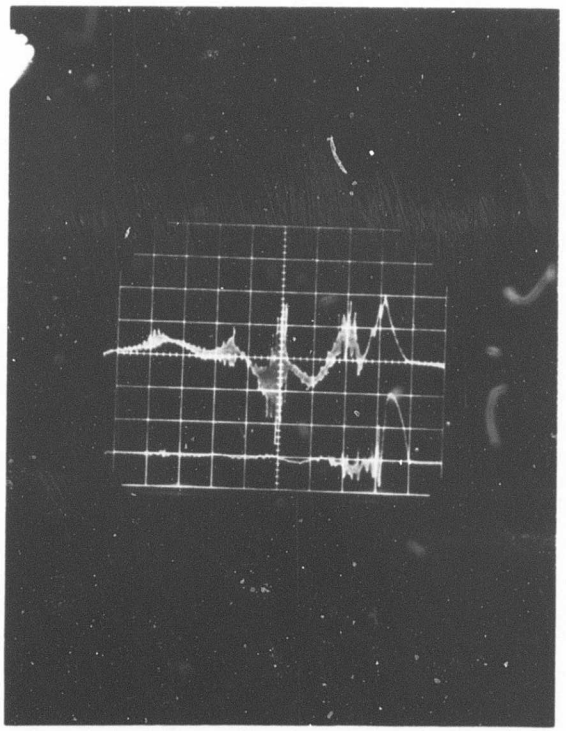

SAW-TOOTH

100# PLATFORM, $\frac{R}{r}$ = -2.40 (RUBBER)

Figure 156. Time History of Experimental Drop Test

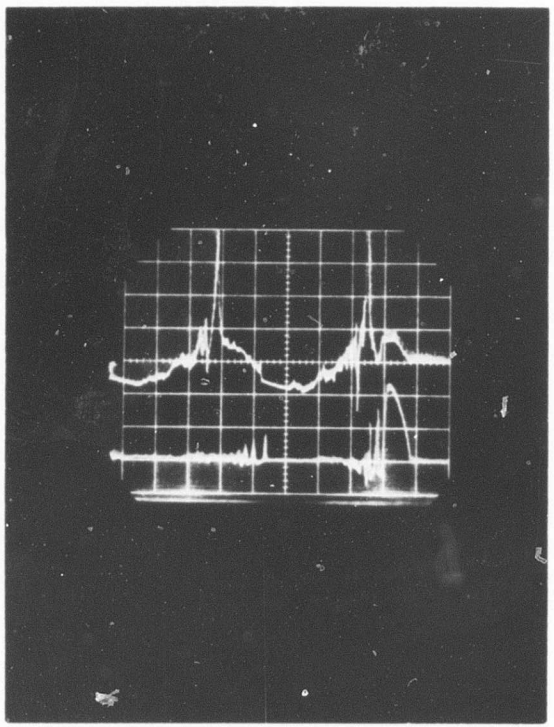

SAW-TOOTH

100# PLATFORM, $\frac{R}{r}$ = -1.135

Figure 157. Time History of Experimental Drop Test

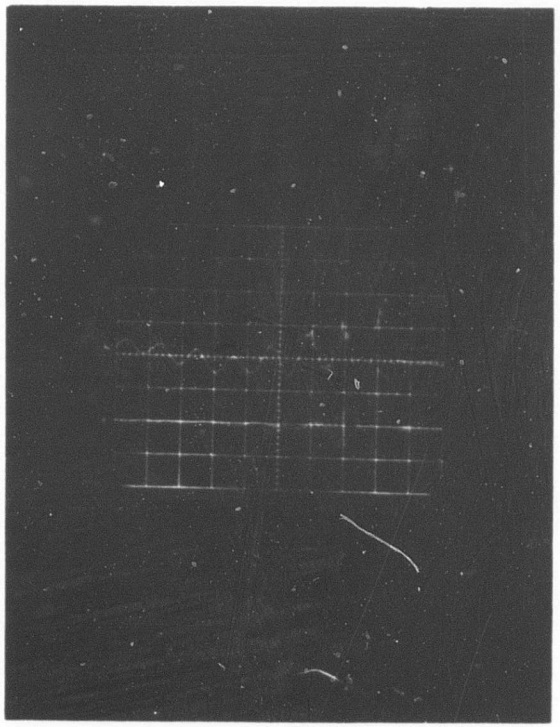

SAW-TOOTH

100# PLATFORM, $\frac{R}{r}$ = 4.842

Figure 158. Time History of Experimental Drop Test

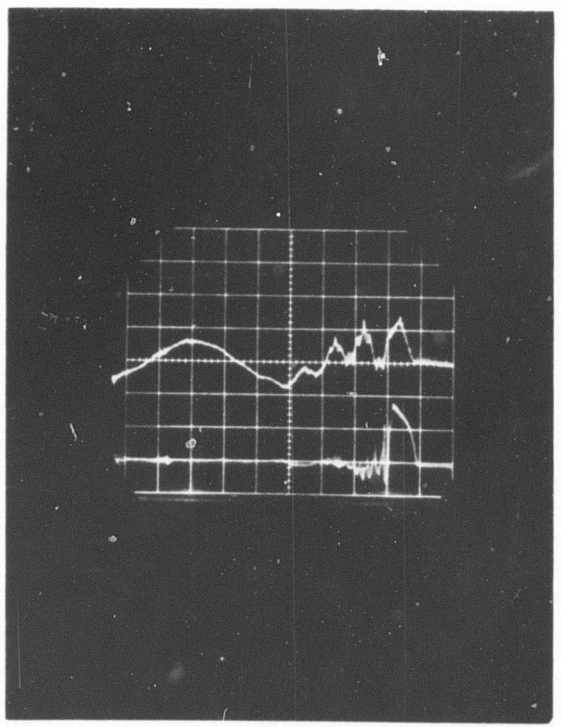

SAW-TOOTH

100# PLATFORM, $\frac{R}{T}$ = 2.95

Figure 159. Time History of Experimental Drop Test

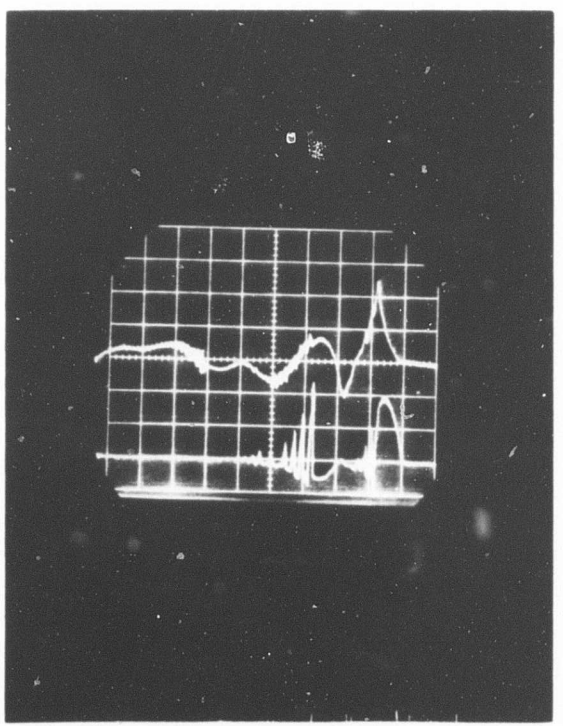

SAW-TOOTH

100# PLATFORM, $\frac{R}{T}$ = 2.95 (RUBBER)

Figure 160. Time History of Experimental Drop Test

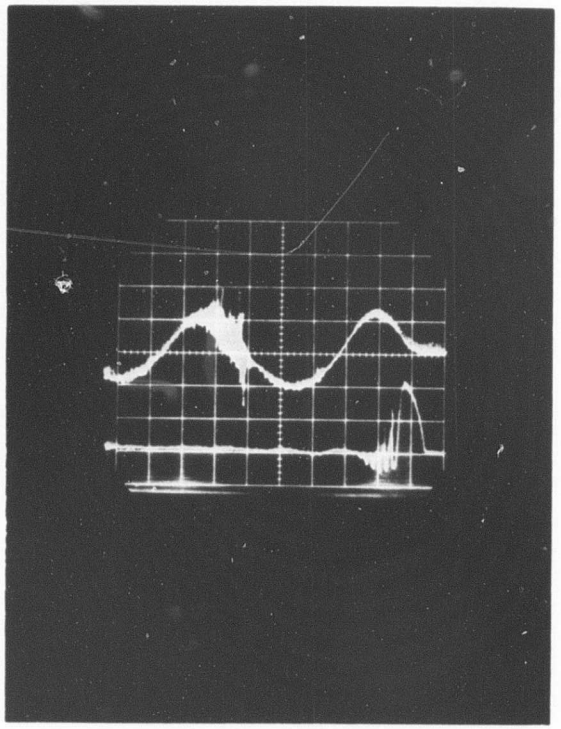

SAW-TOOTH

100 # PLATFORM, CONVENTIONAL

Figure 161. Time History of Experimental Drop Test

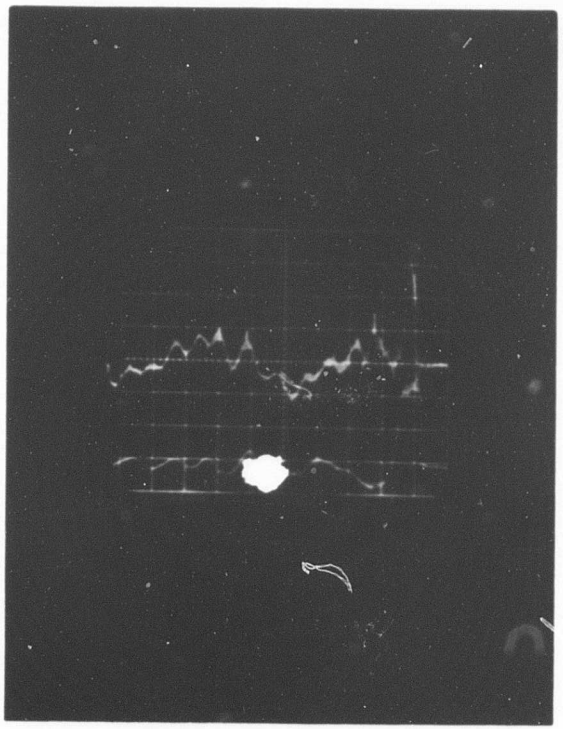

SQUARE WAVE

41 # PLATFORM, $\frac{R}{r}$ = -2.40

Figure 162. Time History of Experimental Drop Test

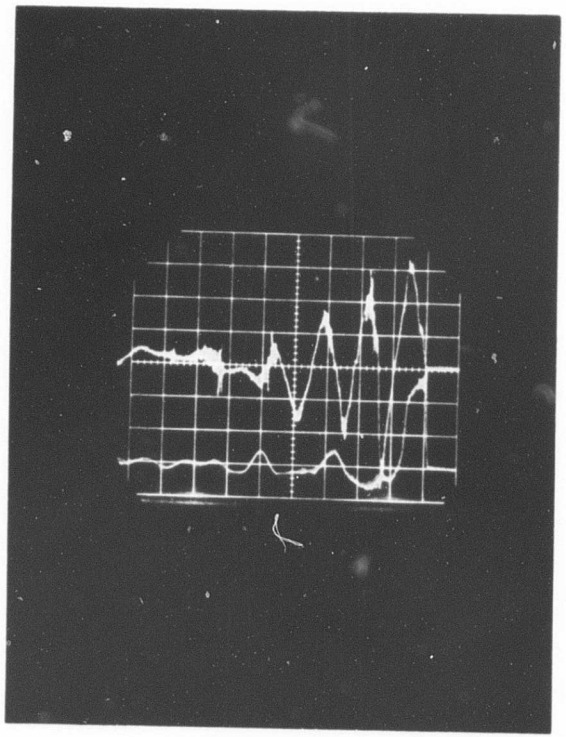

SQUARE WAVE

41# PLATFORM, $\frac{R}{r}$ = -2.40 (RUBBER)

Figure 163. Time History of Experimental Drop Test

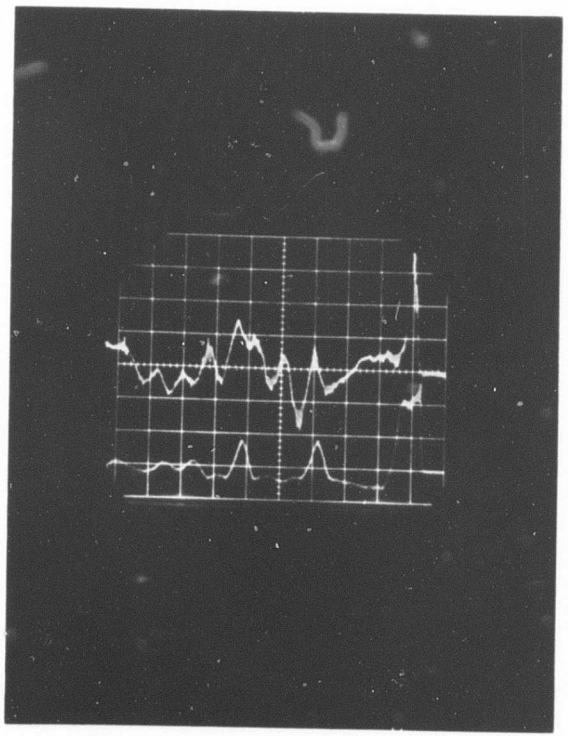

SQUARE WAVE

41# PLATFORM, $\frac{R}{r}$ = 2.95

Figure 164. Time History of Experimental Drop Test

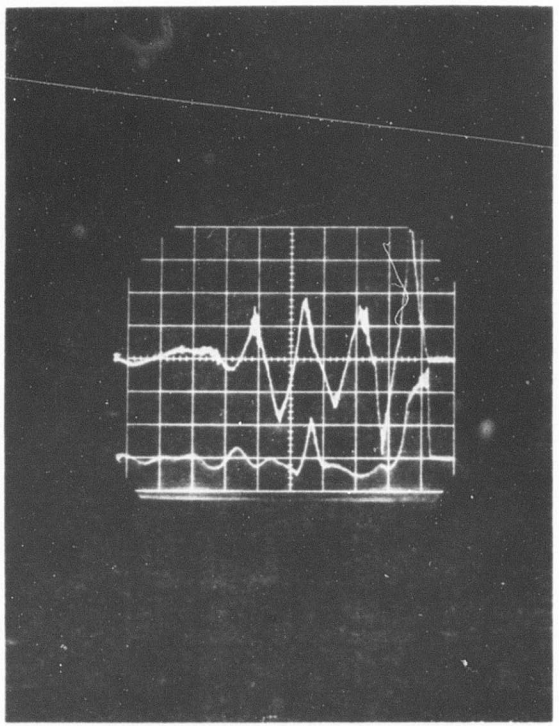

SQUARE WAVE

41# PLATFORM, $\frac{R}{T}$ = +2.95 (RUBBER)

Figure 165. Time History of Experimental Drop Test

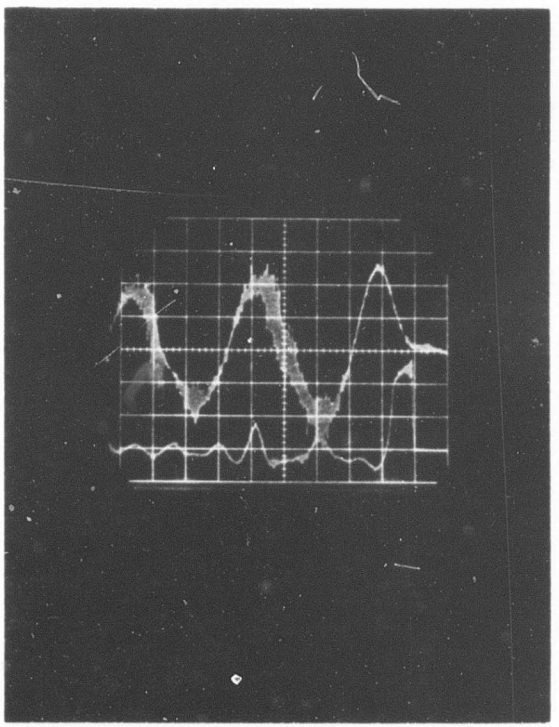

SQUARE WAVE

41# PLATFORM, CONVENTIONAL

Figure 166. Time History of Experimental Drop Test

CONCLUSIONS

From the results of the analysis and model testing, the following conclusions can be made:

1. Correlation of the analytical and test results of the DAVI Alpha was excellent.

2. The natural frequency of the DAVI Alpha was always lower than the natural frequency of the equivalent conventional system.

3. A change in isolated weight did not affect the antiresonant frequency of the DAVI Alpha.

4. The DAVI Alpha can be easily tuned to give the desired antiresonant frequency. In the series of tests on the DAVI Alpha, the DAVI Alpha was tuned to give an antiresonance from 5.6 c.p.s. to 20.5 c.p.s. without changing any hardware.

5. Results of the design study and tests show the DAVI Alpha to be ideally suited for helicopter vibration problems.

6. A two-dimensional DAVI Alpha can be designed with spherical bearings.

7. Analysis and tests show that the series-damped DAVI, that is, the DAVI Beta and Gamma, can be designed to give high-frequency isolation and to retain the DAVI Alpha antiresonance characteristics.

8. Damping in the series element in the DAVI Beta or Gamma can be used to attenuate the natural frequencies of the system, and will still obtain excellent isolation at the antiresonant frequency.

9. The DAVI Beta or Gamma can be designed to give better high-frequency isolation than a conventional isolation system with the same spring rate.

10. The DAVI Beta and Gamma can be designed to give the same results.

11. Correlation of the analytical and test results of the DAVI Beta and Gamma was good.

12. Analysis of the DAVI Delta shows that zero static deflection can be obtained on the inertia bar. However, the DAVI Delta does not have simple tuning capability and cannot be designed as simply as the other DAVI configurations.

13. For the period of the shock input analyzed, the DAVI Alpha has an initial shock transmissibility that is approximately equal to its high-frequency transmissibility. The DAVI Alpha then oscillates in its fundamental mode.

14. A DAVI Alpha can be designed to give better shock attenuation than a conventional isolator of the same stiffness.

15. The DAVI Alpha with radial flexible pivots had higher response due to velocity shock than either the DAVI Alpha with rigid pivots or the conventional isolator. This high response is due to the increased number of degrees of freedom in the DAVI Alpha with radial flexible pivots and all of the modes of motion are excited by the velocity shock input.

16. From the drop test results of the DAVI Alpha with flexible pivots, the initial shock transmissibility that occurred in the DAVI Alpha was eliminated. However, due to the three-degree-of-freedom system, all modes of motion are excited by the shock input, and higher transmissibilities are obtained than in the DAVI Alpha with rigid pivots.

REFERENCES

1. Anderson, R. C., and Smith, M. F., A Study of the Kaman Dynamic Antiresonant Vibration Isolator, USAAVLABS Technical Report 65-75, [illegible]ary 1966.

2. Harris, C. M., and Crede, C. E., Shock and Vibration Handbook, Three Volumes, McGraw-Hill Book Company, Inc., New York, New York, 1961.

3. Crede, C. E., Vibration and Shock Isolation, John Wiley and Sons, Inc., New York, New York, 1951.

4. Den Hartog, J. P., Mechanical Vibrations, Fourth Edition, McGraw-Hill Book Company, Inc., New York, New York, 1956.

UNCLASSIFIED

Security Classification

DOCUMENT CONTROL DATA - R & D

(Security classification of title, body of abstract and indexing annotation must be entered when the overall report is classified)

1. ORIGINATING ACTIVITY (Corporate author)	2a. REPORT SECURITY CLASSIFICATION
Kaman Aircraft Division Kaman Corporation Bloomfield, Connecticut	Unclassified
	2b. GROUP

3. REPORT TITLE

AN ANALYTICAL AND MODEL TEST RESEARCH STUDY ON THE KAMAN DYNAMIC ANTIRESONANT VIBRATION ISOLATOR (DAVI)

4. DESCRIPTIVE NOTES *(Type of report and inclusive dates)*

Final Report

5. AUTHOR(S) *(First name, middle initial, last name)*

Robert Jones

6. REPORT DATE	7a. TOTAL NO. OF PAGES	7b. NO. OF REFS
November 1968	241	4

8a. CONTRACT OR GRANT NO.	9a. ORIGINATOR'S REPORT NUMBER(S)
DA 44-177-AMC-391(T)	
b. PROJECT NO. Task 1F125901A14608	USAAVLABS Technical Report 68-42
c.	9b. OTHER REPORT NO(S) *(Any other numbers that may be assigned this report)*
d.	Kaman Report R-690

10. DISTRIBUTION STATEMENT

This document has been approved for public release and sale; its distribution is unlimited.

11. SUPPLEMENTARY NOTES	12. SPONSORING MILITARY ACTIVITY
	U. S. Army Aviation Materiel Laboratories Fort Eustis, Virginia

13. ABSTRACT

This report is the result of a research study conducted on the Dynamic Antiresonant Vibration Isolator (DAVI). A parametric study was conducted on the basic unidirectional and two-dimensional DAVI Alpha to determine its isolation performance, and a general design criterion was obtained. Theoretical analyses, including damping across the series element, were done on the series-type DAVI's. A comparison was made of the series-type DAVI Beta and Gamma. Shock analyses for various types of inputs were done for the DAVI Alpha configuration. Experimental models of the unidirectional and two-dimensional DAVI Alpha and the series-type DAVI Beta and Gamma were constructed and tested to corroborate the theoretical results. Drop tests with three different inputs were done to determine the shock characteristics of the DAVI Alpha. Results of the analysis and tests show that the DAVI Alpha can be designed to give over 90% isolation at much lower frequencies than a conventional isolator with the same static frequencies. The isolation obtained at the antiresonant frequency is independent of the mass to be isolated. Analysis and tests show that the DAVI Alpha can be designed to give better shock attenuation than the conventional isolator with the same spring rate. Analysis and tests show that a DAVI Beta or Gamma can be designed to retain the advantages of the DAVI Alpha and to obtain better high-frequency isolation than the equivalent conventional isolator. Damping across the series element can be used to attenuate the amplitude obtained at the second natural frequency without affecting the isolation obtained at the antiresonance.

DD FORM 1 NOV 68 1473 REPLACES DD FORM 1473, 1 JAN 64, WHICH IS OBSOLETE FOR ARMY USE.

UNCLASSIFIED

Security Classification

UNCLASSIFIED

Security Classification

14 KEY WORDS	LINK A		LINK B		LINK C	
	ROLE	WT	ROLE	WT	ROLE	WT
Vibration Isolator						
Passive Isolator						
Antiresonant Isolator						
Low Frequency/Stiff Isolator						
Discrete Frequency Isolation						
Series Type Isolator						
Shock Attenuation						
DAVI						

UNCLASSIFIED

Security Classification

1223-68